Investigation of the Photochemical Properties of Ruthenium Polypyridyl Complexes using High Performance Liquid Chromatography (HPLC)

By

Hamid M. Younis Ahmed

A Thesis presented to Dublin City University for the Degree of Doctor of Philosophy

Supervisor Professor Johannes G. Vos

School of Chemical Sciences

Dublin City University

2010

Declaration

I hereby certify that this material, which I now submit for assessment on the programme of study leading to the award of Doctor of Philosophy by research is entirely my own work, that I have exercised reasonable care to ensure that the work is original, and does not to the best of my knowledge breach any law of copyright, and has not been taken from the work of others save and to the extent that such work has been cited and acknowledged within the text of my work.

Signed:----- ----------

Hamid M Younis Ahmed

(Student) ID No.: **99146150**

Date: **29.11.2010**

Acknowledgements

First of all, I would like to thank Prof. Han Vos for the opportunity he gave me and his guide and experience during these last almost 4 years.

Of course to who share with me all worry during study time Hassan Alwael

To Drs. Khaled Ben Younis, Muoth Atma, Shadi Karazi, I really appreciate all the help you gave me in preparing this thesis. I always believe you're my real best friends.

Special thanks to al my family for their patience during my study, also to my special "DCU" friends, both past and present.

Many thanks to the guys in the HVRG, thanks for the great times in lab we had. Doctors, Dinilo Dani, Rob Groarke, Bill Henry, Martin Schulz, Lynda Cassidy, and Brian J. Maclean, and postgraduates researcher Laura Cleary, Jane Inglis, Nadia Coburn, Suraj Soman, Avishek Paul, Gurmeet Singh bindra, Declan Traynor, Saidah Nural and Thanja Lamberts.

Finally I would like to thank the Sirte University for a scholarship and the Embassy of the Libya Peoples in London for their financial support.

I would also like to thank the technical staff John McLaughlin, Mary Ross, Vincent Hooper, Veronica Dobbyn, Ambrose May, Damien McGuirk, and our school secretary Julie McArthur.

There are so many people to thank I'm so sorry I cannot remember all of them.

Abstract

The focus of this thesis is the study of the Photochemical Properties of Ruthenium Polypyridyl Complexes using High Performance Liquid Chromatography (HPLC). In chapter 1, topics relevant to the studies presented in this thesis are introduced. An introduction highlights the literature relevant to the topic.

In Chapter 2, the experimental and optimisation of conditions of the various methods of characterisation and the setup of HPLC are described. A theoretical background for the experimental and computational techniques used is also given.

In Chapter 3, we have presented the separation of the two stereoisomers of $[(Ru(bpy)_2)_2(bpt)](PF_6)_3$; the application of the separation of dinuclear ruthenium(II) polypyridyl complexes is examined. In particular the importance of both by semi preparative HPLC using cation exchange column and ^{1}H NMR spectroscopy.
After three hours of irradiation at 430 nm the isomers constituting fraction A are converted into the isomers forming fraction B as detected through *^{1}H NMR* spectroscopy and HPLC. For both fractions A and B further irradiation produces the fragmentation of the dimetallic complex into monometallic species. Such a photolytic reaction is catalysed by the presence of chloride anions. In particular, photofragmentation of complex consists of the loss of the ruthenium centre bound to the N4-site of the triazole ring.

In Chapter 4, the separation, characterization and photochemical properties of the stereoisomers mono- and dinuclear of $[(Ru(bpy)_2)_2(bpzt)](PF_6)_3$ is examined HPLC and ^{1}H NMR spectroscopy and photophysical and photochemical properties are investigated. In case of the complex, photoisomerization is completed within one hour of irradiation whereas the loss of one metal centre takes place in less than nine hours.

In Chapter 5, photochemically induced ligand rearrangements for the N2 and N4 coordination isomers of the complex $[Ru(bpy)_2(Hpztr)]^{2+}$ and its deprotonated analogue $[Ru(bpy)_2(pztr)]^+$, where bpy is 2,2'-bipyridyl and Hpztr is pyrazine-1,2,4-triazole ligand, are reported. It was found that the N4 isomer is photostable, while the N2 species isomerizes to the N4 species via an intermediate.

In Chapter 6, photochemical reactions of the complexes containing 4,4'-di-tert-butyl-2,2'-bipyridine and Organic ligand (Tetrapyridophenazine, tpphz). $[(tbbpy)_2$ Ru (tpphz)$](PF_6)_2$ (1) , $[(tbbpy)_2$ Ru(tpphz)$PdCl_2](PF_6)_2$ (2), $[(tbbpy)_2$ Ru (tpphz)Ru$(tbbpy)_2](PF_6)_4$ (3), and $[(tbbpy)_3$ Ru$]Cl_2$ (4) in CH_3CN and acetone are studied. Without TEA, all complexes have shown stability, and with TEA the formation of other minor products during irradiation @ 470 nm has been observed.

Finally, we conclude with a summary of the work completed in this thesis and possible future work is presented in chapter 7.

Table of Content

CHAPTER 3

The Separation of the two Stereoisomers of Dinuclear $[(Ru(bpy)_2)_2(bpt)](PF_6)_3$

CHAPTER 4

The Separation, Characterization and Photochemical Properties of The Stereoisomers Mono- and Dinuclear of $[(Ru(bpy)_2)_2(bpzt)](PF_6)_3$

CHAPTER 5

Photochemically Induced Ligand Rearrangements for The N2 and N4 Coordination Isomers of The Complex $[Ru(bpy)_2(Hpztr)]^{2+}$

CHAPTER 6

Photochemical Reactions in This Study of The Complexes Containing 4,4'-di-tert-butyl-2,2'-bipyridine and Organic Ligand (Tetrapyridophenazine, tpphz). $[(tbbpy)_2\ Ru(tpphz)PdCl_2](PF_6)_2$

CHAPTER 7

Appendix

CHAPTER 1

General Introduction

1 General Introduction

1.1 Ruthenium Based Transition Metal Compounds

The interest in the research of ruthenium(II) co-ordination compounds started in the late fifties when $[Ru(bpy)_3]Cl_2$ (bpy is 2,2'-bipyridyl) was recognized as the prototype of luminescent molecule the emission of which originated from a metal-to-ligand charge transfer (MLCT) transition [1]. A further stimulus in the prosecution of the studies on the photophysics and photochemistry of ruthenium-polypyridyl type complexes came from the discovery of their photocatalytic properties in the processes of water dissociation [2], and carbon dioxide reduction [3]. The unique combination of physical and chemical properties of ruthenium polypyridyl compounds, such as high chemical stability, selective excited state reactivity, long-lived excited states, and well defined redox properties caught the attention of many research workers [4]. Since then this interest has continued and led successively to the creation of solar energy conversion devices like Graetzel cells, which are based on the electron transfer properties of excited ruthenium polypypyridyl sensitisers anchored onto semiconductor surfaces [5]. However, the research on ruthenium-polypyridyl complexes was not only confined within the fields of photocatalysis and solar energy conversion [6], but also involved areas of application such as bio, [7] and chemical sensors [8], molecular electronics, [9] nonlinear optics [10] and optical storage [11]. Beside that, ruthenium-polypyridyl complexes played also a relevant role in the development of supramolecular

chemistry [12]. The popularity of ruthenium polypyridyl compounds is based on the special arrangement of the energy levels of the frontier orbitals (Figure 1.1).

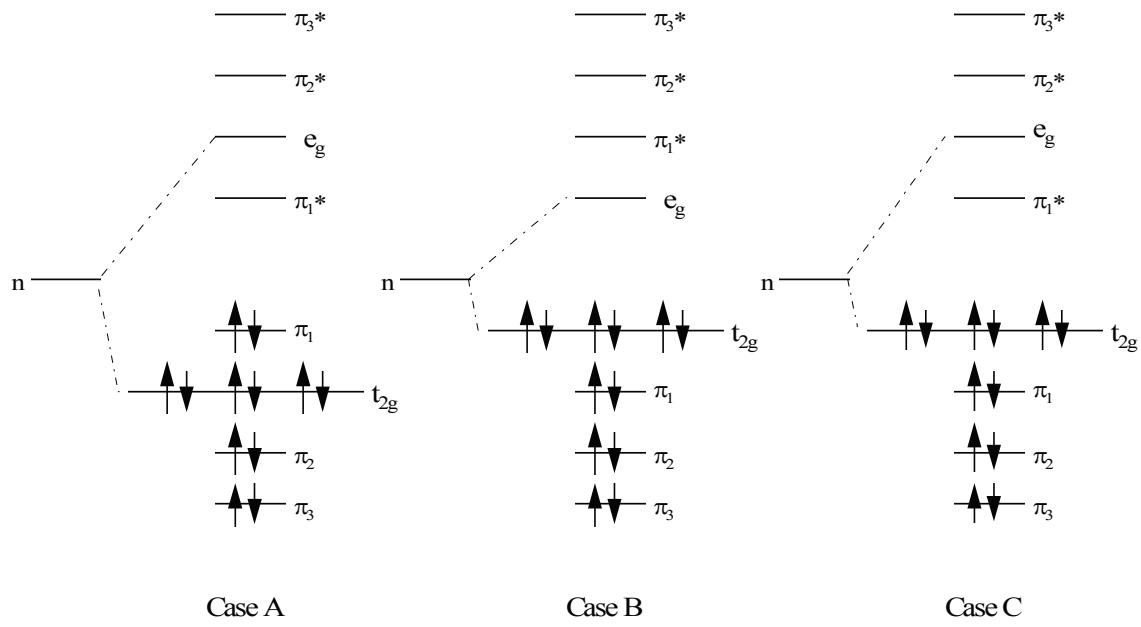

Figure 1.1. *Different possible arrangements of the energy of the frontier orbitals in metal complexes.*

Important in these arrangements is the relative position of the energy levels corresponding to metal and ligand based orbitals: in case A the highest occupied molecular orbital (HOMO) and the lowest unoccupied orbital (LUMO) are ligand based orbitals and both are of the π-type. A complex with this arrangement would act as an organic compound and energy and electron transfer processes would be very difficult since both these orbitals are strongly localized on the same part of the molecule. In case B both HOMO and LUMO are metal based. The features of these two orbitals are explained by the ligand field theory, and since the e_g (LUMO) has an anti-bonding character, its population will lead to the breaking of the metal-ligand bond and may lead to loss or rearrangement of the ligands The most

interesting arrangement is found in case C, which corresponds to the arrangement for ruthenium polypyridyl complexes. The HOMO is metal based while the LUMO in ligand based. This has the result that upon excitation the electron can move from the metal to the ligand (MLCT process) and give rise to further electron and energy transfer processes. These issues are outlined in some more detail in the six points below.

Photochemistry of the complexes can often be observed upon irradiation with visible light since excitation energies are generally lower than in organic compounds. Low-lying, allowed MLCT transitions provide an especially useful gateway through which optical/solar energy is converted into molecular excitation/chemical energy.

Transition metal compounds possess various types of excited states, which differ in their orbital parentage, localisation within the molecule, energy, dynamics and reactivity. This can be exploited to tune their thermodynamics.

As excited state density is much higher in transition metal polypyridyl complexes than most organic molecules several different excited states can occur in a narrow energy range. Hence, excited states of different character can interact with each other, either at the geometry of Franck – Condon (i.e. vertical) excitation or along specific reaction coordinates. This can lead to complex behaviour, which shows competing relaxation and reactivity pathways. Photochemical dynamics and quantum yields often depend on excitation energy and/or temperature due to the

presence of energy barriers on photochemical pathways that originate in avoided crossings between excited state and potential energy surfaces.

Metal complexes exhibit strong spin-orbit coupling, especially when second or third row transition metals are present. Consequently, intersystem crossing is fast and its distinction from internal conversion is blurred. However, for practical purposes it is still possible to use triplet and singlet spin labels, especially for MLCT states. Consequentially, long lived excited states and high quantum yields are common features.

Many transition metal complexes are redox-active in their electronic ground state. Their electron transfer reactions can involve a change in oxidation state of the metal atom, ligand(s) or both. This redox activity is retained in the excited sate. Therefore, many metal complexes can participate in photochemical electron transfer reactions.

Versatile synthetic chemistry allows fine tuning of the excited state character and small structural changes can perturb energy ordering. Knowledge of how to control excited state properties is employed to design new molecular photonic materials, e.g. sensitisers, luminophores, photocatalysts,

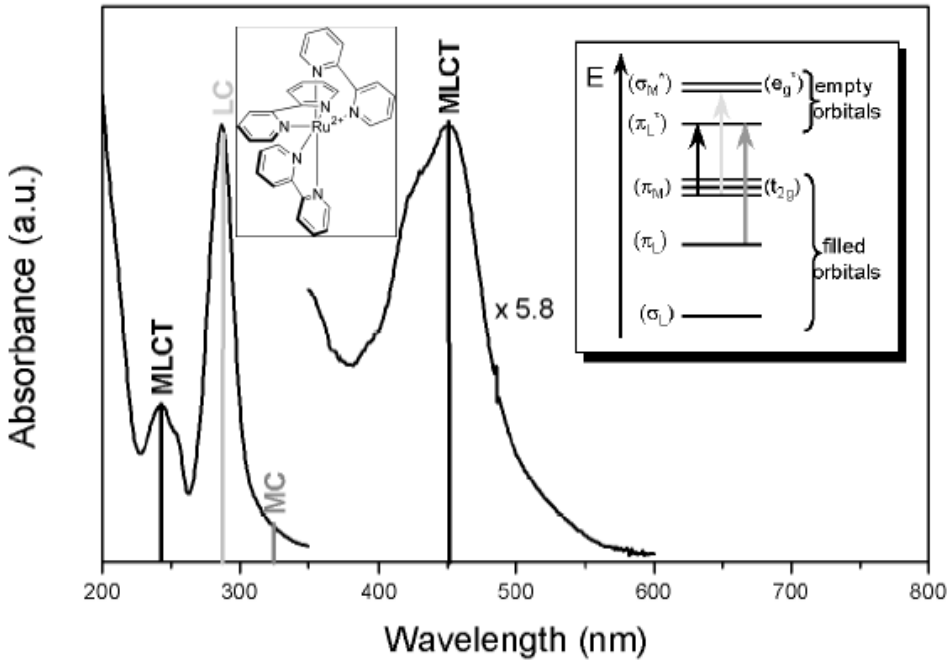

Figure 1.2. *Absorption spectrum of Ru(bpy)3(PF6)2 in acetonitrile showing MLCT, ligand centred (LC) and metal centred (MC) transitions Inset: molecular orbital diagram, where the notation (L or M) indicate where the orbital is mostly localized. The d-orbitals, which are mostly localized on the metal, are split into three lower (t2g) and two higher (eg) orbital energy levels for the presence of the field generated by the bpy-ligands [13]*

luminescent probes or sensors [14]. Finally, transition metal complexes are generally thermally and photochemically stable.

All these aspects make transition metal polypyridyl compounds valuable materials as photosensitisers in artificial photosynthetic systems. In the next section a more detailed description of the "parent compound" $[Ru(bpy)_3]^{2+}$ is given as a general

example of the photophysical properties of compounds of the ruthenium-polypyridyl type.

1. 2 [Ruthenium-tris-(2,2'-bipyridyl)]$^{2+}$: [Ru(bpy)$_3$]$^{2+}$

Ruthenium, when coordinated to a polypyridyl ligand, constitutes one of the most widely studied and better understood examples of complexes of transition metals, in terms of its excited state behaviour and the photophysical processes which it undergoes.

The photophysical properties of the parent compound [Ru(bpy)$_3$]$^{2+}$ will be discussed. Although variation in these properties will occur upon a change of one or more of the ligands, the general principles will remain the same. In the various chapters, an overview of other ruthenium compounds will be given as appropriate.

[Ru(bpy)$_3$]$^{2+}$ is a d_6 complex with octahedral geometry (inset Figure 1.2). Its absorption spectrum is dominated by the two bands at 240 nm and 450 nm (most intense) due to promotion of an electron from a π_M metal orbital to π_L* ligand orbitals (MLCT processes). Ligand centred (LC) bands at 185 nm and 285 nm arise from promotion of an electron from π_L to π_L*. This a C type compound as shown in Figure 1.1. The weak shoulders at 322 and 344 nm are due to the metal centred transitions (MC) from π_M to π_M^* [15]. The versatility of the synthetic chemistry of ruthenium polypyridyl complexes [16] allows the facile variation of the chelating ligands. This mainly produces the alteration, within a certain extent, of the

energy level of the ligand centred LUMO in the complex, with consequent modulation of absorption/emission energies, redox potentials and excited state lifetimes [6,17]. This is because the strength of the ligand field, the substituents on the ligand and the extent of electronic conjugation of the ligand govern the relative position of the energy levels of the orbitals.

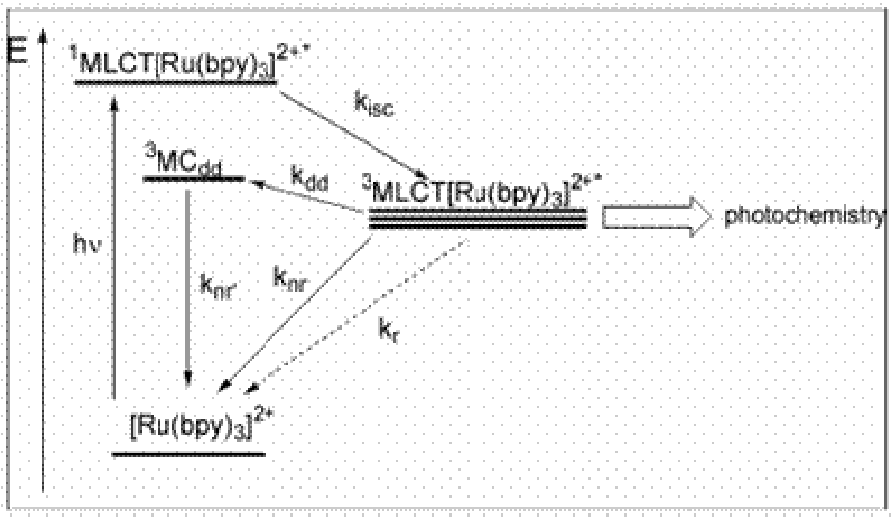

Figure 1.3. *Jablonski diagram for [Ru(bpy)3]2+, showing the excited states after occurrence of the 1MLCT transition [13].*

For $[Ru(bpy)_3]^{2+}$ and most of Ru polypyridine complexes excitation first leads to the populating of the ^{1}MLCT state which successively evolves into the triplet ^{3}MLCT state through an efficient process of intersystem crossing (ISC) (Figure 1.3) [18] The excited triplet state has experimentally been shown to consist of three closely spaced energy levels [19]. Excitation with visible light promotes an electron into the lowest singlet excited state ^{1}MLCT, which within a few hundred femtoseconds, is

converted to the lowest triplet state ^{3}MLCT, via intersystem crossing (ISC) [18]. The quantum yield of the formation of the lowest lying excited state is almost unity, showing that ISC from the upper singlet excited states (obtained by excitation) to the lowest triplet state is very fast and efficient [20]. The radiative (k_r) and non-radiative (k_{nr}) decay pathways of the ^{3}MLCT excited state are also shown in the Jablonski diagram (Figure 1.3). The lifetime of the ^{3}MLCT state at 293 K in deaereted MeCN is 850 ns [18].

Photochemical processes are normally preceded by photoinduced ligand exchange which is one of the most basic photochemical reactions. For transition metals complexes, ligand exchange is associated with the breaking of metal-ligand bonds. Therefore, the photolability of compounds is generally associated with the presence of antibonding metal centred (MC) orbitals. An energy diagram typical for ruthenium polypyridyl complexes is shown in Figure 1.4, outlining the energy levels involved in photochemical processes. In this type of compound excitation from the metal based ground state to a singlet metal-to-ligand charge-transfer state (^{1}MLCT) and fast picosecond intersystem crossing leads to population of a relatively long lived ^{3}MLCT state (triplet metal-to-ligand charge-transfer). The detailed work of Meyer and co-workers on ruthenium polypyridyl complexes has identified the ^{3}MC (metal centered) orbital as being responsible for the photodecomposition observed [21]. For photoactive compounds, population of the antibonding ^{3}MC state from the ^{3}MLCT state takes place at room temperature and the photolability of the complexes is generally related to the energy difference

between the deactivating ^{3}MC state and the emitting ^{3}MLCT level, (See Figure 1.4).

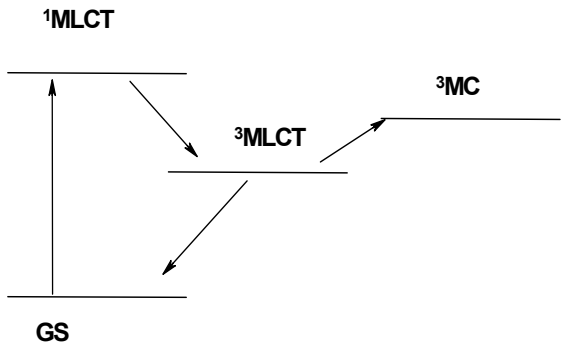

Figure 1.4. *Electronic levels in* $[Ru(bpy)_3]^{2+}$

Meyer and co-workers observed that such photoprocesses may also be strongly dependent on the solvent used. Strong ligands such as acetonitrile and also coordinating counter ions can increase the quantum yield for ligand loss. So while $[Ru(bpy)_3](PF_6)_2$ shows little or no decomposition in CH_2Cl_2, in the presence of Cl^- or NCS^- ions, formation of species such as $[Ru(bpy)_2Cl_2]$ is observed. The photolability of $[Ru(bpy)_3](PF_6)_2$ is much increased in coordinating solvents such as acetonitrile and bpy loss maybe observed [21]. The formation of intermediates containing monodentate coordinated bpy ligands has been observed using ^{1}H NMR [22] coupled with electronic spectroscopy. These studies show clearly that the energy difference between the ^{3}MLCT and the ^{3}MC energy levels is an important parameter, which for a large extent controls the photochemical processes observed.

Apart from the energies and location of excited states, the nature of the ground state is also important for the behaviour of the compounds. Oxidation of $Ru(bpy)_3^{2+}$ occurs at $E_{1/2}$ = +1.5 V vs NHE (NHE = normal hydrogen electrode), and involves the removal of one electron from the metal. The ground state is therefore metal based (again type C in Figure 1.1) Three bpy-based reductions are observed at negative potentials in the range -1.1 → -1.5 V vs NHE. The $[Ru(bpy)_3]^{2+}$ excited state is both a more powerful oxidant (0.82 V vs NHE) and reductant (-0.84 V vs NHE) in comparison to the ground state (Figure 1.4). This feature can be rationalized by considering the excited state to be a combination of Ru^{3+} and a bpy$^{\cdot}$ radical anion. The excited state can be intercepted with quenchers which generate the longer-lived oxidant $[Ru(bpy)_3]^{3+}$ or reductant $[Ru(bpy)_3]^{+}$ [23].

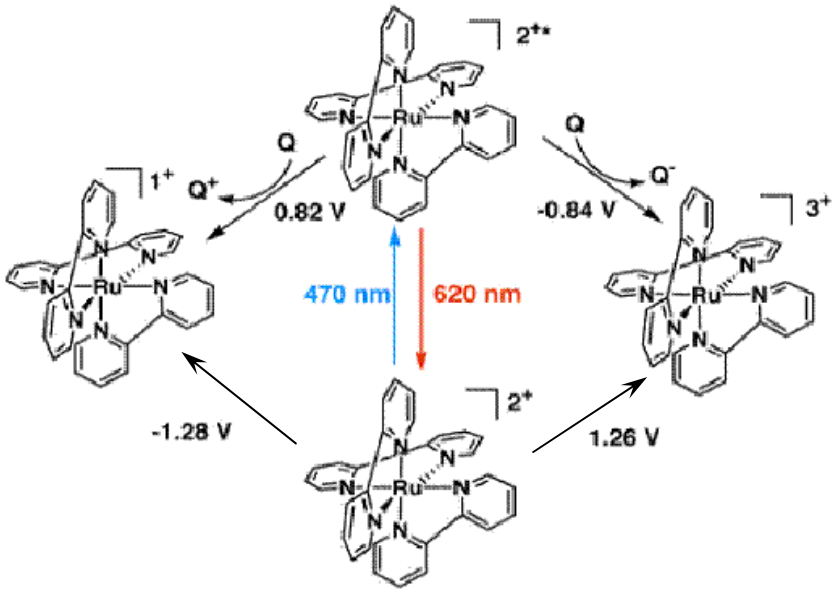

Figure 1.5. *$[Ru(bpy)_3]^{2+}$ redox processes. Bimolecular reaction of $[Ru(bpy)_3]^{2+*}$ with a quencher (Q) can be used to generate $[Ru(bpy)_3]^{3+}$ (1.26 V vs NHE) or $[Ru(bpy)_2(bpy)]^{1+}$ (-1.28 V vs NHE). Blue (red) arrow indicates the wavelength of maximum absorption (emission) in the visible spectrum [24].*

To summarise, the photophysical and photochemical behaviour of these complexes reflect their structural dependence on the nature of their low–lying excited states. The presence of an electron-accepting α-diimine ligand in the coordination sphere allows for charge transfer, CT, through electronic transitions directed to the diimine ligand [promotion of an electron from a $d\pi$(M) metal orbital to the π_L^*, (MLCT)]. In the next sections, a number of photodriven processes such as photoinduced electron and energy transfer will be discussed.

1.3 Photoinduced Electron Transfer

A photoinduced electron transfer (PELT) from a donor (D) to an acceptor (A) results in the formation of a charge separated state that consists of the corresponding radical cation and anion. Such a process is in direct competition with the radiative and nonradiative decay processes that are present in the first formed excited state of the molecule. Therefore, electron transfer can be regarded as another deactivation pathway of the locally excited (singlet) state that can be taken in addition to internal conversion (IC), ISC to the triplet manifold, and fluorescent (or phosphorescent) emission (Figure 1.5). So, PELT can be responsible for emission quenching [25]. The PELT process is involved in many organic photochemical reactions. It plays a major role in photosynthesis and in artificial systems for the conversion of solar energy based on photoinduced charge separation. Fluorescence quenching experiments provide a useful insight into electron transfer processes occurring in these systems. An excited molecule is generally both a better reductant and oxidant than its ground state analogue.

Photoinduced oxidative and reductive electron transfer processes occur according to the following reactions:

$^1D^* + A \longrightarrow D^{\cdot +} + A^{\cdot -}$ Oxidative electron transfer

$^1A^* + D \longrightarrow A^{\cdot -} + D^{\cdot +}$ Reductive electron transfer

The mechanisms for such processes are shown in Figure 1.6.

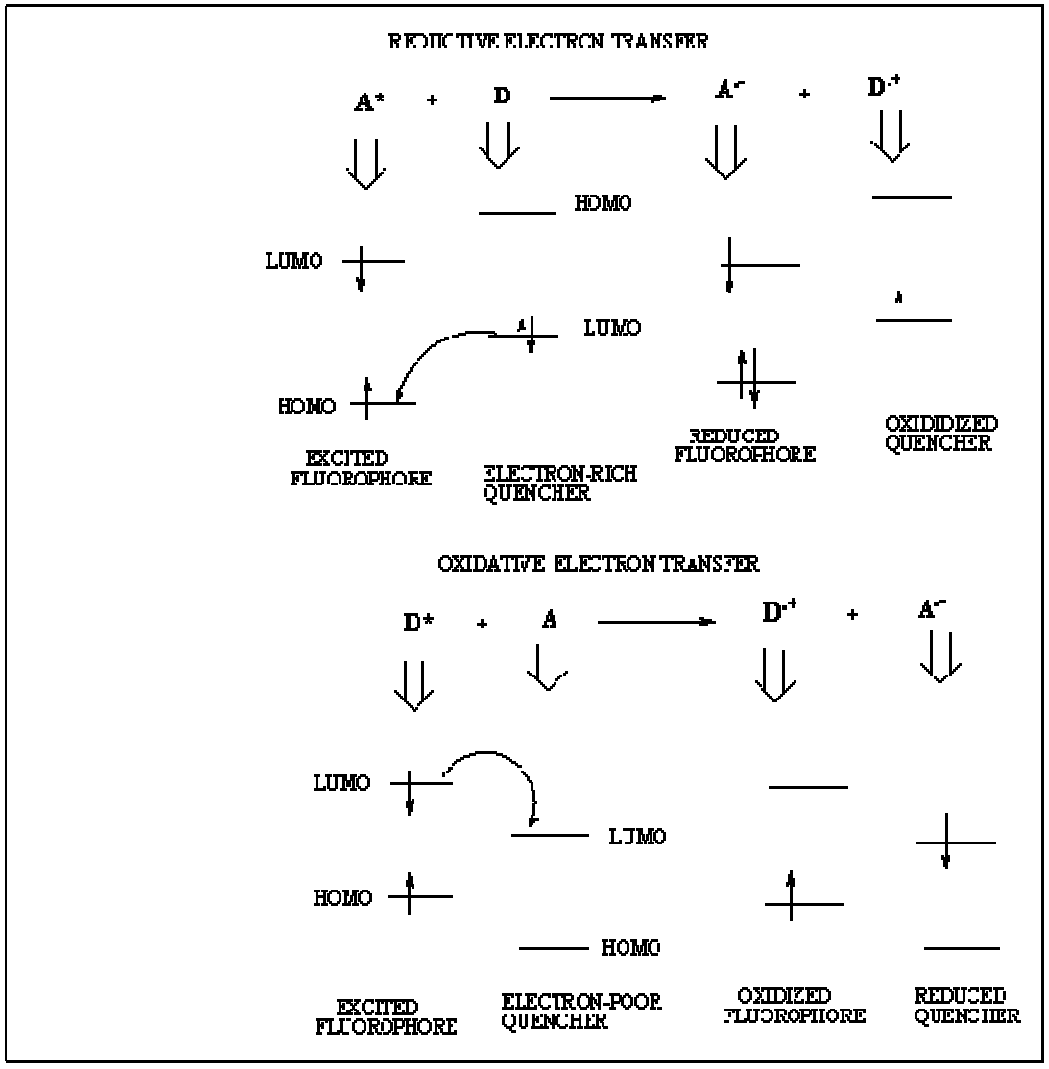

***Figure 1.6**. Reductive and Oxidative electron transfer [14].*

Electron transfer depends on the redox potentials of the donor (E_D^0) and acceptor (E_A^0) together with the excitation energy $E^{0\text{-}0}$ i.e. the difference in the energy between the lowest vibrational levels of the excited state and the ground state. The variations in standard free energy ΔG^0 for the above reactions can be expressed using the redox potentials E^0 and the excitation energy [14].

$$\Delta G^0 = E^0_{D.+/D^*} - E^0_{A/A^{\cdot-}} = E^0_{D.+/D} - E^0_{A/A^{\cdot-}} - \Delta E^{0\text{-}0}(D) \qquad \textit{Equation (1.1)}$$

$$\Delta G^0 = E^0_{D.+/D} - E^0_{A^*/A^{\cdot-}} = E^0_{D.+/D} - E^0_{A/A^{\cdot-}} - \Delta E^{0\text{-}0}(A) \qquad \textit{Equation (1.2)}$$

1.4 Photoinduced Energy Transfer

Non-radiative energy transfer of excitation energy requires some interaction between donor and acceptor molecules, and it can occur if there is overlap between the emission spectrum of the donor and absorption spectrum of the acceptor, so that energy of vibronic transitions in the donor is equal to those transitions in the acceptor. Such transitions are coupled i.e. are in resonance [26].

Energy transfer can result from different interaction mechanisms:

a) Coulombic interaction (Förster mechanism).

b) Intermolecular orbital overlap (Dexter mechanism).

The coulombic interactions consist of long-range dipole-dipole interactions (Förster mechanism). The exchange mechanism (Dexter's mechanism) requires intermolecular orbital overlap, which include electron exchange.

Exchange mechanism is operative only at short distances < 10 Å because it requires orbitals overlap of the molecules. In contrast, the columbic mechanism can still be effective at large distances (up to 80 -100 Å) [14].

Electron exchange mechanisms leading to collisional energy transfer are known as Dexter type. This requires bimolecular collision between the reactants can be visualised as an exchange of electrons taking place when there is simultaneous and favourable overlap of the approaching orbitals. Therefore, the range of effectiveness of these mechanisms is usually restricted to distances ≤ 10 Å. The diagram in Figure 1.7 depicts electron and energy transfer mechanisms [26].

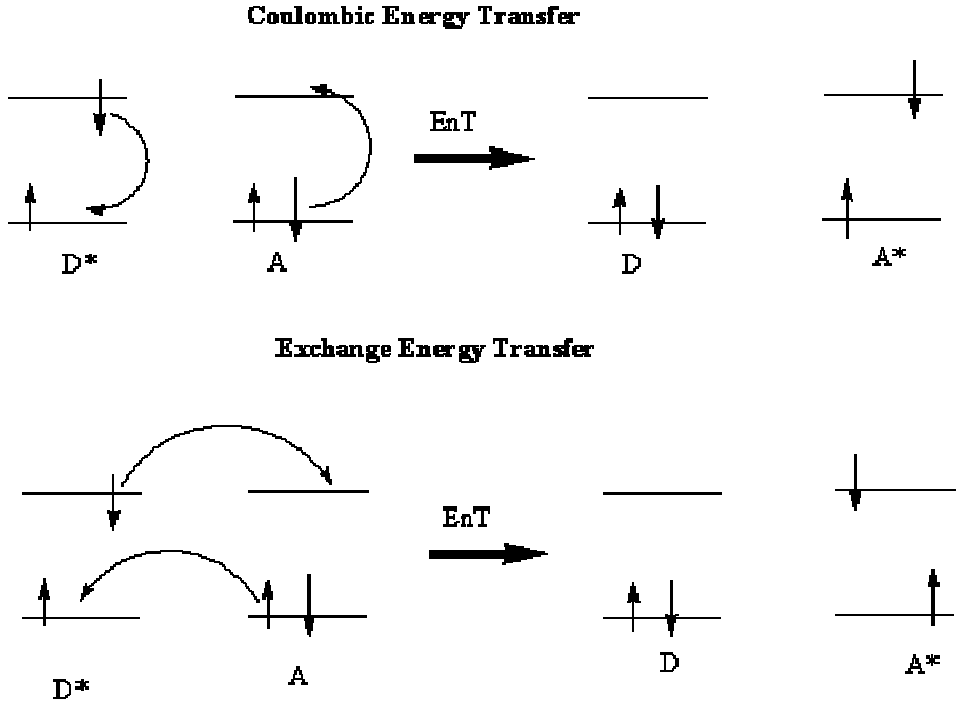

Figure 1.7. *Coulombic and exchange energy transfer [26].*

1.5 Mixed Ligand Ruthenium Polypyridyl Complexes.

There is an extensive literature on the synthesis, chemistry and physical properties of these compounds. The literature is extensive and no attempt will be made to discuss the properties of the many thousands of compounds that have been reported. Many reviews have been reported in the last number of years [27]. In this section an introduction will be given to the structures and properties of ruthenium polypyridyl complexes for which the photochemical processes have been studied in this thesis. Further information about the compounds studied will be given in the relevant chapters.

In this section the electronic and photophysical properties of the compounds of most important to this thesis will be discussed. These are compounds with ligands (L) such as pyridine- and pyrazine-triazoles (Figure 1.8) and polypyridyl complexes with general formula $[Ru(bpy)_2(L)]^{2+}$, where bpy is 2,2'-bipyridine and L is the chelating ligand, were the focus of many investigations. Most of these studies have initially focused on the complexes where L is a bis- chelating ligand possessing two identical coordination sites [27,28]. Of primary interest in this thesis are chelating systems containing asymmetric 1,2,4-triazole containing ligands (HL_1 –L_5 in Figure 1.8), in which the two coordination sites N2 and N4 of the triazole moiety are not equivalent.

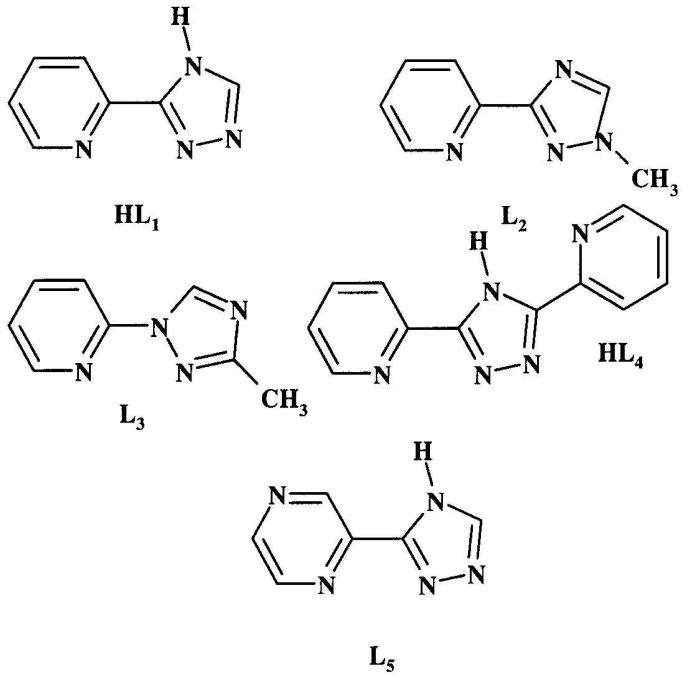

Figure 1.8. *Structure of some ligands that form the ruthenium complexes studied in this thesis [6[c]].*

The extent to which N2 and N4 are coordinated to the metal centre depends on the nature of the substituents on the triazole ring. For example in $[Ru(bpy)_2(\mathbf{L_1})]^+$ the unsymmetrical ligand $\mathbf{L_1}$ can either be bound via the N2 or N4 nitrogen atom of the triazoles unit, Figure 1.9 [16].

The photochemical behaviour of these complexes is affected by the protonation of the triazole ligand. When the triazole ligand is deprotonated the complex is photostable while for that protonated form is photolabile and undergoes photoinduced coordination isomerisation of the triazole ligand. It has been explained that the dissociative state ^{3}MC is populated upon irradiation of either N2 or N4 isomer. The photoproducts have been to be formed were a monodentate

intermediate where the HL1 is coordinated to the metal centre by pyridine ring, followed by rotation of the triazole ring [6[a,b],29].

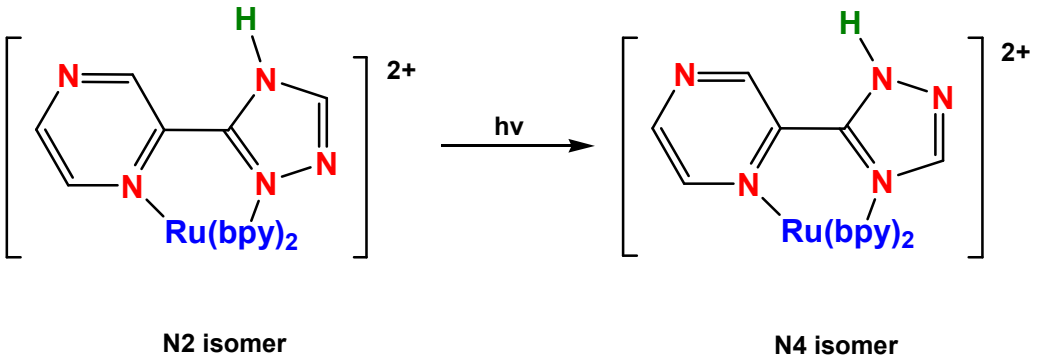

Figure 1.9 *Reversible photoinduced N2-N4 isomerisation of* $[Ru(bpy)_2(HL1)]^{2+}$ *[6].*

Another complex has been reported, $[Ru(bpy)(1Mepytr)]^{2+}$, Figure 1.10 [6]. In this complex when the ligand is methylated on N2 the N 4isomer is obtained as a single product. However, when the complex is directly methylated the N2 isomer can be obtained in high yield. It has been also observed that the N4 is photostable, while N2 isomer undergoes fast photoinduced isomerisation to N4 [29].

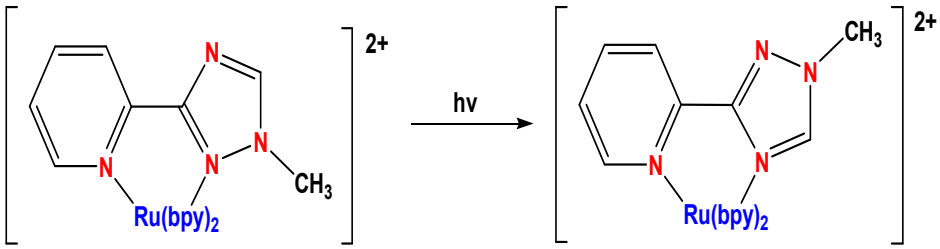

Figure 1.10 *Photo induced irreversible N2 to N4 isomerisation for* $[Ru(bpy)_2(1Mepytr)]^{2+}$.

Preparative photolysis followed by HPLC separation of the $[Ru(bpy)_2L_3]^{2+}$, in acetonitrile or in acetonitrile-containing LiCl , leads to the formation of two products in which the metal is coordinated in a monodentate fashion to the pyridyltriazole ligands. The following photoproducts were obtained, in pure acetontrile $[Ru(bpy)_2(L_3)(CH_3CN)]^{2+}$ and $[Ru(bpy)_2(L_3)Cl]^{+}$ in the presence of LiCl. When these photoproducts are further photolysed the reformation of the parent complex $[Ru(bpy)_2L_3]^{2+}$ was obtained.

The tiazolate moiety can also be used as a part of a bridging ligand to promote interaction between two metal centres in dinuclear species. This idea has been widely exploited to build supramolecular structures that have application in storage and energy conversion devices [12]. In supramolecular structures the perturbation of the photophysical properties occurs due to the electronic interaction between the individual units. The effect of perturbation depends on several factors such as the σ-donor/π-acceptor properties of the ligands and/or the identity of the metal centres. The perturbation may lead to intercomponent energy and electron transfer [27[c]].

The nature of the bridging ligands themselves plays a major role in controlling the photophysical properties of polynuclear complexes, In figure 1.9 the structures of the Hbpt, where Hbpt is (3,5-bis(pyridin-2-yl)-1,2,4-triazole, and Hbpzt, where Hbpzt is (3,5-bis(pyrazin-2-yl)-1,2,4-triazole) homonuclear complexes are shown. All shows strong interaction between the metal centres [16,30], these

dinuclear ruthenium triazole based compounds are discussed in Chapters 3 and 4 with respect to a range of photochemical experiments.

For mixed metal complexes photoinduced energy transfer is also observed in the mixed metal Ru-Os polypyridyl complexes through the bpt based bridging ligand (Figure 1.12)

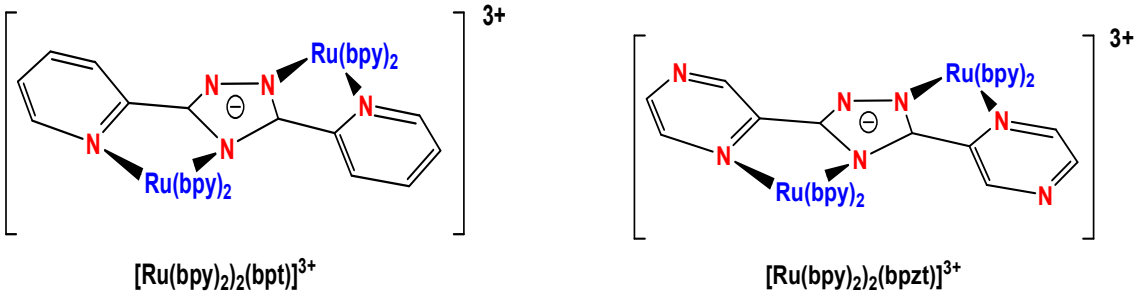

Figure 1.11 *Structures for Hbpt and Hbpzt dimers*

Structures for Hbpt and Hbpzt dinuclear compounds for these compounds only osmium based emission is observed [30[b],30[c]].

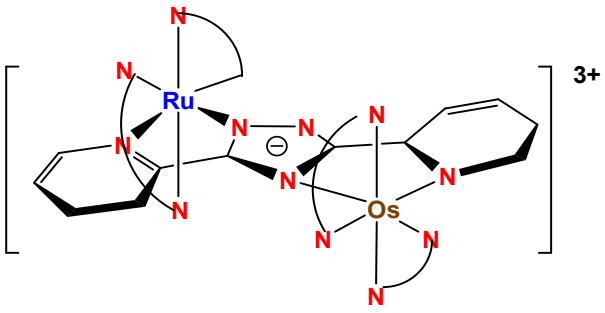

Figure 1.12*. Structure of dinuclear mixed-metal Ru:Os complex of the Hbpt bridging ligand.*

A number of other related dinuclear compounds have also been reported. Halpin *et al.* have reported a series of binuclear osmium and ruthenium [30[a]]. These complexes have been studied to investigate the extent of electronic communication between two metal centres as a function of the bridging ligand and the positioning of the two metal centers. The complexes under investigation were $[(bipy)_2Ru(qpy)Ru(bipy)_2]^{4+}$ **(1)**, $[(bipy)_2Os(qpy)Os(bipy)_2]^{4+}$ **(2)**, $[(bipy)_2Ru(pytr\text{-}bipy)Ru(bipy)_2]^{3+}$ **(3)**, $[(bipy)_2Ru(pytr\ bipy)Os(bipy)_2]^{3+}$ **(4)**, $[(bipy)_2Os(pytr\text{-}bipy)\text{-}Ru(bipy)_2]^{3+}$ **(5)** and $[(bipy)_2Os(bpbt)Os(bipy)_2]^{2+}$ **(6)** {bipy = 2,2-bipyridyl; qpy = 2,2`:5`,5``:2``,2```-quaterpyridyl; pytr-bipy = 3-(2,2`-bipyrid-6-yl)-5-(pyrid-2-yl)-1,2,4-triazolato, and bpbt = 5,5`-bis-(pyrid-2``-yl)-3,3`-bis-1,2,4-triazolato} (Figure 1.13).

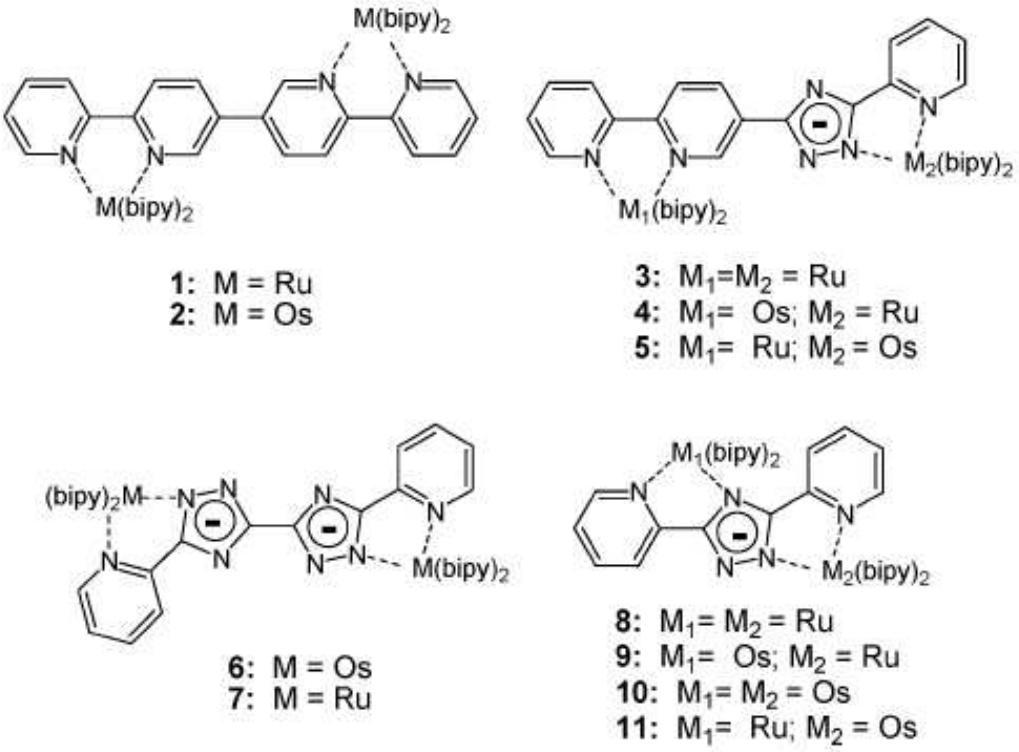

Figure 1.13 *Structures of related binuclear complexes [30[a]].*

$[(bipy)_2Ru(qpy)Ru(bipy)_2]^{4+}$ **(1)**, $[(bipy)_2Os(qpy)Os(bipy)_2]^{4+}$ **(2)**, $[(bipy)_2Ru(pytr\text{-}bipy)Ru(bipy)_2]^{3+}$ **(3)**, $[(bipy)_2Ru(pytr\ bipy)Os(bipy)_2]^{3+}$ **(4)**, $[(bipy)_2Os(pytr\text{-}bipy)\text{-}Ru(bipy)_2]^{3+}$ **(5)** and $[(bipy)_2Os(bpbt)Os(bipy)_2]^{2+}$ **(6)** {bipy = 2,2-bipyridyl; qpy = 2,2`:5`,5``:2``,2```-quaterpyridyl; pytr-bipy = 3-(2,2`-bipyrid-6-yl)-5-(pyrid-2-yl)-1,2,4-triazolato, and bpbt = 5,5`-bis-(pyrid-2``-yl)-3,3`-bis-1,2,4-triazolato} (Figure 1.13). $[(bipy)_2Ru(bpbt)Ru(bipy)_2]^{2+}$(**7**),$[(bipy)_2Ru(bpt)Ru(bipy)_2]^{3+}$(**8**),$[(bipy)_2Ru(bpt)Os(bipy)_2]^{3+}$(**9**),$[(bipy)_2Os(bpt)Os(bipy)_2]^{3+}$(**10**)and $[(bipy)_2Os(bpt)Ru(bipy)_2]^{3+}$ (**11**) (Figure 1.14).

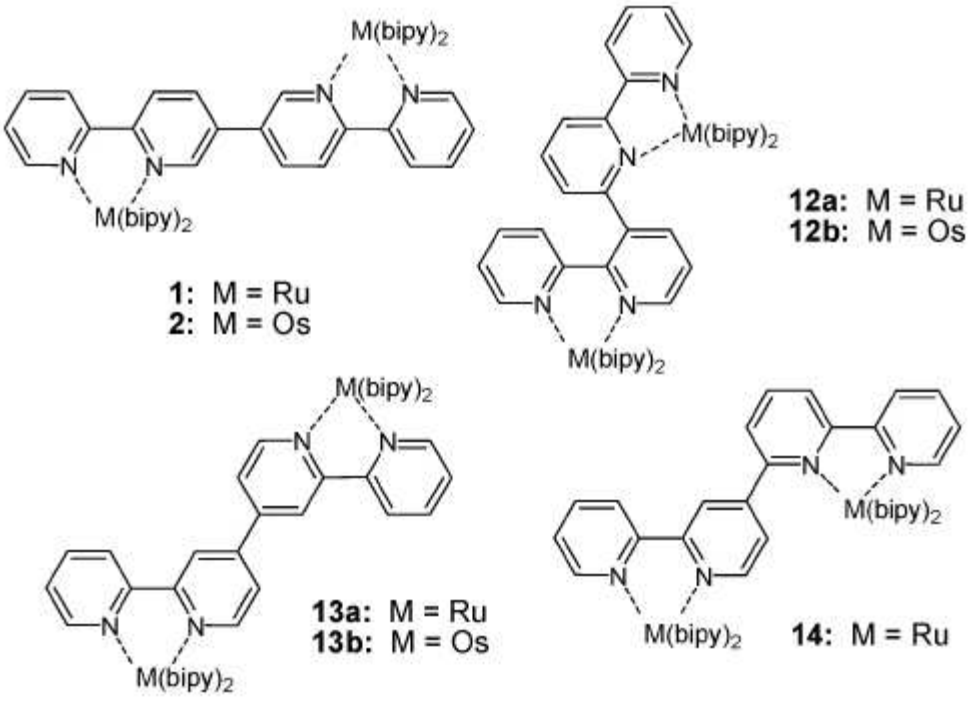

Figure 1.14 *Structures of quaterpyridyl bridged binuclear complexes* ***1***,***2***, $[(bipy)_2M_1(qpy_1)M_2(bipy)_2]^{4+}$ (***12***), $[(bipy)_2M(qpy_2)M(bipy)_2]^{4+}$ (***13***) and $[(bipy)_2M(qpy_3)M(bipy)_2]^{4+}$ (***14***) [30[a]].

All compounds emit at room temperature, however the location of the emitting state in the compounds is at this moment less clear. For compounds 8 and 9 emission is most likely based on the osmium centre. This suggests that the electronic coupling between the metal centres is considerable. For the compounds **6** and **7** the emission is not likely to be located on the triazole based bridging ligand but on the bpy groups this is in agreement with results obtained for compounds **6-11** in Figure 1.13. For compounds **1** and **2** the emission is based on the bridging ligands, based on the electrochemical data obtained. This observation is in agreement with the emission results obtained for the qpy compounds shown in Figure 1.14. However for the "mixed" bpy-pytr bridged complexes the situation is less clear. Further detailed studies are needed to fully understand the photophysical properties of these compounds.

The oxidation potential of the metal centres in quaterpyridyl bridged species **1** and **2** has a weak dependence on the type of quaterpyridyl isomer that bridges the two metal centres, (See Figures 1.14) and first oxidation does not provide evidence for electronic communication between the metal centres of these compounds. Only in **4** and **6** (See Figure 1.13) the electron transfer Ru(II)-[pytr-bipy]-Os(III) → Ru(III)-[pytr-bipy]-Os(II) mediated by bridging ligand is possible because of the larger electron-withdrawing strength of the binding moiety (bipy) that is coordinated by the oxidized metal centre (Os). This implies a HOMO (of the bridging ligand) mediated superexchange mechanism where the energy differences between the HOMOs of the binding sites and the gap between these and the energy levels of

the coordinating metals are the critical parameters [30[a]]. In the case of complexes **6** and **7** differing only in the nature of the metal centres, the weaker intermetallic interaction of osmium complex **6** in comparison to the analogous ruthenium complex **7**, is due to the larger gap between the energy of the metal orbitals of Os with respect to Ru, and the HOMO of the binding unit of the ligand.

1.6 Stereochemistry in Mono- and Poly-Nuclear Complexes

Mononuclear complexes like those of Ru(II) with an hexa-coordinating central metal and octahedral geometry of coordination, present stereoisomerism if the metal coordinates more than one type of ligand. In the simplest case of two distinct mono-dentate ligands, isomeric complexes are formed when identical ligands are in number of two or more. This is a consequence of the six-coordination feature of the central metal, which does not allow more than one spatial distribution for the ligands in octahedral complexes with formula $M(L')(L'')_5$. On the other hand, when the complexes present general formulas $M(L')_2(L'')_4$ and $M(L')_3(L'')_3$ two couples of stereoisomers [*cis* / *trans* in $M(L')_2(L'')_4$, and *fac* / *mer* in $M(L')_3(L'')_3$] are possible (Figure 1.15).

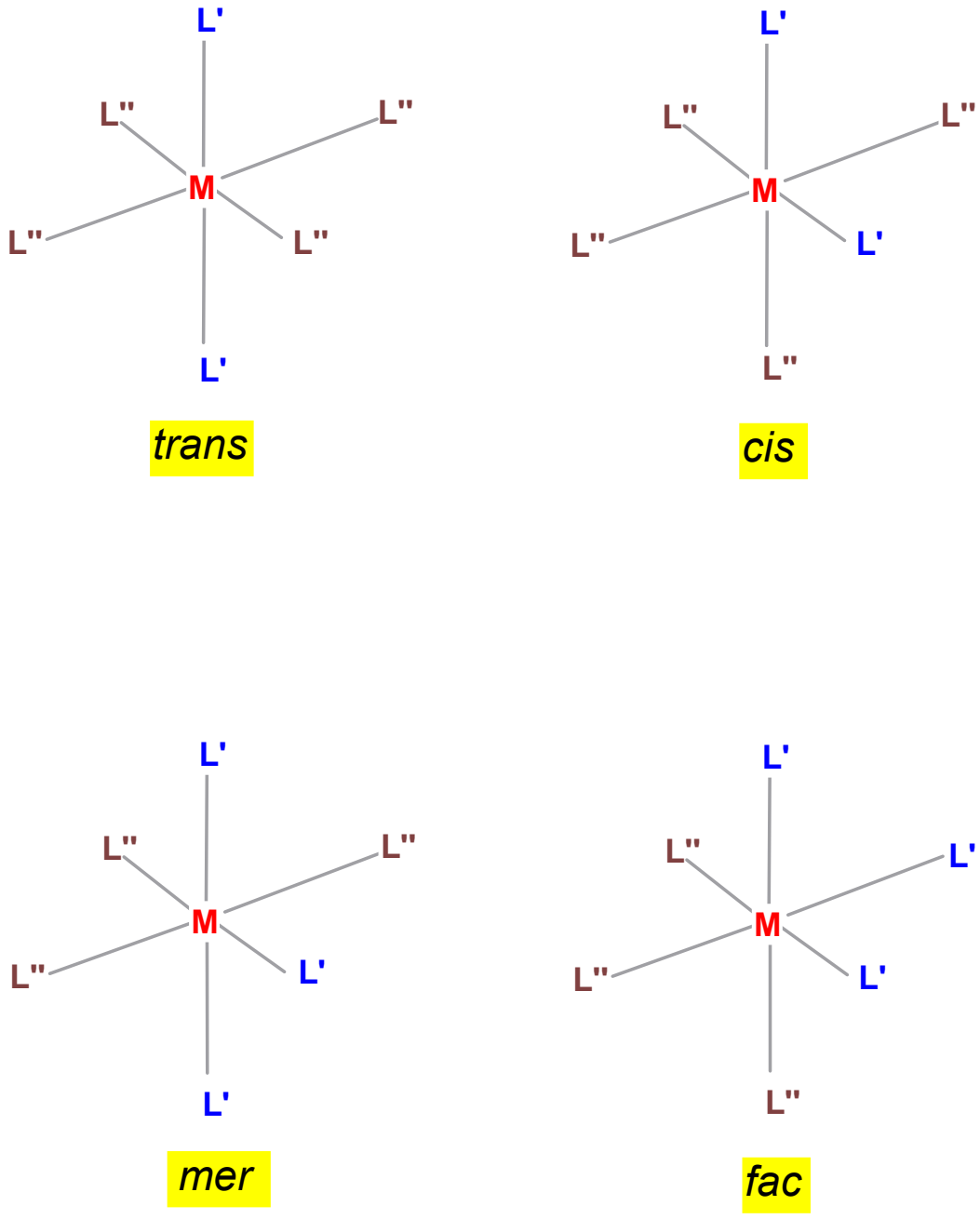

Figure 1.15. *Possible steroisomers in monometallic octahedral complexes with monodentate ligands.*

If the hexavalent metal coordinates bidentate ligands, the resulting octahedral complexes form stereoisomers that differ for the relative orientation of the ligands with respect to the central metal. The simplest case is represented by complexes

of the type $M(L'''')_3$ with three identical bidentate ligands L'''', which present one pair of enantiomers denominated Δ and Λ (Figure 1.16). $[Ru(bpy)_3]^{2+}$ constitutes the prototype of the octahedral complexes of ruthenium within this category.

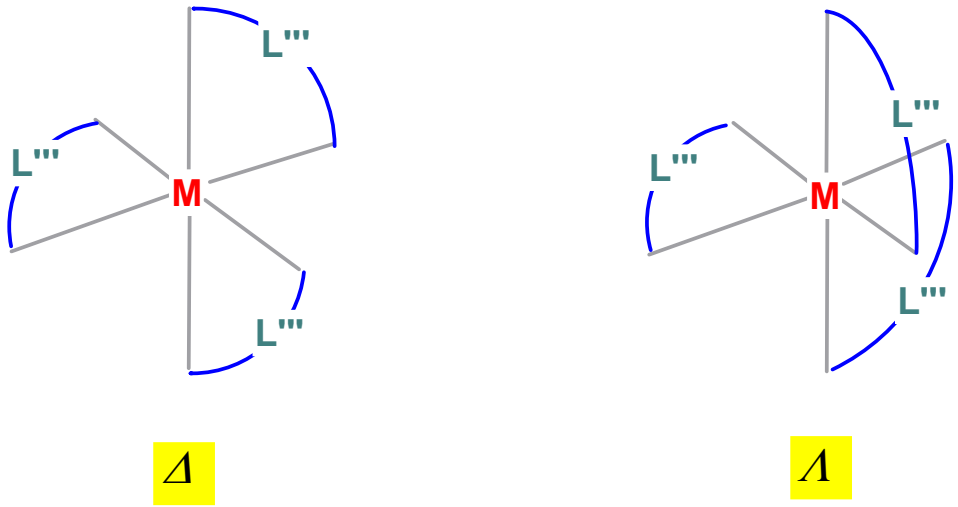

Figure 1.16. *Possible steroisomers in monometallic octahedral complexes with identical bidentate ligands.*

Mononuclear octahedral complexes containing tri-dentate ligands like $[Ru(tpy)_2]^{2+}$ that have generic complex formula: $M(L^{IV})_2$, where L^{IV} is a tridentate ligand, do not present isomers.

The increase of the number of coordinating centres in poly-nuclear complexes is generally accompanied by the increase of the number of possible stereoisomers, the extent of which is directly related to the nature of the various ligands. The stereochemical factor bears quite considerable importance since the spatial

distribution of the ligands can influence the nature of intramolecular electron and energy transfer processes within the complexes.

In the following analysis of the stereochemistry of poly-nuclear complexes the two cases of dinuclear homometallic compounds with symmetrical (BL_{sym}) and unsymmetrical bridging ligand (BL_{uns}) will be considered taking into account the octahedral geometry of coordination for both metal centres. Within these two main groups of complexes, bi-dentate bpy constitutes the peripheral (non-bridging) ligand completing the coordination shell of the two equivalent metal centres [generic formula: $(bpy)_2M(BL)M(bpy)_2$].

Binuclear complexes with symmetrical bridging ligands of the type $(bpy)_2M(BL_{sym})M(bpy)_2$ (complexes **1**, **2**, **6** and **7** in Figure 1.13) form three distinct diastereoisomers Δ/Λ, Δ/Δ and Λ/Λ the latter two of which constitute a pair of enantiomers (Figure 1.17).

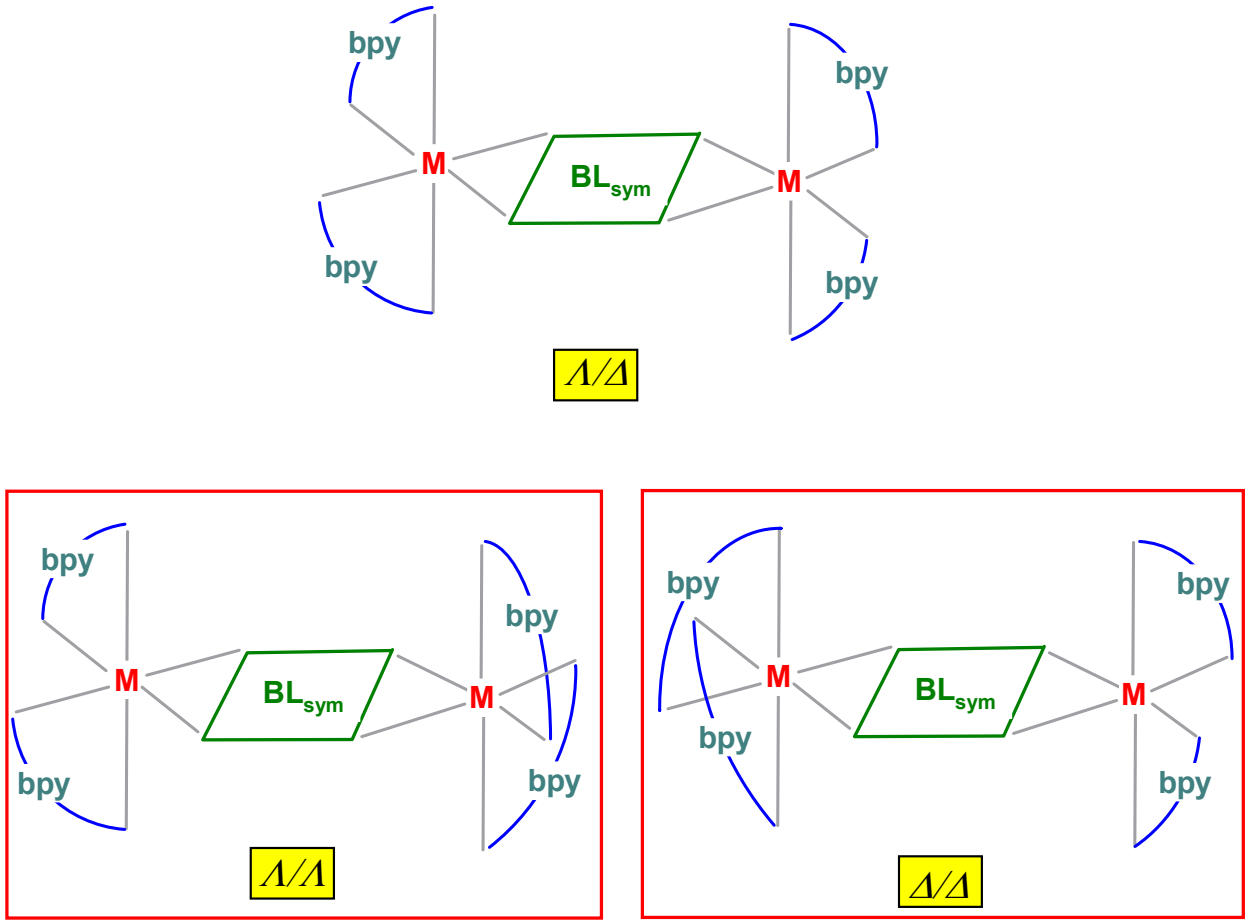

Figure 1.17. *Diasteroisomers of bimetallic complexes with identical peripheral bidentate ligands and symmetrical bridging ligand. Coordination geometry of the metals is octahedral. The pair of enantiomers is framed in red squares.*

Binuclear complexes with unsymmetrical bridging ligands of the type $(bpy)_2M(BL_{uns})M(bpy)_2$ (complexes **3**, **8** and **10** in Figure 1.13) form four distinct diastereoisomers (*Δ*/*Λ*, *Λ*/*Δ*, *Δ*/*Δ* and *Λ*/*Λ*, Figure 1.18). Different to bimetallic complexes of the type $(bpy)_2M(BL_{sym})M(bpy)_2$ the systems with unsymmetrical coordination of the bridging ligand, e.g. $(bpy)_2Ru(bpt)Ru(bpy)_2$ or $(bpy)_2Ru(bpzt)Ru(bpy)_2$, do not generate enantiomeric pairs. In case of

$(bpy)_2Ru(bpt)Ru(bpy)_2$ the separation and identification of all four different isomers was made possible through a combination of HPLC, ^{1}H-NMR, circular dichroism and UV-vis spectroscopy [30,31].

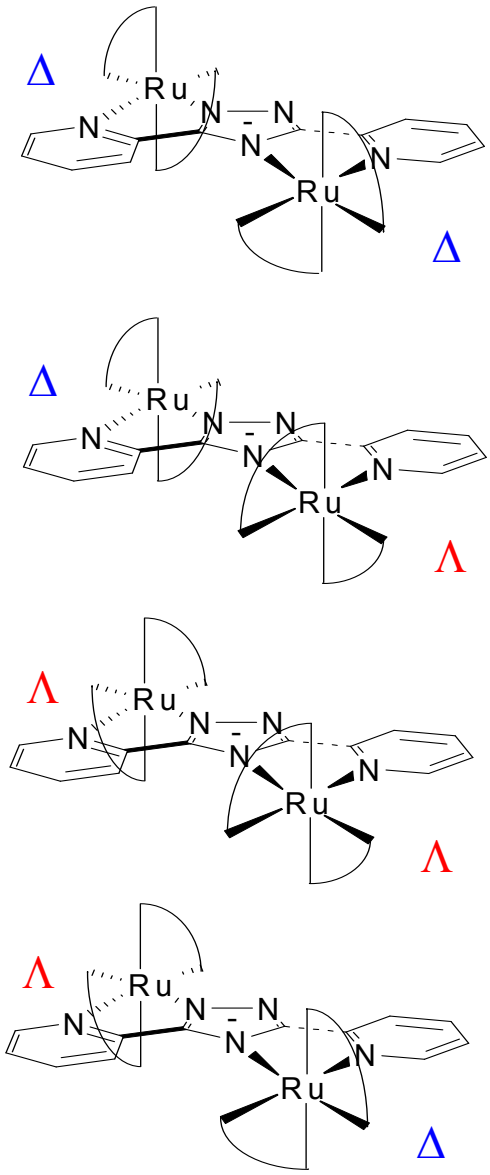

Figure 1.18. *Possible four diasteroisomers of ruthenium complex* ***8*** *(see Fig. 1.16), which constitutes an example of bimetallic complex with identical peripheral bidentate ligands (bpy) and the unsymmetrical bridging ligand bpt. Coordination geometry of the metal centres is octahedral.*

1.7 Aim of the Thesis

The use of high performance liquid chromatography (HPLC) for the monitoring of tris(2,2'-bipyridyl)ruthenium $[Ru(bpy)_3]^{2+}$ reactions has been introduced for the first time by Valently and Behnken in the late seventies [30[l]], using optical absorption at 280 nm as parameter of detection. The high sensitivity of the proposed method and the capability of separating species with very similar structures (either isomers or not) made feasible the identification of the products obtained during the photochemical reaction of a complex of the type $[Ru(bpy)_2(X)]^{n+}$ about ten years later [30[c]]. Thanks to the development of an HPLC method based on a cation exchange column [30[d]]. Semipreparative HPLC proved to be valid also in the separation and identification of isomers in case of ruthenium complexes with asymmetrical ligands like 3-(pyridin-2'-yl)-1,2,4-triazole[30[d,e]], 1-methyl-3-(pyridin-2'-yl)-1,2,4-triazole or 2-(4'*H*-[1,2,4]triazol-3'yl)pyrazine [31], and for the separation of isomers deriving from dimeric ruthenium complexes with tetradentate ligands like 3,5-bis(pyridin-2'-yl)-1,2,4-triazole [30[f]] or 3,5-bis(pyrazin-2'-yl)-1,2,4-triazole [30[d,e]]; Other multinuclear ruthenium complexes that were characterized by means of cation exchange HPLC included 2-phenyl-pyridine [30[f]], and 2,5-bis(5'-methyl-4'H-[1,2,4]triaz-3'-yl)-pyrazine [30] as additional ligands. The use of such a technique has been extended to the separation of bipyridine complexes with metals other than ruthenium, e.g. iron and nickel [30[g]], thus proving its general validity for the purification and characterization of metal complexes with bipyridyl-based ligands.

Besides separation, HPLC has been also employed for the identification of the products of photolysis that were obtained upon irradiation of polypyridyl complexes [30, 31]. In particular, HPLC study of the photoreactions involving the dinuclear complex $[Ru(bpy)_2(bpt)Ru(phen)_2](PF_6)_3$ (bpt = 3,5-bis-(pyridin-2'-yl)-1,2,4-triazole; phen = 1,10-phehanthroline) and its isomer $[Ru(phen)_2(bpt)Ru(bpy)_2](PF_6)_3$, has allowed the identification of the fragmentation products $Ru(bpy)_2^{2+}$, $Ru(phen)_2^{2+}$ and $Ru(bpt)^+$ [30[k]], whereas in case of $[Ru(bpy)_2(tbmbpy)]Cl_2$ irradiation {tbmbpy = *trans*-1,2-bis[4-(4'-methyl)-2,2'-bipyridyl] ethane}, HPLC verified the occurrence of a light-driven dimerization process [32].

In this thesis we report on the use of HPLC for the analysis of the photoreaction products obtained upon irradiation of the binuclear complexes of ruthenium $\{[Ru(bpy)_2]_2L\}^{3+}$ with L = bpt [30] and bpzt [bpzt = 3,5-bis-(pyrazin-2'-yl)-1,2,4-triazole] [30]. (Figure 1.19)

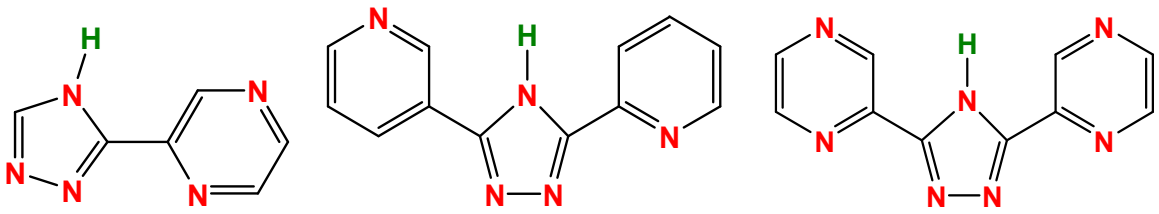

Figure 1.19 *Structural formula for pyrazin-2-yl-1,2,4-triazole (Hpztr), bpt, and bpzt [bpzt = 3,5-bis-(pyrazin-2'-yl)-1,2,4-triazole].*

The interest in the photochemistry of such binuclear systems relies on their possibility of having *intramolecular* transfer of excitation and/or charge between the metal centres [6[b,c]] upon irradiation at the frequencies of metal-to-ligand charge

transfer (MLCT) transitions. In this framework $\{[Ru(bpy)_2]_2L\}^{3+}$ complexes can be considered as supramolecular systems the metal centres of which display different functions in photoactivated processes [32]. The main goal of the present work is to describe the general properties of separation and characterization of the linkage isomers of $\{[Ru(bpy)_2]_2bpt\}^{3+}$ and $\{[Ru(bpy)_2]_2bpzt\}^{3+}$ by ion cation exchange chromatography in semipreparative HPLC using Partisil SCX column and the mixture acetonitrile/water with $LiClO_4$ or LiCl or KNO_3 salts as mobile phase. Complexes $\{[Ru(bpy)_2]_2bpt\}^{3+}$ and $\{[Ru(bpy)_2]_2bpzt\}^{3+}$ have been characterized with ^{1}H-NMR spectroscopy, and their photophysical properties have been determined in acetonitrile at 298 and 77 K.

The aim of this thesis is to investigate the application of high performance liquid chromatography (HPLC) as technique for the investigation of photoinduced processes in a range of mononuclear and dinuclear ruthenium complexes. In Chapter 3 the photochemical behaviour of the homo and heterochiral isomers of the ruthenium dinuclear complex of the ligand (3,5-bis(pyridin-2-yl)-1,2,4-triazole (Hbpt) is investigated while the complexes $[(bpy)_2Ru(bpt)Ru(bpy)_2]^{3+}$ [30] compound is reported. In chapter 4 of the photochemical behaviour of the corresponding pyrazine triazole ligand Hbpzt (3,5-bis(pyrazin-2-yl)-1,2,4-triazole) are discussed in Chapter 4. In Chapter 5 the photochemical behaviour of the N2 and the N4 isomers of the mononuclear ruthenium complex of the ligand 2-pyrazin-2-yl-1,2,4-triazole (Hpztr) (See Figure 1.8 L5) are investigated. Finally in chapter 6 the photochemical behaviour of the compound $[(tbbpy)_2\,Ru\,(tpphz)\,PdCl_2](PF_6)_2$

where, tpphz = tetrapyridol [3,2-a:2`,3`c:3``,2``,h:2```,3```-j] phenazine) and tbbpy = 4,4`-di-tert-butyl-2,2`-bipyridine, which has shown potential as a photocatalyst for the production of hydrogen from water, is investigated [32]. A general discussion of the results obtained and suggested further studies are presented in Chapter 7.

.

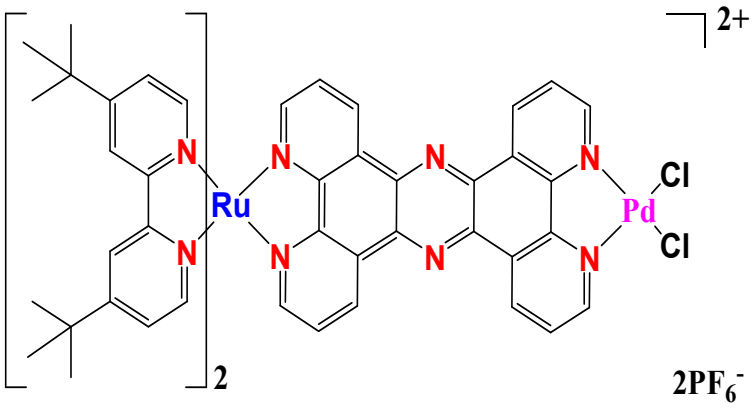

Figure 1.20. *Structural formula for* $[(tbbpy)_2Ru(tpphz)PdCl_2](PF_6)_2$.

References:

[1] J. P. Paris, W.W. Brandt *J. Am. Chem. Soc*. **1959**, *81*, 5001.

[2] V.Balzani, L. Moggi, M.F. Manfrin, F. Bolletta, M. Gleria *Science* **1975**, 189, 852.

[3] R. Ziessel, J. Hawecker, J.M. Lehn *Helv. Chim. Acta* **1986**, 69, 1065.

[4] (a) K. Kalyanasundaram *Coord. Chem. Rev*. **1982**, *46*, 159; (b) A. Juris, V. Balzani, F. Barigelletti, S. Campagna, P. Belser, A. Von Zelewski *Coord. Chem. Rev.* **1988**, 84, 85; (c) V. Balzani, F. Barigelletti, L. De Cola *Top. Curr. Chem.* **1990**, *158*, 31; (d) V. Balzani, A. Juris, M. Venturi, S. Campagna, S. Serroni *Chem. Rev.* **1996**, *96*, 759; (e) S. Campagna, F. Puntoriero, F Nastasi, G. Bergamini, V. Balzani *Top. Curr. Chem.* **2007**, *280*, 117.

[5] (a) B. O'Regan, M. Graetzel *Nature* **1991**, *353*, 737; (b) M.K. Nazeeruddin, S.M. Zakeeruddin, J.J. Lagref, P. Liska, P. Comte, C. Barolo, G. Viscardi, K. Schenk, M. Graetzel *Coord. Chem. Rev.*, **2004**, *248*, 1317; (c) D. Huang, C. Klein, S. Ito, J.E. Moser, R. Humphry-Baker, N. Evans, F. Duriaux, C. Graetzel, S.M. Zakeeruddin, M. Graetzel *Adv. Mat.*, **2007**, *19*, 1133; (d) F. Gao, Y. Wang, D. Shi, J. Zhang, M. Wang, X. Jing, R. Humphry-Baker, P. Wang, S.M. Zakeeruddin, M. Graetzel *J. Am. Chem. Soc.* **2008**, *130*, 10720.

[6] (a) J.G. Vos, M.T. Pryce *Coord. Chem. Rev.* **2010**, *254*, 2519. (b) J.G. Vos and J.M. Kelly, *Dalton Trans*. **2006**, 4869. (c) S.Fanni, T.E. Keyes, C.M. O'Connor, H. Hughes, R. Wang and J.G. Vos. *Coord. Chem. Rev*. **2000** 208, 77.

[7] (a) A.F. Martin, T.A. Nieman *Biosens. Bioelectron.* **1997**, *12*, 479; (b) J.G. Lee, K. Yun, G.S. Lim, S.E. Lee, S. Kim, J.K. Park *Bioelectrochem.* **2007**, 70, 228; (c) H.N. Choi, S.H. Yoon, Y.K. Lyu, W.Y. Lee *Electroanalysis* **2007**, *19*, 459; (d)Y. Li, H. Qi, Y. Peng, Q. Gao, C. Zhang *Electrochem. Comm.***2008**, *10*, 1322.

[8] (a) T.A. Ruda-Eberenz, A. Nagy, W.J. Waldman, P.K. Dutta *Langmuir* **2008**, *24*, 9140; (b) B. Sun, H. Qi, F. Ma, Q. Gao, C. Zhang, W. Miao *Anal. Chem.***2010**, *82*, 5046.

[9] (a) S. Welter, F. Lafolet, E. Cecchetto, F. Vergeer, L. De Cola *ChemPhysChem* **2005**, *6*, 2417; (b) W. Kaim, G.K. Lahiri *Angew. Chem. Int. Ed.* **2007**, *46*, 1778; (c) K. Seo, A.V. Konchenko, J. Lee, G.S. Bang, H. Lee *J. Am. Chem. Soc.* **2008**, *130*, 2553; (d) L. Mercs, A. Neels, M. Albrecht *Dalton Trans.* **2008**, 5570.

[10] (a) B.J. Coe, J.A. Harris, I. Asselberghs, a. Persoons, J.C. Jeffery, L.H. Rees, T. Gelbrich, M.B. Hursthouse *J. Chem. Soc. Dalton Trans.* **1999**, 3617; (b) B.J. Coe, J.L. Harries, M. Helliwell, L.A. Jones, I. Asselberghs, K. Clays, B.S. Brunschwig, J.A. Harris, J. Garin, J. Orduna *J. Am. Chem. Soc.* **2006**, *128*, 12192.
[11] G. Will, G. Boschloo, S. Nagaraja Rao, D. Fitzmaurice *J. Phys. Chem. B* **1999**, *103*, 8067.

[12] (a) J.M. Lehn *Angew. Chem. Int. Ed.* **1988**, *27*, 89; (b) S. Campagna, A. Giannetto, S. Serroni, G. Denti, S. Trusso, F. Mallamace, N. Micali *J. Am. Chem. Soc.* **1995**, *117*, 1754; (c) E.C. Constable *Chem. Comm.* **1997**, 1073; (d) M. Ruben, J. Rojo, F.J. Romero-Salguero, L.H. Uppadine, J.M. Lehn *Angew. Chem. Int. Ed.* **2004**, *43*, 3644; (e) J.M. Lehn "Supramolecular Chemistry" Wiley-VCH, Weinheim, Germany, **1995**; (f) L. Cassidy, S. Horn, L. Cleary, Y. Halpin, W.R. Browne, J.G. Vos *Dalton Trans.* **2009**, 3923; (g) Balzani, *V. Ed.,* "Supramolecular Photochemistry" Reidel, Dordrecht, **1997**; (h) A. K .D. Mesmacker, J.P. Lecomte, J.M. Kelly, *Top. Curr. Chem.*, **1996**, *177,* 25.

[13] http://publications.uu.se/theses/abstract.xsql?dbid=1468

[14] B. Valeur, *Molecular Fluorescence*, Wiley-VCH, New York, **2002**.

[15] G. A. Crosby, Acc. Chem. Res. **1975**, 8, 231.

[16] (a) J.P. Sauvage, J.P. Collin, J.C. Chambron, S. Guillerez, C. Coudret *Chem. Rev.* **1994**, *94*, 993; (b) R. Hage, J.H. Van Diemen, G. Ehrlich, J.G. Haasnoot, D.J. Stufkens, T.L. Snoeck, J.G. Vos, J. Reedijk *Inorg. Chem.***1990**, *29*, 988; (c) B.E. Buchanan, R. Wang, J.G. Vos, R. Hage, J.G. Haasnot, J. Reedijk *Inorg. Chem.* **1990**, *29*, 3263; (d) R. Wang, J.G. Vos, R.H. Schmehl, R. Hage *J. Am. Chem. Soc.* **1992**, *114*, 1964; (e) S.M. Draper, D.J. Gregg, E.R. Schofield, W.R. Browne, M. Duati, J.G. Vos, P. Passaniti *J. Am. Chem. Soc.* **2004**, *126*, 8694.

[17] (a) M. Maestri, N. Armaroli, V. Balzani, E. C. Constable, A. M. W. Cargill Thompson *Inorg Chem*. **1995**, *34*, 2759; (b) G.L. Herzberg *Molecular Spectra and Molecular Structure III. Electronic Spectra and Electronic Structure of Polyatomic Molecules*, ed. Van Nostrand, New York, pp. **1966.** 142,; (c) E. J. Heller, R. L. Sundberg, D. Tannor *J. Chem. Phys*. **1982**, *86*, 1882; (d) A. B. Myers, K.S. Pranata *J. Phys. Chem.* **1989**, *93*, 5079.

[18] N.H. Damrauer, G. Cerullo, A. Yeh; T. R. Boussie; C.V. Shank, J. K. McCusker *Science* **1997**, *275*, 54.

[19] E. M. Kober, T. Meyer. *Inorg. Chem.* **1984**, *23*, 3877.

[20] (a) J.N. Demas, D. G. Taylor *Inorg. Chem.* **1979**, *18*, 3177; (b) J. N. Demas; G. A. Crosby *J. Am. Chem. Soc*. **1971**, *93*, 2841.

[21] (a) B.P. Sullivan, T. J. Meyer, *Inorg. Chem.* **1982**, 21, 1037 (b) B. Durham, J.V. Caspar, J.K Nagle, T.J. Meyer, *J. Am. Chem. Soc.* **1982**, 104, 4803 (c) B. Durham, J.L.Walsh, C.L. Carter, T.J. Meyer, *Inorg. Chem.* **1980**, 19, 860.

[22] S. Tachiyashiki , H. Ikezawa, K. Mizuhiko, *Inorg. Chem.* **1994**, 33, 623.

[23] D.M. Roundhill. *Photochemistry and Photophysics of Metal Complexes*; Plenum Press: New York, **1994**.

[24] http://etd.caltech.edu/etd/available/etd-05302003-172047/unrestricted/ardunn_ch1.pdf

[25] (a) I. Villa, F. Sanchez, T. Lopes, P. Lopez-Cornejo, P. Perez-Tejeda *J. Phys. Chem. A* **2010**, *30*, 7912; (b) M. Ogawa, B. Balan, G. Ajayakumar, S. Masaoka, H.B. Kraatz, M. Muramatsu, S. Ito, Y. Nagasawa, H. Miyasaka, K. Sakai *Dalton Trans.* **2010**, 4421; (c) R.J. Kumar, S. Karlsson, D. Streich, A. Rolandini-Jensen, M. Jaeger, H.C. Becker, J. Bergquist, O. Johansson, L. Hammarstroem *Chem. Eur.J.* **2010**, *16*, 2830; (d) H.A. Meylemans, N.H. Damrauer *Inorg. Chem.* **2009**, *48*, 11161.

[26] J.R. Lakowicz, *Principles of Fluorescence Spectroscopy*; Kluwer Academic/Plenum: New York, **1999**.

[27] (a)K. Kalyanasundaram, '*Photochemistry of Polypyridine and Porphyrin Complexes'*; Academic Press,; London, **1992**; (b) D. M.Roundhill,; *Photochemistry and Photophysics of Metal Complexes*; Plenum: New York, **1994**; p 165-215; (c) V. Balzani, F. Scandola, *Supramolecular Photochemistry*; Ellis Horwood: Chichester, **1991**; (d) S. Rau, D. Walther and J. G. Vos, *Dalton Trans.*, **2007**, 915; V. Balzani, A. Juris, M. Venturi, S. Campagna and S. Serroni, *Chem. Rev.*, 1996, **96**, 759; (e) J. G. Vos and J. M. Kelly, *Dalton Trans.*, **2006**, 4869.

[28] (a) A.J. Downard, G.E. Honey, L.F. Phillips, P.J. Steel *Inorg. Chem.***1991**, *30*, 2259; (b) P. Rillema, K.B. Mack *Inorg. Chem.* **1982**, *21*, 3849.

[29] (a) A.F. Martin, T.A. Nieman *Biosens. Bioelectron.* **1997**, *12*, 479; (b) J.G. Lee, K. Yun, G.S. Lim, S.E. Lee, S. Kim, J.K. Park *Bioelectrochem.* **2007**, 70, 228; (c) H.N. Choi, S.H. Yoon, Y.K. Lyu, W.Y. Lee *Electroanalysis* **2007**, *19*, 459; (d)Y. Li, H. Qi, Y. Peng, Q. Gao, C. Zhang *Electrochem. Comm.* **2008**, *10*, 1322.

[30] Y. Halpin, L. Cleary, L. Cassidy, S. Horne, D. Dini, W. R. Browne, and J. G. Vos, *Dalton Trans*. **2009**, 4146. (b) H.P. Hughes and J.G. Vos *Inorg. Chem*., **1995**, *34*, 4001. (c) H.P. Hughes, D. Martin, S. Bell, J.J. McGarvey and J.G. Vos. *Inorg. Chem.,* **1993**, *32*, 4402. (d) R. Hage, J.G. Haasnoot, J. Reedijk, R. Wang, and J.G. Vos. *Inorg. Chem*., **1991**, *30*, 3263. (e) L. De Cola, F. Barigelletti, V. Balzani, R. Hage J.G. Haasnoot, J. Reedijk, and J.G. Vos. *Chem. Phys. Letters*. **1991**, *178,* 491. (f) R. Hage, J.G. Haasnoot, H.A. Nieuwenhuis, J. Reedijk, D.J.A. De Ridder and J.G. Vos. *J. Am. Chem. Soc.,* **1990**, *112*, 9245. (g) F. Barigelletti, L. De Cola, V. Balzani, R. Hage, J.G. Haasnoot, J. Reedijk, and J.G. Vos. *Inorg. Chem*. **1991**, *30,* 641. (h) F. Barigelletti, L. De Cola, V. Balzani, R. Hage, J.G. Haasnoot, J. Reedijk, and J.G. Vos. *Inorg. Chem.,* **1989**, *28*, 4344. (i) R. Hage, J.G. Haasnoot, D.J. Stufkens, T.L. Snoeck, J.G. Vos and J. Reedijk. *Inorg. Chem*., **1989**, *28*, 1413. (j) R. Hage, A.H.J. Dijkhuis, J.G. Haasnoot, R. Prins, J. Reedijk, B.E. Buchanan and J.G. Vos. *Inorg. Chem*. **1988**, *27*, 2185. (k) R. Hage, R. Prins, J.G. Haasnoot, J. Reedijk, and J.G. Vos. *J. Chem. Soc., Dalton Trans*., **1987**, 1389. (l) S.J. Valently, P.E. Behnken, *Anal. Chem.* **1978**, *50*, 834.

[31] W. R. Browne, D. Hesek J. F. Gallagher, C. M. O'Connor, J. S. Killeen, F. Aoki, H Ishida. Y. Inoue, C. Villani.J. G. Vos, *Dalton Trans*. **2003,** 2597.

[32] (a) S. Rau, B. Schaefer, D. Gleich, E. Anders, M. Rudolph, M. Friedrich, H. Goerls, W. Henry, J.G. Vos, *Angew. Chem. Int. Ed.* **2006**, *45*, 6215; (b) B. Gholamkhass, H. Hiroaki Mametsuka, K. Koike, T. Tanabe, M. Furue, O. Ishitani, *Inorg. Chem.* **2005**, *44*, 2326; (c) S. Sato, K. Koike, H. Inoue, O. Ishitani, *Photochem. Photobiol. Sci.* **2007**, *6*, 454.

CHAPTER 2

Experimental and Optimisation of Conditions of the Various Methods of Characterisation a setup of HPLC

2.1 Introduction

The use of high performance liquid chromatography (HPLC) for the monitoring of tris(2,2'-bipyridyl)ruthenium $[Ru(bpy)_3]^{2+}$ reactions has been introduced for the first time by Valently and Behnken in the late seventies [1], using optical absorption at 280 nm as parameter of detection. The high sensitivity of the proposed method and the capability of separating species with very similar structures (either isomers or not) made feasible the identification of the products obtained during the photochemical reaction of a complex of the type $[Ru(bpy)_2(X)]^{n+}$ about ten years later [2], thanks to the development of an HPLC method based on a cation exchange column [3]. Semipreparative HPLC proved to be valid also in the separation and identification of isomers in case of ruthenium complexes with asymmetrical ligands like 3-(pyridin-2'-yl)-1,2,4-triazole [3,4], 1-methyl-3-(pyridin-2'-yl)-1,2,4-triazole or 2-(4'*H*-[1,2,4]triazol-3'yl)pyrazine [5], and for the separation of isomers deriving from dimeric ruthenium complexes with ligands like 3,5-bis(pyridin-2'-yl)-1,2,4-triazole [6] or 3,5-bis(pyrazin-2'-yl)-1,2,4-triazole [3,4,7]; Other multinuclear ruthenium complexes that were characterized by means of cation exchange HPLC included compounds containing ligands such as 2-phenyl-pyridine [8], and 2,5-bis(5'-methyl-4'H-[1,2,4]triaz-3'-yl)-pyrazine [9]. The use of such a technique has been extended to the separation of bipyridine complexes with metals other than ruthenium, e.g. iron and nickel [10], thus proving its general validity for the purification and characterization of metal complexes with bipyridyl-based ligands. The separation of two possible coordination isomers for [Ru(bpy)2(Hpytr)]2+, has been reported [11]. In this complex the the Hpytr ligand

is bound *via* either the N2 or the N4 nitrogen atom of the triazole ring as shown in .Figure 2.1.

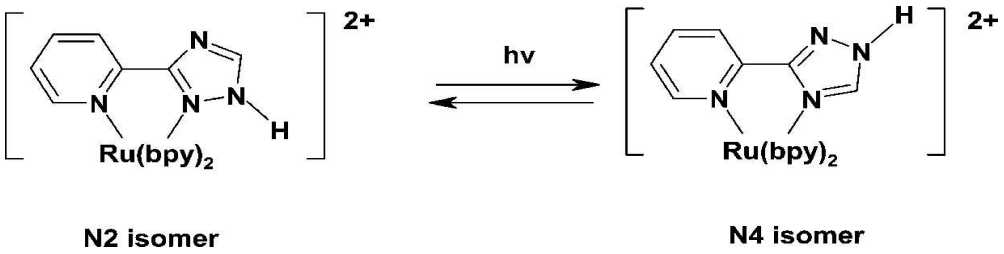

Figure 2.1 *The Hpytr ligand is bound via either theN2 or the N4 nitrogen atom of the triazole ring*

HPLC was useful in the separation and identification of both isomers. The HPLC traces of the photolysis of these isomers in CH_2Cl_2 showed apart from the solvent peak two peaks, the first one was for N2 isomer and peak 3 was N4 isomer.

HPLC has been also employed for the identification of the products of photolysis that were obtained upon irradiation of related polypyridyl complexes [7,12]; In particular, HPLC study of the photoreactions involving the dinuclear complex $[Ru(bpy)_2(bpt)Ru(phen)_2](PF_6)_3$ (bpt = 3,5-bis-(pyridin-2'-yl)-1,2,4-triazole; phen = 1,10-phehanthroline) and its isomer $[Ru(phen)_2(bpt)Ru(bpy)_2](PF_6)_3$, has allowed the identification of the fragmentation products $Ru(bpy)_2^{2+}$, $Ru(phen)_2^{2+}$ and $Ru(bpt)^+$ [7], whereas in case of $[Ru(bpy)_2(tbmbpy)]Cl_2$ irradiation {tbmbpy = *trans*-1,2-bis[4-(4'-methyl)-2,2'-bipyridyl] ethane}, HPLC verified the occurrence of a light-driven dimerization process [12].

In the present work, we report further on the use of HPLC for the analysis of the photoreaction products obtained upon irradiation of the binuclear complexes of

ruthenium $\{[Ru(bpy)_2]_2L\}^{3+}$ with L = bpt [13] and bpzt [bpzt = 3,5-bis-(pyrazin-2'-yl)-1,2,4-triazole] [3] and of related mononuclear pyrazinetriazole complexes.

The interest in the photochemistry of such binuclear systems relies on their possibility of having *intramolecular* transfer of excitation and/or charge between the metal centres [14] upon irradiation at the frequencies of metal-to-ligand charge transfer (MLCT) transitions. In this framework $\{[Ru(bpy)_2]_2L\}^{3+}$ complexes can be considered as supramolecular systems, the metal centres of which display different functions in photoactivated processes [15]. The photochemical behaviour of dinuclear compounds (See Figure 6.2) capable of producing hydrogen from water and solar light will described in Chapter 6.

2.1.1 Introduction to HPLC

High performance liquid chromatography (HPLC) is a powerful tool for the characterization of synthetic and natural polymers by separating individual fractions by molecular weight, chemical composition, functional groups, etc. It is also used for isolation and purification of biopolymers and analysis of additives in complex polymer formulations. As in any chromatographic technique, separation occurs due to thermodynamic partitioning between the sample components in the mobile and stationary phases. In HPLC, this process takes place in solution inside a chromatographic column packed with inorganic (usually, silica-based) or organic (synthetic resin, such as polystyrene–divinely benzene and acrylic-based materials) porous particles, capable of resisting the high pressure created by a

moving liquid (mobile phase) mechanically pumped through the column. Depending on application, isocratic (constant mobile phase composition) or gradient (variable composition) modes of separation can be employed, which significantly extends the capabilities of the technique [16]. The separation of mixture of components is based on differences in migration rates between each component as shown in Figure 2.2 [17,18].

2.1.2 Classification of HPLC Methods

There are many ways to classify liquid column chromatography. If this classification is based on the nature of the stationary phase and the separation process, three modes can be specified [17].

2.1.2.1 A. Adsorption Chromatography
The stationary phase is an adsorbent (like silica gel or any other silica based packing) and the separation is based on repeated adsorption-adsorption steps.

2.1.2.2 B. Partition or Distribution
These are similar terms and are sometimes used interchangeably. They relate to the general process by which a system comes to equilibrium.

2.1.2.3 C. Size Exclusion
This relates to separations based on size or shape, where certain molecules are excluded from the stationary phase, resulting in separation.

2.1.2.4 D. Ion Exchange
This process relates to exchange of a given ion, cation, or anion during the separation process [19].

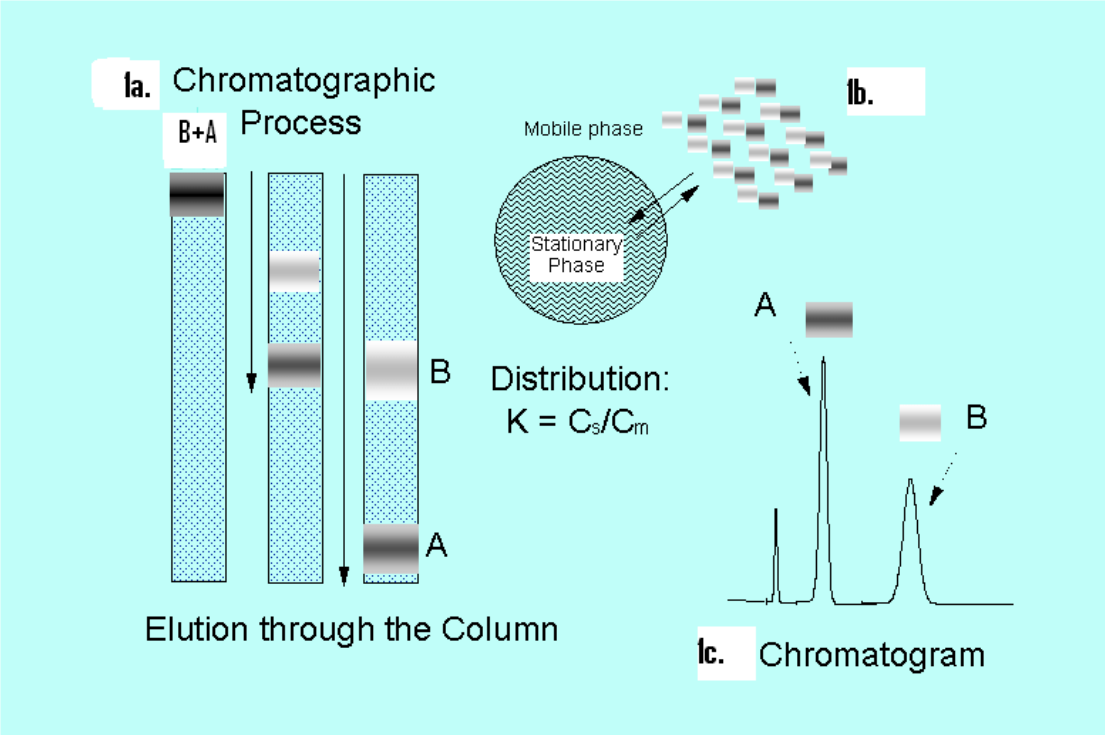

Figure 2.2. *(a) Schematic of the chromatographic process showing the migration of two bands of components down a column. (b) Microscopic representation of the partitioning process of analyte molecules A and B into the stationary phase bonded to a spherical solid support. (c) A chromatogram plotting the signal from a UV detector displays the elution components A and B. [19].*

2.1.2.5 Ion- Exchange Chromatography (IEC)

In ion-exchange chromatography [20,21], the separation model is based on the exchange of ionic analytes with the counter-ion of the ionic groups attached to the solid support (Figure 2.3). Typical stationary phases are cationic exchange (sulfonate), or anionic exchange (quaternary ammonium) groups bonded to polymeric or silica materials. Mobile phases consist of buffers, often with increasing

ionic strength, to force the migration of the analytes. Common applications are analysis of ions and biological components such as amino acids, proteins/peptides, and polynucleotides.

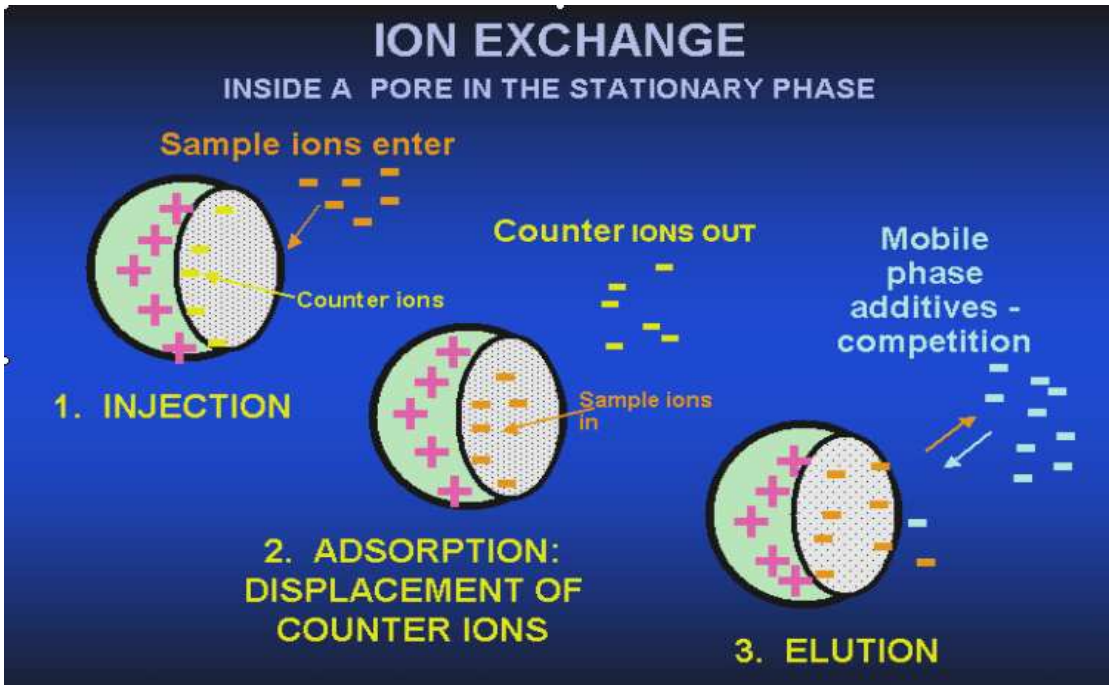

Figure 2.3 A pore in the stationary phase in ion exchange chromatography [21].

Immediately following the introduction of commercial HPLC equipment in 1968, ion-exchange chromatography (IEC) was an important HPLC method [20]. During the next decade, however, its application for the separation of most sample types gradually diminished compared to other HPLC methods. Today it is used infrequently, except for certain “special” samples. These include mixtures of biological origin (amino acids, oligonucleotides, peptides, proteins, and nucleic acids), inorganic salts, and some organometallics.

2. 2 Theory of Ion Exchange

Ion exchangers are by definition insoluble solid materials that contain charge centers and exchangeable counterions of opposite charge. When the ion exchanger is in contact with a solution of an electrolyte, its counterions can be exchanged for an equivalent amount of ions of the same charge provided by the electrolyte. If the exchangeable counterion provided by insoluble solid substance is a cation, it is participating in cation exchange and the solid substance is commonly called a cation exchanger. If it is an anion, anion exchange is taking place and the substance is called an anion exchanger [22].

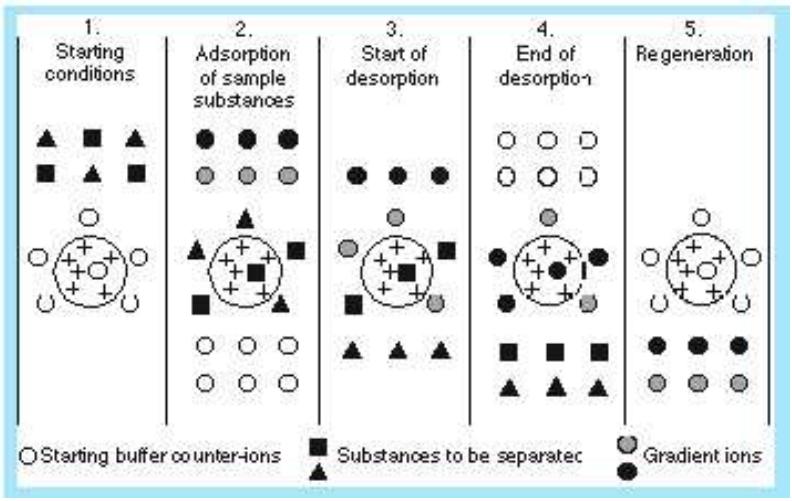

Figure.2.4: *Schematic diagram showing the set-up in ion exchange chromatography [22].*

Separation in ion exchange chromatography depends upon the reversible adsorption of charged solute molecules to immobilized ion exchange groups of

opposite charge. Most ion exchange experiments are performed in five main stages. These steps are illustrated schematically in Fig.2.4.

The first stage is equilibration in which the ion exchanger is brought to a starting state, in terms of pH and ionic strength, which allows the binding of the desired solute molecules. The exchanger groups are associated at this time with exchangeable counter-ions (usually simple anions or cations, such as chloride or sodium).

The second stage is sample application and adsorption, in which solute molecules carrying the appropriate charge displace counter-ions and bind reversibly to the gel. Unbound substances can be washed out from the exchanger bed using starting buffer.

In the third stage, substances are removed from the column by changing to elution conditions unfavourable for ionic bonding of the solute molecules. This normally involves increasing the ionic strength of the eluting buffer or changing its pH. In Figure 2.4 desorption is achieved by the introduction of an increasing salt concentration gradient and solute molecules are released from the column in the order of their strengths of binding, the most weakly bound substances being eluted first.

The fourth and fifth stages are the removal from the column of substances not eluted under the previous experimental conditions and re-equilibration at the starting conditions for the next purification.

Separation is obtained since different substances have different degrees of interaction with the ion exchanger due to differences in their charges, charge densities and distribution of charge on their surfaces. These interactions can be controlled by varying conditions such as ionic strength and pH. The differences in charge properties of biological compounds are often considerable, and since ion exchange chromatography is capable of separating species with very minor differences in properties, e.g. two proteins differing by only one charged amino acid, it is a very powerful separation technique.

In ion exchange chromatography, one can choose whether to bind the substances of interest and allow the contaminants to pass through the column, or to bind the contaminants and allow the substance of interest to pass through. Generally, the first method is more useful since it allows a greater degree of fractionation and concentrates the substances of interest.

In addition to the ion exchange effect, other types of binding may occur. These effects are small and are mainly due to van der Waals forces and non-polar interactions. Ion exchange separations may be carried out in a column, by a batch procedure or by expanded bed adsorption. All three methodologies are performed in the stages of equilibration, sample adsorption etc… described previously [23].

2. 2.1 Ion Exchangers for HPLC

An effective stationary phase in HPLC must possess a set of physical properties, in addition to properties which influence analyte-stationary phase retention that leads to a favorable flow of mobile phase and produces narrow, well-defined chromatographic peaks. The closer these properties are to the optimum, the more efficient the column operation becomes and the better its ability to resolve mixtures of analytes assuming other factors that influence analyte-stationary phase interactions are favourable. Table 2.1 summarizes the key stationary phase physical properties that must be satisfied for an efficient column operation.

Table 2.1 *Key stationary phase physical properties*

1. Uniform particle size
2. Microsize particles
3. Rigid particles
4. Physical strength to resist fracture due to column pressure drop
5. Spherical particles
6. Porous properties that provide access to retention sites
7. Chemical stability toward a wide range of mobile phase conditions

An ion exchanger suitable for HPLC applications must provide the following basic components:

It should possess an ionogenic group.

The ionogenic groups within the ion exchanger must be accessible.

A favourable number (ion exchange capacity) of the ionogenic groups should be present.

A preference of one analyte over another (ion exchange selectivity) should be present.

The ion exchange should be reversible and follow mass action effects

The kinetics of the exchange (rate of exchange) should be rapid enough to permit a column operation.

Ion exchangers suitable for HPLC applications are of four basic types:

- Organic polymeric ion exchanger
- Bonded phase ion exchanger
- Pellicular ion exchanger
- Inorganic oxide ion exchanger

Figure 2.5 indicates their basic physical form. A macroporous structure is achieved by the network of mcrospheres that are jointed together or by the channels that are present in the matrix. Since the ionogenic groups are attached to the matrix, they are accessible because of the porosity. This leads to a favourable effect on mass transfer and column efficiency. The pellicular-type ion exchanger differs from the

others in that the macroporous network, which contains the ionogenic group, is at the surface. Since its thickness over the inert core is about 1-3 μm rather than throughout the bead, mass transfer is even more favorable. The useful result, however, is partially offset by the subsequent decrease in the number of ionogenic groups present and the difficulty in preparing the pellicular form in a <10μm size ad a narrow reproducible size range.

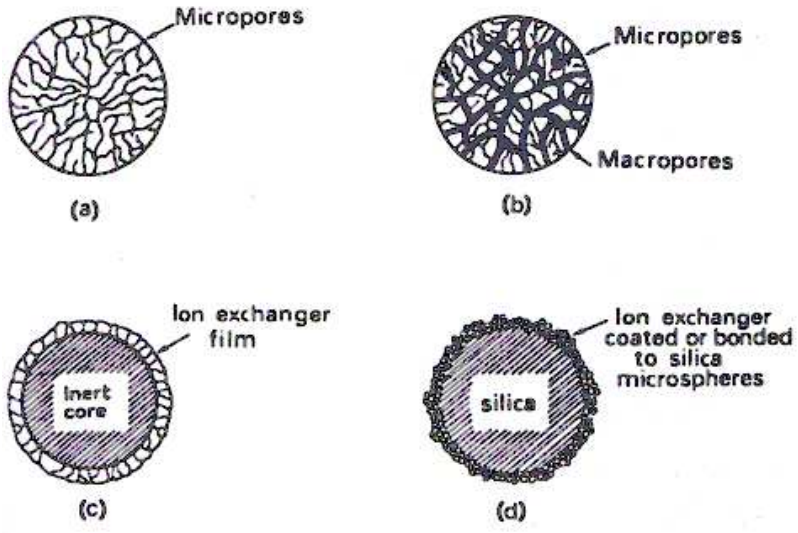

Figure 2.5 *Types of ion exchangers. (a) microporous or gel organic polymaeric ion exchangers; (b) macroporous organic polymeric ion exchanger; (c) pellicular ion exchanger; (d) bonded phase ion exchanger [17].*

2. 2. 2 Bonded Phase Ion Exchanger

Introduction of the bonded stationary phase to HPLC was a major turning point in the development of HPLC. This type of stationary phase is widely used and accounts for a large majority of HPLC applications. The bonded phase has the

physical strength of an adsorbent and the resolving power associated with a partitioning system provided by a stationary phase coated with a liquid layer. Since the bonded phase involves chemical bonding of the phase layer to the stationary phase, it is not lost during elution with mobile phase. Bonded phases are made by chemically bonding hydrocarbon groups to a microsilica particle. If polar groups are contained on the hydrocarbon, then the bonded phase exhibits normal phase chromatographic properties while if they are absent it exhibits reversed phase chromatographic properties. If the hydrocarbon group contains an ionogenic group or one is chemically attached to it in a subsequent reaction, then the bonded phase is an ion exchanger. The chemistry of chemically bonding a group onto silica can be accomplished in several ways [22,23]. One approach is based on the conversion of the silanol by reaction with an alcohol to form a silicate ester as shown in Eq. 2.1. The silanol group will readily undergo

$$\equiv Si-OH + ROH \rightarrow \equiv Si-OR \qquad \textit{Equation (2.1)}$$

reactions with organochlorosilanes (Eq. 2.2). If an organodichlorosilane is used, a terminal –OH group is obtained which can then be reacted with another type of organochlorosilane.

$$\equiv Si-OH + R_3 SiCl \rightarrow \equiv Si-O-SiR_3 \qquad \textit{Equation (2.2)}$$

The silanol can be converted into chloride, e.g., by reaction with thionyl chloride, and the resulting chloride is treated with a Grignard organolithium reagent to give the product as shown in eq.2.3.

$$\equiv Si-OH + SOCl_2 \rightarrow \equiv Si-Cl + LiR \rightarrow \equiv Si-R \qquad \textit{Equation (2.3)}$$

The silane chemistry in eq. 2.2 offer the better and more versatile synthetic routes to the bonded phase ion exchangers. If aromatic groups are attached, then these can be sulfonated to yield a strong-acid cation exchanger [23].

Ion-exchange packings with silica supports have several advantages over polystyrene based ones, in addition to the difference in selectivity. The glass or silica core of the resins makes them stronger structurally. Thus, there are seldom any problems with swelling or bed settling. Generally, it is possible to change buffer salts and even use mixed solvents without suffering a loss of column efficiency due to swelling of the particles. High temperatures (up to 80°C) do not affect the packings with bonded resin. But extremely acidic (pH<2) or mildly basic (pH>8) conditions may lead to attack of the silica supporting the bonded phases and destroy the column resistance and a simultaneous decrease in column efficiency.

2. 2. 3 Inorganic Groups

The presence of charged groups is a fundamental property of an ion exchanger. The type of group determines the type and strength of the ion exchanger; their total number and availability determines the capacity. A cation ion exchanger has a

strong acid or weak acid inorganic group while an anion exchanger has a strong base or weak base group. There is a variety of groups which have been chosen for use in ion exchangers; some of these are shown in Table 2.2.

Table 2.2 *Functional groups used on ion exchangers.*

Anion exchangers **Functional group**		
Quaternary ammonium	strong	$-O-CH_2N^+(CH_3)_3$
Diethylaminoethyl	weak	$-O-CH_2CH_2N^+H(CH_2CH_3)_2$
Diethylaminopropyl	weak	$-O-CH_2CHOHCH_2N^+H(CH_2CH_3)_2$
Cation exchangers **Functional group**		
Sulfopropyl	strong	$-O-CH_2CHOHCH_2OCH_2CH_2CH_2SO_3^-$
Methyl sulfonate	strong	$-O-CH_2CHOHCH_2OCH_2CHOHCH_2SO_3^-$
Carboxymethyl	weak	$-O-CH_2COO^-$

Sulphonic and quaternary amino groups are commonly used to form strong ion exchangers; the other groups form weak ion exchangers. The terms strong and weak refer to the extent of variation of ionization with pH and not the strength of binding. Strong ion exchangers are completely ionized over a wide pH range whereas with weak ion exchangers, the degree of dissociation and thus exchange capacity varies much more markedly with pH.

Some properties of strong ion exchangers are:

- Sample loading capacity does not decrease at high or low pH values due to loss of charge from the ion exchanger.
- A very simple mechanism of interaction exists between the ion exchanger and the solute.

2. 3 Basis of Retention

Columns used for ion exchange are characterized by the presence of charged groups covalently attached to the stationary phase: anion-exchange columns carry a positive charge (usually a quaternary ammonium or amine group) and cation-exchange columns carry a negative charge (sulfonate or carboxylate groups). Cation-exchange columns are used for the separation of cations such as protonated bases, and anion-exchange columns are used for anionic or acidic samples [24].

If the stationary phase is represented by R^- (cation exchanger) or R^+ (anion exchanger), and the sample by X^+ (cation) or X^- (anion), retention in IEC can be represented as follows:

$$X^+ + R^-K^+ \Leftrightarrow X^+R^- + K^+ \qquad \textit{(cation exchange)} \qquad \textit{Equation (2.4)}$$

$$X^- + R^+Cl^- \Leftrightarrow X^-R^+ + Cl^- \qquad \textit{(anion exchange)} \qquad \textit{Equation (2.5)}$$

Here it is assumed that the counterion in the mobile phase is either K^+ or Cl^-, and the sample ion is univalent.

The effect of the counterion concentration on retention can be generalized for a sample ion of charge *z* and a univalent counterion as

$$k' = \frac{constant}{\left(counterion\ \ concentration\right)^z} \qquad \textbf{Equation (2.6)}$$

where $k' = retention\ \ factor$, and

$$K_D = k'\frac{V_S}{V_R} = \frac{K_E^S C_R^{y/x}}{\left[E^x\right]_S^{y/x}} \qquad \textbf{Equation (2.7)}$$

being K_D = distribution coefficient, V_S = volume of the stationary phase, V_R = volume of the mobile phase, K_E^S = selectivity coefficient, C_R = exchange capacity, $\left[E^x\right]_S$ = eluent ion concentration in the solution of the mobile phase, y,x = charges on sample and eluent ions, respectively.

Thus an increase in salt or buffer concentration in IEC results in decreased retention, and the effect is greater for more highly charged sample compounds (z >1). The ionic strength of the mobile phase is normally varied to control sample retention for 0.5 > k > 20, and selectivity will also be affected for any two compounds of differing charge (Eq.2.6).

2. 3.1 pH Effects

IEC is typical used for acidic or basic sample. Since retention (Eqs.2.4 and 2.5) requires that the sample molecule carries a charge opposite to that on the column, only the ionized from of the acid or base will be retained significantly. This allows

the effects of pH on retention in ion exchange to be understood and controlled. An increase in pH leads to greater sample ionization and retention in anion-exchange separation of acids, while a decrease in pH favours the retention of bases by cation exchange HPLC. Varying pH is usually a preferred way to change selectivity in ion exchange separations [24,25] according to:

$$K_H^{Na} = \frac{[Na^+]_R [H^+]_S}{[H^+]_R [Na^+]_S} \qquad \textit{Equation (2.8)}$$

where the subscripts R and S refer to the stationary and solution phases, respectively.

2. 3.2 Salt or Buffer Types

Different mobile-phase anions or cations are retained more or less strongly in ion exchange, and sometimes a particular salt is selected to provide stronger or weaker retention. Therefore, we can speak of strong or weak ionic displacers or counter-ions; a strong displacer reduces sample retention more than the same concentration of a weak displacer. In general, more highly charged displacers are stronger [26]. The relative strength of different displacers in anion-exchange chromatography is F^- (weak) < OH^- < acetate$^-$ < Cl^- < SCN^- < Br^- < $NO3^-$ < I^- < oxalate^{2-} < SO_2^{2-} < citrate^{-3} (strong)

Similarly, displacer strength in cation-exchange chromatography varies as

Li^+ (weak) < H^+ < Na^+ < $NH4^+$ < K^+ < Rb^+ < Cs^+ < Ag^+ < Mg^{2+} < Zn^{2+} < Co^{2+} Co^{2+} < Cd^{2+} < Ni^{2+} < Ca^{2+} < Pb^{2+} <Ba^{2+} (strong).

A change in the salt used for ion exchange chromatography can also affect selectivity [26].

2. 3. 3 Organic Solvents

For addition of an organic solvent to the mobile phase results in decreased retention, just as in the case of reversed-phase HPLC [18,25]. Solvents such as methanol or acetonitrile are also often used in ion exchange to create changes in selectivity.

2. 3. 4 Column Type

Four kinds of ion-exchange column can be distinguished: weak and strong cation exchangers (WCX and SCX, respectively) and weak and strong anion exchangers (WAX and SAX, respectively).

Strong ion exchangers carry ionic group whose ionisation dose not change over the usual pH range ($2 < pH < 12$) [e.g., $-SO_3^-$ groups for cation exchange and $-N(CH_3)^+_3$ groups for anion exchange]. Weak ion exchangers lose their change and sample retention for certain pH ranges (e.g., $^-COO^-$ groups for cation exchange show a progressive loss in charge for $pH< 5$) [18,24,25].

Most applications of ion- exchange chromatography (except the separation of biological samples) make use of strong ion exchangers. Weak ion-exchange columns can be used as a means of changing selectivity or for reduced retention.

2. 4 Resolution in Ion Exchange Chromatography

This section discusses the main theoretical parameters which affect the separation in ion exchange chromatography. The result of an ion exchange experiment, as with any other chromatographic separation, is often expressed as the resolution between the peaks of interest. The resolution (R_S) is determined from the chromatogram as shown in Figure 2.6 [22,23,26].

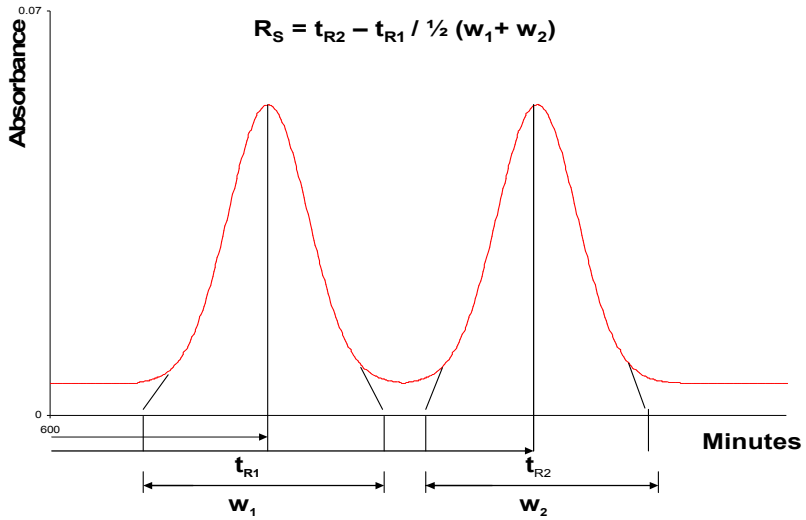

Figure 2.6 *Determination of the resolution (Rs) between two peaks.*

The resolution is defined as the distance between peak maxima compared with the average base width of the two peaks. Elution volumes and peak widths should be

measured with the same units to give a dimensionless value to the resolution. R_s is a measure of the relative separation between two peaks and can be used to determine if further optimization of the chromatographic procedure is necessary. If R_s = 1.0 (Fig.2.6) then 98% purity has been achieved at 98% of peak recovery, provided the peaks are Gaussian and approximately equal in size. Baseline resolution requires that R_s =1.5. At this value purity of the peak is 100%. Note: A completely resolved peak is not equivalent to a pure substance. This peak may represent a series of components that are not resolvable using the selected separation parameter. The resolution achievable in a system is proportional to the product of the selectivity,

The efficiency and the capacity of the system are the two most important parameters to control column chromatography performance. The analytical expression for R_s is:

$$R_s = \frac{1}{4}\frac{\alpha - 1}{\alpha} \text{ X } \sqrt{N} \text{ X } \frac{k}{k+1} \qquad \textbf{Equation (2.9)}$$

selectivity efficiency capacity

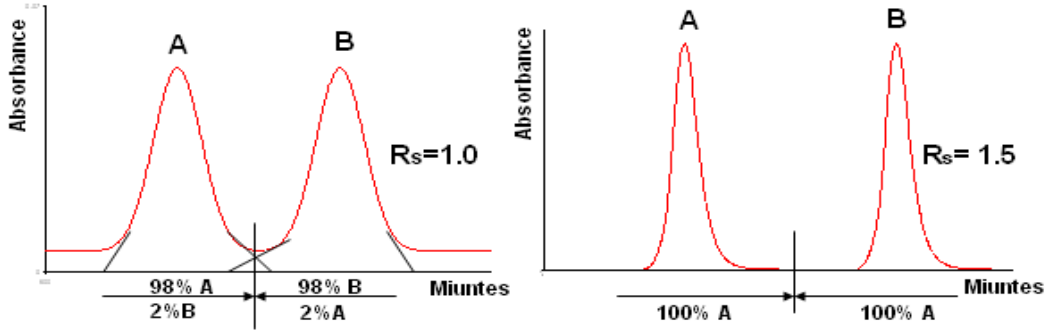

Figure 2.7 *Chromatograms results with different resolutions, R_S = 1.0 and R_S = 1.5.*

2. 4. 1 Capacity Factor

The capacity or retention factor k is a measure of the retention of a component and should not be confused with loading capacity (mg sample/ml) or ionic capacity (mmol/ml). The capacity factor is calculated for each individual peak. For example k for peak in Figure 2.7 is derived from the equation:

$$\textit{Capacity factor } k = \frac{t_R - t_0}{t_0} \qquad \textbf{\textit{Equation (2.10)}}$$

In the equation for R_s, k is the average of k_1 and k_2. The quantities V are the retention times of the solutes and can be measured as times, volumes of solvent or distances on the recorder chart. Adsorption techniques such as ion exchange chromatography can have high capacity factors since experimental conditions can be chosen which lead to peak retention volumes greatly in excess of V_0. This can be seen in contrast with the technique of gel filtration where capacity is limited since all peaks must elute within the volume (t_R - t_0).

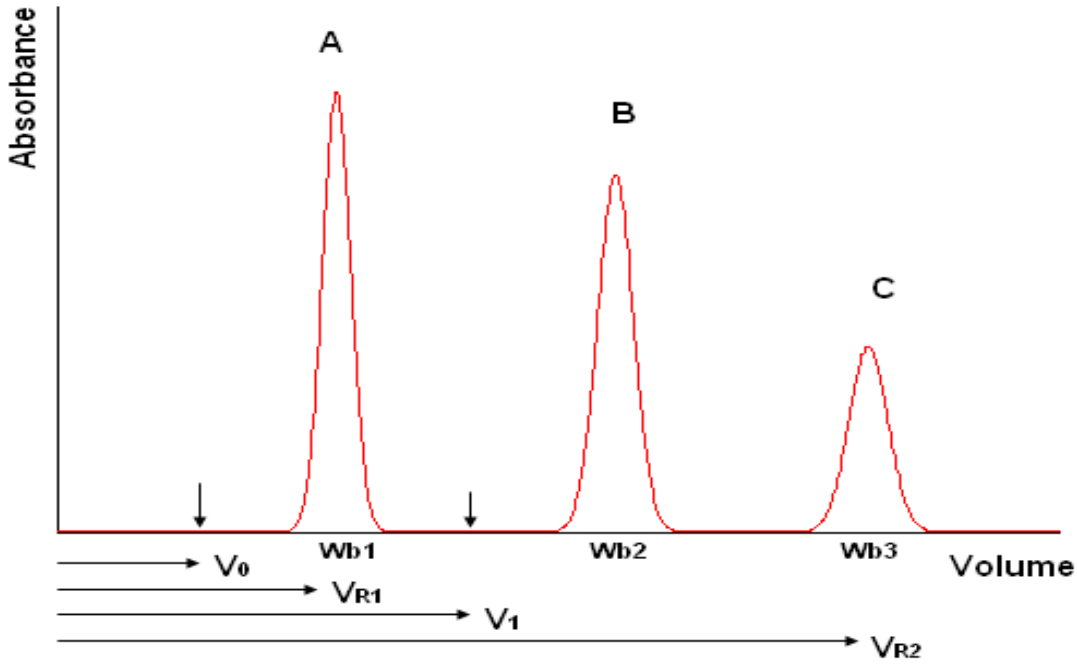

Figure 2.8 *Hypothetical chromatogram.*

V_0 = void volume.

V_{R1} = elution volume for peak 1, wb1 = peak width for peak 1

V_{R2} = elution volume for peak 2, wb2 = peak width for peak 2

V_t = total volume.

2.4.2 Column Efficiency

The column efficiency is related to the zone broadening which occurs on the column and can be calculated from the expression:

$$N = 16\left(\frac{V_R}{w}\right)^2 \quad \text{or} \quad N = 5.54\left(\frac{V_R}{w_{1/2}}\right)^2 \qquad \textit{Equation (2.6)}$$

(where w and $w_{1/2}$ are respectively the peak width and the peak width at half peak height) and is expressed as the number of theoretical plates (N) for the column under specified experimental conditions.

The plate model supposes that the chromatographic column is contains a large number of separate layers, called theoretical plates [19,23,27].

Separate equilibrations of the sample between the stationary and mobile phase occur in these "plates". The analyte moves down the column by transfer of equilibrated mobile phase from one plate to the next.

It is important to remember that the plates do not really exist; they are a figment of the imagination that helps us understand the processes at work in the column. They also serve as a way of measuring column efficiency, either by stating the number of theoretical plates in a column, N (the more plates the better), or by stating the plate height; the Height Equivalent to a Theoretical Plate (the smaller the better). If the length of the column is L, then the HETP is

$$HETP = L / N$$

A more realistic description of the processes at work inside a column takes account of the time taken for the solute to equilibrate between the stationary and mobile phase (unlike the plate model, which assumes that equilibration is infinitely fast). The resulting band shape of a chromatographic peak is therefore affected by the rate of elution. It is also affected by the different paths available to solute molecules, since they travel between particles of stationary phase. If we consider the various mechanisms that contribute to band broadening, we arrive at the Van Deemter equation for plate height [26]

$HETP = A + B / u + C.u$

Where u is the average velocity of the mobile phase. A, B, and C are factors which contribute to band broadening.

A - Eddy diffusion

The mobile phase moves through the column that is packed with stationary phase. Solute molecules will take different paths through the stationary phase at random. This will cause broadening of the solute band, because different paths are of different lengths.

B - Longitudinal diffusion

The concentration of analyte is less at the edges of the band than at the center. Analyte diffuses out from the center to the edges. This causes band broadening. If the velocity of the mobile phase is high then the analyte spends less time on the column, which decreases the effects of longitudinal diffusion.

C - Resistance to mass transfer.

The analyte takes a certain amount of time to equilibrate between the stationary and mobile phase. If the velocity of the mobile phase is high, and the analyte has a strong affinity for the stationary phase, then the analyte in the mobile phase will move ahead of the analyte in the stationary phase. The band of analyte is broadened. The higher the velocity of mobile phase, the worse the broadening becomes Van Deemter plots [26].

A plot of plate height vs. average linear velocity of mobile phase.

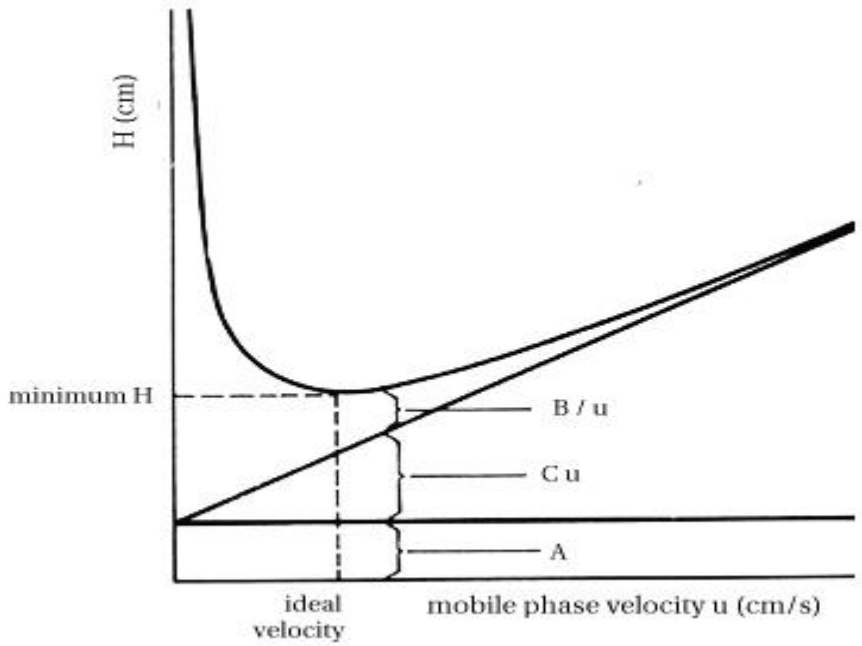

Figure 2.9 *Van Deemter plot [26]*

Such plots are of considerable use in determining the optimum mobile phase flow rate. Since the observed value for N depends on experimental factors such as flow rate and sample loading, it is important that comparisons are done under identical conditions. In the case of ion exchange chromatography, efficiency is measured under isocratic conditions, using a substance that does not interact with the matrix, e.g. acetone. One of the main causes of zone broadening in a chromatography bed is longitudinal diffusion of the solute molecules. The effect is minimized if the distances available for diffusion, in both the mobile phase and stationary phase, are minimized. In practice this is achieved by using small uniform bead sizes and important developments in ion exchange chromatography have been the

introduction of 10 μm and 15 μm diameter particles. The highest efficiency is achieved with the non-porous, 3 μm diameter, designed for analytical and micropreparative applications. After bead size, the second major contributory factor to efficiency is good experimental technique. Badly, unevenly packed chromatography beds and air bubbles will lead to channelling, zone broadening and loss of resolution. Good separations require well packed columns and the importance of column packing increases in direct proportion to the performance required.

2. 4. 3 Selectivity

The selectivity (α) defines the ability of the system to separate peaks i.e. the distance between two peaks. The selectivity factor can be calculated from the chromatogram (Figure 2.10) using the expression [27].

$$\alpha = \frac{k_2}{k_1} = \frac{V_{R2} - V_0}{V_{R1} - V_0} \qquad \textit{Equation (2.7)}$$

Good selectivity is a more important factor than high efficiency in determining resolution (Figure 2.10) since Rs is linearly related to selectivity but quadratically related to efficiency. This means that a four fold increase in efficiency is required to double the resolution under isocratic conditions.

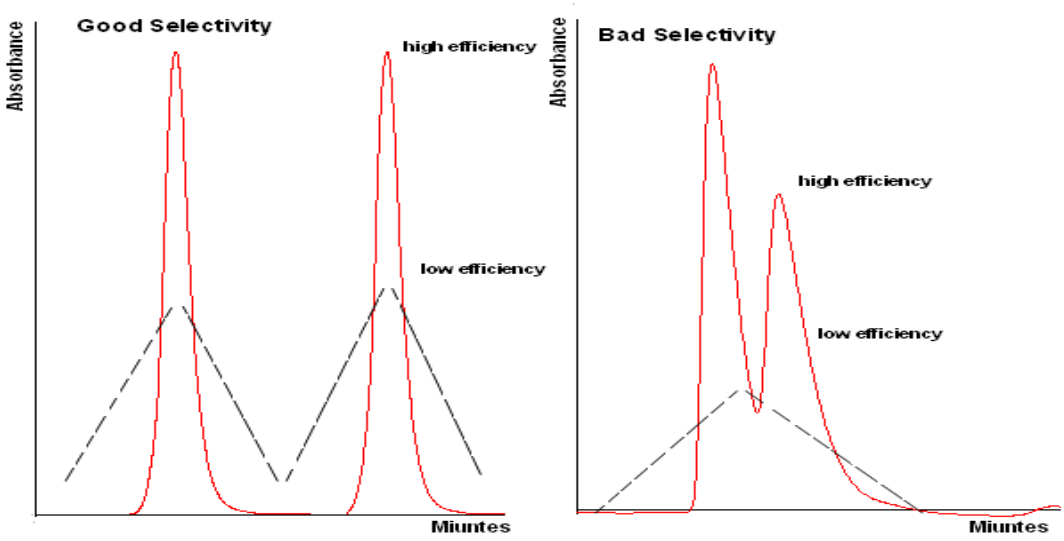

Figure 2.10 *Effects of selectivity and efficiency on retention*

Selectivity in ion exchange chromatography depends not only on the nature and number of the ionic groups on the matrix but also on the experimental conditions, such as pH and ionic strength. It is the case and predictability with which these experimental conditions, and thus the selectivity, can be manipulated which gives ion exchange chromatography the potential of extremely high resolution.

2. 4.4 Capacity

The capacity of an ion exchanger is a quantitative measure of its ability to take up exchangeable counter-ions and is therefore of major importance. The capacity may be expressed as total ionic capacity, available capacity or dynamic capacity. The total ionic capacity is the number of charged substituent groups per gram dry ion exchanger or per ml of swollen gel. Total capacity can be measured by titration

with a strong acid or base. The actual amount of electrolyte that can be bound to an ion exchanger, under defined experimental conditions, is referred to as the available capacity for the gel. If the defined conditions include the flow rate at which the gel was operated, the amount bound is referred to as the dynamic capacity for the ion exchanger [28,29].

Available and dynamic capacities depend upon:

- The properties of the electrolyte.
- The properties of the ion exchanger.
- The chosen experimental conditions.

The properties of the electrolyte which determine the available or dynamic capacity on a particular ion exchange matrix are its molecular size and its charge/pH relationship. The capacity of an ion exchanger is thus different for different electrolytes [16,19,23].

2. 5 Optimization of Chromatographic Condition Used During this Study.

2. 5.1 Salt or Buffer Type

Different mobile-phase anions or cations are retained more or less strongly in ion exchange, and sometimes a particular salt is selected to provide stronger or weaker retention. Therefore, we can speak of strong or weak ionic displacers or counter-ions; a strong displacer reduces sample retention more than the same concentration of a weak displacer. In general, more highly charged displacers are stronger.

This series indicates that an eluent made up using a potassium salt will be a stronger eluent than one using a sodium salt, if ion exchange is the only mechanism in operation.

A change in the salt used for ion exchange chromatography can also affect selectivity described previously [26].

For addition of an organic solvent to the mobile phase results in decreased retention, just as in the case of reversed- phase HPLC. Solvents such as methanol or acetonitrile are also often used in ion exchange to create changes in selectivity.

The optimum conditions for many separations of Ru complexes were investigated employing many buffers as a mobile phase. In the past, ammonium acetate (NH_3COOCH_3), lithium chloride (LiCl) and lithium perchlorate $LiClO_4$, were used as buffer, many reported has been done for the separation of mononuclear Ru complexes. Unfortunately, no separation of Ru-Ru dimers was obtained after many runs in this work using previously reported salts. The used conditions turned out to be inappropriate for highly charged of ruthenium complexes. A possible way to improve separation of the Ru-Ru dimers could be the use of the eluent in gradient mode or the modification of KNO_3 concentration and mixture amount of acetonitrile / water/ methanol.

2.5.2 Effect of acetonitrile/water/methanol proportion on retention at KNO_3 concentration and flow rate constant.

Effect of KNO_3 concentration on a series of injections by varying the acetonitrile/water/methanol proportion was carried out to investigate its effect on

the retention time (Table 2.2). The effect of changes in this parameter of the mobile phase on the retention of $[Ru(bpy)_3]^{2+}$ and the peak shape is obvious.

The compound studied showed marked decreases in retention on reducing the eluent water content from 30 to 20% (v/v) on the SCX column. In addition, a certain amount of tailing was observed; this was reduced by decreasing the water content in the mobile phase. Retention at acetonitrile/water/methanol proportion, pH and flow rate constant.

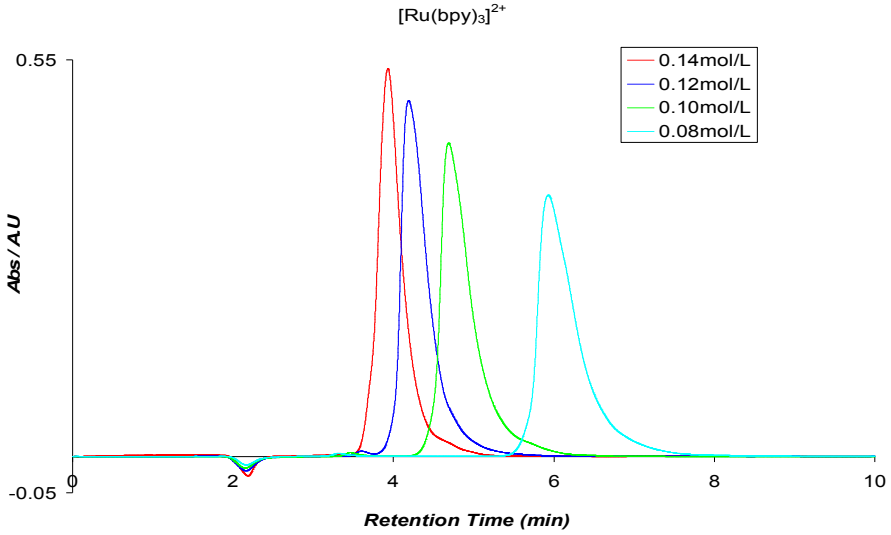

Figure 2.11 *Effect of KNO_3 concentration on the peak shape and retention time.*

Table 2.2 *Effect of acetonitrile/water/methanol ratio on retention in 0.12 KNO_3 and 2ml/min flow rate constant.*

Acn/water/methanol (v/v/v)	retention time(min)	peak width (sec)	P (Bars)
65 / 30 / 5	7.0	36.6	137
70 / 25 / 5	6.1	31.1	197
75 / 20/ 5	5.7	26.9	182
80 / 15 / 5	5.8	23.9	142

Effects of variations in potassium nitrate concentration on the retention time was investigated. The results showed that the retention is dependent on the KNO_3 concentration (Table 2.3). The peak shape is also affected by the concentration (Figure 2.11). Increases in KNO_3 concentration leads to a reduction of the retention time and a decrease of the peak tailing effect. It seems therefore that the $[Ru(bpy)_3]^{2+}$ SCX column interaction process was dependent on the adsorption of K^+ cation on the SCX column. The diffusion is dependent on the KNO_3 concentration.

***Table 2.3**. Effect of KNO_3 on retention at acetonitrile/water/methanol (75 / 20 / 5; v/v/v), pH 3.7 and 2.0ml/min flow rate constant.*

$[KNO_3]$ (mol/L)	retention time (min)	peak width (sec)	P (Bars)
0.14	3.9	19.0	242
0.12	4.2	20.0	215
0.10	4.7	23.5	210
0.08	5.9	29.6	197

2.5.3 Effect of flow rate on retention at acetonitrile/water/methanol proportion and KNO_3 concentration constant.

This series of injections of $[Ru(bpy)_3]^{2+}$ at flow rates of 2, 3 and 4ml/min revealed, as expected, that the retention time decreases as the flow rate increases from 2 to

4ml/min. (Table 2.4). In addition, the amount of tailing was reduced by increasing the flow rate of the mobile phase (Figure 2.12).

Table 2.4 *Effect of the flow rate on retention at acetonitrile/water/methanol (75/20/5; v/v/v) and 0.12 MKNO$_3$ constant.*

flow rate (ml/min)	retention time (min)	P (Bars)	Peak width (sec)
2	5.8	142	25.3
3	3.8	210	17.4
4	2.8	272	12.4

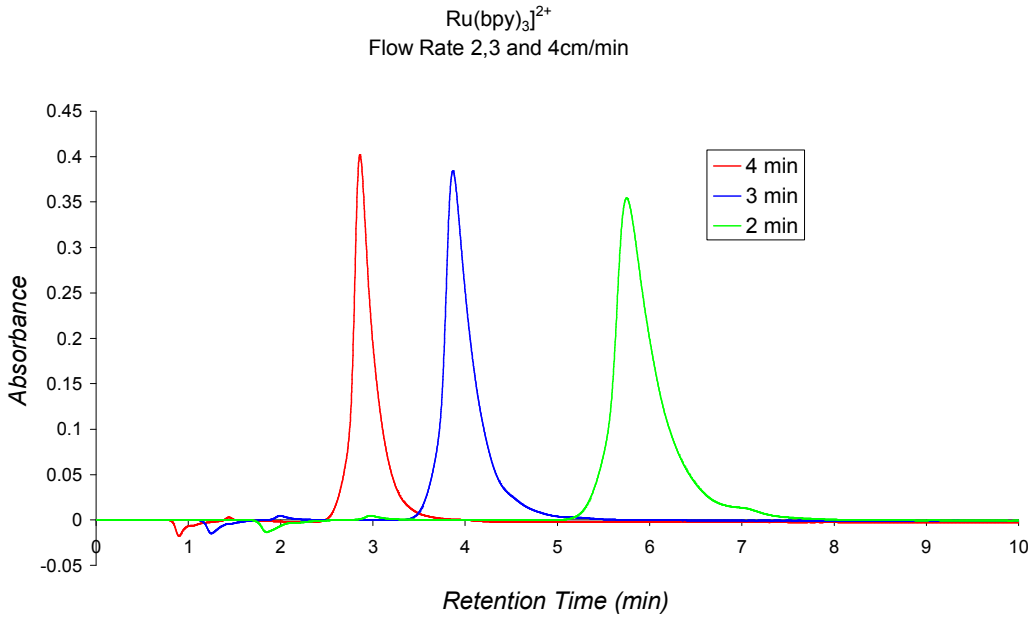

Figure 2.12 *Effect of the flow rate on retention at acetonitrile/water (75/20/5; v/v/v).*

2.5.4 Effect of pH on retention.

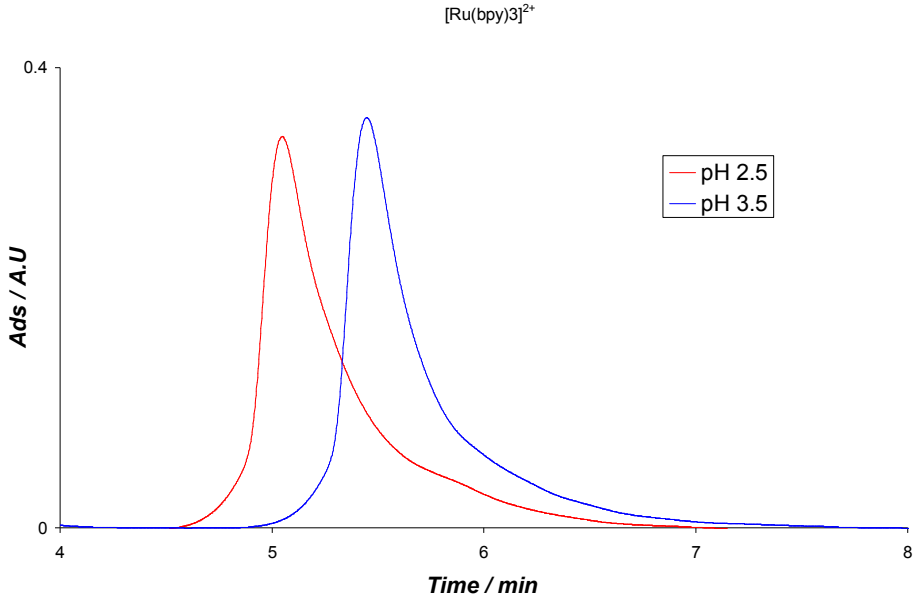

Figure 2.13 *Effect of pH on retention at acetonitrile/water/methanol proportion, flow rate and KNO_3 concentration constant.*

The effects of pH on retention in ion exchange could be understood and controlled. An increase in pH leads to greater sample ionzation and retention in anion-exchange separation of acids, while a decrease in pH favors the retention of bases by cation exchange HPLC (the opposite of RPC retention). Varying pH is usually a preferred way to change selectivity in ion exchange separations.[1]

It was expected that low pH values would shorten the retention time and the tailing effect. A set of injections was carried out under different pH values. The pH of the acetonitrile/water /methanol (75 / 20 / 5; v/v/v) containing 0.12 M KNO_3 is 3.7. This pH was changed to 2,3 by addition of concentrated HCl. Table 2.4 shows that the

retention times of some ruthenium compounds could be shortened by lowering the pH. However, bad peak shape were obtained under pH 2.3 conditions (Figure 2.13).

Table 2.5 *Effect of pH variation on retention time at acetonitrile/water/methanol (75/ 20/ 5; v/v/v), 0.12 M KNO_3 and flow rate 2.0 ml/min constant.*

compound	Retention time (min)		Peak width (sec)	
	pH 2.3	pH 3.7	pH 2.3	pH 3.7
$[Ru(bpy)_3]^{2+}$	4.09	4.23	17.4	12.3
$[(Ru(bpy)_2)_2\ bpt]^{3+}$	7.75	8.26	37.8	22.2
$[(Ru(bpy)_2)_2\ bpzt]^{3+}$	11.81	12.57	64.5	37.4

2. 6 Discussion

The results reported above showed that the composition of the mobile phase, including acetonitrile /water/methanol proportion, salt concentration, flow rate and pH, has a direct effect on the interaction between the ruthenium compounds and the SCX-column. To choose a reliable mobile phase composition, we have to take the retention time, the peak shape and the pump pressure into account.

Experiments carried out using acetonitrile/water/methanol (80 / 15 / 5; v/v/v) containing 0.08 M KNO_3 as a mobile phase and a flow rate of 2.0 cm^3/min seemed to be suitable for the separation of pure $[Ru(bpy)_2)_2\ bpt]^{3+}$ ruthenium compounds. $CH_3CN:H_2O$ 80:20 containing 0.12 M KNO_3 (flow rate 2.0-4.0 cm^3/min) for $[(Ru(bpy)_2)_2\ bpzt]^{3+}$ in CH_3CN, and acetonitrile/water/methanol (75 / 20 /5; v/v/v) containing 0.1 M KNO_3 at a flow rate of 2.0 cm^3/min seemed to be suitable for the separation of pure $[Ru(bpy)_2\ pztr]^{+}$.

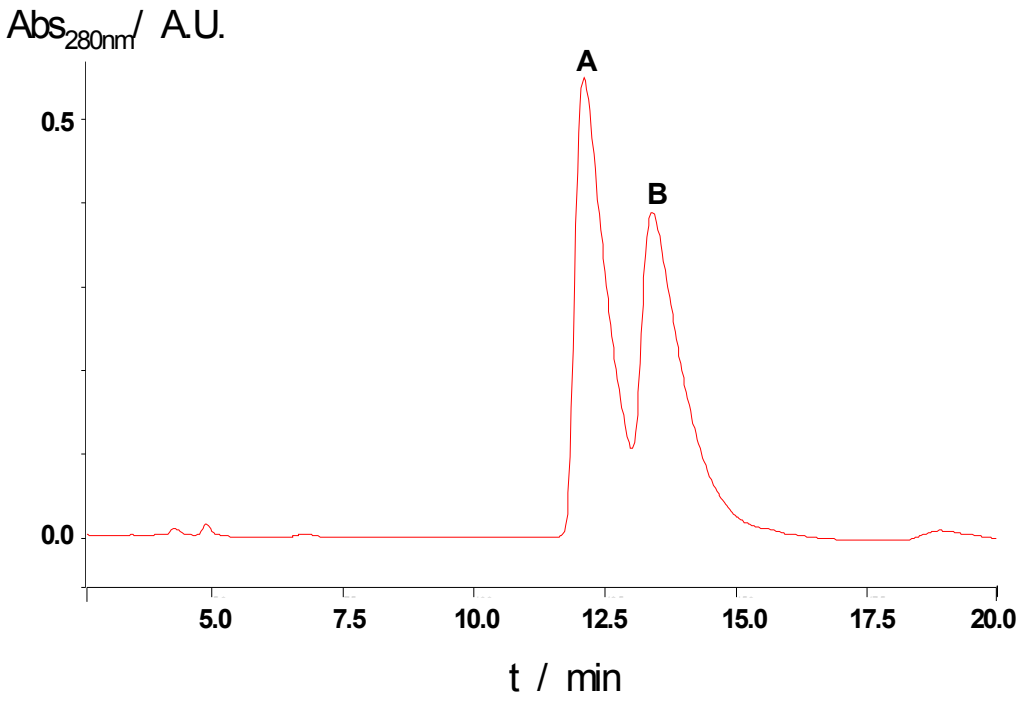

Figure 2.14 *Separation of* $[Ru(bpy)_2)_2\ bpt]^{3+}$*. Condition using acetonitrile/water/ methanol (80 / 15 / 5; v/v/v) containing 0.1 M* KNO_3 *as a mobile phase and a flow rate of 2.0* $cm^3\ min^{-1}$*.*

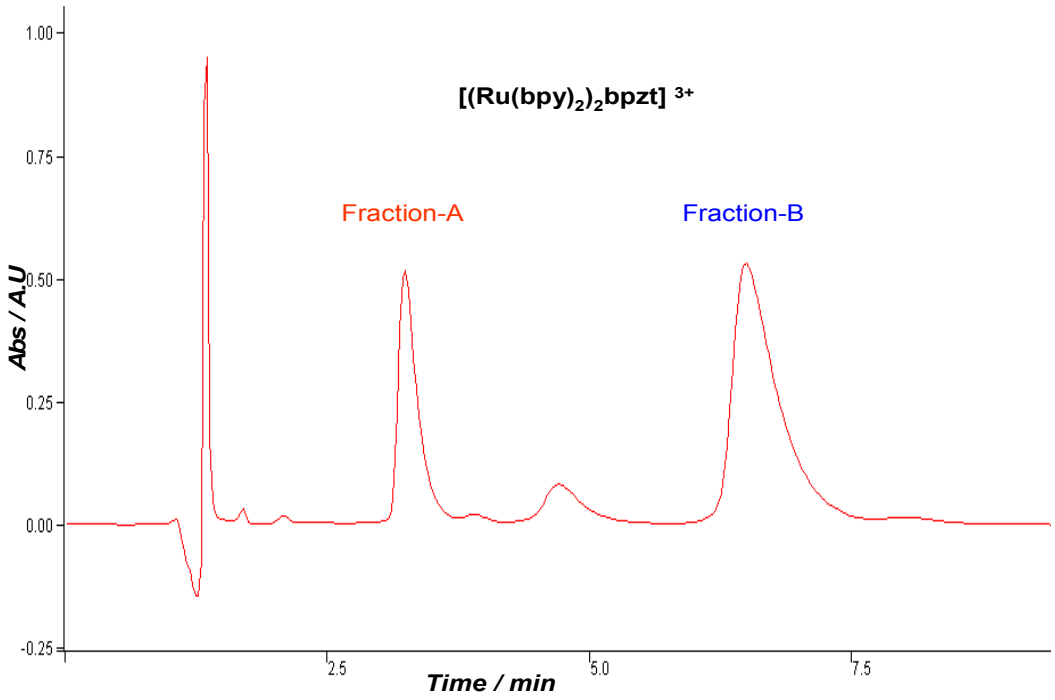

Figure 2.15 *Separation of $[(Ru(bpy)_2)_2\ bpzt]^{3+}$ in 80:20 $CH_3CN:H_2O$ containing 0.12 M KNO_3 (flow rate 4.0 $cm^3\ min^{-1}$).*

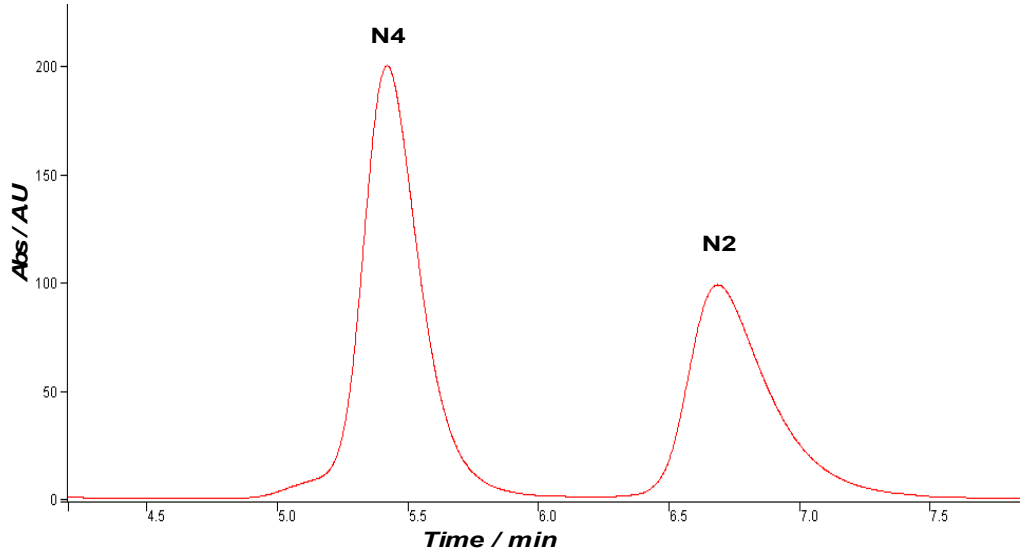

Figure 2.16 *Separation of $[Ru(bpy)_2pztr]Pf_6$. Condition using acetonitrile/water/methanol (75 /20/ 5; v/v/v) containing 0.1 M KNO_3 as a mobile phase and a flow rate of 2.0 $cm^3\ min^{-1}$.*

2. 7 Experimental Section and Measurements Techniques.

2. 7. 1 Materials

The ruthenium compounds were prepared by our group research and Prof Sven. All solvents employed were of HPLC grade or better and used as received unless otherwise stated. Water was prepared with water purification System model Milli-Q (Millipore, Bedford, MA, USA). All samples were filtered through Nylaflo® nylon membrane filter units of 0.45 µm pore diameter (Millipore). All mobile Phases were degassed prior to use.

2.7.2 Semi-Preparative HPLC:

Semi-preparative HPLC was carried out on a model Varian 230 pump, (model230.01) (see figure 2.17) and Varian detector (Model 330.71) fitted with a 200 µm injection loop and a magnum- Partisil 10 SCX cation exchange column (4.6mm x 25cm) provided by HICHROM; the most intense band in the absorption spectrum for the complexes studied was between 270nm and 290nm. So 280 nm was chosen as the detection wavelength. With an acetonitrile/water/methanol (80/15/5;v/v/v) mixture during 30 minutes. Then the column was washed with mobile phase containing potassium nitrate KNO_3 as a buffer during 30 minutes. After use, the Column was rinsed with an acetonitrile/water/methanol (80/15/5; v/v/v) mixture (30 min) and the flow rate used was 2.0-4.0 ml/min.

Figure 2.17 *Varian ProStar 230 HPLC System.*

2.7.3 Analytical HPLC:

High performance liquid chromatography (HPLC) was carried out on using a Varian Pro Star photodiode array as detecting system in conjunction with Varian Star software, a Varian 230.0 pump, a 20μL injector loop and a strong cation exchange Luna SCX column (25cm x4.6mm) provided by HICHROM. This column is a silica-based sorbent derivatized with benzenesulfonic acid phase. The column is packed with 5μm particles and the operating pH range is between 2.0 and 7.0.

- The pump, UV/Vis detector was switiched on. The pump flow rate should be at 0mL/min and the pressure at 0 Psi.

- Before using the column was washed with HPLC Grade acetonitrile/water (50/50 v/v) mixture this primes column for use.
- The system was initially purged. The purge valve was turned to the (Open) position and the purge button was pressed. The system was purged for 30-60 seconds. The purge valve was turned back to the (Close) position. The system was purged for every change of mobile phase than the system was allowed to equilibrate for 20-30 minutes. The flow rate was set depending on experimental between 1.5-3.5mL/min and pump was pressed. The pressure increases to highly depending on increasing of flow rate and differential buffers on use maximum pressure on the setup pump was 6000 Psi.
- In any changing of buffers the system was cleaned for 20-30 minutes.
- When the absorbance reading on the detector was stable the Software shows the message “ready for injection”.
- The injection loop and syringe was cleaned with the mobile phase. The injection loop was cleaned by placing the loop in the (load) position and injecting the mobile phase. This was repeated for every change of mobile phase and samples.
- The samples were prepared by dissolving a small amount of sample, for example for semi-prep experiments large amount may needed to get enough amount for each separation fractions <200mg, in approximately 10-20mL of mobile phase. The sample was filtered and placed in injection syringe. The syringe was placed in the injection loop in the (load) position.

- The absorbance detector was set at 0.4AU, detection wavelength at 280/430 nm depending on solvents.
- The time of injection was changing up to flow rate and mobile phase using and type of experimental.
- Al mobile phases were preparation, each mobile phase was vacuum filtered through 0.5µm membrane filters and then degassed in Ultra Sonic for 15-20 minutes.

2.7.4 Photochemical Studies:

The photochemical experiments were carried out at room temperature in air-equilibrated solution in a 1 cm quartz cell or by placing samples in NMR tubes and placing them before a 10 W blue lamb (LED emitting diodes 470 nm) or 100 W Tungsten filament light source slide projector (Kodak EKTAPRO 3000). This produces light with a broad spectrum similar to that of solar energy, a glass filter lens (λ > 390 nm) to prevent UV radiation reaching the sample. The sample heating was prevented using a water filter.

- It has two removable fans whose flow direction and intensity can be set separately. The position of the fans is variable, so that it at an angle of 90 ° or 180 ° to each other can see. Therefore, investigations under irradiation both at right angles, as well as at 180 °.

Light sources For illumination, we used LED light emitting diodes λ = 470 nm LAMP type L-7113PBC-BLUE. *S. Meyer et al [30].*

- In the sample holder can be used as well as round-cornered reactors (such as cuvettes or standard GC - Vial) be integrated. You can also opposed to any arbitrary sample holder to be replaced if, for example, larger or more reactors to be irradiated. The LED Bar is interchangeable and can thus the wavelength of the irradiation can be varied. The position of the LED bar is also variable.

2.7.5 Spectroscopic Measurements:

^{1}H-NMR. ^{1}H-NMR spectra were recorded on a Bruker Avance 400 (400 MHz) NMR Spectrometer. All measurements were carried out in [D_6]-DMSO for ligands [D_6]-acetonitrile and acetone for complexes. Peak positions are relative to residual solvent peaks – Mass spectra were obtained using a Bruker-Esquire LC_00050 electrospray ionization mass spectrometer at positive polarity with cap-exit voltage of 167 V. Spectra were recorded in the range of 50-2200 m/z with an acquisition time of between 300 and 900 μs and a potential of between 30 and 70 V. Each spectrum was recorded as a summation of 20 scans.

2.7.6 UV-Vis Spectroscopy:

UV-vis absorption spectra (accuracy: ± 2 nm) were recorded in 10 mm thick quartz cuvettes on a Shimadzu UV-vis-NIR 3100 spectrophotometer interfaced with an Elonex PC466 using UV/Vis data manager. UV-vis spectra of the products obtained after separation with HPLC were carried out with a Varian Cary 50 Scan UV-vis spectrophotometer run under Varian`s Cary WinUV software. Molar

absorption coefficients have an error of +/- 10%. Emission spectra (accuracy ± 5 nm) were recorded at 298 K using a LS50B luminescence spectrophotometer, equipped with a red sensitive Hamamatsu R928 PMT detector, interfaced with an Elonex PC466 employing Perkin-Elmer FL WinLab custom built software. Emission and excitation slit widths were 10 nm. Emission spectra were not corrected for photomultiplier response.

2.7.7 Preparation of Samples for Photo-Catalysis

All samples were used as received, with no further purification. All measurements were performed in air unless otherwise stated. Preparation of sample solutions was carried out in the absence of ambient light, and solutions were wrapped in aluminium foil and carefully sealed to avoid exposure to light, and evaporation. Samples were always prepared fresh, immediately prior to the measurements.

Samples were deoxygenated using Argon with triethylamine (TEA) for about 30 minutes. A ~ $1x10^{-4}$M solution of complexes in Acetonitrile, and in Acetone $1*10^{-4}$ M without TEA/ or with TEA 20 ml of solvent (Acetonitrile, Acetone (20ml) + TEA (sacrificial agent) and took 5 ml sample of above concentration solution for irradiation at 470nm (blue light) (irradiation time).

Figure 2.18 *shows the reactor where the catalytic solutions were irradiated by blue LEDs (470 nm wavelength).*

References:

[1] S.J. Valently, P.E. Behnken, *Anal. Chem.* **1978**, *50*, 834.

[2] B.E. Buchanan, E. McGovern, P. Harkin, J.G. Vos, *Inorg. Chim. Acta* **1988**,154,1.

[3] (a) B.E. Buchanan, R. Wang, J.G. Vos, R. Hage, J.G. Haasnoot, J. Reedijk, *Inorg. Chem.* **1990**, *29*, 3263; (b) H.A. Nieuwenhuis, J.G. Haasnoot, R. Hage, J. Reedijk, T.L. Snoeck, D.J. Stufkens, J.G. Vos, *Inorg. Chem,* **1991**, 30, 48.

[4] (a) R. Hage, R. Prins, J.G. Haasnoot, J. Reedijk, J.G. Vos, *J. Chem. Soc. Dalton Trans.* **1987**, 1389; (b) R. Wang, J.G. Vos, R.H. Schmehl, R. Hage, *J. Am. Chem. Soc.* **1992**, 114, 1964.

[5] W.R. Browne; D. Hesek, J.F. Gallagher, C.M. O'Connor, J.S. Killeen, F. Aoki, H. Ishida, Y. Inoue, C. Villani, J.G. Vos, *Dalton Trans.* **2003**, 2597.

[6] (a) R. Hage, A.H.J. Dijkhuis, J.G. Haasnoot, R. Prins, J. Reedijk, B.E. Buchanan, , J.G. Vos, *Inorg. Chem.* **1988**, 27, 2185; (b) H.P. Hughes, D. Martin, S. Bell, J.J. McGarvey; J.G. Vos, *Inorg. Chem.* **1993**, 32, 4402; (c) R. Hage, J.G. Haasnoot, J. Reedijk, R. Wang, J.G. Vos, *Inorg. Chem.* **1991**, 30, 3263; (d) L. De Cola, F. Barigelletti, V. Balzani, R. Hage, J.G. Haasnoot, J. Reedijk, J.G. Vos, *Chem. Phys. Lett.* **1991**, 178, 491.

[7] (a) H.P. Hughes, J.G. Vos, *Inorg. Chem.* **1995**, 34, 4001; (b) W.R. Browne, C.M. O'Connor, C. Villani; J.G. Vos, *Inorg. Chem.* **2001**, 40, 5461.

[8] J.H. Van Diemen, R. Hage, J.G. Haasnoot, H.E.B. Lempers, J. Reedijk, J.G. Vos, L. De Cola, F. Barigelletti, V. Balzani, *Inorg. Chem.* **1992**, 31, 3518.

[9] W.R. Browne, N.M. O'Boyle, W. Henry, A.L.. Guckian, S. Horn, Fett, T.; O'Connor, C.M.; Duati, M.; De Cola, L.; Coates, C.G.; Ronayne, K.L.; McGarvey, J.J. J.G. Vos, *J. Am. Chem. Soc.* **2005**, 127, 1229.

[10] A. Mangia, M.T. Lugari, *J. Liq. Chromatogr. Rel. Techn.* **1983**, 6, 1073.

[11] S.Fanni, T.E. Keyes, C.M. O'Connor, H. Hughes, R. Wang and J.G. Vos. *Coord. Chem. Rev*. **2000**, 208, 77-86.

[12] (a) H. Zhang, C.S. Rajesh, P.K. Dutta, *J. Phys. Chem. A* **2008**, *112*, 808; (b) M. Thomalla, H. Tributsch, *Compt. Rend. Chimie* **2006**, *9*, 659; (c) Y. Cho, Y. Park, W. Choi, *J. Ind. Eng. Chem.* **2008**, 14, 315.

[13] (a) P. Passaniti, W.R. Browne, F.C. Lynch, D. Hughes, M. Nieuwenhuyzen, P. James, M. Maestri, J.G. Vos, *J. Chem. Soc. Dalton Trans.* **2002**, 1740; (b) W.R. Browne, C.M. O'Connor, H.P. Hughes, R. Hage, O. Walter, M. Doering, J.F. Gallagher, J.G. Vos, *J. Chem. Soc. Dalton Trans.* **2002**, 4048.

[14] J.G. Vos, J.M. Kelly, *Dalton Trans.* **2006**, 4869.

[15] (a) S. Rau, B. Schaefer, D. Gleich, E. Anders, M. Rudolph, M. Friedrich, H. Goerls, W. Henry, J.G. Vos, *Angew. Chem. Int. Ed.* **2006**, 45, 6215; (b) B. Gholamkhass, H. Hiroaki Mametsuka, K. Koike, T. Tanabe, M. Furue, O. Ishitani, *Inorg. Chem.* **2005**, *44*, 2326; (c) S. Sato, K. Koike, H. Inoue, O. Ishitani, *Photochem. Photobiol. Sci.* **2007**, 6, 454.

[16] W. R. Brown, *HPLC and CE Principles and Practice*, USA, **1997**.

[17] L. R. Snyder, J. L. Glajch, J. J. Kirklan, *Practical HPLC Method Development* second edition Wiley & Sons, USA **1997**.

[18] D. A. Skoog, D. M. West, F. J.Holler, *Fundamental of Analytical Chemistry*, seventh edition, USA, **1996.**

[19] M. W. Dong, Modern HPLC for Practicing Sciences, Wiley & Sons, USA, **2006.**

[20] K. Unger, Packings and Stationary Phase in Chromatographic Techniques (*Chromatographic Science*), Marcel Dekker, New York, **1990**.

[21] K. Unger, Porous Silica , *Journal of Chromatography Library*, Volume 16, Elesevier Scientific Publishing Co., New York, **1979**.

[22] D. A. Wellings, A Practical Handbook of Preparative HPLC, Elsavier Ltd **2006**.

[23] J. Barnes, *High Performance Liquid Chromatography,* John Wiley & Sons **1992**.

[24] A. Pryde, J*. Chromatographie. Sci*., **1974**, 12, 438.

[25] D. C. Harris, *Quantitative Chemical Analysis*, seventh edition,. W. H. Freeman & Company. USA, **2007**.

[26] *Ion Exchange Chromatography Principle and methods*. Handel Book Amersham Biosciences.**2004**.

[27] D. A. Skoog, F. J. Holler, T. A. Nieman, *Principles of Instrumental Analysis*, fifth edition. , USA, **1998**.

[28] R. E. Majors and M. J. Hopper, J**.** *Chromatography. Sci*., **1974**, 12, 974.

[29] S. Ahuja, *Chromatography and Separation Science*, V4, **2003**.

[30] S. Meyer, D. Tietze, S. Rau, B. Schäfer, G. Kreisel, *Journal of Photochem and Photobio A: Chemistry*, ***2007***, *186, 248*.

CHAPTER 3

The Separation of the two Stereoisomers of Dinuclear $[(Ru(bpy)_2)_2(bpt)](PF_6)_3$

3.1 Introduction

Extensive studies have been reported on the synthesis, electrochemical, photochemical and photophysical properties of ruthenium (II) complexes with chelating ligands such as pyridyltriazoles and pyrazinyltriazoles.[1, 2] In the asymmetric triazole containing ligands two different coordination sites are in principle available for coordination to the $Ru(bipy)_2$ moiety, namely the N2 and N4 atoms of the triazole ring. See Figure 3.1

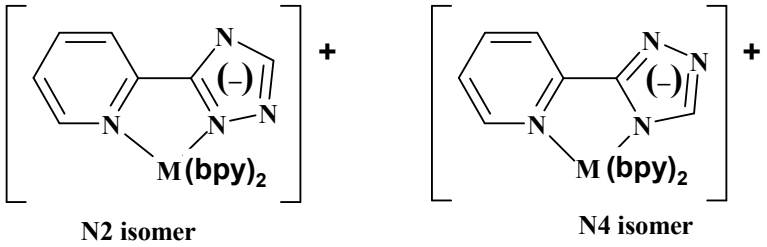

***Figure 3.1**. N2 and N4 coordination isomers for pyridine triazole ligands.*

Interestingly, there are substantial differences in the electrochemical and excited state properties of the two isomers and also in their ground state and in the excited state acid-base properties.

A series of mononuclear complexes of $Ru(bpy)_2$ and pyridine-2-yl-1,2,4-trazoles has been prepared and characterized by ^1H , ^{13}C NMR spectra . The ligands have been used in this study are shown in Figure 3.2 [2], the coordination modes has an influence on the electronic and electrochemical properties due to the π-acceptor property of the ligand. Coordination to the triazole ring can occur through either the N2 or the N4 atom. The proton NMR of the compounds has confirmed a *cis* geometry of all compounds.

It has also been reported that the triazole ring in HL^3 is bound through N2 atom while that in L^4 through the N4 atom, and the triazole ring in L^1 through the N2 atom. For the L^5 only one chelating co-ordination has been assumed namely through the pyridine nitrogen and N2.

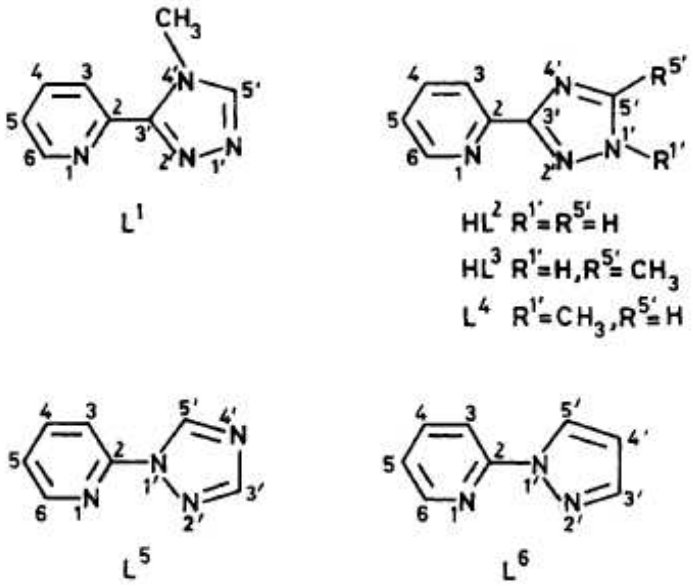

Figure 3.2 *Structures of ligands L^1,HL^2,HL^3,L^4,L^5 and L^6 Ref [2].*

Moreover, the electrochemical data suggested that all the ligands except L^5 are weaker π-acceptor than bpy. Deprotonation of HL^2 and HL^3 complexes leads to a shift to lower energy of the MLCT band. This was explained by an increase of the σ-donor properties of the deprotonated ligand. All compounds with deprotonated ligands do emit at room temperature [2].

Synthesis of mono- and dinuclear $Ru(bpy)_2$ complexes with 3,5-bis-(pyridin-2'-yl)-1,2,4-triazole (Hbpt) were reported by Hage and Vos [3]. Two isomers of the dinuclear compound were suggested for a typical example see Figure 3.3.

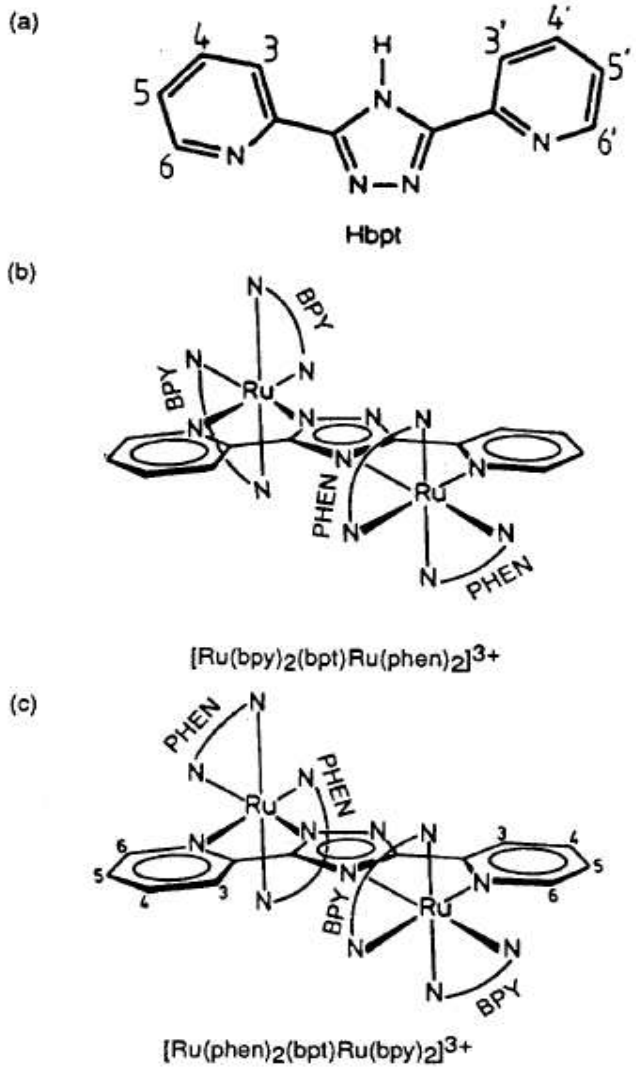

Figure 3.3 *Structure of (a) 3,5-bis(pyridin-2-y1)-1,2,4-triazole and two coordination isomers of the dinuclear ruthenium compounds. b) $[Ru(bpy)_2(bpt)Ru(phen)_2](PF_6)_3$ and (c) $[Ru(phen)_2(bpt)Ru(bpy)_2](PF_6)_3$ [4].*

This was confirmed using NMR studies. A strong metal-metal interaction in this compound was observed which is facilitated by the negative charge on the bridging triazole ligand.

The photophysical and photochemical properties of mononuclear and dinuclear complexes of Ru(II) containing bpy as a terminal ligand and bpt as a bridging ligand were also investigated. The mononuclear compound exhibits an

emission and absorption bands at λ_{max}= 480 nm and λ_{max}=678 nm, respectively. While the dinuclear complex exhibits absorption and emission bands at λ_{max}= 453 nm and λ_{max}= 648 nm, respectively. Because of the σ-donor ability of bpt^- causes an increase in the electronic charge of the Metal-Ligand-Charge transfer (Ru-bpy) absorption and emission bands coordination of a second metal centre to the bpt^- results in a blue shift of the MLCT [5]. Resonance Raman spectroscopy studies suggested that MLCT is a bpy-based and not bpt based in the compound as the bpy ligand vibrations dominated rR spectra of the complex [6]. The photolysis of the dinuclear compound results in the formation of the mononuclear complex and $[Ru(bpy)_2Cl_2]$ [5]. This result in turn indicates that photoreaction takes through population of a ^3MC level centred on the Ru-bpy unit attached to the N4 position [7].

Dinuclear mixed polypyridyl compounds containing both phen and bpy have also been reported. The aim of those reports was to use these dinuclear complexes to investigate the differences between the photophysical properties of bpy and phen. In these complexes $Ru(bpy)_2$ and $Ru(phen)_2$ can be coordinated in a controlled manner to either to N1 and N4 site yielding $[Ru(bpy)_2(bpt)Ru(phen)_2]^{3+}$ and $[Ru(phen)_2(bpt)Ru(bpy)_2]^{3+}$, Figure 3.3

The rR spectroscopy and electrochemical studies have confirmed that the lowest emitting state in the compounds is bpy-based [7]. Five photoproducts have been obtained from these complexes. Using UV-Vis and HPLC analysis, these products were identified as $[Ru(phen)_2Cl_2]$, $[Ru(bpy)_2Cl_2]$, and $[Ru(bpy)_2(MeCN)Cl]^{3+}$, and another two bpt^- - containing mononuclear

complexes. This shows that decomposition occurs at both the N2 and the N4 positions in the dinuclear compound.

Heteronuclear Ruthenium-Osmium complexes with asymmetric triazolate bridge were also reported by Haasnoot and Vos [5,6] heteronuclear compounds $[(bpy)_2Ru(bpt)Os(bpy)_2](PF_6)_3$ (RuOs) and $[(bpy)Os(bpt)Ru(bpy)_2](PF_6)_3$ where synthesized and characterized using NMR and X-Ray analysis. The two metal centres are coordinated via N(1) and N(4) of the triazole ring, the ruthenium is coordinated via N(1), whereas Osmium binds via N(4) of triazole with similar metal-nitrogen distances as observed for the ruthenium homonuclear complexes, Figure 3.3

The NMR data confirmed that the OsRu isomer has a similar structure to RuOs except in the former the osmium bound via N(1) and ruthenium is coordinated via N(4) of the triazole ring. The electrochemical data showed that the oxidation potentials of the differences in the oxidation potentials of the mixed-metal complexes (RuOs) and (OsRu) gives information about the influence of the different coordination sites of the bridging triazole ligand. If both coordination sites are equivalent then the oxidation potentials of both dinuclear complexes should be the same. The results obtained in that report confirmed that the oxidation potentials of the mixed-metal complexes (RuOs) and (OsRu) are quite different. In (RuOs) the osmium ion bound via N4 of the triazole ring is oxidized at 0.73 V while in (OsRu) the osmium ion is bound to N1 and subsequently is oxidized at lower potential of 0.65 V. In the RuOs dinuclear compound the N1-bound ruthenium ion is oxidized at at 1.2 V while in OsRu the N4-bound ruthenium ion is oxidized at 1.3 V.This has been explained by assuming that N1 of the triazole ring is better a σ-donor that the N4 atom

As interest in both polynuclear and asymmetric ruthenium(II) complexes increases, so does the issue of isomerism, in terms of both connectivity [1] and stereochemistry [8]. Since through-space interactions are often as significant as through bound interactions. Obtaining inorganic complexes with well defined spatial and electronic structures is viewed as a necessity for the successful development of molecular devices [10]. It has been recognized for some time that the use of bidentate ligands results in formation of stereoisomers. For example, Keen and co-workers have reported differences in luminescence lifetimes between the hetero-and homochiral isomers for the dinuclear $[Ru(bpy)_2)_XHAT]^{2x+}$ complexes [9]. (where x = 1-3, LL = 2,2`-bipyridine or 1,10-phenanathroline, and HAT = 1,4,5,8,9,12-hexaazatriphenylene) and for the charge separated state of a series of four geometric isomers of a ruthenium(II) mononuclear chromophore quencher system [9].

Browne *et al.* have reported the separation of the four stereoisomers of the complex $[(Ru(bpy)_2)_2bpt](PF_6)_3$ (See Figure 3.4) [10]. For mononuclear metal complexes the chiral compounds that can in principle be obtained are either Δ or Λ. However in dinuclear compounds such as the complexes studied in this chapter, both metal centres have their own stereochemistry and as a result heterochiral species such as $\Delta\Lambda$ can be obtained. It is furthermore important to note here that, as already pointed out in the introduction, the N2 and N4 coordination sites of the bridging ligand are not identical. As a result two rather than one heterochiral species are obtained.

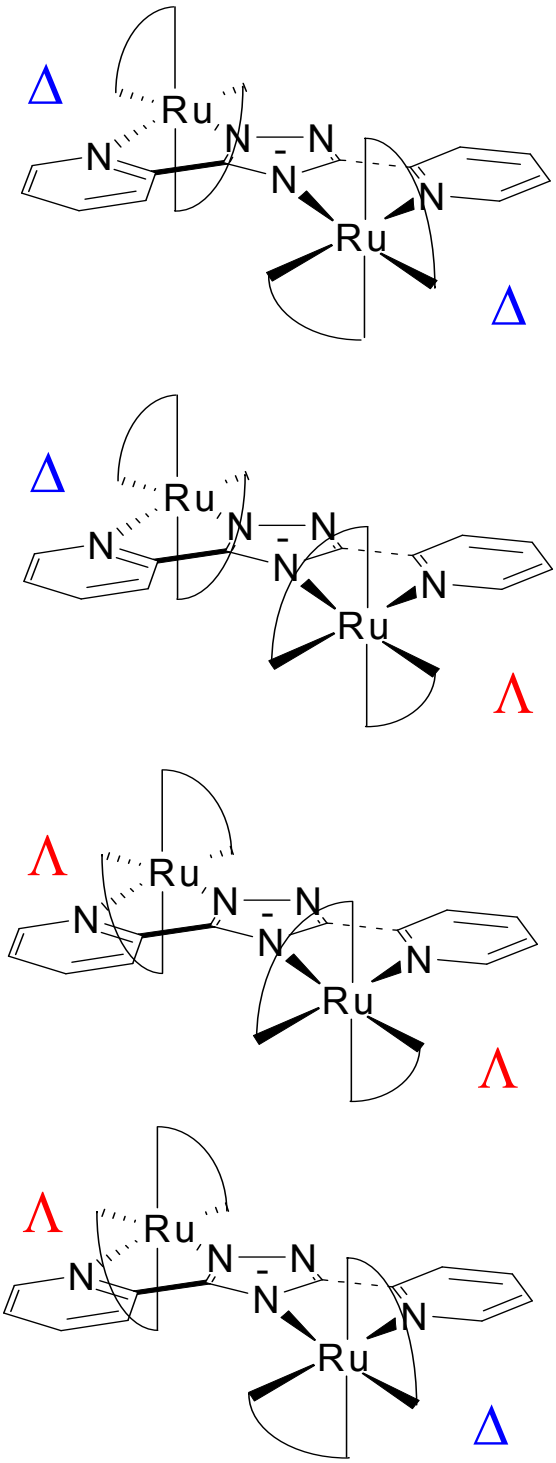

Figure 3.4 *The four possible stereoisomers of* $[Ru(bpy)_2)_2bpt]^{3+}$.

If the bridging ligand is symmetrical the ΔΛ and ΛΔ isomers are the same but because of the asymmetry in the bpt bridging ligand, they are not. The ^{1}H NMR

spectra and photophysical properties of these four stereoisomers reported in this reference showed very little difference.

The interest in the photochemistry of such binuclear systems is based on their possibility of having *intramolecular* transfer of excitation and/or charge between the metal centres [11] upon irradiation at the frequencies of metal-to-ligand charge transfer (MLCT) transitions. In this framework $\{[Ru(bpy)_2]_2L\}^{3+}$ complexes can be considered as supramolecular systems the metal centres of which display different functions in photoactivated processes [12]. A detailed study of their photophysical and photochemical behaviour is therefore of great importance.

Surprisingly HPLC analysis in $[Ru(bpy)_2]_2(bpt)](PF_6)_3$ (**1**) [bpy = 2,2'-bipyridyl, Hbpt = 3,5-bis-(pyridin-2'-yl)-1,2,4-triazole], with a standard cation exchange column shows the presence of two fractions; A and B. These two species have been analysed with ^{1}H-NMR and UV/vis spectroscopy and each constituted an enantiomeric pair and together form the set of chiral compounds shown in Figure 3.4.

In this chapter, the photochemical behaviour of the enantiomeric pairs of the $[(Ru(bpy)_2)_2bpt](PF_6)_3$ complex, is reported. The resultant photochemical ligand exchange reactions are also considered.

3.2 Experimental Section

3.2.1. Materials

The synthesis and purification of $[(Ru(bpy)_2)_2(bpt)](PF_6)_3$. 1 where (bpy = 2,2`-bipyridine, Hbpt = 3,5- bis(pyridine-2-yl)-1H-1,2,4-triazole) where carried out using previously reported methods. [1] All solvents employed were of HPLC grade or better and used as received unless otherwise stated. Water was prepared with water purification System model Milli-Q (Millipore, Bedford, MA, USA). All samples were filtered through Nylaflo® nylon membrane filter units of 0.45 μm pore diameter (Millipore). All mobile phases were degassed prior to use.

3.2.2. High Performance Liquid Chromatography

The separation of the stereoisomers was carried out on using a semi preparative method, as described in Chapter 2.

The conditions used for the separation are as follows. The mobile phase used was CH_3CN: H_2O: CH_3OH with volume ratio 75:15:10 containing 0.12 M KNO_3) with at a flow rate of 4 cm^3 min^{-1}. The detection wavelength used was 280 nm. Two fractions were collected. The first contained isomer one (fraction A), and the second isomers two contained isomer 2 (fraction B). The separation process and the characterisation of the products obtained were carried out using ^1H-NMR, UV/vis spectroscopy, and HPLC techniques. See Chapter 2 for further experimental techniques and details**.**

3.3 Results and Discussion

3.3.1 Separation of Isomers

The chromatogram obtained upon injection of a $\{[Ru(bpy)_2]_2\ bpt\}^{3+}$ sample as obtained from the literature synthesis is shown in Figure 3.4 below. The trace shows the presence of species with the main compounds having retention times of 6.0, 15.2, 16.2 and 19.2 minutes, something generally observed when unpurified samples of the dinuclear compound are analysed by HPLC. The species observed at about 5 min has been identified by UV/Vis and ^1H NMR spectroscopy as the mononuclear $[Ru(bpy)_2bpt]^+$ species by comparison with a separately prepared sample and has a lowest energy absorption maximum of 465 nm. The main fraction with a retention time of around 15 minutes shows two fractions with very similar peak area. The two main fractions were isolated by semi-preparative HPLC as shown in Figure 3.5. The spectral features of these two peaks are identical as shown in Figure 3.7. These species were further purified by additional semi-preparative techniques as shown in Figure 3.6 and 3.8. The compounds obtained were further characterised by ^1H NMR spectroscopy as shown below in the ^1H NMR spectra in Figure 3.9.

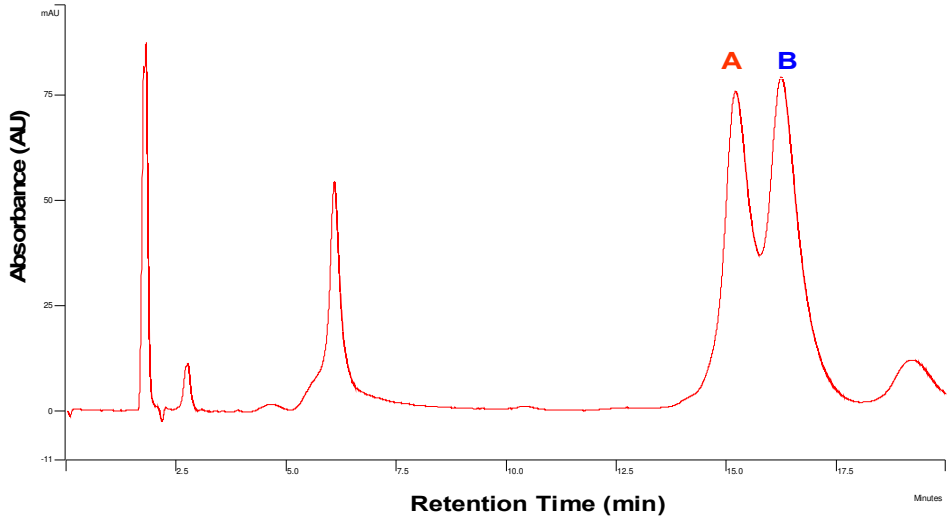

.

Figure 3.5. *HPLC trace for impure {[Ru(bpy)$_2$]$_2$ bpt}$^{3+}$ in CH_3CN (mobile phase CH_3CN: H_2O: CH_3OH with volume ratio 75:15:10 containing 0.12 M KNO_3). Flow rate: 2.0 cm^3 min^{-1}; detection wavelength at 280 nm.*

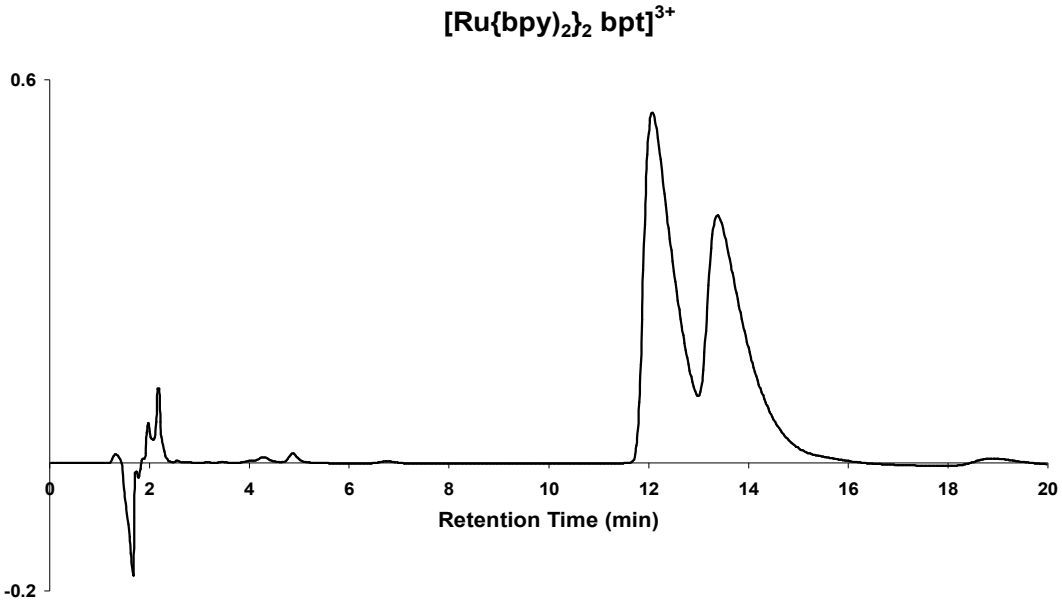

Figure 3.6 *Chromatogram taken after first purification step of {[Ru(bpy)$_2$]$_2$ bpt}$^{3+}$ (mobile phase CH_3CN: H_2O: CH_3OH with volume ratio 75:15:10 containing 0.12 M KNO_3). Flow rate: 2.0 cm^3 min^{-1}; detection wavelength at 280 nm.*

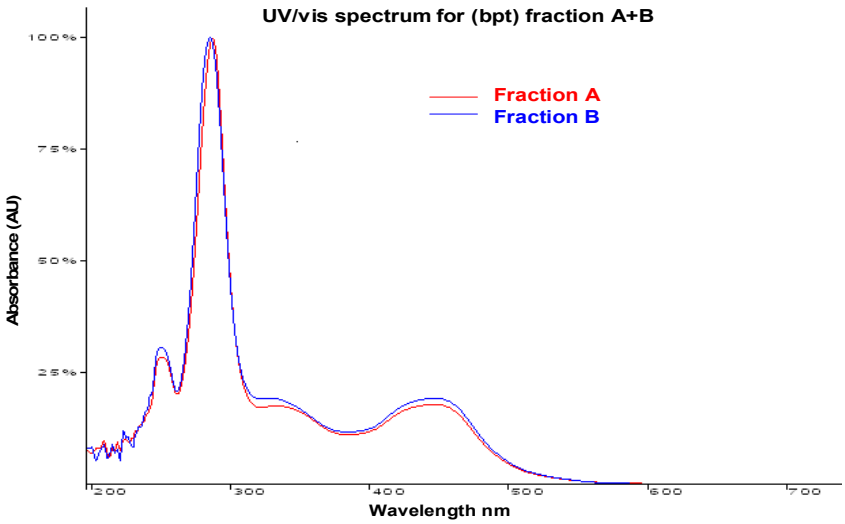

Figure 3.7 *UV/vis spectra for fraction A and B shown in Figure 3.5.*

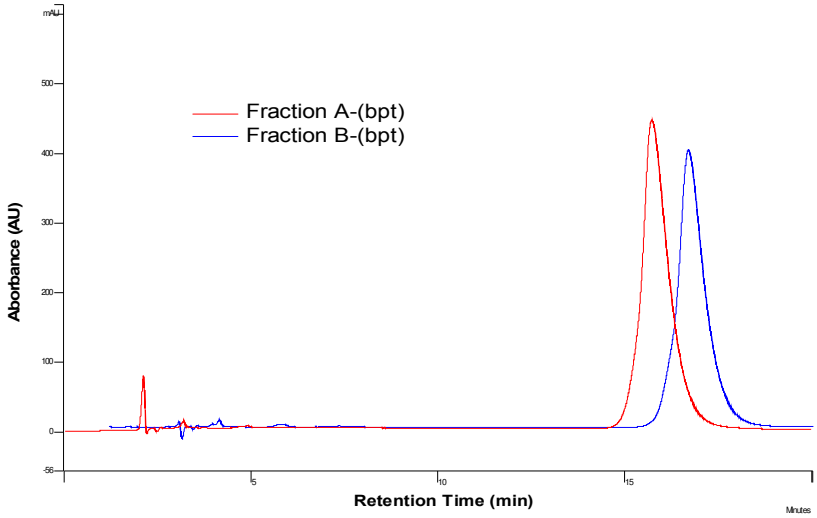

Figure 3.8 *HPLC trace for fraction A and B taken after second semi-preparative purification step of* $\{[Ru(bpy)_2]_2\ bpt\}^{3+}$ *(mobile phase* CH_3CN*:* H_2O*:* CH_3OH *with volume ratio 75:15:10 containing 0.12 M* KNO_3*). Flow rate: 2.0* $cm^3\ min^{-1}$*; detection wavelength at 280 nm*

The absorption spectra shown in Figure 3.7 are in agreement with those reported in earlier investigations for bpt based dinuclear compounds [3]. The complexity of the ^1H NMR spectra shown does not allow for their detailed interpretation. The spectra obtained for the different fractions are, however, different in some important details, such as the doublets observed around 6.5

ppm. The value obtained for Fraction B is at about 6.45 ppm while for fraction A a value of 6.55 ppm is observed. Comparison with literature [10] data shows that the homochiral ΔΔ and ΛΛ species have the same ^{1}H NMR spectra while also the two heterochiral species show the same spectra. On the basis of these observations fraction A can be assigned to a mixture of the homochiral species while fraction B contains the heterochiral isomers. For structures see Figure 3.4. With the present column it was not possible to separate these isomers any further. In order to do that, chiral columns have to be used [10].

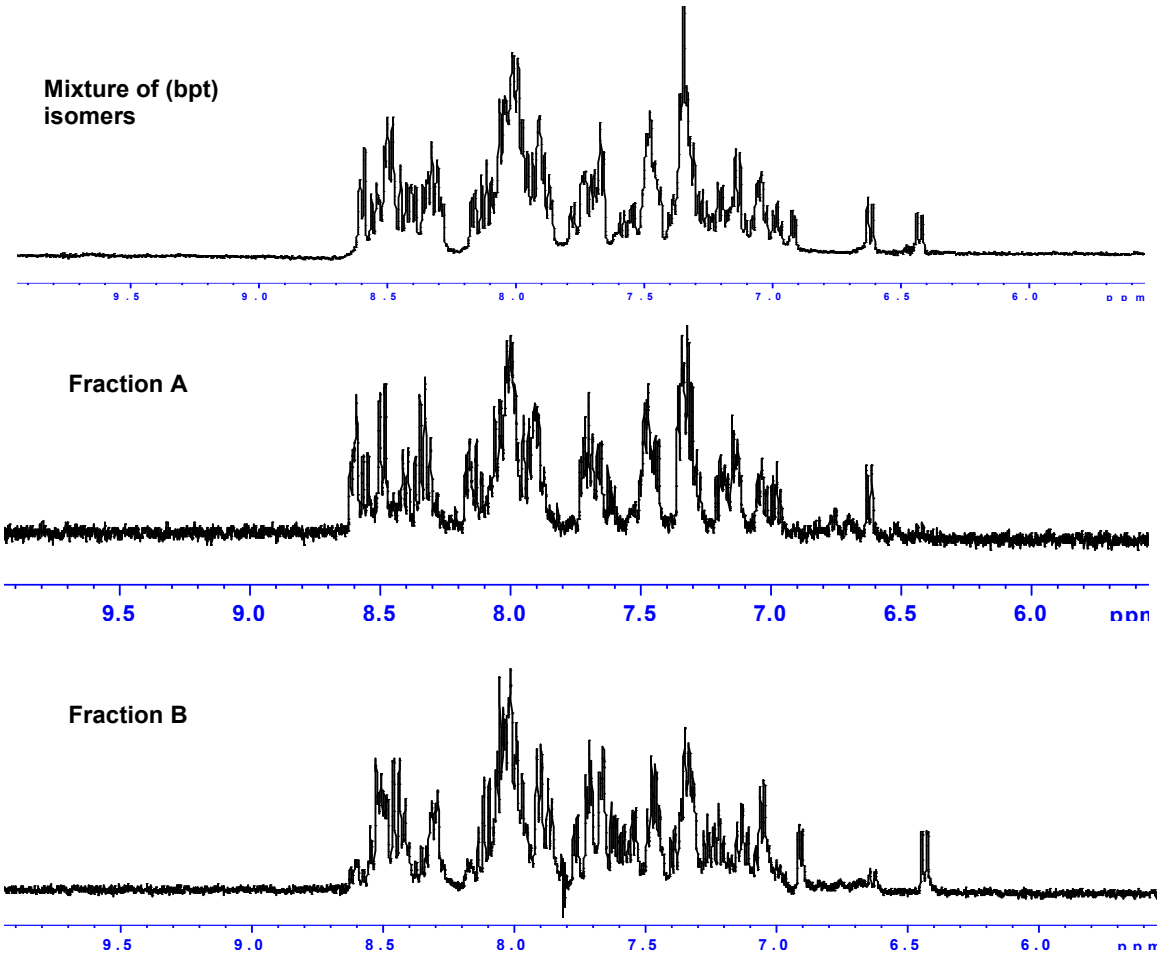

Figure 3.9 *^{1}H-NMR spectra obtained of the fractions A, B and the mixture of ruthenium compounds in d_3 acetonitrile.*

It is interesting that the cation exchange column used is able to separate the two enantiomeric pairs. As discussed already in the introductory chapter irradiation of the compounds lead often to ligand loss. Very little is however known about the actual behaviour of the different chiral isomers. In the next section we investigate the photochemical behaviour of the two enantiomeric pairs the homochiral ΔΔ and ΛΛ (Fraction A) and the heterochiral species ΔΛ and ΛΔ (Fraction B). For simplicity the terms Fraction A and B are used in the manuscript rather than using the chiral labels.

3.3.2 Photolysis of Fraction A in Acetonitrile.

Both Fractions were photolysed in acetonitrile. The photochemical processes were followed by UV/Vis spectroscopy and HPLC. The results obtained with UV/Vis spectroscopy are shown in Figure 3.15.

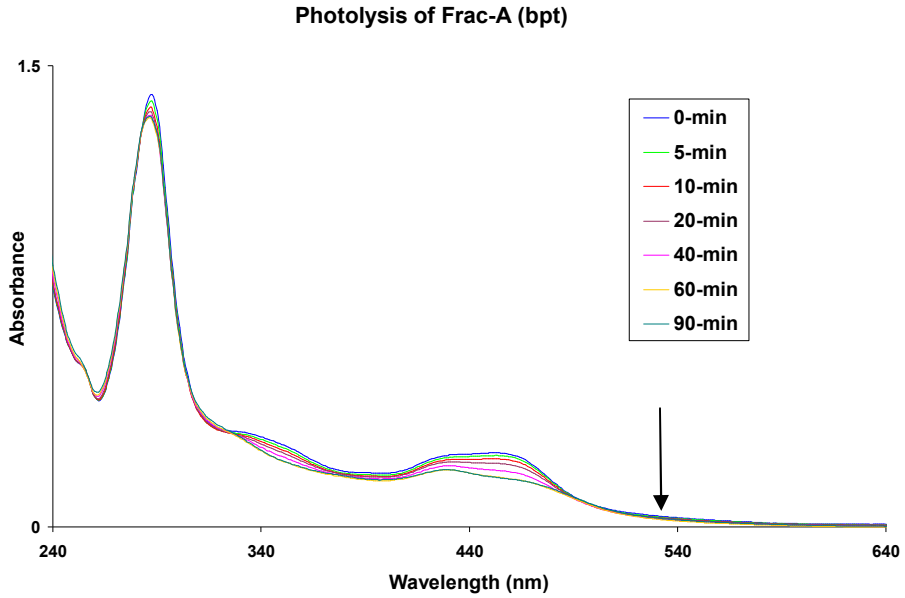

Figure 3.10 *UV/vis obtained during photolysis of fraction A in CH_3CN*

The absorption features observed are located over a large range of the UV/vis spectrum starting at approximately 550 nm. Two distinct peaks were observed. These peaks were located in the 420-450 and 280-290 nm regions. The assignments for the absorption bands were made on the basis of the well documented electronic transitions in $[Ru(bpy)_3]^{2+}$ [5,6]. The absorption between 420-450 nm were assigned to metal-to ligand charge transfer (MLCT) transitions ($d\pi \rightarrow \pi^*$) (bypyridine)). The second transition higher energy (280-290 nm) were assigned to ligand centred charge transfer, which were consistent with other reported LC ($\pi \rightarrow \pi^*$) transitions for these type of complexes. Figure 3.10 shows a shift of the absorption maximum with increasing irradiation time, with the maximum moving from about 450 to 425 nm. The UV/vis spectrum changes in several ways. The $\pi \rightarrow \pi^*$ (bpy) bands at 280-290 nm lose some intensity but not significantly shifted. Irradiation caused a shift of the absorption maximum of the reaction solution from 451 to 424 nm. The absence of a set of isosbestic points in the UV/vis spectra suggested the formation of more than one product. The change of the MLCT ($d\pi \rightarrow \pi^*$) from 451 nm to 424 nm is consistent with the photolysis leading to the loss of the (bpt) ligand with subsequent replacement by CH_3CN. This suggests that the end product of the reaction is $[Ru(bpy)_2(CH_3CN)_2]^{2+}$. Since the absorption spectra observed for the different chiral compounds are the same, UV/Vis spectroscopy is not expected to provide information about a possible change in the chirality of the species. Therefore HPLC experiments were carried out to obtain further information and the HPLC traces obtained for the photolysis of fraction A in acetonitrile are shown in Figure 3.11.

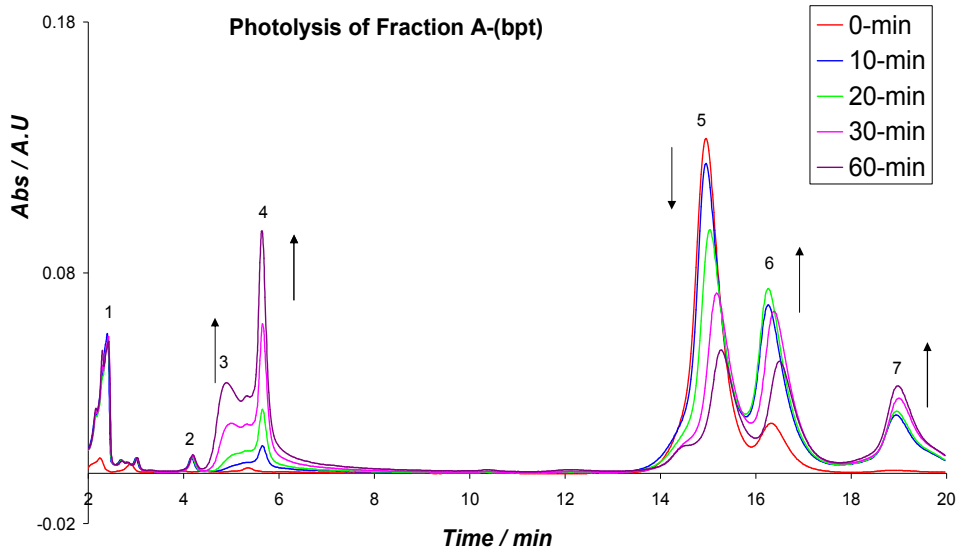

***Fig 3.11**. HPLC trace during Photolysis of fraction A of {[Ru(bpy)$_2$]$_2$ bpt}$^{3+}$ in CH_3CN. (mobile phase CH_3CN: H_2O: CH_3OH with volume ratio 75:15:10 containing 0.12 M KNO_3). Flow rate: 2.0 cm^3/min^{-1}; detection wavelength at 280 nm.*

The UV/Vis spectra of the main photoproducts present after 30 minutes of irradiation are shown in Figure 3.12 and 3.13.

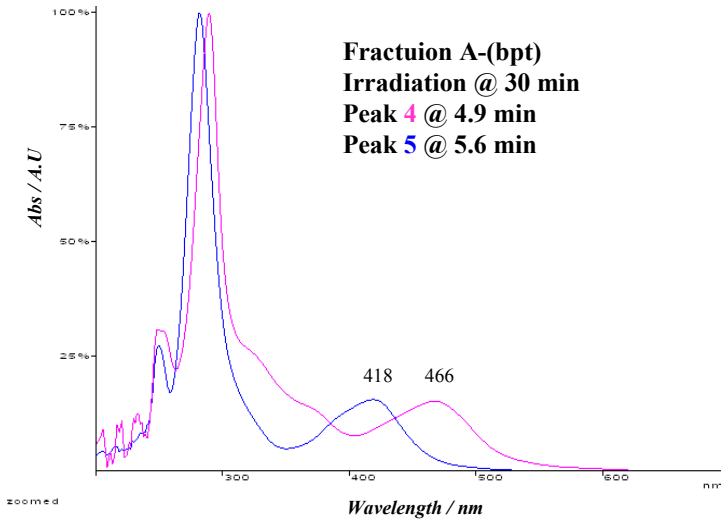

***Fig 3.12** UV/vis spectrum of the products of the Irradiation of fraction A of {[Ru(bpy)$_2$]$_2$ bpt}$^{3+}$ Irradiation time 30-minutes. Red trace, retention time 4.9 min, Blue trace 5.6 min.*

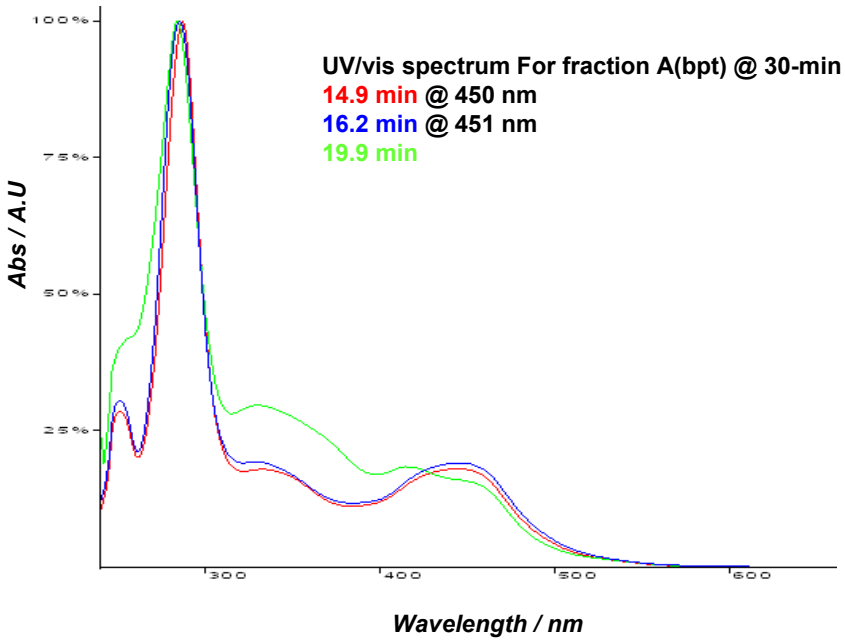

Figure 3.13 *UV/vis spectrum of the products of the Irradiation of fraction A of* $\{[Ru(bpy)_2]_2\ bpt\}^{3+}$ *Irradiation time 30-minutes. Red trace; retention time 14.9 min, blue 16.2 min and green 18.9 minutes.*

From these traces and the corresponding UV/Vis spectra 4 main photoproducts can be observed after 30 min of the photolysis of fraction A. The starting material fraction A has a retention time of 14.9 min and a λ_{max} of 451 nm. The product with a retention time of 5.6 min and an absorption maximum of 422 nm was identified as $[Ru(bpy)_2(CH_3CN)_2]^{2+}$, secondly peak 4 which was assigned as $[Ru(bpy)_2bpt]^{+}$, with an λ_{max} of 466 nm and a retention time 4.9 min. A further photoproduct with a retention time 16 min at same λ_{max} 451 nm was obtained which can be identified as fraction B by its spectral features and its retention time. Finally a last product with a retention time of 19.0 min has been tentatively assigned to the species $[Ru(bpy)_2]_2bpt\ (CH_3CN)]^{+}$ where the bpt ligand is bound in a monodentate fashion. This species will be discussed below in more detail together with a more detailed overview of the photoinduced processes observed. At this stage it is important to note that transformation

from the homochiral to the heterochiral species is obtained and that this transformation seems faster than photolabilisation of ligands.

3.3.3 Photolysis of Fraction B in Acetonitrile

The heterochiral set of isomers, fraction B, was also studied in acetonitrile using both UV/Vis spectroscopy and HPLC. The data observed for the spectroscopic studies are shown in Figure 3.14. A typical set of HPLC traces is shown in Figure 3.15.

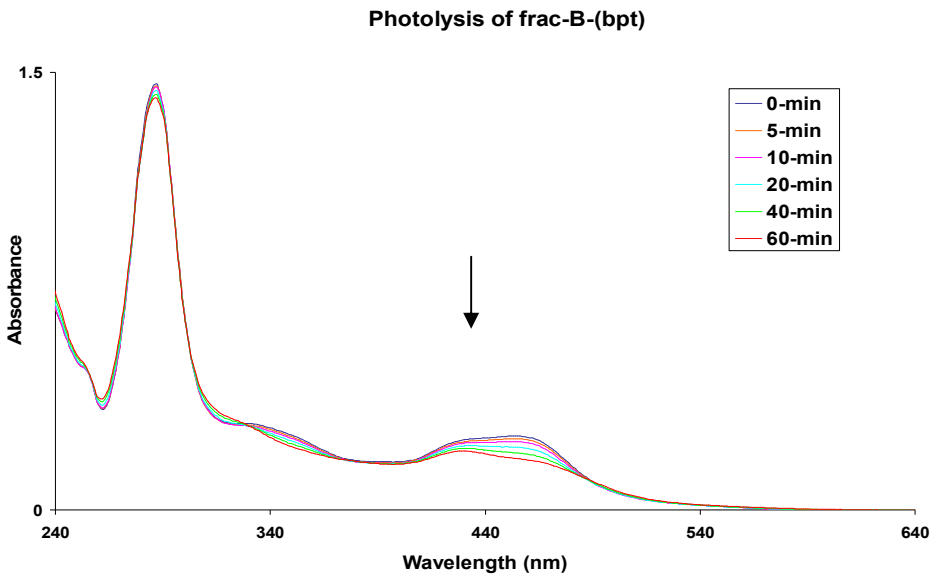

Figure 3.14 *UV/vis spectra during photolysis for fraction* ***B*** *in* CH_3CN

Figure 3.14 shows that, as already observed for fraction A, little detail can be obtained from the UV/Vis analysis of the photochemical reaction concerning the nature of the products observed. The features observed are very similar to those obtained for fraction A. Again HPLC shows to be better suited for the analysis of the photoinduced processes observed as shown in Figure 3.15.

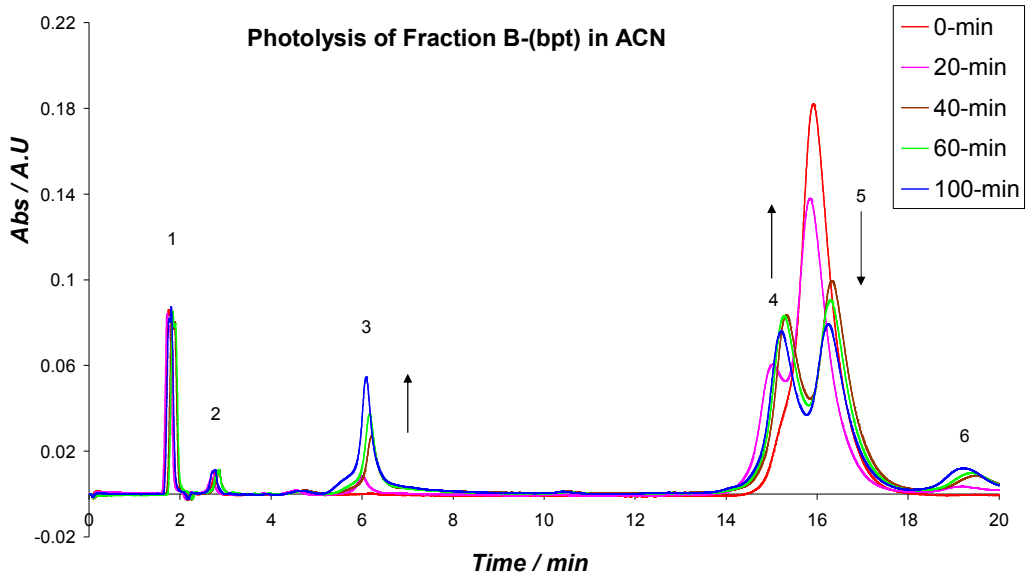

Figure 3.15 *HPLC trace during Photolysis of Fraction* ***B*** *in CH_3CN, (mobile phase CH_3CN: H_2O: CH_3OH with volume ratio 75:15:10 containing 0.12 M KNO_3). Flow rate: 2.0 cm^3 min^{-1}; detection wavelength at 280 nm.*

The photolysis of fraction B was carried out under the same conditions as that of fraction A. Although the processes observed are similar there are some differences. As observed for fraction A isomerisation between A and B fractions is observed, with in this case the formation of fraction A from fraction B. The process seems slower and both sets of chiral species is still present in appreciable amounts after 100 min. This increased stability is reflected in the reduction in the formation of further photoproducts such as $[Ru(bpy)_2bpt]^+$ or $[Ru(bpy)_2\ (CH_3CN)]^{2+}$ (retention time 6.2 min) as observed for fraction A. It needs to be pointed out however that the solution used for the irradiation is slightly more concentrated than in the experiments carried out with fraction A (see peak heights at time = 0 min). Nevertheless some qualitative observations can be made, although the effect of concentration cannot be ruled out. A slow increase of a series of species with a retention time of 6 min is observed. The

peak is asymmetric and therefore contains more than one component. Only one clear spectrum can be identified for this peak and this has an absorption maximum of 422 nm, which suggests the presence of the bis acetonitrile complex $[Ru(bpy)_2(CH_3CN)_2]^2$. The second spectral feature observed is very weak but similar. These two species may be related and can possibly be assigned as the N2 (retention time 4.7) and N4 isomers (5.7 min) of the mononuclear $[Ru(bpy)_2bpt]^+$ species. Finally a species at a retention time of 19.4 min is also observed and is again assigned to an intermediate containing a monodentate coordinated bpt ligand as already mentioned for fraction A and this species will be discussed in more detail below.

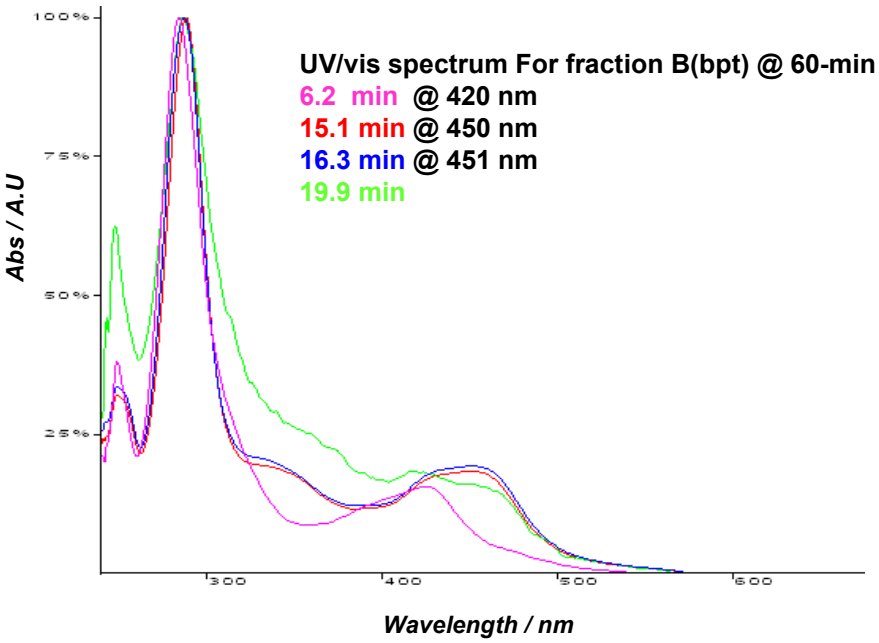

Figure 3.16 *UV/vis spectrum of the products after 60 min of the Irradiation of* $\{[Ru(bpy)_2]_2bpt\}^{3+}$ *For fraction* ***B****. 6.2 min pink 420 nm,* $[Ru(bpy)_2(CH_3CN)_2]^{2+}$ *, 15.1 min red 450 nm, 16.3 min blue 451 nm (fractions A and B) 19.9 min green* $Ru(bpy)_2(bpt)(CH_3CN)]^+$

So again photoinduced transformations are observed which are at short time scale related to the rearrangement rather than loss of ligand and suggest changes in the nature of the chiral species present.

3.3.4. Photolysis of Fraction A

To investigate this proposal further the photolysis was also followed by NMR spectroscopy to try to uncover the nature of the species produced. Figure 3.18 shows the evolution of the HPLC data of the sample during its irradiation in D_3-CH_3CN.

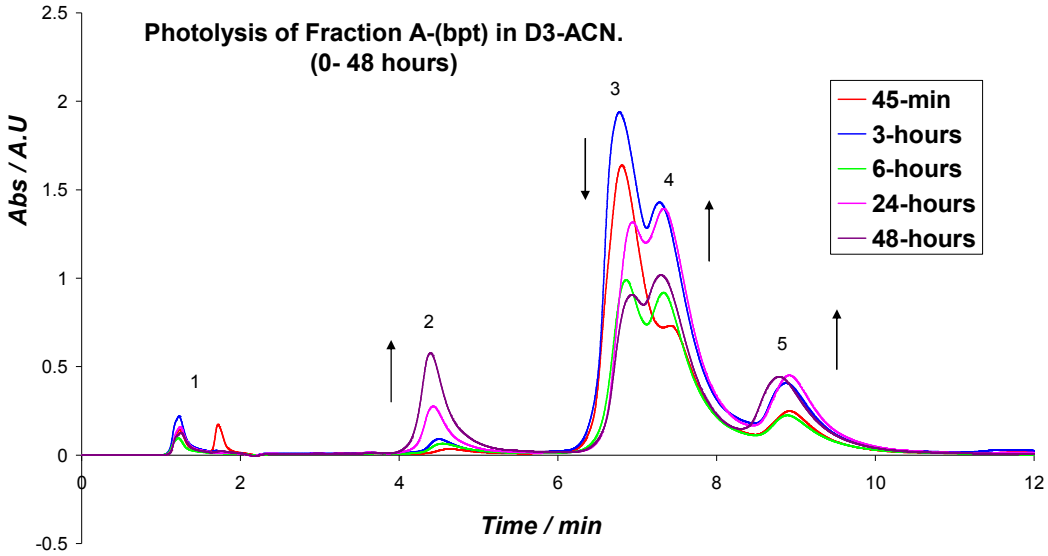

Figure 3.17 *HPLC trace during photoreactions of Fraction* ***A****, in deuteriated acetonitrile. Mobile phase ACN/H_2O (80/20 v/v) 0.12 M KNO_3, Flow rate: 4.0 cm^3 min^{-1}; detection wavelength at 280 nm.*

Note that a different mobile phase is used, this results in shorter retention times. In addition, the sample was irradiated in an NMR tube at much higher concentrations to achieve the concentration of the products necessary for NMR

spectroscopy. As a result it is clear from these traces that the irradiation times are considerably longer. The results obtained are however comparable with those obtained at lower concentrations as discussed above. The major products are peaks 2 and 5, with retention times of 4.5 and 8.9 respectively. The absorption features obtained for these peaks (not shown) are in agreement with those obtained at lower concentrations and suggest the formation of a mixture of $[Ru(bpy)_2bpt]^+$ and $[Ru(bpy)_2(CH_3CN)_2]^{2+}$ at about 4.5 min and $[(Ru(bpy)_2)_2bpt(CH_3CN)]^{3+}$ at 8.9 min. but mainly the isomerisation from Fraction A to fraction B.

The HPLC data observed for the experiment with fraction B are very much in agreement with those shown for fraction A. Increased concentrations give rise to longer irradiation times and slower decomposition of the compounds

The ^1H NMR spectra taken during the photolysis are shown below in Figures 3.18 and 3.19. As pointed our earlier (See Figure 3.9) fraction A can be identified by a doublet at 6.55 ppm, while in the spectrum obtained for fraction B this proton is observed at 6.45 ppm. In the spectrum obtained after 9 hours of irradiation the growth of a signal at 6.45 ppm is observed. This is an indication of the formation of fraction B but at longer irradiation times other processes are observed as well. The growing of signal at about 9.5 ppm is particularly evident. This resonance is most likely explained by the interaction of an H6 proton of a bpy ring with a non-aromatic ligand [13].

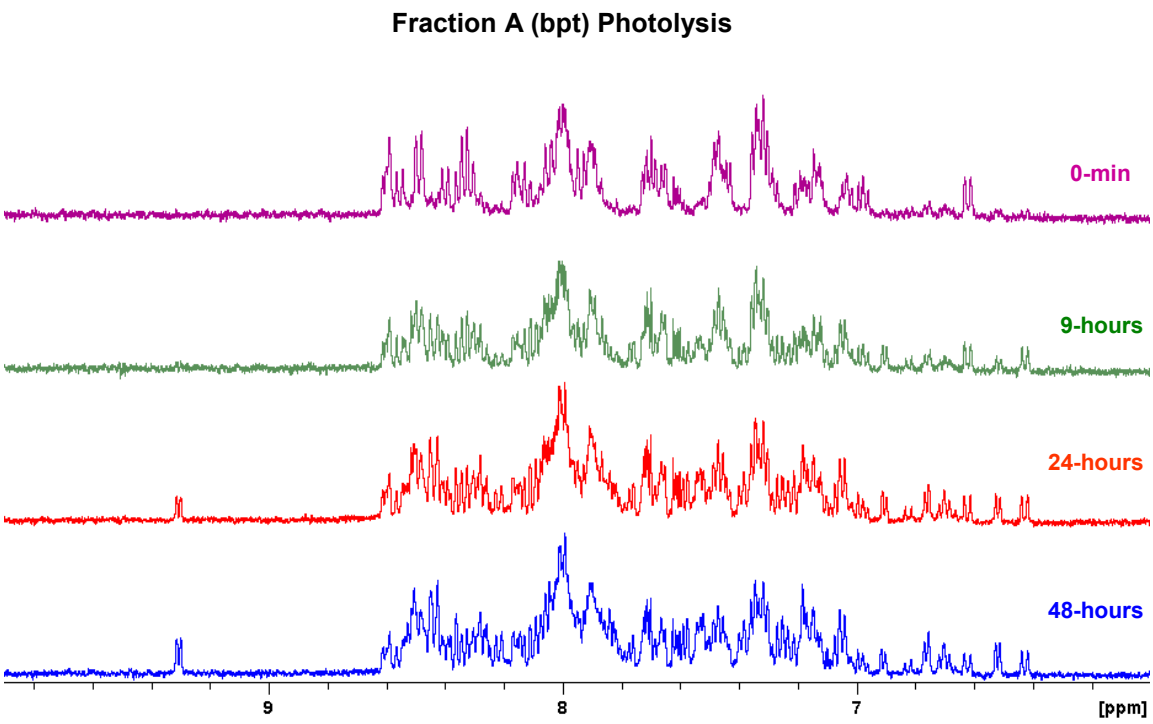

Figure 3.18 *^{1}H-NMR data of the fractions **A**-(bpt) during photolysis. in d_3 acetonitrile.*

The fact that only one signal is observed in this range suggest a symmetric molecule where two non-aromatic ligands are present. The ^{1}H NMR spectra obtained after 48 hours of photolysis suggests the formation of the bis acetonitrile species $[Ru(bpy)_2(CH_3CN)_2]^{2+}$, in agreement with the absorption maxima of this compound observed in the HPLC traces. The features of this spectrum are identical to that observed for the bis(acetonitrile) compound discussed in Chapter 5.

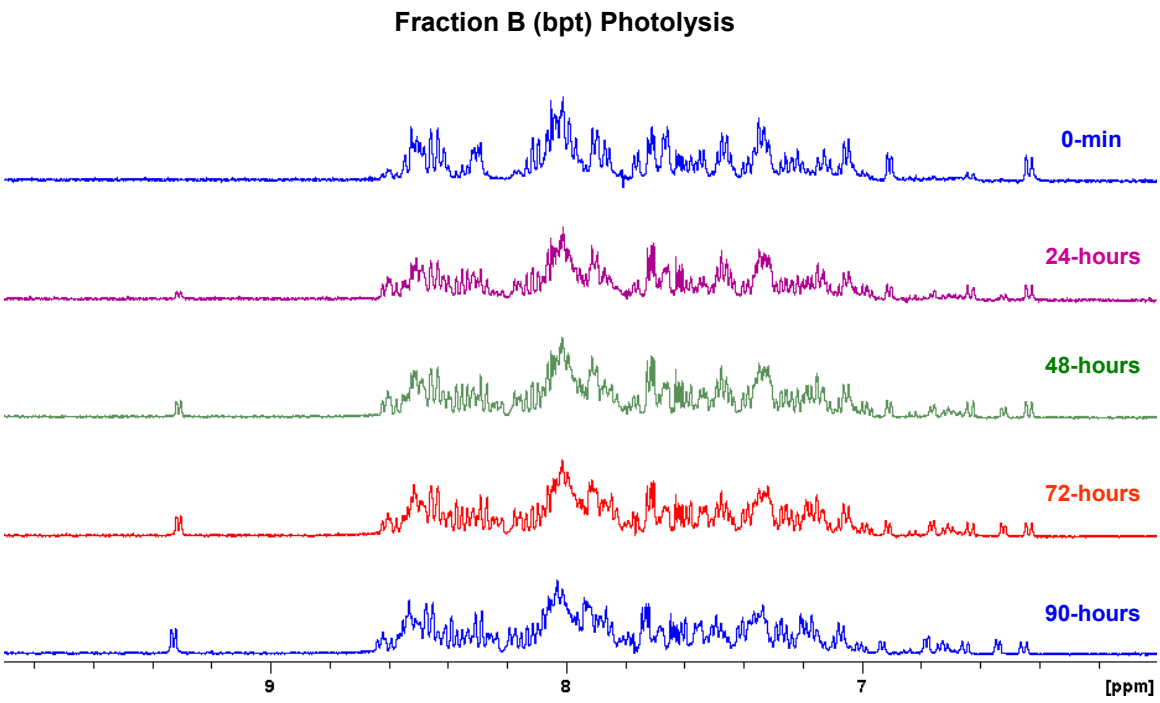

Figure 3.19 *^{1}H-NMR* data of the fraction **B** during Photolysis. in D3 acetonitrile

Analogously the irradiation of fraction **B** of $Ru(bpy)_2bpt(CH_3CN)]^{2+}$ leads initially to a process of photoisomerization into the components of fraction **A**. For both fractions **A** and **B** of $[Ru(bpy)_2bpt(CH_3CN)_2]^{3+}$ further irradiation produces the fragmentation of the dimetallic complex into monometallic species.

3.4 Conclusion

The results obtained indicate clearly that upon irradiation in acetonitrile a range of photoproducts is obtained, the nature of which is dependent on the duration of the irradiation. First of all interconversion of Fraction A and B is observed a typical example is shown below in Figure 3.20. For this to occur bond breaking between the ligand and the metal centre needs to occur.

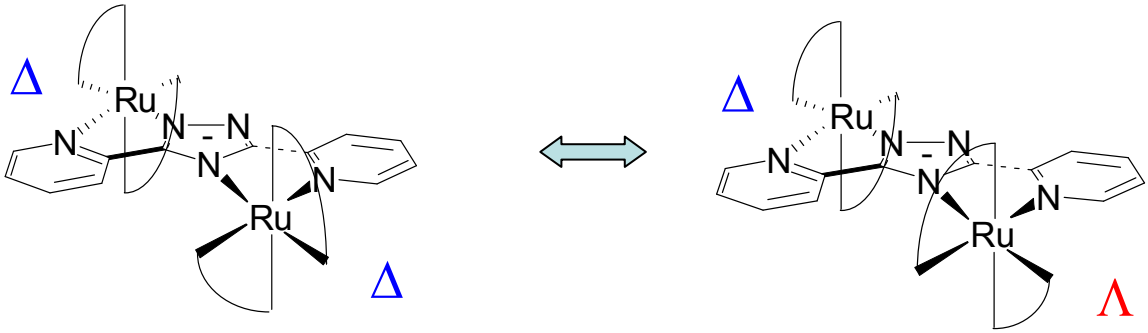

Figure 3.20. *Example of photoinduced interconversion of chiral isomers.*

In case of the process outlined above the ligands are not replaced but rearrangement takes place from the homochiral to the heterochiral structures (A to B) and the other way around. In all cases two end products are obtained mainly the $[Ru(bpy)_2bpt]^+$ mononuclear species and $[Ru(bpy)_2(CH_3CN)_2]^{2+}$. The occurrence of these species together is to be expected and both have been reported before in other similar studies. Another species is observed at a retention time of about 19 minutes. The retention time of this species suggests that its charge is 3+ as observed for Fractions A and B, while its absorption spectrum (See Figure 3.16) is rather unusual and cannot be a known compound. At present it is not possible to positively identify the nature of this compound, but since its concentration in the HPLC traces remains fairly

constant upon irradiation the formation of a species with a monodentate bound bpt ligand is proposed as shown in Figure 3.21. Similar species are observed for other pyridine- and pyrazine triazoles as outlined in Chapters 1 and 5. For this

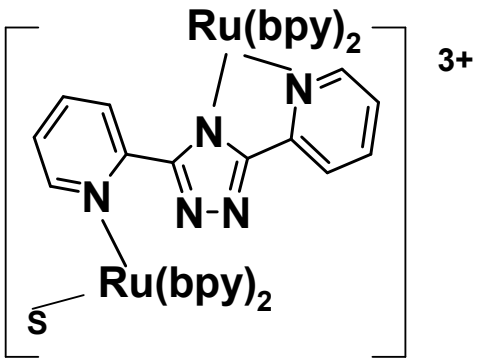

Figure 3.21. *Potential structure of monodentate coordinated species. S = solvent and may be CH_3CN or H_2O.*

species the bpt ligand may either be re-coordinated to form Fraction **A** or **B** or the dinuclear structure is broken up to produce the bpt monomer and the bis acetonitrile complex. So based in this evidence the photochemical processes taking place after the isomerisation of the chiral species are based on the decomposition of the dinuclear bpt complex and the formation of two mononuclear species as outlined in the following equations;

$$[(Ru(bpy)_2)_2(bpt)]^{3+} \xrightarrow{h\nu} [(Ru(bpy)_2)_2(bpt_{monodentate})(CH_3CN)]^{3+} \quad \textbf{Equation 5.1}$$

$$[Ru(bpy)_2(bpt_{monodentate})(CH_3CN)]^{3+} \xrightarrow{h\nu} [Ru(bpy)_2(CH_3CN)_2]^{2+} + Hbpt \quad \textbf{Equation 5.2}$$

References:

[1] B. E. Buchannan, J. G. Vos, M. Kaneko, W. J. M. Van der Putten, J. M. Kelly, R. Hage, R. A. G. De Graaff, R. Prins, J. G. Haasnoot and J. Reedijk, *J. Chem. Soc. Dalton Trans*., **1990**, 2425.

[2] R. Hage, R. Prins, J.G. Haasnoot, J. Reedijk, and J.G. Vos. *J. Chem. Soc., Dalton Trans*., **1987**, 1389.

[3] R. Hage, A. Dijkhuis, J. Haasnoot, R. Prins, J. Reedijk, B. Buchanan, and J. Vos, Inorg. Chem. **1988**, 27, 2185-2189.

[4] H.P. Hughes, D. Martin, S. Bell, J.J. McGarvey and J.G. Vos. *Inorg. Chem.,* **1993**, *32*, 4402

[5] R. Hage, J.G. Haasnoot, D.J. Stufkens, T.L. Snoeck, J.G. Vos and J. Reedijk. *Inorg. Chem*., **1989**, *28*, 1413

.

[6] F. Barigelletti, L. De Cola, V. Balzani, R. Hage, J.G. Haasnoot, J. Reedijk, and J.G. Vos. *Inorg. Chem.,* **1989**, *28*, 4344

[7] (a) P. Passaniti, W.R. Browne, F.C. Lynch, D. Hughes, M. Nieuwenhuyzen, P. James, M. Maestri, J.G. Vos, J. Chem. Soc. Dalton Trans. **2002**, 1740; (b) W.R. Browne, C.M. O'Connor, H.P. Hughes, R. Hage, O. Walter, M. Doering, J.F. Gallagher, J.G. J. Vos, Chem. Soc. Dalton Trans. **2002**, 4048.

[8] (a) F. R. Keen, *Coord. Chem. Rev*. 1997, 166, 121; (b) F. R. Keen, *Chem. Soc. Rev*. **1998**, 27, 185.

[9] T. J. Rutherford, O. V. Gijte, A. Kirsch-DeMesmaeker, F. R. Keene, Inorg. Chem. **1997**, 36, 4465.

[10] W. R. Browne, C. M. O`Connor, C. Villani, Johannes G. Vos. *Inorg. Chem*. **2001**, 40, 5461-5464.

[11] J.G. Vos, J.M. Kelly, *Dalton Trans.* **2006**, 4869.

[12] (a) S. Rau, B. Schaefer, D. Gleich, E. Anders, M. Rudolph, M. Friedrich, H. Goerls, W. Henry, J.G. Vos, *Angew. Chem. Int. Ed.* **2006**, 45, 6215; (b) B. Gholamkhass, H. Hiroaki Mametsuka, K. Koike, T. Tanabe, M. Furue, O. Ishitani, *Inorg. Chem.* **2005**, 44, 2326; (c) S. Sato, K. Koike, H. Inoue, O. Ishitani, *Photochem. Photobiol. Sci.* **2007**, 6, 454.

[13] A.L. Guckian, W.R. Browne, J.Hjelm J.G. Vos. *J. Chin. Chem. Soc*. **2007**, 54, 1151

CHAPTER 4

Photochemical Properties of Mononuclear and Dinuclear bis(pyrazine)triazole Complexes.

4.1 Introduction

Multinuclear metal polypyridyl complexes are of particular interest in regard to transfer of either electronic charge or energy from one site of coordination to the other via π-delocalized bridging ligands [1]. In principle, such intramolecular charge transfer in binuclear complexes can be exploited for the realization of miniaturized devices where electrons or photons dispatch signals between specific sites within distances of the order of a few angstroms [2]. A key challenge therefore is to be able to control not only the strength of the interaction between the two metal centers both in the ground and excited state but also the direction of such processes. This can be achieved through the structural changes in the bridging ligand and the variation of the nature of the coordinating metal centers [3].

For many years, ruthenium(II) and osmium(II) polypyridyl complexes have attracted attention due to the possibility of producing complexes that have applications in energy conversion, sensing and interactions with DNA [4]. The spectroscopic, photophysical, photochemical, and electrochemical properties of ruthenium(II) and osmium(II) polypyridyl complexes make them excellent candidates in the construction of supramolecular systems that may lead to the above applications [5,6,7]. For the above reason, there has been a considerable interest in the study of mononuclear and multinuclear of ruthenium(II) polypyridyl and / or osmium(II) polypyridyl complexes connected together via a bridging ligand.

As already discussed in Chapter 3 in dinuclear complexes the nature of the bridging ligand is an important factor which may influence the properties and behaviour of the compounds. The bridging ligand is a key component in controlling intercomponent processes occurring within the compound such as the direction of energy and electron transfer. The bridging ligand also controls the distance between the two metal centers. Several triazole based bridging ligands have been under extensive research some of them are shown in Figure 4.1 others have already been shown in Chapter 3. The goal of these studies was to examine the effect of the bridging ligand on the excited states properties of these complexes.

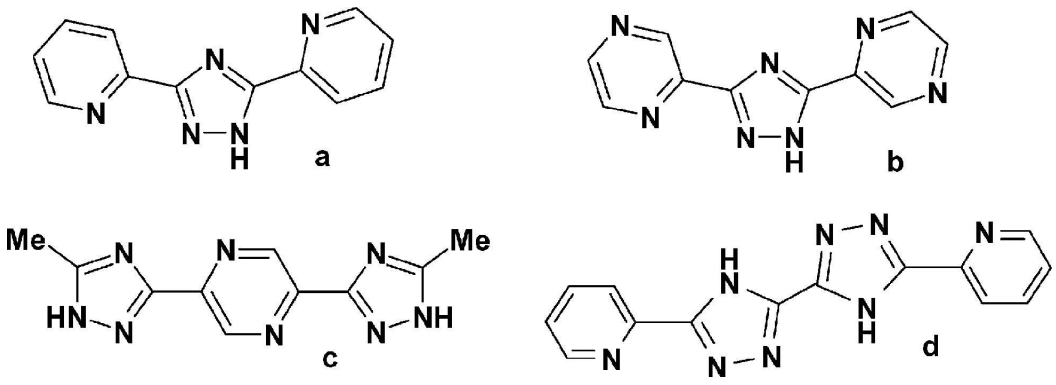

Figure 4.1 *Structures of some triazole based bridging ligands;* ***a****, Hbpt,* ***b,*** *Hbpzt,* ***c****, 2,5-bis(5'-methyl-4'H-[1,2,4]triaz-3'-yl)-pyrazine,* ***d****, 5', 5'-bis (pyridine-2''-yl)-3,3-bis (1,2,4-triazole) [4].*

Among these ligands , the anions of 3,5-bis(pyridin-2`-yl)-1H-1,2,4-triazole (Hbpt) [8] and 3,5- bis(pyrazin-2`-yl)-1H-1,2,4-triazole) (Hbpzt) [9], (Figure 4.1) have been extensively investigated by our research group. Upon coordinated to the metal centre, Hbpt and Hbpzt deprotonation results in a negative charge on the bridging

ligand. The two coordination sites of the triazole (N2 and N4) are non equivalent, N2 is a better σ-donor than the N4 position as already outlined in Chapter 3.

In Chapter 3 the photochemical behaviour of a Hbpt based dinuclear compound was reported. In this Chapter the pyrazine analogue Hbpzt is investigated. It is known that ligands such as pyrazine or bipyrazine have a weaker σ-donor potential and stronger π-acceptor properties than pyridine or bipyridine [10]. On the basis of this chemistry it is expected that there will be a differences between the photophysical properties of the compound containing pyridyltriazoles and pyrazinyltriazoles. Of interest, for example, is the location of the lowest energy excited state.

Vos *et al* have reported the synthesis of several mononuclear and dinuclear $Ru(bpy)_2$ complexes with 1,2,4- triazole containing pyrazine based ligands [7]. A series of mononuclear $[Ru(bpy)_2(L)](PF_6)_2$ complexes, where bpy = 2,2'-bipyridine and L = 3-(pyrazin-2-yl)-1,2,4-triazole (HL1), 3-methyl-5-(pyrazin-2-yl)- 1,2,4-triazole (HL2) 1-methyl-3-(pyrazin-2-yl)-l,2,4-triazol(L3) have been prepared and characterized. For ligand structures see Figure 4.2 [11].

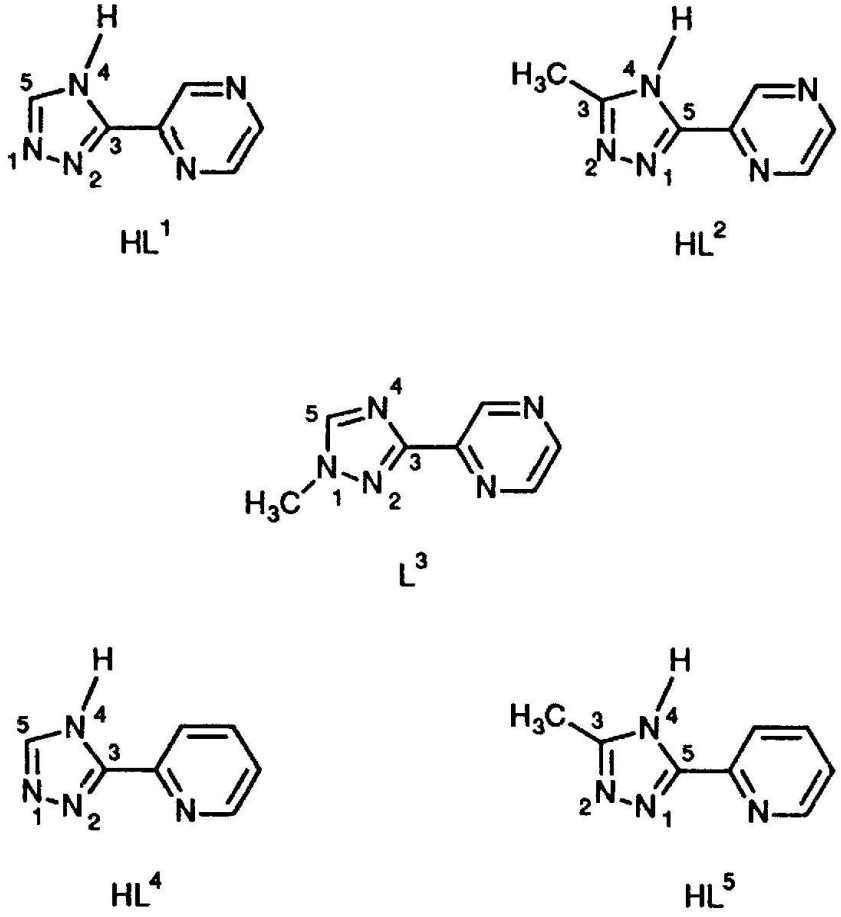

Figure 4.2 *Ligand structures of pyrazine based triazole ligands L = 3-(pyrazin-2-yl)-1,2,4-triazole (HL^1), 3-methyl-5-(pyrazin-2-yl)-1,2,4-triazole (HL^2) 1-methyl-3-(pyrazin-2-yl)-l,2,4-triazol(L^3) and related pyridine analogues 3-(pyridine-2'yl)-1,2,4-triazole (HL^4), 3-methyl-5-(pyridin-2'-yl)- 1,2,4-triazole (HL^5).*

This report indicates that the lowest *π levels in compounds containing protonated or N-methyl-substituted pyrazinyltriazole ligands are pyrazinyltriazole based, while for the complexes with deprotonated ligands the lowest *π are located on the bpy ligands. These results have been confirmed using spectroscopic and electrochemical studies. In this report emission spectroscopy has shown that the

emitting states can be changed from bpy to pyrazinyltriazole upon lowering the pH for the $[Ru(bpy)_2(HL1)]^+$ and $[Ru(bpy)_2(HL2)]^+$ complexes where bpy = 2,2'-bipyridine and L = 3-(pyrazin-2-yl)-1,2,4-triazole (HL1), and 3-methyl-5-(pyrazin-2-yl)- 1,2,4-triazole (HL2), [11].

The synthesis and characterization of the dinuclear $[(Ru(bpy)_2)_2bpzt]^{3+}$ and $[(Ru(bpy)_2)_2\ bpt]^{3+}$ Figure 4.3, have been reported [12, 13]. The major difference between Hbpt and the Hbpzt based complexes is that the lowest unoccupied molecular orbital (LUMO) in the dinclear bpt^- complexes is bpy based, while in the dinuclear $bpzt^-$ complexes it is based on the pyrazine rings of the bridging ligand. Photophysical, resonance Raman spectroscopy, and electrochemical studies have been carried out to investigate the effect of these differences on the photochemical and the photophysical properties of the dinuclear compounds [14]. The $[(Ru(bpy)_2)_2\ bpzt]^{3+}$ complex showed a strong emission at 671 nm at room temperature.

One of the interesting properties of these dinuclear compounds is that they feature strong interactions between metal centers [15]. Resonance Raman (RR) spectroscopy has been very useful in defining the nature of the excited state in mixed metal complexes, in mononuclear and dinuclear $[Ru(bpy)_2(bpzt)]^+$ (**1**) and $[(Ru(bpy)_2)_2(bpzt)]^{3+}$ (**2**)

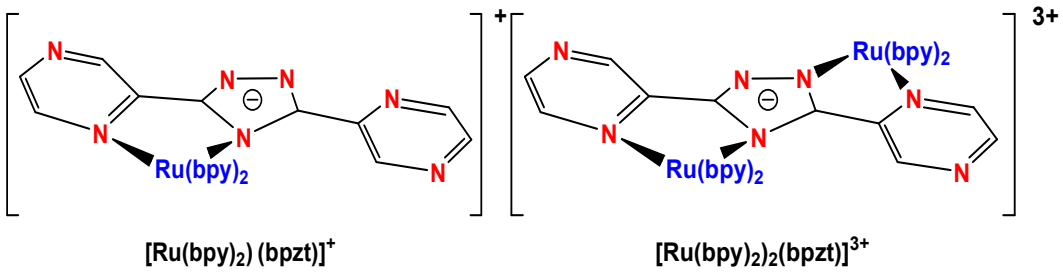

Figure 4.3 *Mononuclear $[Ru(bpy)_2(bpzt)]^+$ (**1**) and dinuclear $[(Ru(bpy)_2)_2(bpzt)]^{3+}$ (**2**).*

Excited state rR of **1** and **2** have shown that protonation of the bpzt ligand or addition of a second metal centre, result in a switching of the ligand on which the LUMO is based. Exciting the complex in its absorption band and measuring the rR spectra will give evidence about the nature of the excited state. The resonance Raman spectra of **1** indicate localization of the ^{3}MLCT on a bpy ligand. Excitation of the complex **2** using the same excited wavelength, of 355 nm, shows a set of features which provides evidence for the location of the emitting ^{3}MCLT state on a pyrazine ring of the bridging ligand. This suggest that in the two compounds the excited state is located on different ligands. It has been suggested that the emitting state is located on the N2 site of the triazole ring, while photosubstitution occurs at N4. The emission lifetimes of the complex 2 are 0.2 and 7.0 μs at room temperature and 77K, respectively. The temperature dependent lifetime studies indicates that the triplet metal centred ^{3}MC can be populated at room temperature and it therefore expected that the dinuclear compounds will be photolabile and this is indeed observed [13[a], 14,16].

As indicated in Chapter 3 dinuclear complexes of this type may be obtained as a series of 4 optical isomers. In Chapter 3 it was shown that for the bpt- dinuclear species these optical isomers could be separated in two sets of two homochiral and heterochiral isomers. It was also shown that interconversion between these two types of optical isomers could be obtained. In this chapter we wish to investigate whether this can also be achieved for the bpzt compounds. In addition the photochemical properties of the compounds obtained will be investigated. In this study we wish to utilise again HPLC techniques. Semi preparative HPLC is often the only way to achieve ultrapure compounds. The samples are first investigated using analytical HPLC and after a separation method is developed, semipreparative separation can be used. For the average ruthenium complex cation exchange chromatography is most helpful [17] although alternative enantioselective separations using column chromatography and other HPLC columns have also been reported [18].

4.2 Experimental Section

4.2.1 Materials

The compound $[(Ru(bpy)_2)_2(bpzt)]^{3+}$ was available from previous experiments and was prepared by Ms Nadia Coburn. All solvents used were HPLC grade or better and used without purification.

4.2.2 Chromatographic Analysis

High performance liquid chromatography (HPLC) was carried out using a Varian Pro Star 230 HPLC system with photodiode array as outlined in Chapter 2. The mobile phase used for routine work was $CH_3CN:H_2O$ (volume ratio = 80:20) containing 0.08 M LiCl. For photolysis experiments, a more efficient separation of the fractions was required and the retention time was increased using 80:20 CH_3CN: H_2O (volume ratio = 80:20) containing 0.06 M LiCl. The flow rate for routine work was 2.0-4.0 cm^3min^{-1} in case of photochemical experiments.

4.2.3 Semi-Preparative HPLC

Semipreparative HPLC was carried out on a model Varian 230 pump, (model 230) and Varian detector (Model 330.71) fitted with a 200 μm injection loop and a magnum- Partisil 10 SCX cation exchange column (4.6mm x 25cm). The mobile phase employed was 80:20 CH_3CN: H_2O containing 0.1M KNO_3 for mononuclear complexes and 0.15 M KNO_3 for dinuclear complexes. The flow rate ranged

between 2 and 4.0 cm^3 min^{-1}. The detection wavelength was 280 nm where ruthenium complexes display the most intense absorption band.

All samples were dissolved in the eluent (100 mg/mL) and filtered through a 0.45 micron filter prior to injection. Typical column loading were 10-20 mg per run, CH_3CN:H_2O 80:20 with 0.12 M KNO_3 mobile phase.

Many injections were required to separate small amounts for both species A and B. After removal of the mobile phase, both complexes were dissolved in minimum amount of H_2O, followed by the addition of saturated aqueous KPF_6 solution. Occasionally it was found that some product was difficult to re-dissolve in H_2O. In these cases, a few drops of acetone were added. After adding to an aqueous solution of KPF_6, the precipitate of both fractions were filtered, washed with H_2O to remove excess KPF_6 and then dried in vacuo. About 25 mg of pure Fraction **A** and 35 mg of pure Fraction **B** were collected. HPLC shows that both species were obtained in high purification.

4.3 Results and Discussion

4.3.1 Chromatographic Behaviour of Compounds.

The chromatogram obtained for the dinuclear compound is shown in Figure 4.3. As observed for the bpt analogue, two peaks are obtained. These were separated and the UV-vis spectra of the two products obtained are shown in Figure 4.4. The chromatographic spectra obtained for the two species are shown in Figure 4.5.

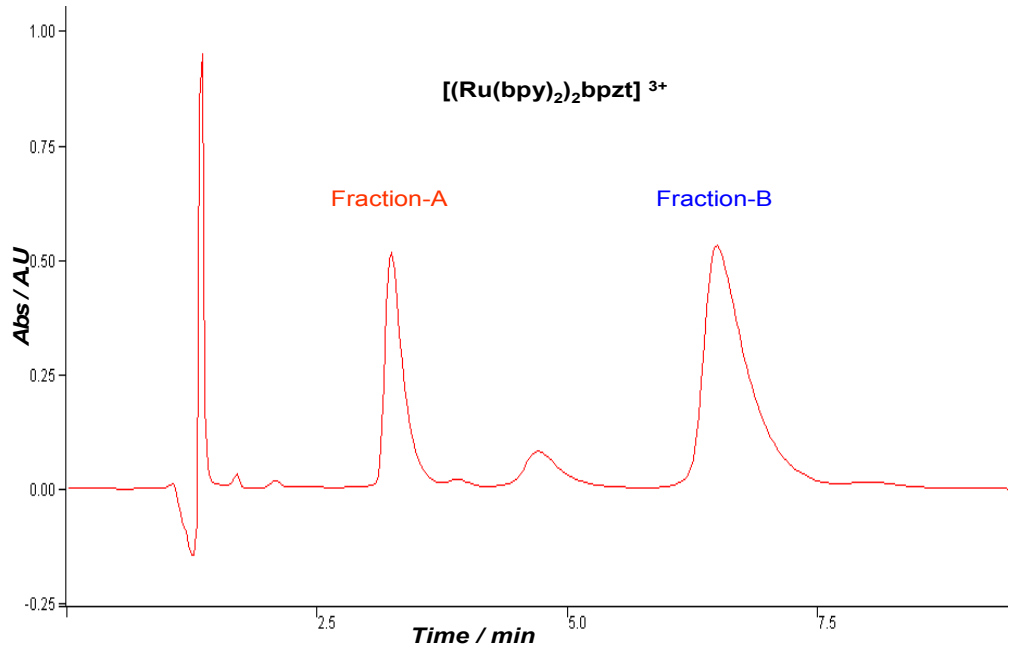

Figure 4.3: *HPLC trace taken during purification of $[(Ru(bpy)_2)_2\ bpzt]^{3+}$ in CH_3CN 80:20 $CH_3CN:H_2O$ 0.12 M KNO_3 flow rate 4.0 $cm^3\ min^{-1}$ at 280 nm.*

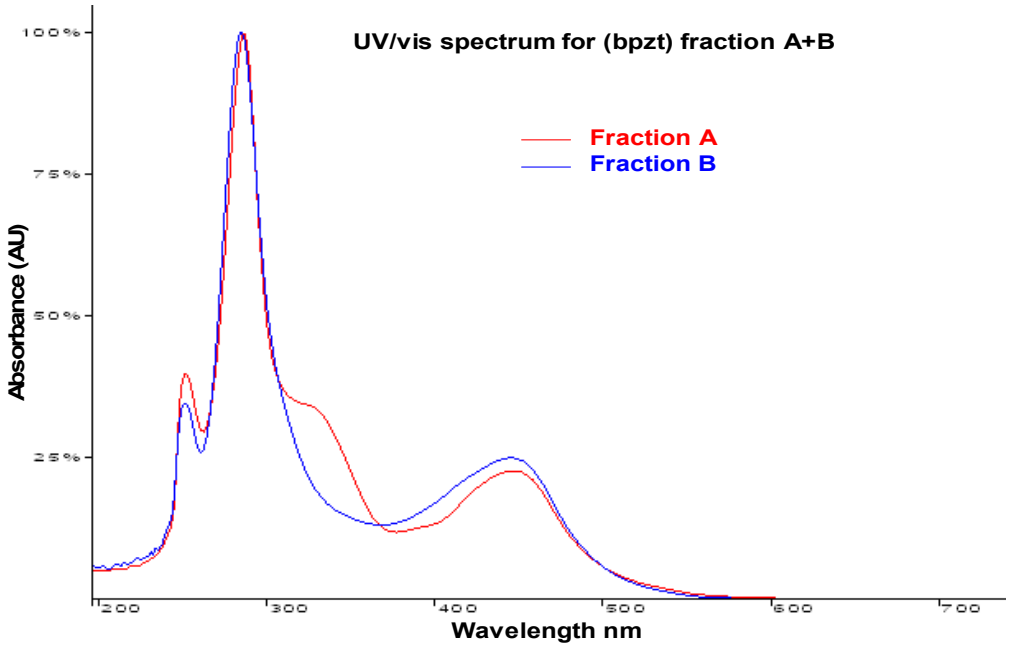

Figure 4.4: *UV/vis spectra of Fraction A+B of $[(Ru(bpy)_2)_2\ bpzt]^{3+}$ after semi-prep separation in CH_3CN 80:20 $CH_3CN:H_2O$ 0.12 M KNO_3 flow rate 4.0 $cm^3 min^{-1}$ at 280 nm. Concentrations of fraction A and B : 10^{-3} M.*

Comparison of the chromatogram shown in Figure 4.3 with that obtained for the bpt analogue in Figure 3.5 shows that the difference in retention time for the two fractions is considerable more for the bpt fractions discussed in Chapter 3. It should be noted that the mobile phases used for both compounds are different, however it is not expected that the large differences observed in retention time are only due to these differences. It is proposed that the presence of free nitrogen atoms at the outside of the molecules will substantially affect the retention times. What is also surprising is that the two spectra obtained for the two fractions of the bpzt compound are considerably different while for the bpt species the spectra as shown in Figure 3.6 are basically identical. These spectra remain the same after both fractions are separated.

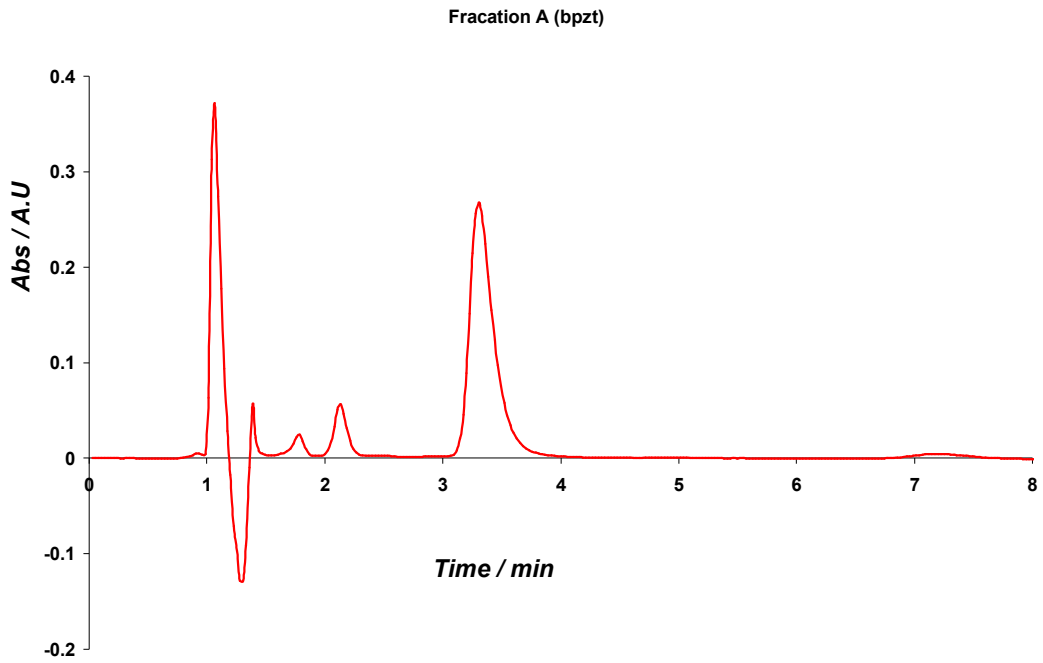

Figure 4.5 *Fraction A of $[(Ru(bpy)_2)_2\,bpzt]^{3+}$ after semi-prep separation in CH_3CN 80:20 $CH_3CN:H_2O$ 0.12 M KNO_3 flow rate 4.0 $cm^3\ min^{-1}$, retention time 3.5 min at 280 nm.*

Comparison with literature values [12,13,15] suggests that while Fraction B can be identified by its UV/vis spectra as the dinuclear bpzt complex, fraction A is the mononuclear species $[Ru(bpy)_2(bpzt)]^+$. This assessment is confirmed by the ^1H NMR spectra [12] obtained for the purified species shown in Figure 4.7.

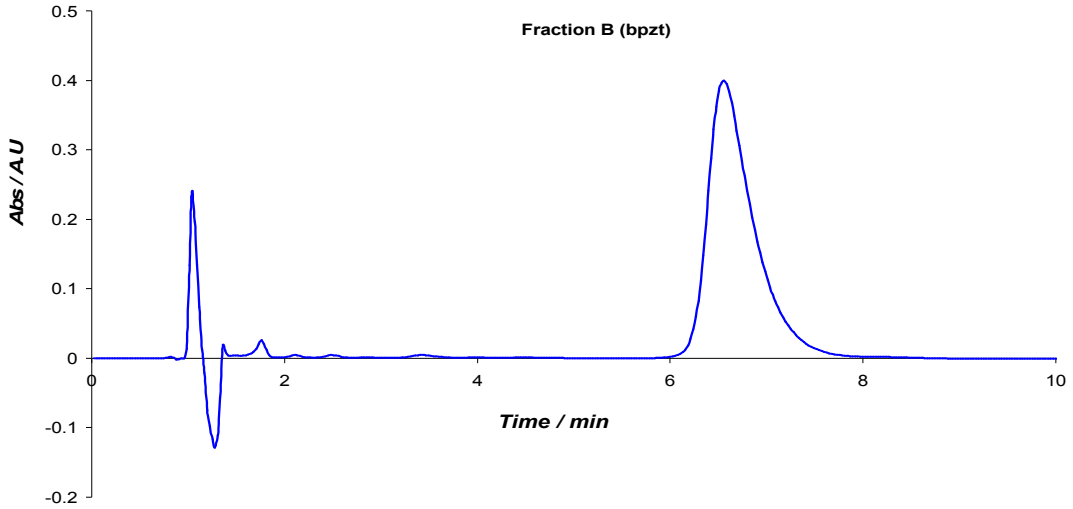

Figure 4.6: *Fraction B of $[(Ru(bpy)_2)_2\,bpzt]^{3+}$ after semi-prep separation in CH_3CN 80:20 $CH_3CN:H_2O$ 0.12 M KNO_3 flow rate 4.0 $cm^3\ min^{-1}$, retention time 6.5 min at 280 nm.*

It is clear from the spectra shown in this figure that they are complex and this has so far prevented a complete analysis of all the resonances present. This does, however, not hinder the application of the spectra for identification purposes and for the study of photoinduced ligand exchange processes. Two areas of the spectrum are particularly useful for this. Compound **1** is easily identified by the two

signals observed at about 9.30 and 9.23 ppm. These have been assigned as the H3 pyrazine protons of the bridge [12]. The difference between the two is explained by the fact that the two pyrazine rings in compound **1** are different; one is coordinated to the metal centre and the other is free. For the dinuclear compound **2**, the assignment is made even more complicated since as for the dinuclear compound for bpt **4** optical isomers are obtained. It has so far however not been possible to isolate these optical isomers in a pure state. Indicative for compound **2** are the signals at about 9.2 ppm again H3 and at 7.1 ppm. The latter signal is assigned to two second H3 proton of the bridging ligand. Both the strong differences between these spectra are, therefore, indicative for the nature of the species obtained, namely Fraction A can be assigned to compound **1** and fraction **B** to a mixture of chiral isomers of compound **2**.

A disappointing observation is that for the dinuclear compound only one peak is observed. Different to bpt analogue, no separation of optical isomers was observed. This may be associated with the presence of the free nitrogen atoms in the pyrazine rings which are expected to interact differently with both mobile phase and stationary phase.

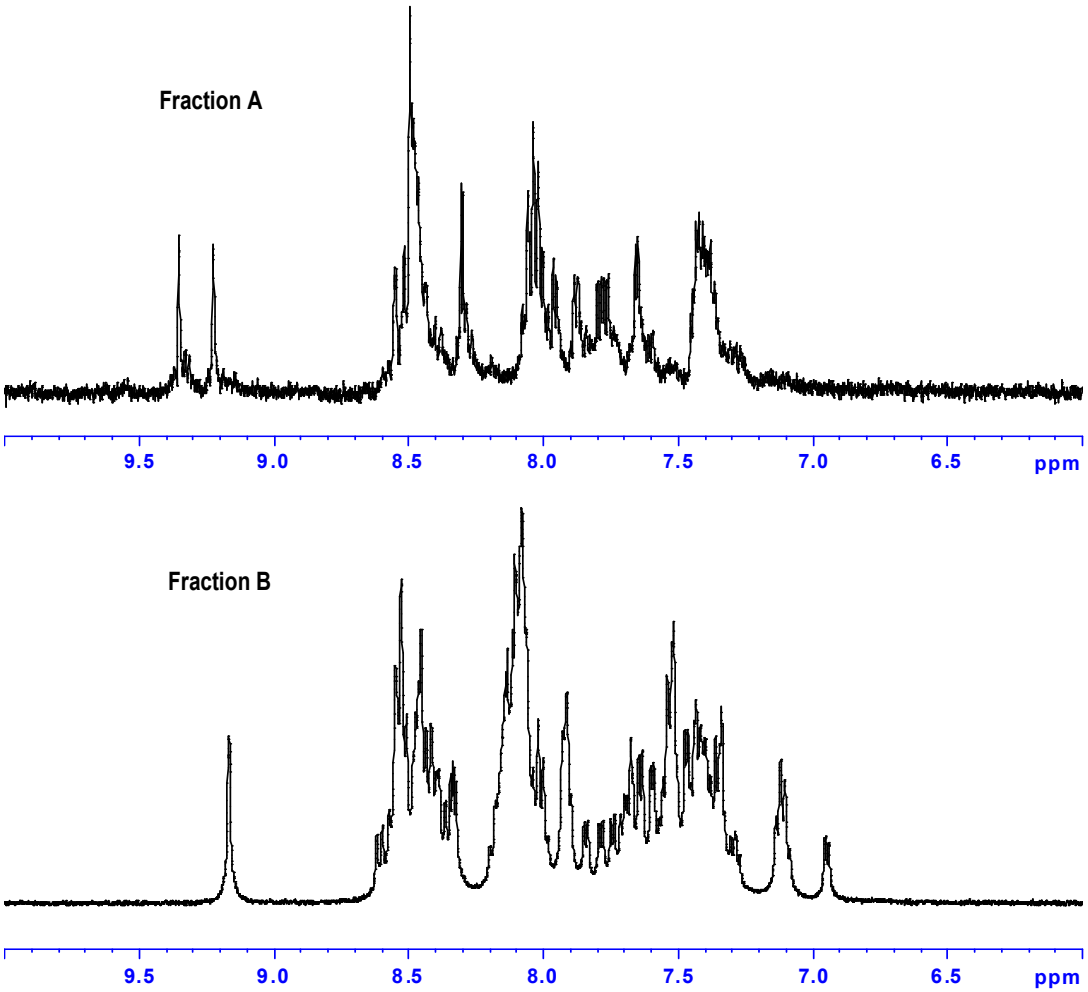

Fig 4.7: *^{1}HNMR spectra of fractions A and B, in d_3-acetonitrile.*

This is disappointing since a possible interconversion between optical isomers as observed for the bpt dinuclear species can not be studied. It was however decided to carry out a limited study on the photostability of the two fractions obtained. This will allow comparing the behaviour of the bpt and bpzt compounds under the same conditions. Note that from now on the species so far called fraction 1 and fraction 2 will for the rest of the document be called the mononuclear compound $[Ru(bpy)_2bpzt]^+$, compound **1** and the dinuclear compound $[(Ru(bpy)_2)_2bpzt]^{3+}$, compound **2** (See Figure 4.3). It is important that in the synthetic approach made to

obtain these compounds it has been established that in compound **1**, the ruthenium centre is coordinated to the N2 nitrogen atom of the triazole ring. This can be explained by steric considerations; the presence of the second pyridine ring strongly effects access to N4 but for coordination to N2 to steric hindrance is expected [8].

4.3.2 Photochemical Studies

The photochemical behaviour of both fractions was studied in CH_3CN. The chromatograms obtained for irradiation of the mononuclear species compound **1** and the dinuclear compound **2** is given in Figures 4.8 and 4.9, respectively.

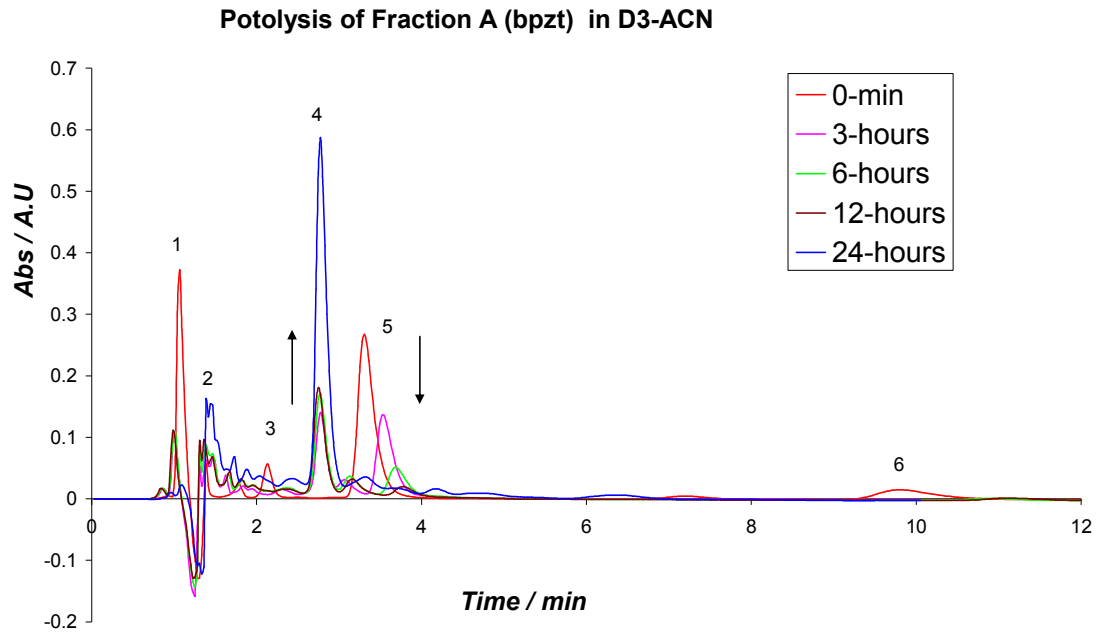

Figure 4.8: *HPLC trace of Photolysis of Fraction **A**; $[(Ru(bpy)_2\ bpzt]^+$ in ACN 80:20 $CH_3CN:H_2O$ 0.12 M KNO_3 flow rate 4.0 $cm^3\ min^{-1}$; detection wavelength at t 280 nm.*

Figure 4.8 shows that upon irradiation the intensity of the starting material at about 3.5 minutes decreases and that one main product is observed at 2.7 minutes. The absorption spectrum of this product has a maximum at 420 nm, and this is in agreement with the formation of the compound - $[(Ru(bpy)_2(CH_3CN)_2]^{2+}$ [19]. The nature of the minor species formed was not determined but they are likely to be compounds where the triazole containing ligand is bound in a monodentate fashion as reported before for similar pyridine triazole based metal complexes [19]. It is somewhat surprising that the compound **1** is showing photoinduced ligand exchange since based on the electronic properties of this compound, which are similar to those of the bpt monomer this compound was considered photostable [14]. However in that study the irradiation times were considerably shorter with a maximum irradiation time of 17 min. A different, less intense light source was also used in that study. As Figure 4.8 shows irradiation times in this study are up to 24 hours.

The photochemical behaviour of the dinuclear compound **2** is shown in Figure 4.9. Figure 4.9 indicates that irradiation of the dinuclear compound **2** leads to the formation of two main products, which have retention times at 3.5 and 2.7 minutes. After 24 hours only a single product remains.

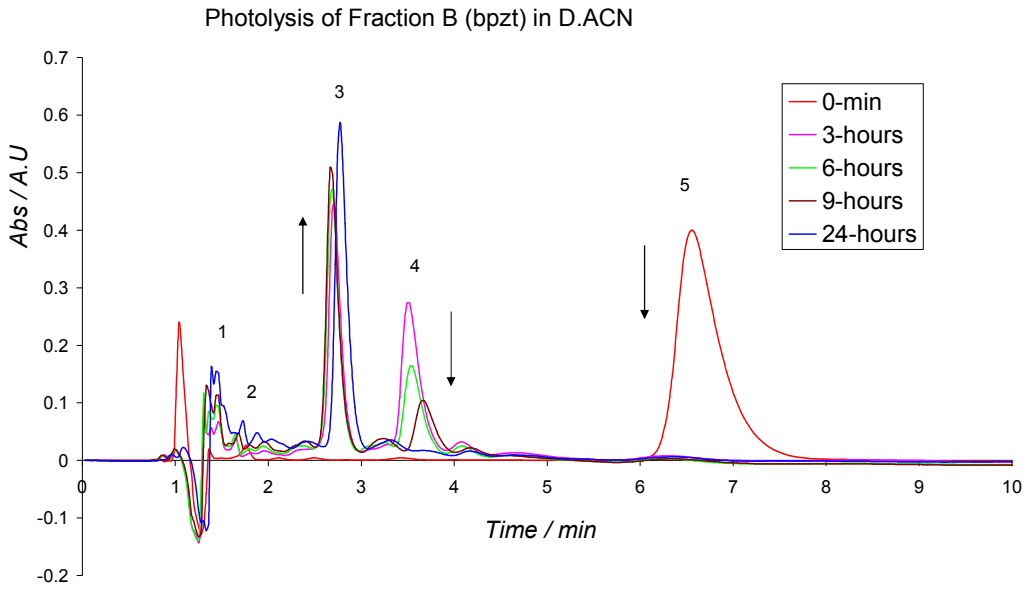

Figure 4.9: *HPLC trace of Photolysis of* $[(Ru(bpy)_2)_2\ bpzt]^{3+}$ *in acetonitrile Mobile phase ACN 80:20* $CH_3CN:H_2O$ *0.12 M* KNO_3 *flow rate 4.0* $cm^3\ min^{-1}$*; detection wavelength 280 nm.*

The UV/vis spectra obtained for these two species are shown in Figure 4.10 and these indicate that the mononuclear compound **1** is formed first (peak 4 in Figure 4.9) and that this species is later transformed into $Ru(bpy)_2(CH_3CN)_2]^{2+}$, (peak 3 in Figure 4.9) It is noteworthy that the photodecomposition of the dinuclear compound **2** is considerable faster than that observed for compound **1**. The photochemical processes observed are the decomposition of compound **2** in the first 3 hours with the photochemistry of compound **1** being observed between 3-24 hours. Since we were unable to separate the enantiometric pairs no evidence for their interconversion could be obtained.

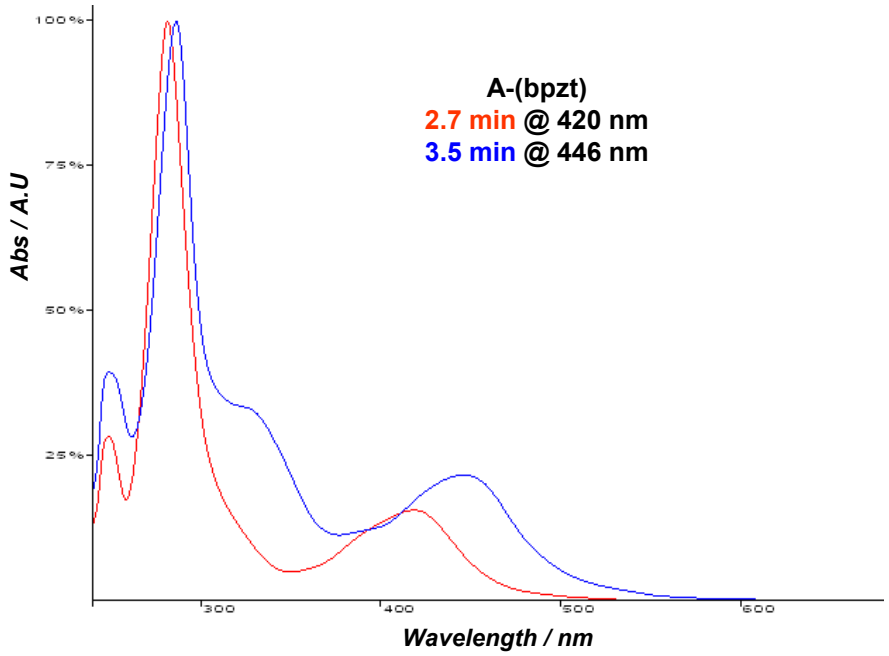

Figure 4.10: *UV/vis Spectrum of irradiation products obtained for $[(Ru(bpy)_2)_2 bpzt]^{3+}$ in CH_3CN.*

The photolytic process was also investigated using NMR spectroscopy. The spectra obtained for the photolysis of Compounds 1 and 2 are shown in Figures 4.11 and 4.12 respectively.

The ^{1}H NMR spectrum at the top of Figure 4.11 shows the features expected for compound **1**. Two singlets are observed at around 9.3 ppm as discussed above. The following spectra show the appearance of a series of new features the clearest of these is a doublet at 9.3 ppm. After 40 hours of irradiation, a simplified spectrum is obtained, with 8 sets of resonances; 4 doublets and 4 doublets of doublets. The doublets can be assigned to the H6 and H3 protons of the bpy ligands, while the others are associated with the protons H5 and H4. All signals are found in the

region expected for a compound with the general formula; $[Ru(bpy)_2(L)_2]^{2+}$. The absorption maximum observed in the UV/vis spectrum (See Figure 4.10) for the species with a retention time of 2.4 minutes indicates that L = acetonitrile. This is not unexpected as this is the solvent used for the photochemical experiments. This indicates that the bpzt ligand has been replaced by CH_3CN and that the following reaction has taken place;

$$[Ru(bpy)_2(bpzt)]^{+} \xrightarrow{h\nu} [Ru(bpy)_2(CH_3CN)_2]^{2+} + Hbptz \qquad \textbf{Eq 4.1}$$

Apart from the resonances associated with the bis(CH_3CN) complex a number of broadened features are seen that can not be identified. These features are very similar to those observed in the final spectrum in Figure 4.12. These may be associated with the production of the fraction **A** monomer. This compound is however not very soluble in acetonitrile and this may affect the signals obtained.

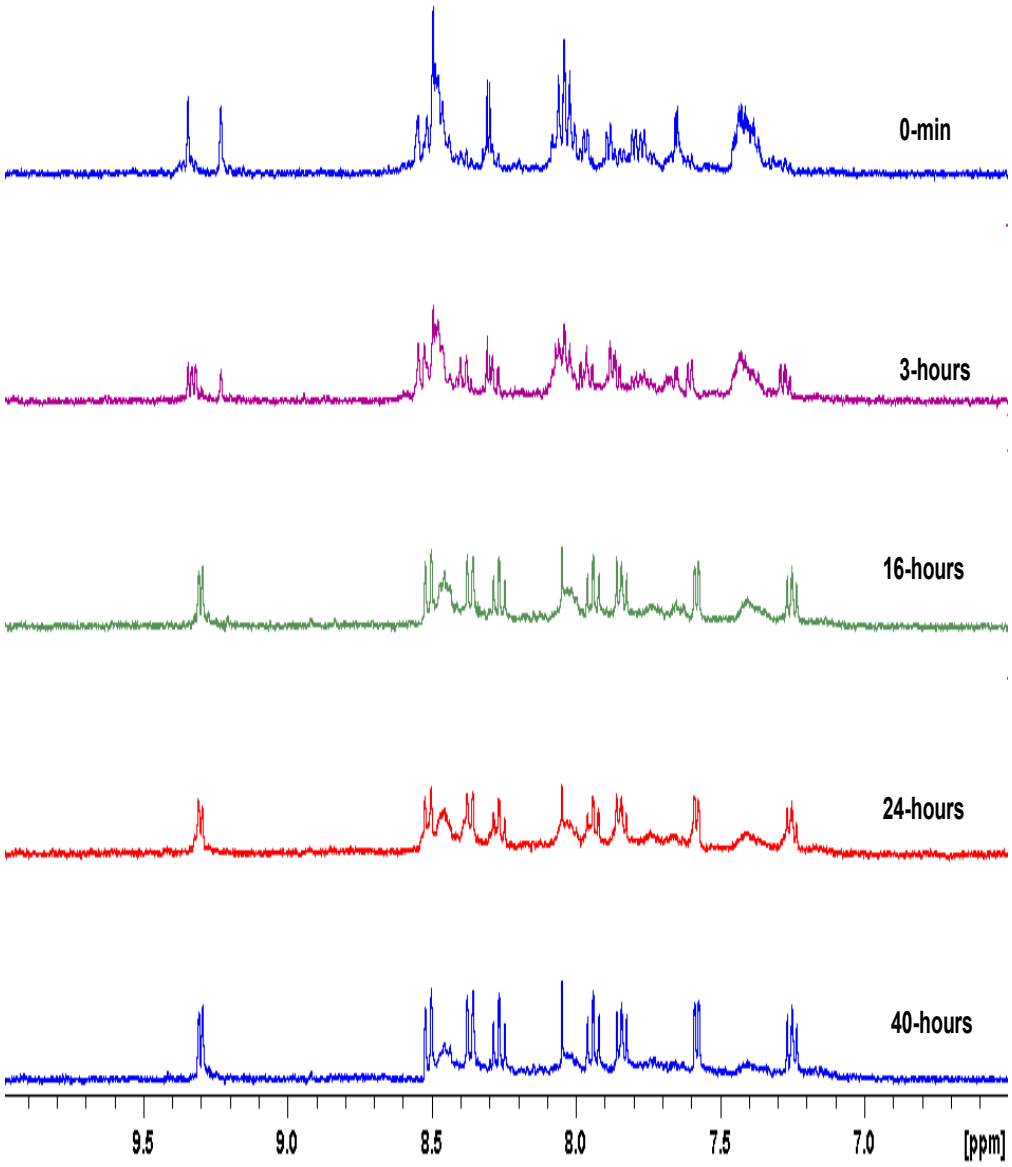

Figure 4.11: *^{1}H NMR* during Irradiation of compound 1 in d_3-acetonitrile.

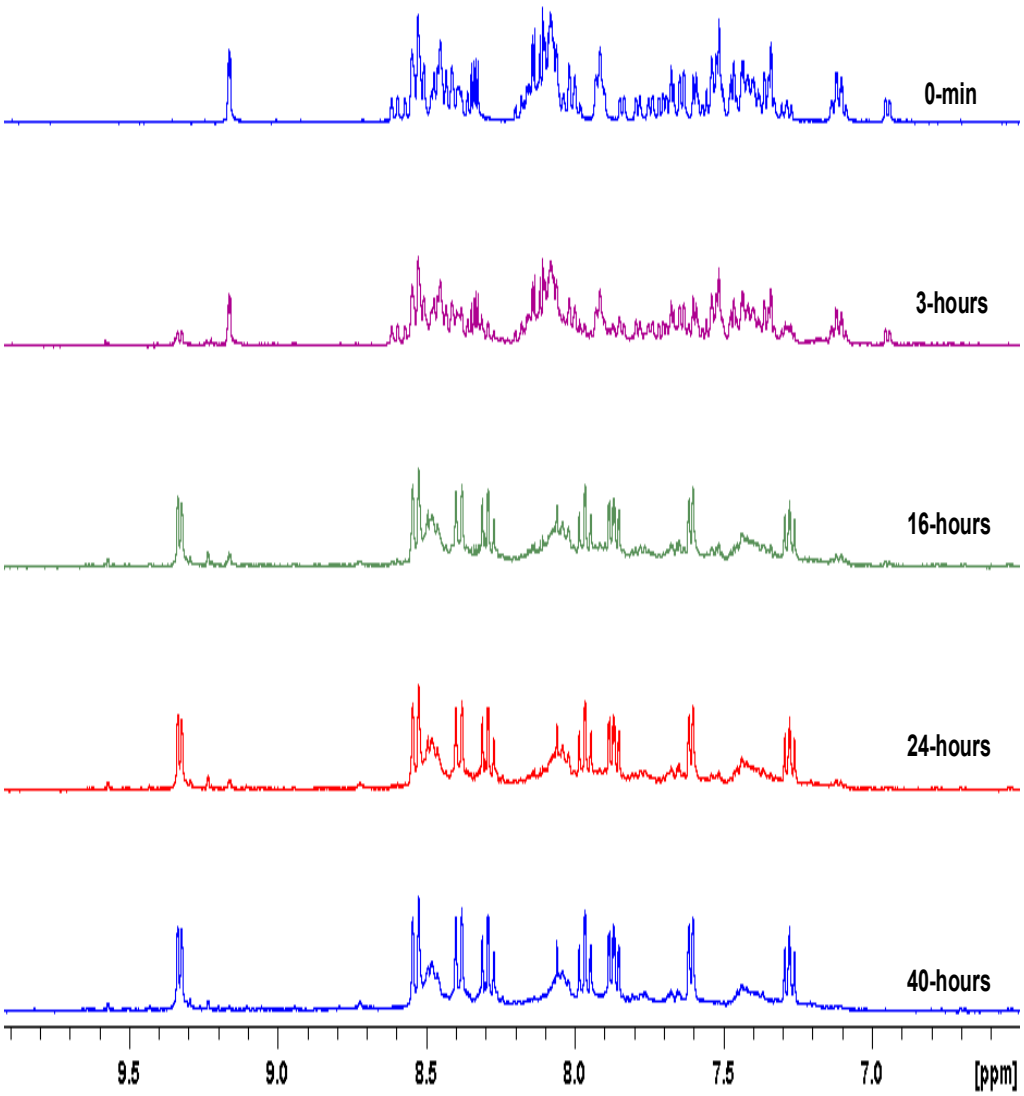

Figure 4.12: *^{1}H NMR during Irradiation of compound 2 in d_3 -acetonitrile.*

In Figure 4.12 the resonances typical for Compound **2** at about 9.2 and 7.0 ppm as shown in the top spectrum are deceasing with increasing radiation time, until the spectrum typical for $[Ru(bpy)_2(CH_3CN)_2]^{2+}$ is obtained. In addition a new species showing 2 signals between 9.2 and 9.3 ppm is observed. This species is assigned to the formation of compound **1**. This is confirmed by the HPLC traces shown in Figure 4.9. The formation of free ligand is observed; see for example the formation

of a sharp peak to about 8.1 ppm in both sets of spectra, another signal is expected at about 9.3 but this overlaps with bpy related signals.

These observations suggest that for compound 2 the following photoinduced processes are taking place in two stages.

$$[Ru(bpy)_2(bpzt)]^+ \xrightarrow{h\nu} [Ru(bpy)_2(bpzt)(CH_3CN)]^+ \quad \textbf{Eq 4.2}$$

$$[Ru(bpy)_2(bpzt)(CH_3CN)]^+ \xrightarrow{h\nu} [Ru(bpy)_2(CH_3CN)_2]^{2+} + (bpzt)^- \quad \textbf{Eq 4.3}$$

4.4 Conclusions

The photochemical processes observed are, in a general sense, in agreement with these obtained before. For the first time the obtained products have been identified by NMR spectroscopy, being semi-preparative HPLC used. The instability of Compound **1** is surprising since in earlier studies its decomposition was not observed. Also for the analogous bpt mononuclear compound temperature dependent measurements have predicted its photochemical stability. Its decomposition in this study is most likely due to the much longer irradiation times and the use of a stronger more focused light source with λ_{max} 430 nm. The inability to separate the two enantiomers of compound **2** was disappointing. This prevents a direct comparison of the photochemical behaviour of the bpt and bpzt dinuclear complexes. Nevertheless the observation that for both compounds the mononuclear compounds will decompose when more intense light and longer irradiation times are used is an important observation.

References:

[1] V. Balzani, A Juris, A. Venturi,; S. Campagna, S. Serroni, *Chem. Rev.* **1996**, *96*, 759.

[2] (a) D. M. D'Alessandro, F. R. Keene, *Pure Appl. Chem.* **2008**, *80*, 1-16; (b) D. M. D'Alessandro, F. R. Keene, *Chem. Rev.* **2006**, *106*, 2270-2298; (c) Launay, J. P. *Chem. Soc. Rev.* **2001**, *30*, 386.

[3] R. Hage, A. H. Dijkhuis, J. G. Haasnoot, R. Prins, J. Reedijk, B. E. Buchanan, J. G. Vos, *Inorg. Chem.* **1988**, *27*, 2185.

[4] J.G. Vos and J.M. Kelly, *Dalton Trans*., **2006**, 4869.

[5] (*a*) V. Balzani and F. Scandola, *Supramolecular Photochemistry*, Ellis Horwood, Chichester, **1991**; V. Balzani (Editor), *Supramolecular Photochemistry*, Reidel, Dordrecht, **1997**.

[6] (a) A. Juris, V. Balzani, F. Barigelletti, S. Campagna, P. Belser and A. von Zelewsky, *Coord. Chem. Rev.*, **1988**, 84, 85; (b) T. J. Meyer, *Acc. Chem. Res.*, **1989**, 22, 163; (c) B. O'Regan and M. Graetzel, *Nature (London)*, **1991**, 335, 737; (d) L. De Cola and P. Belser, *Coord. Chem. Rev.*, **1998**, 177, 301; (e) C. A. Bignozzi, J. R. Schoonover and F. Scandola, *Prog. Inorg. Chem.*, **1997**, 44, 1; (f) M.-J. Blanco, M. C. Jiménez, J.-C. Chambron, V. Heitz, M. Linke and J.-P. Sauvage, *Chem. Soc. Rev.*, **1999**, 28, 293.

[7] (a) V. Balzani, A. Juris, M. Venturi, S. Campagna and S. Serroni, *Acc. Chem. Res.*, **1998**, 31, 26; (b) C. A. Slate, D. R. Striplin, J. A. Moss, P. Chen, B. W. Erickson and T. J. Meyer, *J. Am. Chem. Soc.*, **1998**, 120, 4885; (c) Y.-Z. Hu, S.

Tsukiji, S. Shinkai, S. Oishi and I. Hamachi, *J. Am. Chem. Soc.*, **2000**, 122, 241, (d) V. Balzani, A. Juris, M. Venturi, S. Campagna and S. Serroni, *Chem. Rev.*, **1996**, 96, 759.

[8] (a) R. Hage, R. Prins, J. G. Haasnoot, J. Reedijk, J. G. Vos, *J. Chem. Soc., Dalton Trans.* **1987**, 1389. (b) H. A. Nieuwenhuis, J. G. Haasnoot, R. Hage, J. Reedijk, T. L. Snoeck, D. J. Stufkens, J. G. Vos, *Inorg. Chem.* **1990**, 30, 48. (c) B. E. Buchanan, R. Wang, J. G. Vos, R. Hage, J. G. Haasnoot, J. Reedijk, *Inorg. Chem.* **1990**, 29, 3263. (d) Browne, W. R.; O'Connor, C. M.; Villani, C.; Vos, J. G. *Inorg. Chem.* **2001**, 40, 5461. (e) R. Wang, J. G. Vos, R. H. Schmehl, R. Hage, *J. Am Chem. Soc*. **1992**, 114*,* 1964.

[9] (a) R. Hage, A. H. Dijkhuis, J. G. Haasnoot, R. Prins, J. Reedijk, B. E. Buchanan, J. G. Vos, *Inorg. Chem*. **1988**, 27, 2185. (b) F. Barigelletti, L. De Cola, V. Balzani, R. Hage, J. G. Haasnoot, J. G. Vos, *Inorg. Chem*. **1989**, 28, 4344.

[10] R. J. Crutchley, A. B. P, Lever *Inorg. Chem*. **1982**, 21, 2277.

[11]. R. Hage, J.G. Haasnoot, H.A. Nieuwenhuis, J. Reedijk, R. Wang, and J.G. Vos. *J. Chem. Soc., Dalton Trans*., (1991), 3271**.**

[12] R. Hage, J.G. Haasnoot, J. Reedijk, R. Wang, and J.G. Vos. *Inorg. Chem*., **1991**, 30, 3263.

[13] (a) F. Barigelletti, L. De Cola, V. Balzani, R. Hage, J. G. Haasnoot, J. Reedijk, J. G. Vos, *Inorg. Chem.* **1989,** 28**,** 4344. (b) H. P. Hughes, D. Martin, S. Bell, J. J. McGarvey, J. G. Vos, *Inorg. Chem.* **1993,** 32*,* 4402.

[14] (a) H. P. Hughes and H. Vos, *Inorg. Chem,* 15, **1995,** 34, 4003. (b) C.G. Coates, T.E. Keyes, H.P. Hughes, P.M. Jayaweera, J.J. McGarvey and J.G. Vos. *J. Phys. Chem.A* **1998**, 102, 5013.

[15] R. Hage, J. G. Haasnoot, H. A. Nieuwenhuis, J. Reedijk, D. J. A. De Ridder, J. G. Vos, *J. Am. Chem. Soc*. **1990**, *112*, 9249.

[16] J.G. Vos, M.T. Pryce *Coord. Chem. Rev.* **2010**, 254, 2519.

[17] B. E. Buchanan, R. Wang, J. G. Vos, R. Hage, J. G. Haasnoot and J. Reedijk, *Inorg. Chem.*, **1990**, 29, 3263.

[18] (a) For a review see: F. R. Keene, *Coord. Chem. Rev.*, 1007, 121, 159; (b) W. R. Browne, C. M. O'Connor, C. Villani and J. G. Vos, *Inorg. Chem.*, **2001**, 40, 5461; (c) W. R. Browne, D. Hesek, J. F. Gallagher, C. M. O'Connor, J. S. Killeen, F. Aoki, H. Ishida, Y. Inoue, C. Villani and J. G. Vos, *Dalton Trans.*, **2003**, 2597; (d) D. Hesek,Y. Inoue, S.R. L. Everitt, H. Ishida, M.Kunieda andM.G. B.Drew, *Inorg. Chem.*, **2001**, 39, 317.

[19] B.E. Buchanan, H. Hughes, P. Degn, J.M. Pavon Velasco, B.S. Creaven, C. Long, J.G. Vos, R. A. Howie, R. Hage, J.H. van Diemen, J.G. Haasnoot, and J. Reedijk. *J. Chem. Soc., Dalton Trans*., **1992**, 1177.

CHAPTER 5

Photoinduced Ligand Isomerisation in a Pyrazine Containing Ruthenium Polypyridyl Complex

5.1 Introduction

Following the early work of Adamson [1] and others [2], the investigation of photoinduced processes has developed substantially over the last 50 years. This development was further intensified with the application of ruthenium polypyridyl complexes as dyes for solar cells [3], oxygen sensors [4], and as bioprobes [5] and molecular machines and devices, such as molecular wires, motors and switches [6]. Recently these studies have received further interest due to the potential application of polypyridyl compounds in the development of sustainable and environmentally friendly energy such as photocatalytic hydrogen generation [7] and CO_2 reduction [8].

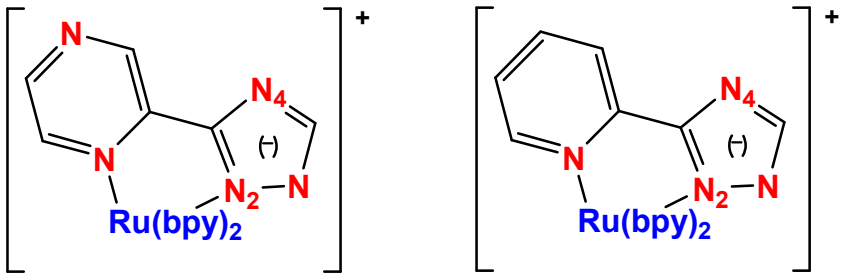

Figure 5. 1. *N2 isomers of* $[Ru(bpy)_2(pztr)]^{2+}$ ***1,*** *(left) and* $[Ru(bpy)_2(pytr)]^{2+}$ ***2,*** *(right), bpy = 2,2'-bipyridine*

Over the last number of years we have reported a series of studies of photoinduced ligand rearrangements of ruthenium polypyridyl complexes containing pyridine-1,2,4-triazole (Hpytr) ligands. Recently such ligands have seen widespread application in iridium(III) based OLED systems also [9]. The complex $[Ru(bpy)_2(pytr)]^+$ (Fig. 5.1), which contains a deprotonated pyridine-1,2,4-triazolato

ligand is photostable upon irradiation in basic acetone and acetonitrile. This photostability is related to the strong σ-donor capacity of the deprotonated triazole ring that provides for a considerable destabilization of the ^{3}MC state that has been indentified as being involved in the photochemical activity of ruthenium polypyridyl complexes [10]. Because of the destabilisation, this excited state is not populated significantly at room temperature. However, for complexes containing protonated or methylated triazole ligands the ^{3}MC level is stabilised and photolability observed [11,12,13], As a result photoinduced ligand dissociation processes are observed where the triazole ligand is not anionic. For $[Ru(bpy)_2(Hpytr)]^{2+}$ there are two coordination isomers possible where the Hpytr ligand is bound either via the N2 or the N4 nitrogen atom of the triazole ring (Fig 5.2). Irradiation in CH_2Cl_2 of either the N2 or N4 isomer leads to a photostable state with a N4:N2 ratio of 4:1

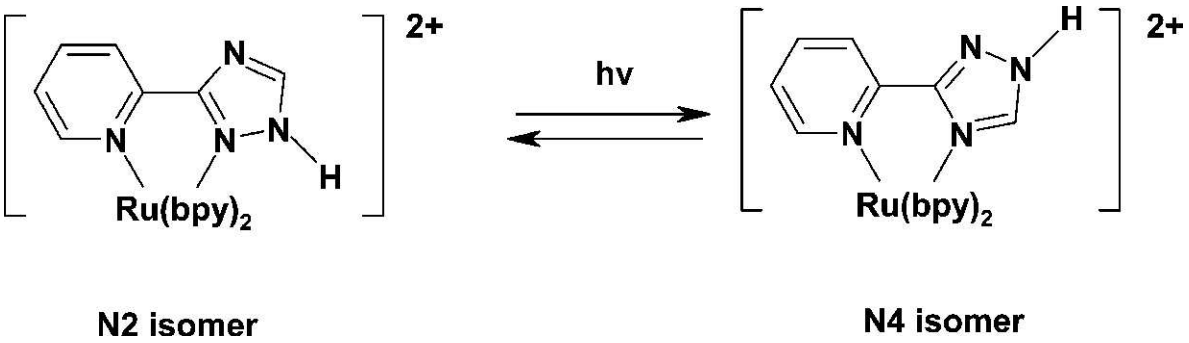

Figure. 5.2*. Reversible N2-N4 isomerisation observed for compound* ***2H****.*

For the analogous pyrazine triazole (Hpztr) based complexes (*e.g.*, Fig. 5.1) photochemically induced ligand isomerisations have not been reported. There have however been extensive photophysical studies [14,15] that have shown that

contrary to that which is observed for the Hpytr based complexes, where the emitting state is bpy based, the lowest energy triplet state in complexes containing the protonated ligand is based on the pyrazine ring.

In this contribution we report the photochemically induced rearrangements observed for the complex $[Ru(bpy)_2(Hpztr)]^{2+}$ (**1H)**. The photochemical processes observed are discussed in terms of the structure and the electronic properties of the complex and are compared with those observed for the analogous complex **2H** based on the Hpytr ligand.

5.2 Experimental Section

5.2.1 Synthesis and Materials

All solvents employed in spectroscopic measurements were of spectroscopic grade (Sigma-Aldrich). All other solvents were of HPLC grade or better. *cis*-$[Ru(bpy)_2Cl_2]$. $2H_2O$ [16], the isomer mixture of $[Ru(bpy)_2(pztr)](PF_6)_2$ **1** [14[a],15[a,c]]. and $[Ru(bpy)_2(CH_3CN)_2](PF_6)_2$ were available from earlier studies [13[b]].

^{1}H-NMR spectra were recorded on a Bruker Advance 400 MHz NMR spectrometer. Data are relative to residual solvent absorptions. UV/vis absorption spectra were recorded on a JASCO 570 UV/vis/NIR spectrophotometer using a 1 cm pathlength quartz cells. Temperature dependent luminescence lifetime studies were carried out using a Spectra Physics Q-switched Nd-YAG laser system as described elsewhere [14[e]]. Analytical High Performance Liquid Chromatography (HPLC) experiments were carried out using an analytical HPLC system consisting

of a Varian Prostar HPLC pump fitted with a 20 µL injection loop, a Varian Prostar PDA detector connected to a dedicated PC, and a HiChrom Partisil P10SCX-3095 cation exchange column. Mobile phase CH_3CN: H_2O: CH_3OH with volume ratio 75:20:5 containing 0.12 M KNO_3. Flow rate: 2.0 cm^3 min^{-1}; detection wavelength: 430 nm. The photochemistry of complexes **1**, **2, 1H** and **2H** was monitored by HPLC and ^1H NMR spectroscopy. HPLC samples were irradiated in acetonitrile or acetone with an array of 60 Kingbright L-7113PBC-Gblue 470$\pm$ 20 nm LEDs. Photolysis studies monitored by ^1H NMR spectroscopy were carried out by irradiating the compounds in NMR tubes and placing them before a 20 W Tungsten filament light source slide projector (Kodak Carousel S-AV 2020). Sample heating was prevented using a water filter. The protonation state of the triazole ring of the complexes was controlled by addition of 100 µl triethylamine or trifluoroacetic acid to the 2 cm^3 NMR sample.

5.3 Results and Discussion

Both isomers show strong ^{1}MLCT bands in the visible part of the spectrum as expected.[15c] the absorption maxima of both compounds are very similar with a λ_{max} of 440 nm for the N2 isomer and a value of 439 nm for the N2 species. Upon protonation the absorption maxima of the N2 and N4 isomers shift to 456 and 457 nm respectively. Because of the similarity of these values and also in the shape of the absorption spectra can not be used to discriminate between the two isomers. As shown before it is expected that the photochemical properties of the pyrazine

triazole compounds will be strongly affected by the protonation state of the triazole ring. In the next section a brief background to the acid/base properties of these compounds is given [17].

5.3.1 The Acid-Base Properties of Transition Metal Complexes.

In general the acid-base properties of metal complexes containing acidic groups can be treated in the same manner as for other more standard acids and the following equation holds;

$$AH + H_2O \longrightarrow A^- + H_3O^+ \qquad \text{Equation 5.1}$$

Earlier studies have shown that for ruthenium polypyridyl complexes containing the pyridinetriazole ligands containing NH groups pK_a values of about 6-4 are obtained , while for the corresponding pyrazine analogues values of about 5-3 are obtained. For example the pKa value for the N2 isomer of the complex containing the unsubstituted pyridine triazole ligand is 6.0 while for the N4 isomer a value of 4.07 is obtained [11[a]]. This indicates that the N2 and N4 isomers have very different properties. For the corresponding pyrazine triazole complexes the values obtained for the N2 and N4 isomers are 5.3 and 3.7 respectively [18]. Since the pK_a values of the free pyridine and pyrazine ligands are 9.2 and 8.7 respectively it is clear that the coordinated ligands are more acidic than their unbound analogues. In addition second acid/base equilibrium is observed for the pyrazine complexes at

a pH of -1.8 which is related to the protonation of the pyrazine ring. The latter process is not of importance for the studies carried out in this chapter. More important is however the fact that the acidity of a compound in the excited state different from that observed in the ground state as outlined below.

In the case where acids and bases are stronger in the excited state than the ground state, photoinduced proton transfer may occur upon excitation and this process is outlined in scheme 5.1

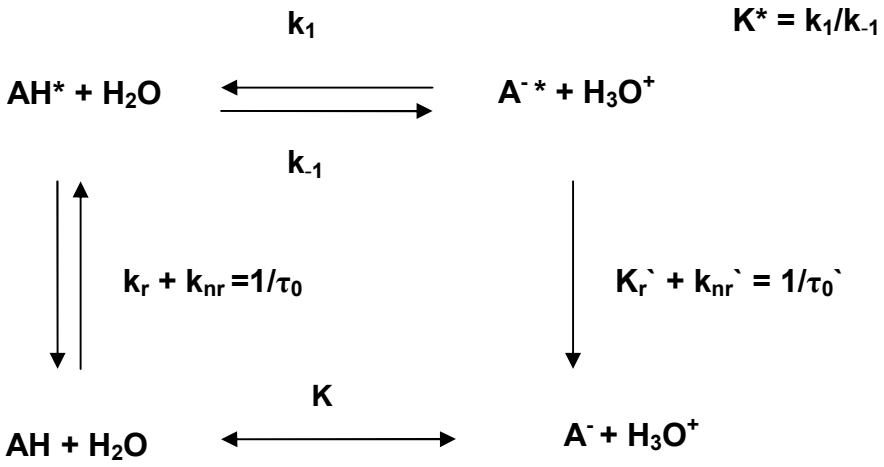

Scheme 5.1. *The processes associated with the excitation of Acid in aqueous solution.*

In this scheme τ_0, τ_0' are the excited state lifetimes of the acidic (AH*) and basic (A^-*) forms, respectively, and k_1 and k_{-1} are the rate constants for deprotonation and protonation. Respectively, k_r and k_r' are the radiative rate constants. The excited-state equilibrium constant is $K_a^* = k_1 / k_{-1}$ [19].

Using this approach, one can estimate the excited state pK_a or pK* by means of Förster cycle as shown in this scheme by using spectroscopic parameters as

shown in Equation 5.2. This equation below is generally used when the excited state emission lifetime of the protonated and deprotonated species are not known:

$$pK^* = pK + 2.1 \times 10^{-3} (\bar{\nu}_{A^-} - \bar{\nu}_{AH}) \qquad \textbf{Equation 5.2}$$

$\bar{\nu}_{A^-}, \bar{\nu}_{AH}$ corresponds to the AH and A^- and they are usually estimated by means of the average of the wavenumbers corresponding to the maxima of absorption and emission:

$$\nu_{0-0} = \frac{\bar{\nu}_{abs}^{\max} + \bar{\nu}_{em}^{\max}}{2} \qquad \textbf{Equation 5.3}$$

When lifetimes are known however the emission data can be used to calculate a more accurate estimate of pK*. The inflection point, pH_i obtained from the emission titration curve can be corrected for the difference in the lifetimes of the protonated (τ_{HA}) and the deprotonated (τ_{A^-}) species according to the following equation [20]:

$$pK_a^* = pH_i + \log \frac{\tau_{acid}}{\tau_{base}} \qquad \textbf{Equation 5.4}$$

Using this method excited state pKa values of 5.5 and 3.8 are obtained for the N4 and N2 isomers respectively. Importantly the acid –base properties of transition metal complexes containing ionizable ligands such as carboxy polypyridyls, triazole, imidazoles and CN^- can provide important information about the nature and the location of the excited state [17]. A small change or decrease in the acidity from the ground state to the excited states this often implies that acid-base functional groups located on this ligand- are not involved in the excited state. However, when the ligand with the acid-base group is the location of the excited

state then the acidity is decreased in the excited state. The acid-base properties of transition metal complexes containing ionisable ligands have been used towards designing pH probes [21,22 23].

An interesting consequence of these acid/base properties is that for pyridine triazolato compounds of the type $[Ru(bpy)_2(pytr)]^+$ are photostable due to the strong σ donor ability of the deprotonated triazole ligand. On the other hand, in the complexes where the protonated or methylated triazole ligands exist, the complexes undergo photoinduced ligand rearrangements due to the population of low lying ^{3}MC at room temperature. This behaviour has been outlined in the $[Ru(bpy)_2(Hpyrt)]^{2+}$, Figure 5.1. A detailed study of this behaviour has been carried out by Wang *et al* have reported the effect of protonation and deprotonation on the photoreactvivity of Ru(II) pyridyltriazole complexes [24]. They reported that protonation of the the N-2 bound and the N-4 bound isomers isomers results in a decrease in the luminescence lifetime in solution and an increase in reactivity upon photolysis in CH_2Cl_2. Photolysis of either protonated isomer in CH_2Cl_2 results in linkage isomerisation with a N4:N2 equilibrium established for photolysis of 4:1 .

5.3.2 Identification of Isomers

For the studies carried out in this chapter, it is important to determine the protonation state of the complexes. In the photochemical experiments this is achieved by the addition of acid or base if required to create solutions with the required acidity. Another important issue is what the protonation state of the

compounds under investigation is when injected onto the HPLC column since considering how easy the triazole is deprotonated, it is likely that the protonation state achieved in the sample during photolysis is changed upon injection on the column. The behaviour observed is shown in Figures 5.3A and B. The absorption spectra obtained for the different species are shown in Figures 5.4 A and B. The spectra observed are very similar, however the spectra obtained in a acidified mobile phase have an absorption maximum at slightly higher energy 440 vs 450 nm for the non-acidified mobile phase. These values are in agreement with values reported for the protonated and deprotonated species as reported in the literature [14].

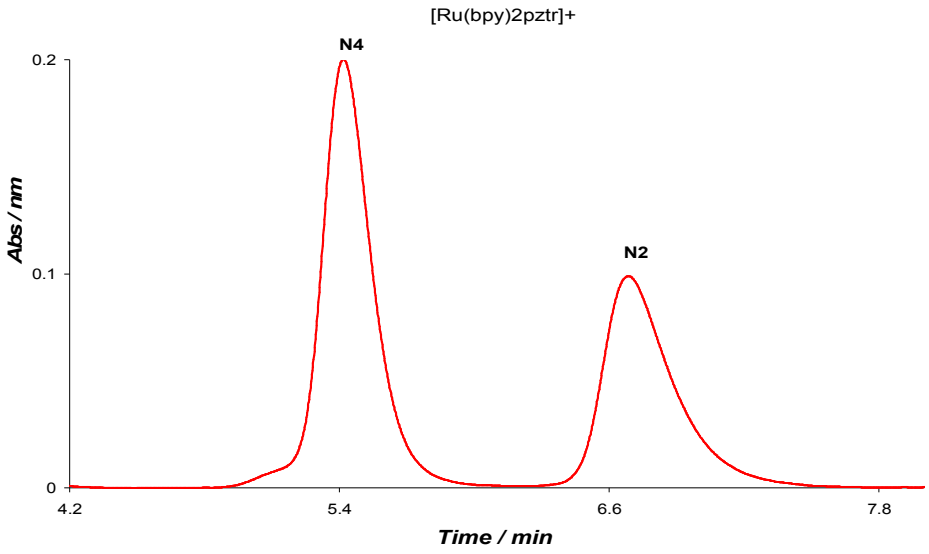

Figure. 5.3A *HPLC trace of N2 and N4 isomers of* ***1*** *injected as mixture. Mobile phase CH_3CN: H_2O: CH_3OH with volume ratio 75:20:5, 0.12 M KNO_3 Flow rate: 2.0 cm^3 min^{-1}; detection wavelength at 430 nm, at 20^o C.*

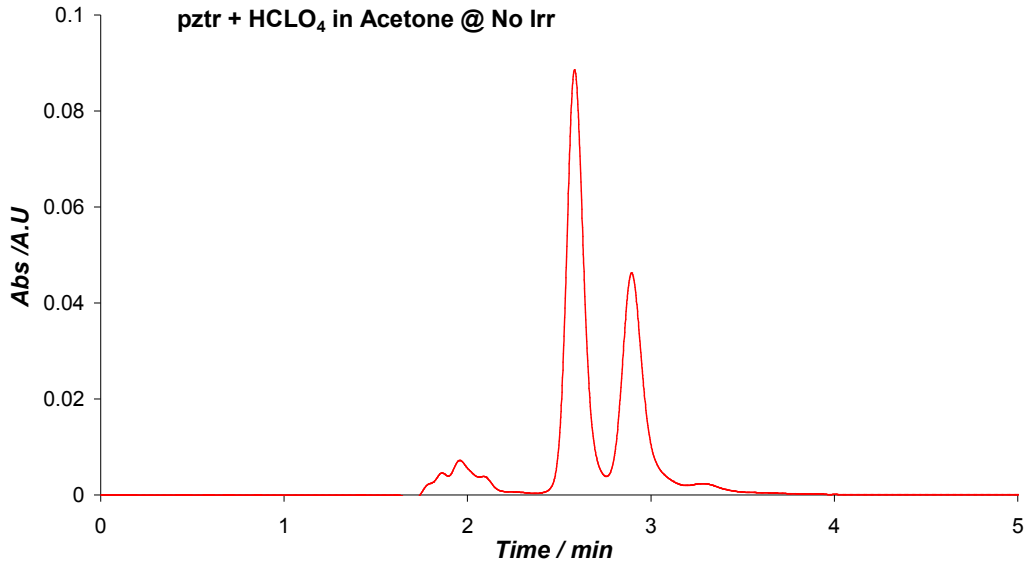

Figure 5.3B *HPLC trace of N2 /N4 mixture of compound 1 , @ 430 nm and 20° C, (Mobile phase CH_3CN: H_2O: CH_3OH with volume ratio 75:20:5 0.12 M KNO_3). Flow rate: 2.0 cm^3 min^{-1}; detection wavelength at 430 nm. Mobile phase containing $HClO_4$,*

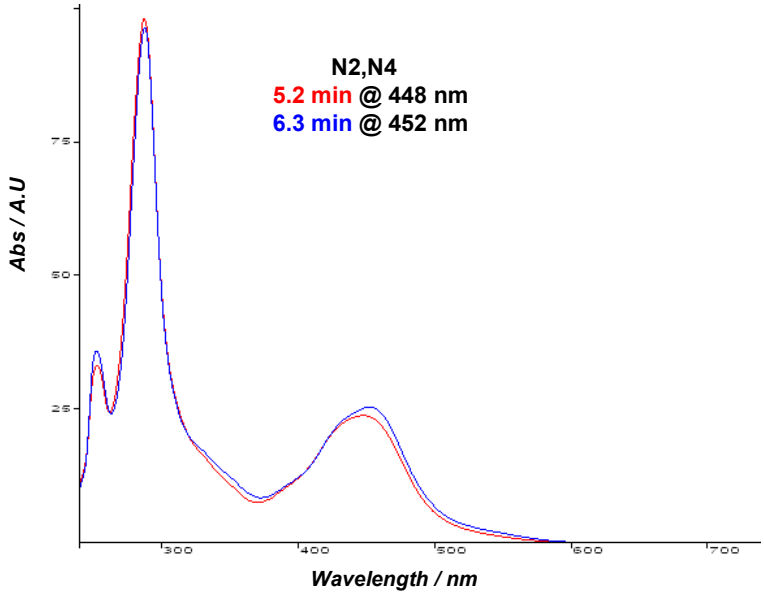

A

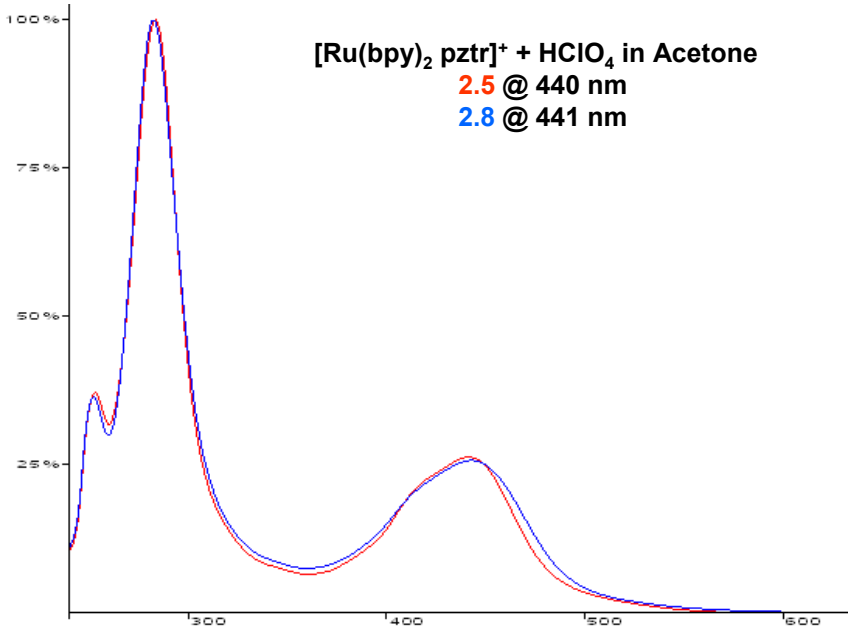

B

Figure 5.4 *Absorption spectra observed for N2/N4 isomers of Compound 1 in) neutral (A) and B) acidic mobile phase (B) See Figure 5.3*

Since it is expected that the compound upon protonation will have a higher charge it is somewhat surprisingly that the retention time of the species in considerably reduced in acidic solution. This may be a result of the change in the chromatographic behaviour with the acidic mobile phase. Importanty when complexes which were dissolved in an acidic solution for photolysis experiments are injected in the non-acidified mobile phase they appear as deprotonated species on the column. In the experiments discussed below the mobile phases used will not contain any acid. The species present in the mobile phase after injection will therefore be deprotonated.

The HPLC chromatogram obtained for a mixture of the N2 and N4 isomers is shown in Figure 5.3. The N4 isomer is observed to have a retention time of 5.4 min, while the N2 is observed at 6.7 min. The same elution order is observed for the pyridinetriazole analogues (*e.g.,* **2**) [11]. In contrast to **2**, the UV/Vis spectra of the two isomers of **1**/**1H** are almost identical and cannot be used for identification as a result. The two species are identified by their ^{1}H NMR spectra however as shown in Figures 5.5 and 5.6. The atom numbering of the ligand is shown below;

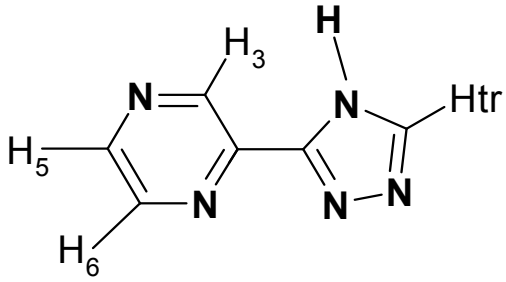

Scheme 5.2*. Numbering of protons in Hpztr ligand*

The assignment is as shown in reference [14]. The bpy signals are not considered here since they do not allow for the identification of the different isomers.

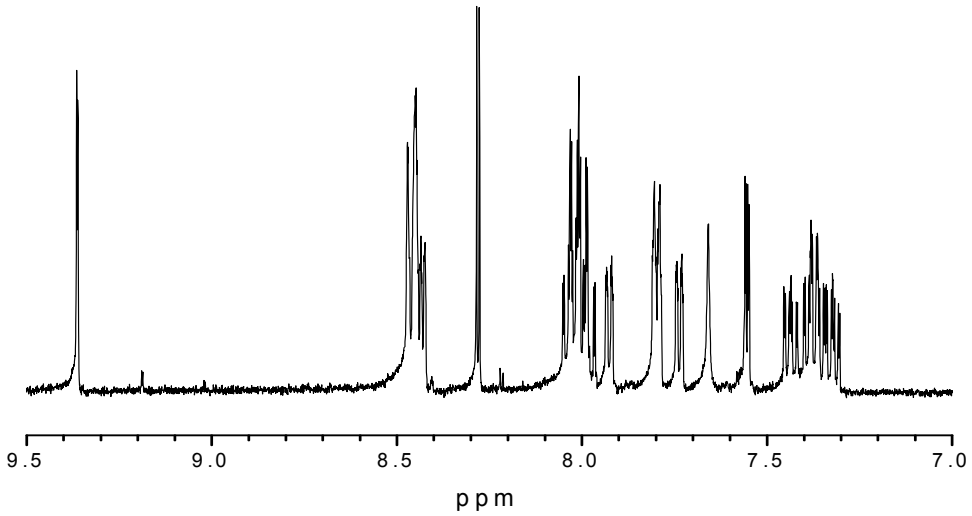

***Figure 5.5**: ^{1}H NMR (CD_3CN, 400 MHz) of N4-[$Ru(bpy)_2(pztr)$]PF_6*

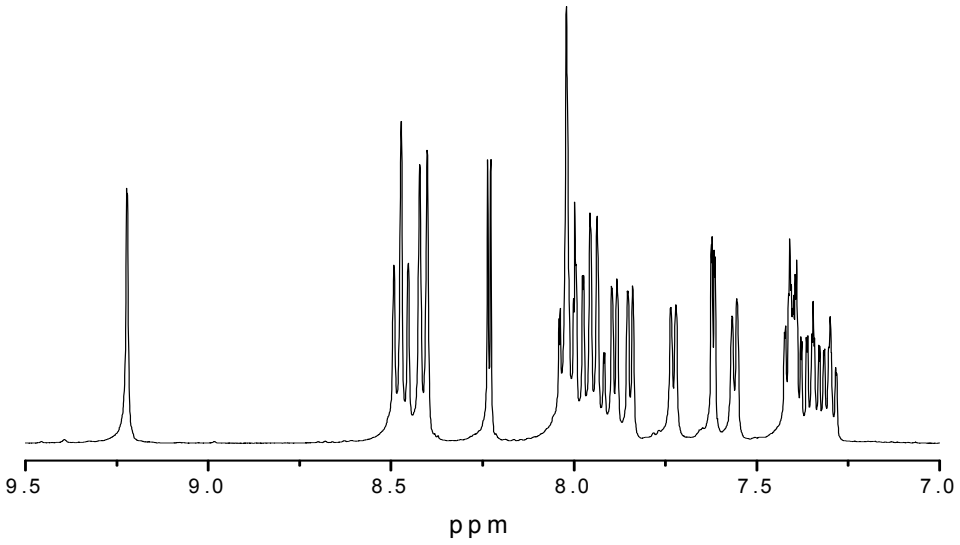

***Figure 5.6**: ^{1}H NMR (CD_3CN, 400 MHz) of N2-[$Ru(bpy)_2(pztr)$]PF_6*

Of most importance for the identification of the nature of the isomer obtained are the ^{1}H NMR absorptions than can be attributed to the pyrazine and the triazole rings. The pyrazine absorptions appear as a singlet (H3) in the range 9.1-9.5 ppm, while H5 appears at ca. 7.8 ppm and H6 at ca. 8.2 ppm ; the exact location depending on whether the compound is protonated or not. The most indicative feature identifying the isomeric form is the position of the H3 proton of the pyrazine ring and the H5 proton of the triazole ring. For the protonated N2 isomer the H5 proton is observed at 8.91 ppm and for the deprotonated N2 isomer at 8.0 ppm. For the N4 isomer the corresponding values are at ca. 8.4 and 7.55 ppm respectively. The H3 proton of the pyrazine ring for the deprotonated N2 isomer is found at 9.18 ppm, while in the protonated species a value of 9.63 ppm is observed. For the N4 isomer values of 9.3 and 9.57ppm are observed. These values were obtained in acetone however and vary depending on the amount of acid added and the water content of the solvent. The rather large difference between the values observed for the H5 protons for the two isomers is related to the through space interaction between these protons and neighbouring bpy ligands especially in the case of the N4 isomer [$15^{c,}25$]. This through space interaction results in the considerable shift to lower ppm values for the proton in the N4 isomer compared with the N2 species.

5.3.3 Irradiation in Acetonitrile

The photochemical properties of **1** and **1H** were investigated using ^{1}H NMR spectroscopy and HPLC. Irradiation of the compounds was carried out in both acetonitrile and acetone.

HPLC and ^{1}H NMR spectroscopic studies indicate that both isomers of the deprotonated compound **1** are photostable in the presence of the base TEA in acetonitrile and in acetone. This is in agreement with the reported behaviour of compound **2** [11]. However, acidification of the solution prior to irradiation allows for photoinduced changes to be observed. The photoinduced changes for N4 in acidified acetonitrile monitored by HPLC are shown in Fig. 5.7.

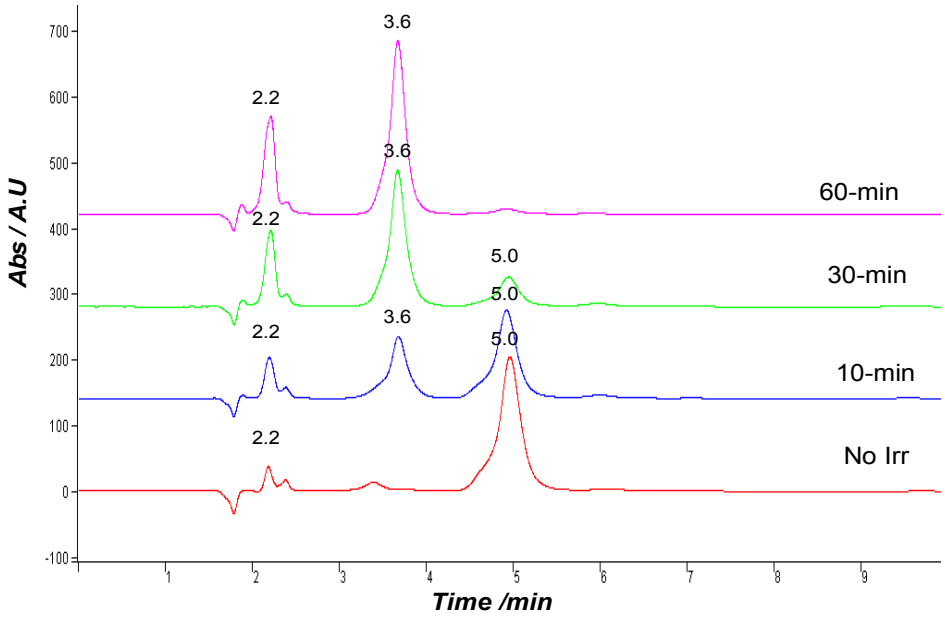

Figure 5. 7. *HPLC trace following the irradiation of the N4 isomer in CH_3CN with CF_3CO_2H (Mobile phase CH_3CN: H_2O: CH_3OH with volume ratio 75:20:5; 0.12 M KNO_3. Flow rate .2.0 cm^3 min^{-1}; detection wavelength at 430 nm, 20° C*

The decrease in the signal for the N4 isomer (retention time of 5.0 min) with irradiation is accompanied by the appearance of a new peak at 3.6 min. This signal which shows an absorption maximum at 425 nm is identified

The irradiation of the protonated N2 isomer in acetonitrile was monitored by ^{1}H NMR spectroscopy also (Fig. 5.8). ^{1}H NMR spectra show that upon irradiation of both the N2 and the N4 isomers of **1H** in acidic acetonitrile results in formation of the same final product, $[Ru(bpy)_2(CH_3CN)_2]^{2+}$ (Fig. 5.), which was confirmed by comparison with the spectrum of an authentic sample. The appearance of a second product with a retention time of 2.2 min (λ_{max} = 472 nm) is observed also. The nature of these species could not be determined unambiguously but may be related to the intermediate observed in the ^{1}H NMR spectrum in Fig. 5.8

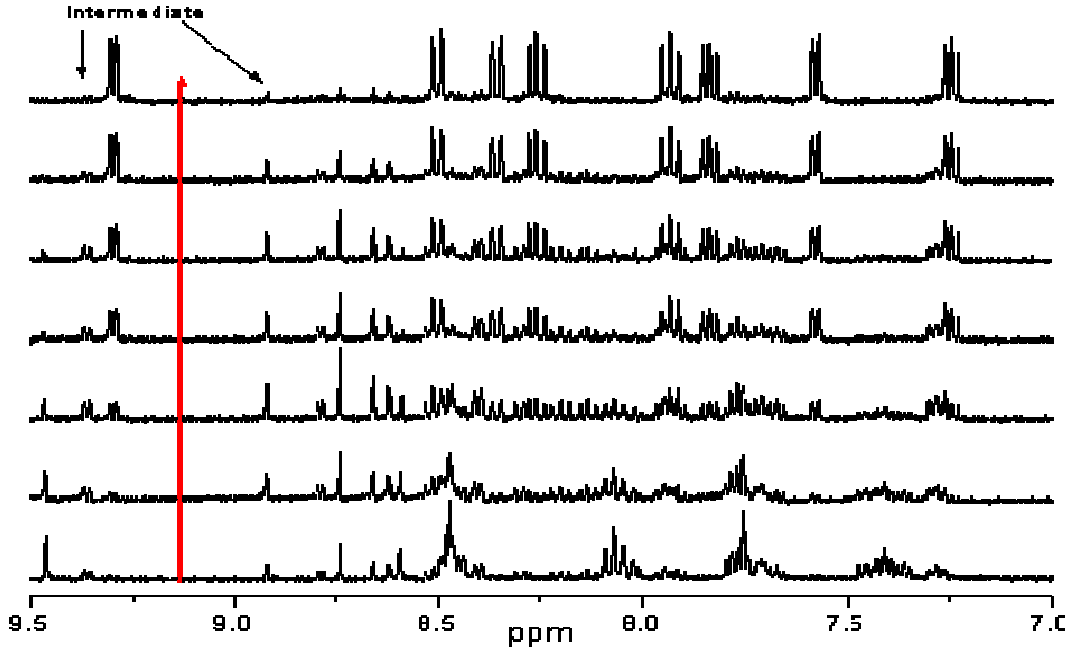

Figure. 5.8 *^{1}HNMR spectra obtained during irradiation of N2 isomer of $[Ru(bpy)_2(Hpztr)]^{2+}$ in acetonitrile with CF_3CO_2H.*

In this Figure an intermediate is also observed with signals at 8.0, 8.9 pm and 9.3 pm which disappears upon further photolysis. The observed process could suggests that in this intermediate the pyrazine ring remains attached to the metal centre, since this allows for reorientation of the triazole ring in the sterically most favoured position. However, our earlier studies have shown that an alternative intermediate species is formed upon photolysis of the related complex $[Ru(bpy)_2(L\text{-}L')]^{2+}$ where L-L' is 4-methyl-3-(pyridine-2-yl)-1,2,4-triazole. In this intermediate the triazole ring is bound to the N1 atom as shown in Figure 5.6 [13[b]]. Such a species can be formed starting from both **1H** isomers and hence the formation of the isomer where the triazole ring is coordinated to the metal centre via the N1 atom of the triazole ligand can not be excluded.

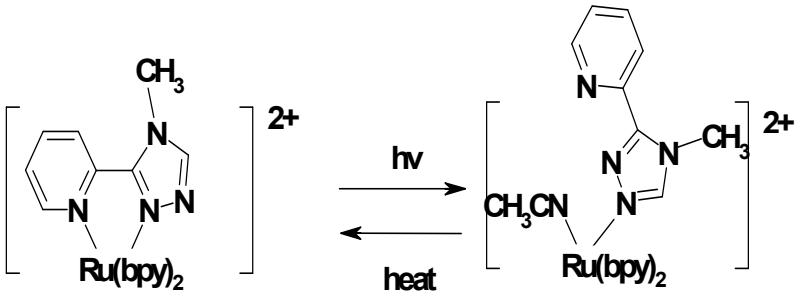

Figure. 5.9 *Photo- and thermally induced coordination changes for* $[Ru(bpy)_2(L\text{-}L')]^{2+}$ *where L-L' is 4-methyl-3-(pyridine-2-yl)-1,2,4-triazole.*

So both protonated isomers undergo ligand exchange processes when irradiated in acidic acetonitrile. The end product is the bis(acetonitrile) complex while an intermediate species most likely containing a monodentate coordinated pyrazine ligand is observed by ^{1}H NMR.

5.3.4 Irradiation in Acetone

The photostability of the protonated complex **1H** in acetone was investigated. Surprisingly, irradiation of the N4 isomer of **1H** does not result in any observed changes over at least a 2 h period. The N2 isomer, by contrast, shows photoreactivity as illustrated in Fig. 5.10. Initally the N2 isomer is observed at a retention time of 7.4 min. After irradiation the N4 isomer is present as the main product with a retention time of 5.9 min. As observed in the ^{1}H NMR spectra the formation of other minor products is observed also (Fig. 5.11).

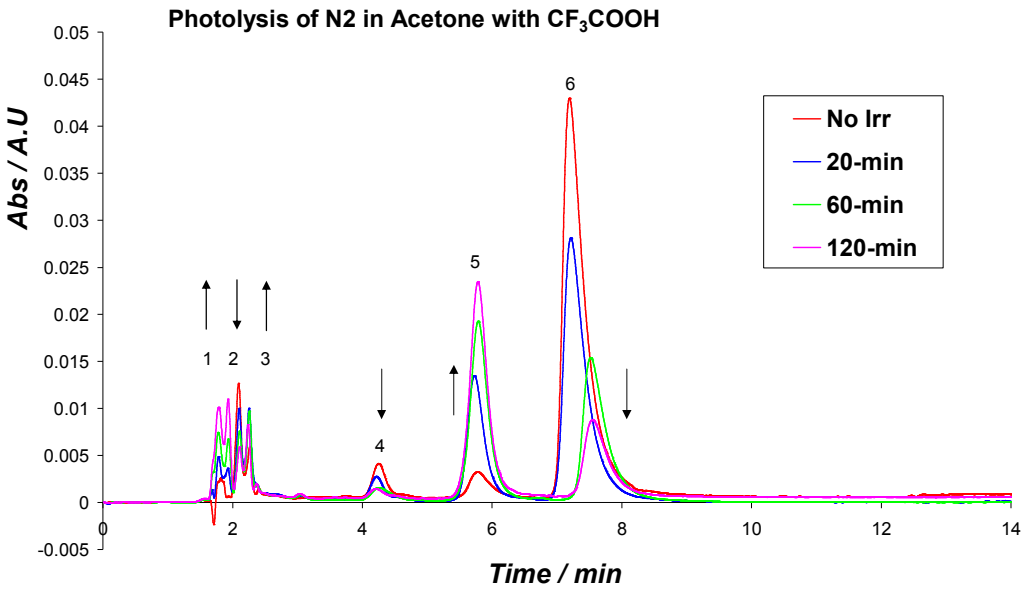

Figure 5.10 *HPLC assessment of the photoisomerisation of N2 isomer of* ***1H*** *in acetone in the presence of CF_3COOH.*

Most indicative for the isomerisation from the N2 to the N4 isomer are the changes observed for the pzH3 peak which changes from 9.63 ppm for the N2 isomer to

9.54 pm. Additionally the peak of the pzH5 shifts from 8.58 pm to 8.61 pm. During irradiation two peaks appear at 9.1 pm and 9.17 pm and disappear in the final spectrum, indicating (as in the HPLC traces, i.e. at 4.2 and 2.0 min) the formation of a small amount of an intermediate. The concentrations of these species are however to low to allow for definitive assignment.

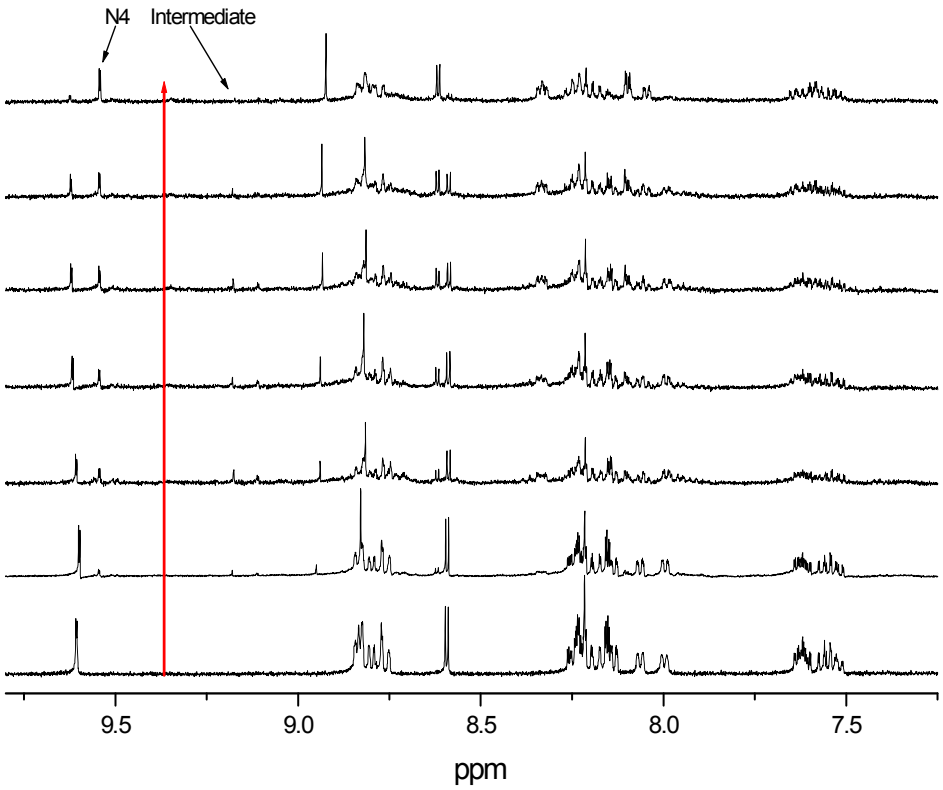

a)

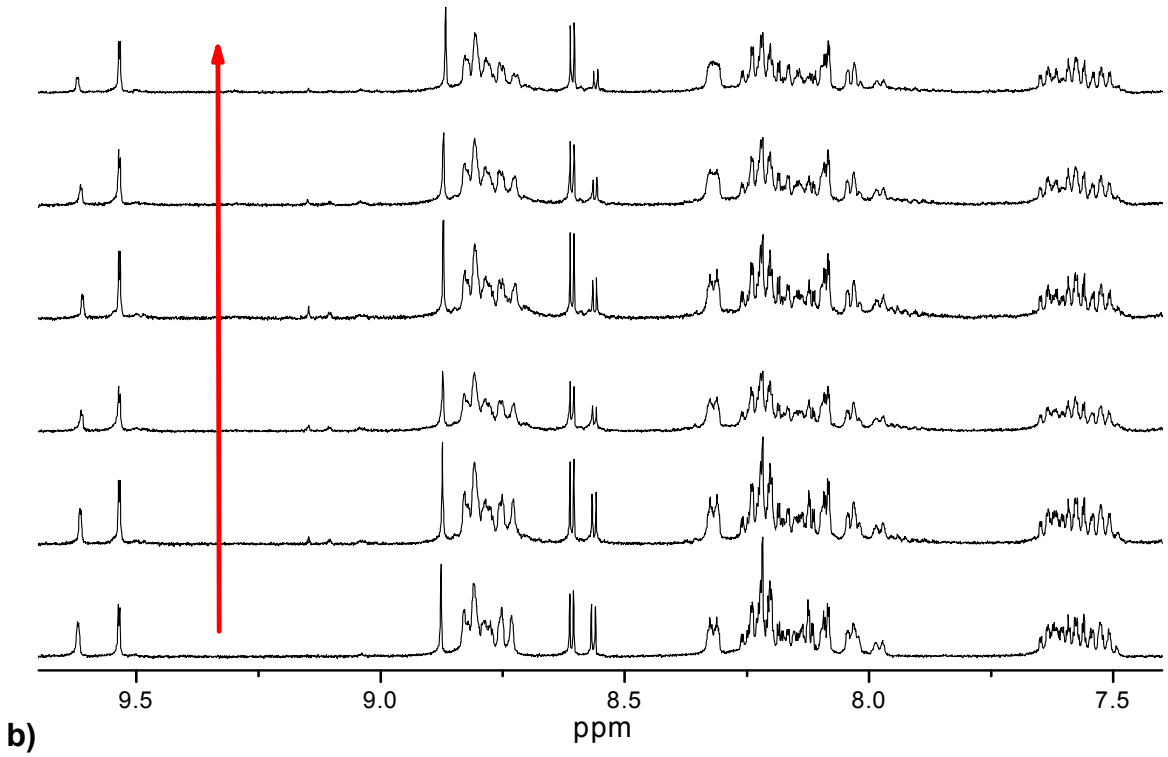

***Figure. 5.11**. a) Irradiation of the N2 isomer of $[Ru(bpy)_2(Hpztr)]^{2+}$ (**1H**) in acetone with CF_3CO_2H. (b) Irradiation of a 1:1 mixture of the N2 and N4 isomer of $[Ru(bpy)_2(Hpztr)]^{2+}$ (**1H**) in acetone with CF_3CO_2H. Spectra run from bottom to top in each case.*

5.3.5 Activated Crossing from the ^{3}MLCT to ^{3}MC States

Ligand exchange via cleavage of metal–ligand bonds is a paradigm photochemical reaction and is central to results discussed here. Meyer and co-workers [26], in their studies of ruthenium(II) polypyridyl complexes, identified the triplet metal centred (^{3}MC) state as being responsible for the photochemical ligand dissociation observed for these compounds. The state corresponds to population of the antibonding (e_g) orbitals which is accessed at room temperature from the lowest ^{3}MLCT state manifold. This process is thermally activated and the difference in

energy between the ^{3}MLCT and ^{3}MC states can be estimated indirectly from the temperature dependence of the emission lifetime. The activation parameters obtained in an ethanol/methanol (4:1) solvent system over the temperature range 150-300 K are shown in Table 5.1 and are compared with related data for Hpytr based compounds *N2***2** and *N4***2**. Values of the ^{3}MLCT – ^{3}MC energy gap for **1H** complexes are similar to those obtained for their **2H** analogues.

Table 5.1. *Activation parameters and kinetic data for ruthenium(II) pyrazine triazole complexes and related pyridine triazole analogues.*

	E_a / cm^{-1} [a]	A / s^{-1}	k_{77K} / s^{-1}
*N4***1**	1300	5.1×10^{9}	2.2×10^{5}
*N2***1**	1200	3.6×10^{9}	2.4×10^{5}
*N4***1H**	2950	1.5×10^{13}	1.5×10^{5}
*N2***1H**	2200	9.0×10^{11}	1.4×10^{5}
*N4***2** [b]	600	3.1×10^{7}	6.4×10^{5}
*N2***2** [b]	550	4.7×10^{7}	4.1×10^{5}
*N4***2H** [b]	2850	9.2×10^{13}	2.8×10^{5}
*N2***2H** [b]	1700	6.0×10^{10}	2.8×10^{5}

[a]Data obtained in ethanol/methanol (4:1) at temperatures 150-300 K. Rate constant errors ± 5%, activation parameters ± 10%. [b] values obtained from reference [11].

The temperature dependent lifetime data in the temperature range 150-300 K were analysed by assuming that the excited state decay consists of a temperature independent intrinsic decay from the ^{3}MLCT state and a single thermally activated non-radiative decay process according to the equation 1:

$$\frac{1}{\tau_{obs}} = k_{77\,\mathrm{K}} + A\exp(\frac{-E_a}{RT}) \qquad \textbf{Equation 5.5}$$

Where $k_{77K} = k_{nr} + k_r$ (the sum of the temperature independent radiative and non-radiative decays from the ^{3}MLCT direct to the ground state), A is the preexponential factor and E_a is the activation energy for crossing from the ^{3}MLCT to the ^{3}MC excited state. k_{77K} is obtained at 77 K, assumes that k_{nr} and k_r are temperature independent above 77 K and that population of the ^{3}MC states is effectively prevented at 77 K

Activation parameters obtained for ruthenium polypyridyl complexes usually fall into one of two categories:

a) Small activation energies (< 800cm^{-1}) and low prefactors (<10^9 s^{-1}).

b) Large activation energies (> 2000 cm^{-1}) and large prefactors (> 10^{11} s^{-1}).

Complexes exhibiting the former behaviour are typically unreactive towards photosubstitution. This is indeed observed for the deprotonated species**.** The low prefactor suggests the process involves the population of an MLCT state of largely singlet character that is weakly coupled to the **^{3}**MLCT state.[27] Complexes exhibiting the second type of behaviour are typically photochemically active and the

activation process has been ascribed as being due to population of a ^{3}MC state. If relaxation of the ^{3}MC state is rapid relative to crossover from the ^{3}MC state back to the ^{3}MLCT state, the measured E_a represents the activation energy for ^{3}MLCT–^{3}MC internal conversion. For such a process the prefactor is expected to be large (10^{13}-10^{14}). The N4 isomers for both **1H** and **2H** fall in this category.

The N2 isomer of $[Ru(bpy)_2(Hpztr)]^{2+}$ (i.e. *N2***1H**) intermediate behaviour was observed, with an activation barrier of 2200 cm^{-1} and a prefactor of 9.0 x 10^{11}. This may indicate that the ^{3}MLCT and ^{3}MC states are in equilibrium [28]. For compound *N2***2H** this intermediate behaviour was also observed [11].

Population of the ^{3}MC state is a key step in the photochemistry of the protonated pyrazyltriazole complexes. pK_a data indicate that triazole is a stronger σ-donor when coordinating via the N2 nitrogen than via the N4 nitrogen [11,14[a]]. Hence for the N2 isomers of **1H** and **2H** the ^{3}MC state would be expected to lie higher in energy than the for the corresponding N4 isomers. Consequently the larger activation energy for population of the ^{3}MC state from the ^{3}MLCT state is expected to be higher for the N2 isomers compared with the N4 isomers. However, this is not found to be the case, suggesting that population of the ^{3}MC excited state is not the rate determining step in the photochemistry of the protonated pyridine triazole complexes. Instead, the rate-determining step may be governed by the formation of the monodentate species during the photoisomerisation and the subsequent ground state thermal self-healing process. This may be related to the difference observed between the N4 and N2 isomers in the deactivation

mechanism for the ^{3}MC state. While the prefactors for the N2 isomers suggest the existence of an equilibrium with the ^{3}MCLT state, fast deactivation of the ^{3}MC state is taking place via other pathways.

5.4 Conclusions

The aim of this study is to compare the photochemical properties of the $[Ru(bpy)_2(pztr)]^+$ **1**, and $[Ru(bpy)_2(pytr)]^+$ **2** and their protonated analogues **1H** and **2H**. Earlier studies have shown that for **1**, **2** and **2H** the LUMO and lowest emissive ^{3}MLCT state is based on the bpy ligands [11], while for **1H** the LUMO and lowest emissive ^{3}MLCT state is pyrazine based [14[d,e]]. The purpose of this study is therefore to investigate whether the difference in the location of the LUMO/^{3}MLCT state affects the photolability of the complexes. The deprotonated complexes **1** and **2** are both photostable in acetonitrile and acetone. This is not unexpected since the activation parameters (Table 1) for these compounds indicate the population of the ^{3}MC excited state is not significant. The photolability of **1H** and **2H** in CH_3CN is again the same, with ligand loss occurring with the formation of $[Ru(bpy)_2(CH_3CN)_2]^{2+}$ as the final product. Differences are however observed upon photolysis in acetone. As reported earlier photoinduced interconversion of the N2 and N4 isomers of **2H** is observed in CH_2Cl_2, with steady-state equilibrium of N4:N2 of 4:1. Upon irradiation of **1H** however, it was found that the inactive N4 isomer is photostable while the N2 species isomerises to the N4 species via an intermediate. The results obtained therefore indicate that for these compounds the location of the LUMO in **1H** and **2H** does not affect the photolytic behaviour

fundamentally. The photostability of the N4 isomer of **1H** is however an important point but is likely to be associated with the thermal stability of the primary photoproduct, i.e the species that contains a monodentate coordinated ligand.

References:

[1] (a)W. A. Adamson, *J. Phys Chem*., **1967**, 79, 798; (b) W. A. Adamson, *Adv. Chem. Series, No. 49,* American Chemical Society, Washington, D. C., **1965**.

[2] L. G. Vanquickenborne and A. Ceulemans, *J. Am Chem. Soc*., **1977**, 99, 2208.

[3] (a) B. O'Regan and M. Grätzel, *Nature* **1991**, 353, 737; (b) A. Hagfeldt and M. Grätzel, *Acc. Chem. Res.*, **2000**, 33, 269.

[4] (a) A. P. Doherty, M. A. Stanley, D. Leech and J. G. Vos. *Anal. Chim. Acta*, **1996**, 319, 111; (b) A. Lobnik, I. Oehme, I. Murkovic and O. S. Wolfbeis, *Anal. Chim. Acta,* **1998**, 367, 159; (c) J. N. Demas and B. A. DeGraff, *J. Chem. Edu*., **1997**, 74, 690.

[5] (a) J. K. Barton, A. T. Danishefsky and J. M. Goldberg, *J. Am. Chem. Soc*., **1984**, 106, 2172; (b) J. K. Barton, J. M. Goldberg, C. V. Kumar and N. J. Turro, *J. Am. Chem. Soc*., **1986**, 108, 2081; (c) J. M. Kelly, A. B. Tossi, D. J. McConnell and C. OhUigin. *Nucleic Acid Res.*, **1985**, 13, 6017; (d) L. Jacquet, J. M. Kelly and A. Kirsch-De Mesmaeker, *J. Chem. Soc. Chem. Comm*. **1995**, 913; (e) L. Jacquet, R. J. H. Davies, A. Kirsch-De Mesmaeker and J. M. Kelly, *J. Am. Chem. Soc.,* **1997**, 119, 11763; (f) L. M. Wilhelmsson, F. Westerlund, P. Lincoln and B. Norden, *J. Am. Chem. Soc.***, 2002**, 124, 12092.

[6] (a) V. Balzani, M. Venturi and A. Credi, *Molecular Devices and Machines*, Wiley-VCH, Weinheim **2003**; (b) J-P. Sauvage, *Acc. Chem. Rev.*, **1998**, 31, 611; (c) V. Balzani, *Small*, **2005**, 1, 278, (d) P. Mobian, J-M. Kern and J-P Sauvage, *Angew. Chem. Int. Ed*. **2004**, 43, 2392.

[7] S. Rau, D. Walther and J. G. Vos, *Dalton Trans*., **2007**, 915 and references therein.

[8] (a) H. Takeda, K. Koike, H. Inoue and O. Ishitani, *J. Am. Chem. Soc*., **2008**, 130, 2033; (b) Y. Hayashi, S. Kita, B. S. Brunschwig and E. Fujita, *J. Am. Chem. Soc*., **2003**, 125, 11976.

[9] (a) S-C Lo, C. P. Shipley, R. N. Bera, R. E. Harding, A. R. Cowley, P. L. Burn and I. D. W. Samuel, *Chem. Mater*., **2006**, 18, 5119; (b) E. Orselli, G. S. Kottas, A. E. Konradsson, P. Coppo, R. Fröhlich, L. De Cola, A. van Dijken and H. Börner, *Inorg. Chem*. **2007**, 46, 11082; (c) M. Felici, P. Contreras-Carballada, Y. Vida, J. M. M. Smits, R. J. M. Nolte, L. De Cola, R. N. Williams and M. C. Feiters, *Chem. Eur. J*, **2009**, 15, 13124; (d) C-H. Yang, S-W. Li. Y Chi, Y-M. Cheng, Y-S. Yeh, P-T. Chou, G-H. Lee, C-H. Wang and C-F. Shu, *Inorg. Chem*., **2005**, 44, 7770.

[10] (a) W. M. Walcholtz, R. A. Auerback, R. H. Schmehl, M. Ollino and W. R. Cherry, *Inorg. Chem.,* **1985**, 24, 1758; (b) G. H. Allen, R. P. White, D. P. Rillema and T. J. Meyer, *J. Am. Chem. Soc.,* **1984,** 106, 2613; (c) F. Barigelletti, A. Juris, V. Balzani, P. Belser and A. von Zelewsky, *Inorg. Chem*., **1983**, 22 ,3335.

[11] (a) R. Wang, J. G. Vos, R. H. Schmehl and R. Hage. *J. Am Chem. Soc*., **1992**, 114, 1964; (b) B.E. Buchanan, J.G. Vos, M. Kaneko, W.J.M. van der Putten, J.M. Kelly, R. Hage, R. Prins, J.G. Haasnoot, J. Reedijk and R.A.G. de Graaff. *J. Chem. Soc., Dalton Trans*., **1990**, 2425.

[12] S. Fanni, F. M. Weldon, L. Hammarström, E. Mukhtar, W. R. Browne, T. E. Keyes and J.G. Vos, *Eur. J. Inorg. Chem*., **2001**, 529.

[13] (a) B. E. Buchanan, H. Hughes, J. van Diemen, R. Hage, J. G. Haasnoot, J. Reedijk and J. G. Vos. *J. Chem. Soc, Chem. Commun*. **1991**, 300; (b) B. E. Buchanan, H. Hughes, P. Degn, J. M. Pavon Velasco, B. S. Creaven, C. Long, J. G. Vos, R. A. Howie, R. Hage, J. H. van Diemen, J. G. Haasnoot and J. Reedijk. *J. Chem. Soc., Dalton Trans*., **1992**, 1177.

[14] (a) H. P. Hughes and J. G. Vos *Inorg. Chem*., **1995**, 34, 4001; (b) H. E. B. Lempers, J. G. Haasnoot, J. Reedijk, R. Hage, F. M. Weldon and J. G. Vos, *Inorg. Chim. Acta*., **1994**, 225, 67; (c) R. Hage, H. E. B. Lempers, J. G. Haasnoot, J. Reedijk., F. M. Weldon and J. G. Vos. *Inorg. Chem*., **1997**, 36, 3139; (d) T. E. Keyes, C. M. O'Connor and J. G. Vos, *Chem. Commun*., **1998**, 889; (e) T. E. Keyes, C. M. O'Connor, U. O'Dwyer, C. C. Coates, P. Callaghan, J. J. McGarvey and J. G. Vos. *J. Phys*. *Chem. A*, **1999**, 103, 8915.

[15] (a) H. A. Nieuwenhuis, J. G. Haasnoot, R. Hage, J. Reedijk, T. L. Snoeck, D. J. Stufkens and J. G Vos, *Inorg. Chem.* **1991**, 30, 48; (b) R. Hage, J. G. Haasnoot, J. Reedijk, R. Wang, and J. G. Vos. *Inorg. Chem*., **1991**, 30, 3263; (c) R. Hage, J. G. Haasnoot, H. A. Nieuwenhuis, J. Reedijk, R. Wang, and J. G. Vos, *J. Chem. Soc., Dalton Trans*., **1991**, 3271; (d) C. G. Coates, T. E. Keyes, H. P. Hughes, P. M. Jayaweera, J. J. McGarvey and J. G Vos, *J. Phys. Chem. A,* **1998**, 102, 5013; (e) W. R. Browne, N. M. O'Boyle, W. Henry, A. L. Guckian, S. Horn, T. Fett, C. M. O'Connor, M. Duati, L. De Cola, C. G. Coates, K. L. Ronayne, J. J. McGarvey and J. G. Vos, *J. Am. Chem. Soc*., **2005**, 127, 1229.

[16] B. P. Sullivan, D. J. Salmon and T. J. Meyer, *Inorg. Chem.,* **1978**, 17, 3334.

[17] J.G. Vos. *Polyhedron*, Polyhedron, **1992**, *11*, 2285.

[18] R. Hage, J.G. Haasnoot, H.A. Nieuwenhuis, J. Reedijk, R. Wang, and J.G. Vos. *J. Chem. Soc., Dalton Trans*., **1991**, 3271.

[19] B. Valeur, Molecular Fluorescence; Principles and Applications, **2002**, Wiley, Weinheim.

[20] W. Browne, N. M. O'Boyle, J. J. McGarvey, and J. G. Vos, Chem. Soc. Rev., **2005**, 34, 641.

[21] C.-H. Su, H.-Y. Chen, K. Y-D. Tsai, and I-J. Chang, J. Phys. Chem. B, **2007**, 111, 6857.

[22] E. C. Constable, C. E. Housecroft, A. C. Thompson, P. Oasssaniti, S. Silvi, M. Maestri, A. Credi, Inorganica Chimica Acta , **2007**, 360 , 1102.

[23] S. Campagna, F. Puntoerio, F. Nastasi, G. Bergamini, V. Balzani, Top Curr Chem DOI 10.1007/128-2007-133.

[24] R. Wang, J. G. Vos, R. H. Schemhl, and R. Hage , J. Am. Chem. Soc., **1992**, 114, 1964.

[25] B. E.Buchanan, R. Wang, J. G. Vos, R. Hage, J. G. Haasnoot and J. Reedijk, *Inorg. Chem.,* **1990**, 29, 3263.

[26] (a) B.P. Sullivan and T. J. Meyer, *Inorg. Chem*., **1982**, 21, 1037; (b) B. Durham, S. R. Wilson, D. J. Hodgson and T. J. Meyer, *J. Am. Chem. Soc.,* **1980**, 103, 600; (c) B. Durham, J. V. Caspar, J. K Nagle and T. J. Meyer, *J. Am. Chem. Soc*., **1982**, 104, 4803; (d) B. Durham, J. L. Walsh, C. L. Carter and T. J. Meyer, *Inorg. Chem*., **1980**, 19, 860.

[27] (a) T. J.Meyer, *Pure Appl. Chem.,* **1986**, 58, 1193, (b) Y. Kawanishi, N. Kitamura, and S. Tazuke, *Inorg. Chem*., **1989**, 28*,* 2968.; (c) E. M. Kober and T. J. Meyer, *Inorg. Chem*., **1982,** 21, 3967.

[28] W. F. Wacholtz, R. A. Auerbach and R. H. Schmehl, *Inorg. Chem*., **1986**, 90, 2285.

CHAPTER 6

Photochemical properties of a Ru/Pd based photocatalyst for the solar driven generation of hydrogen.

6.1 Introduction

In the light of the rapidly increasing need for sustainable energy interest in the conversion of solar energy is growing. Solar energy is utilized as a source for thermal or electrical energy (photovoltaic cells) [1], however, its application in light driven catalytic systems may open a route towards highly energy efficient chemical reactions. One of the approaches used is the use of catalytic systems that include light harvesting transition-metal complexes for the photolysis to convert the light energy into chemical energy [2,3]. Transition-metal complexes have a distinct advantage over semiconductors as their photophysical properties can be tuned through ligand modification. Especially transition metal cations and their complexes are well explored and are very suitable as photo- chemically active substances. Aided by this versatility, researchers have devised a variety of catalytic systems capable of performing the reduction half-reaction of water cleavage, in which the excited state of the transition-metal complex is quenched by charge transfer to an electron relay [4]. Early works report the successful use of $[Ru(bpy)_3]^{2+}$ (bpy=2,2'-bipyridine) as a photo sensitizer, in combination with an electron relay species, and typically employ a platinum catalyst [5,6].. In this report Ru-complexes were used to study if they are appropriate to cleave water and so produce hydrogen.

The central processes in natural photosynthesis are light driven electron transfer from the special-pair to the primary acceptor, and the subsequent charge separation to enable the reduction of substrates. The transfer of these design

principles to artificial systems has led to the development of catalytic multi-component systems for the photo catalytic production of hydrogen [7]. In these systems, photoredox-active metal complexes and separate redox catalysts are used to facilitate directed photo induced electron transfer. For example, Grätzel et al. showed that heterogeneous photo catalyst systems can be used for the generation of hydrogen [8], and Currao et al. reported the photochemical [9] splitting of water with a system consisting of a photoactive silver/silver chloride anode and a silicon solar cell acting as a cathode. However, in these heterogeneous systems, the electron-transfer processes depend on many interfacial parameters that are difficult to influence. Homogeneous systems, consisting of a photoactive Ru complex and an electron relay of Pd/Pt complexes, which generate H_2 in intermolecular reactions, have also been described. Their effectiveness is limited by the instability of the reduced photo catalysts. [4]

In an intramolecular photocatalyst it should be easier to control photoinduced electron transfer by precise tuning of the physical properties and orientation of the molecular components. If it were also possible to slow down charge recombination processes, efficient photocatalytic systems may become feasible. Rau and coworkers recently reported a dinuclear compounds (See Figure 6.1) which produces hydrogen upon irradiation with a turn-over-number of (TON) of 56 [10], recently values of up to 250 have been obtained in the presence of water [11]. Other such catalysts have also been reported [4,12].

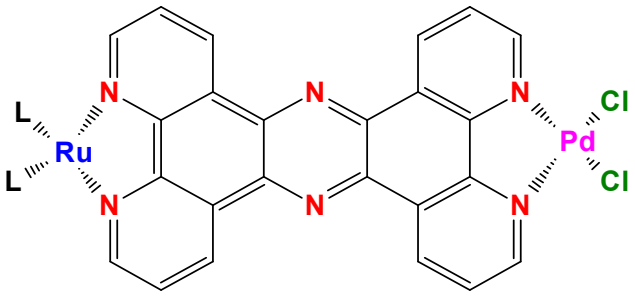

Figure 6.1 *Structure of $[(tbbpy)_2Ru(tpphz)PdCl_2]^{2+}$ where L = 4,4'-di-tert-butyl-2,2'-bipyridine and tpphz = tetrapyrido[3,2-a:2',3'c:3'',2'',- h:2''',3'''-j]phenazine.*

The hetero-dinuclear Ru–Pd complex used as photocatalyst consists of the following three components:-

– A photoactive ruthenium (II) fragment acting as a light absorber. [13]

– A $PdCl_2$ unit which, when coordinated at the other end of the assembly, acts as a catalytic centre.

–A bridging unit connecting the two metal centres through conjugated reducible π-electron system.

In the presence of the sacrificial agent triethylamine (TEA) efficient hydrogen formation is observed [10].The photoinduced electron-transfer processes taking place to allow for the intramolecular hydrogen evolution $[(tbbpy)_2Ru(tpphz)PdCl_2]^{2+}$ (RuPd), where tbbpy=4,4'-di-tert-butyl-2,2'-bipyridine and tpphz=tetrapyrido[3,2-a:2',3'c:3'',2'',- h:2''',3'''-j]phenazine) have been studied by resonance Raman and ultrafast time-resolved absorption spectroscopy. By comparing the photophysics of the $[(tbbpy)_2Ru(tpphz)]^{2+}$ precursor with that of the supramolecular catalyst RuPd [14] a reaction scheme was proposed as shown in (Figure 6.2 and Scheme 6.1).

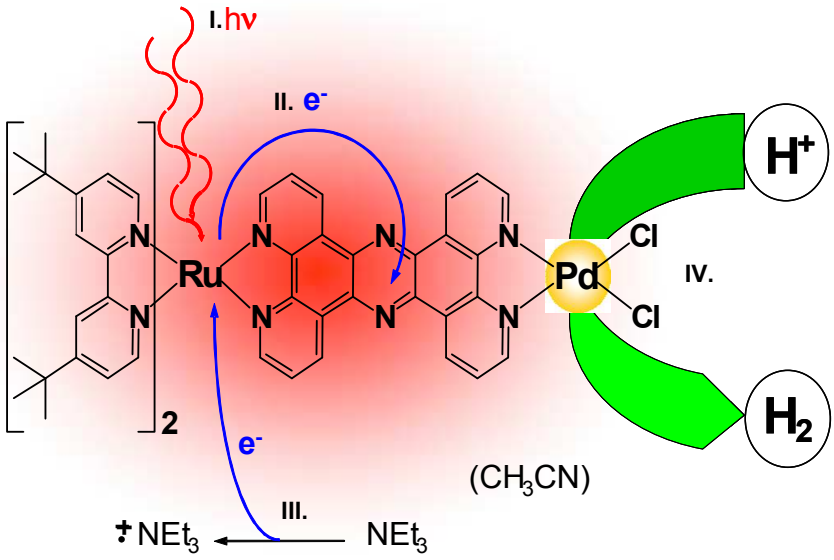

***Figure 6.2**. Schematic presentation of the photoinduced hydrogen generation process [10].*

The individual processes are outlined below in Scheme 6.;

$$\text{Ru(II)-B-Pd(II)} \xrightarrow{h\nu} \text{Ru(II)*-B-Pd(II)}$$

$$\text{Ru(II)*-B-Pd(II)} \rightarrow \text{Ru(III)-B}^{-}\text{-Pd(II)}$$

$$\text{Ru(III)-B}^{-}\text{-Pd(II)} \xrightarrow{\text{TEA}} \text{Ru(II)-B}^{-}\text{-Pd(II)}$$

$$\text{Ru(II)-B}^{-}\text{-Pd(II)} \rightarrow \text{Ru(II)-B-Pd(I)}$$

$$\text{Ru(II)-B-Pd(I)} + \text{H}^{+} \rightarrow \text{Ru(II)-B-Pd(II)} + 1/_2\text{H}_2$$

***Scheme 6.1**. Proposed reaction pathway based on Figure 6.2. B =bridging ligand [10].*

Although as outlined above photophysical studies on this Ru/Pd photocatalytic system have been carried out. Nothing is known about the photochemical stability

of the photocatalyst. UV/Vis studies have been carried out during the photocatalytic reactions as shown in Figure 6.3.

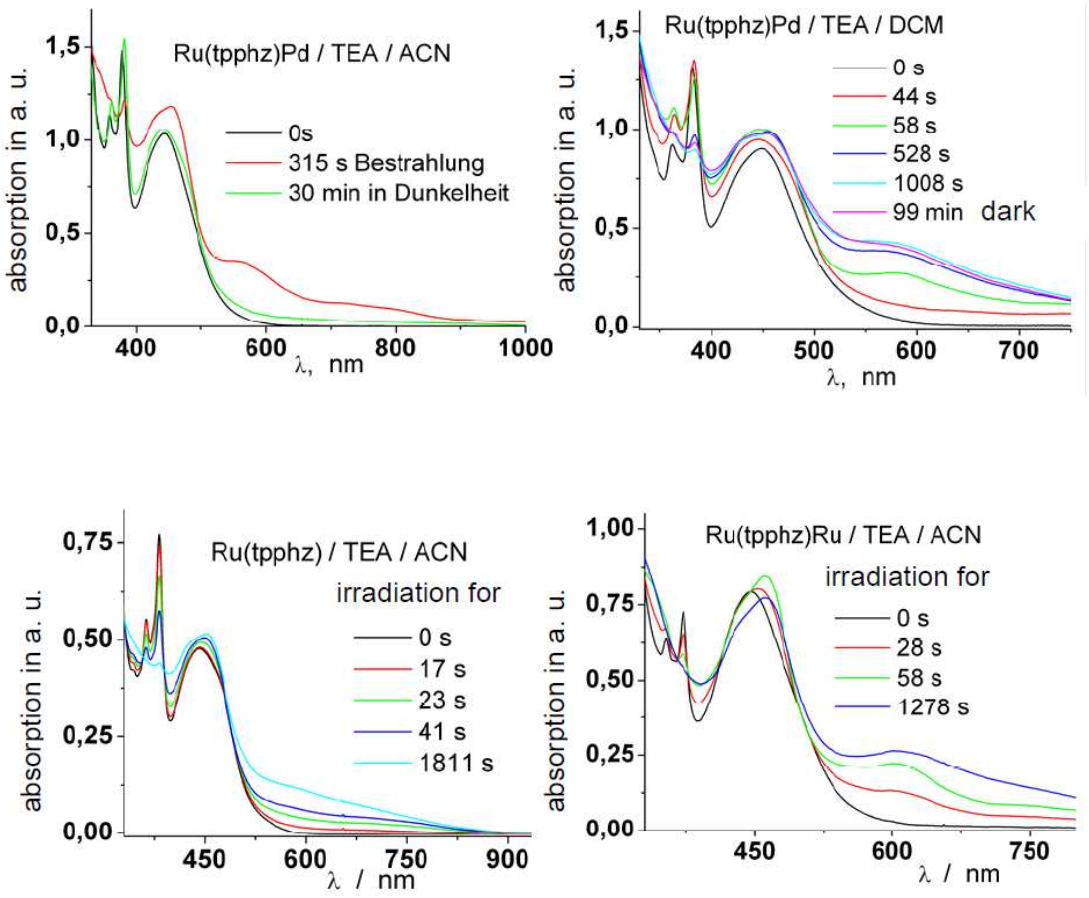

Figure 6.3 *UV/vis spectra of Ru(tpphz) compound 1, Ru(tpphz)Ru , compound 3 and Ru(tpphz)Pd, compound 2, with visible light (470nm) [11].*

These studies do show the formation of photoinduced intermediates as evidenced by species with absorption maxima at up to 600 nm, involving reduced bridging ligands such as shown in the following structure.

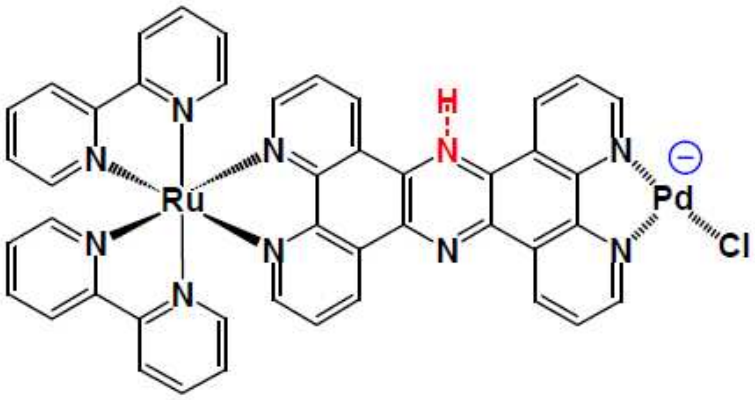

***Figure 6.4**. Structure of potential intermediate shows a reduced bridging ligand and a loss of chloride [11].*

No information concerning the photostability of the photocatalyst is available. In this chapter we wish to carry out HPLC studies to investigate the issue of the photostability of the photocatalyst. The photochemical properties of this complex together with a number of analogues compounds (See Figure 6.5 below) will be investigated initially in acetonitrile, subsequently their stability under photocatalytic conditions, in the presence of TEA and an under argon atmosphere.

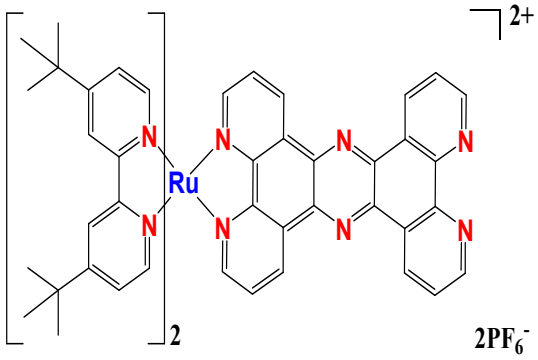

[(tbbpy)$_2$Ru(tpphz)](PF$_6$)$_2$

Compound 1

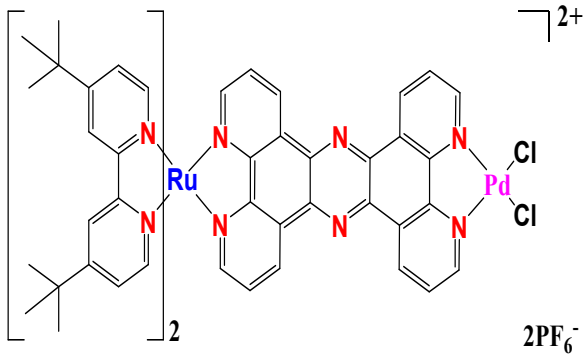

[(tbbpy)$_2$Ru(tpphz)PdCl$_2$](PF$_6$)$_2$

Compound 2

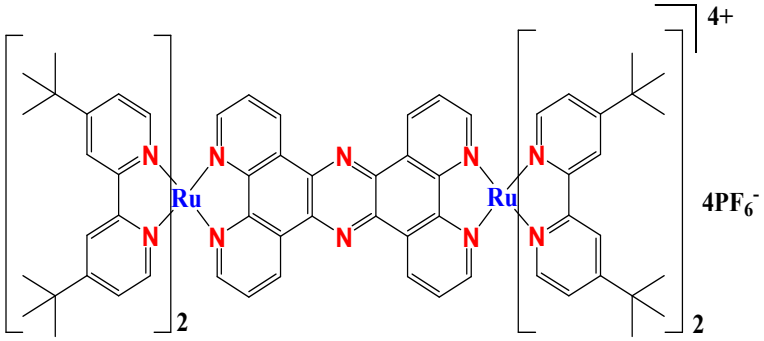

[(tbbpy)$_2$Ru (tpphz)Ru(tbbpy)$_2$](PF$_6$)$_4$

Compound 3

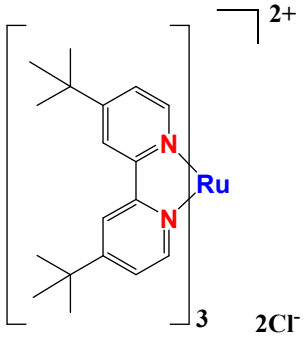

[(tbbpy)$_3$Ru]Cl$_2$

Compound 4

Figure 6.5 *Chemical structures of the systems investigated in this study: The mononuclear building block compound **1**, compound **2**, compound **3** and the reference compound [Ru(tbbpy)$_3$]$^{2+}$ compound **4**.*

6.2 Experimental Section

6.2.1 Material and Methods

All complexes investigated were synthesized by and received from the group of Prof Sven Rau, Erlangen, Germany. All samples were used as received, with no further purification. All solvents employed were of HPLC grade or better and used as received unless otherwise stated.

6.2.2 Chromatographic Analysis

For the investigation the following chromatographic conditions were used.

High performance liquid chromatography (HPLC) was carried out on using a Varian Pro Star photodiode array as outlined in Chapter 2. All Samples were dissolved in the eluent in CH_3CN and filtered through a 0.45 micron filter prior to injection. The samples- $[(tbbpy)_2Ru(tpphz)](PF_6)_2$ (1) , $[(tbbpy)_2Ru(tpphz)\ PdCl_2](PF_6)_2$ (2), $[(tbbpy)_2Ru(tpphz)Ru(tbbpy)_2](PF_6)_4$ (3), and $[(tbbpy)_3Ru]Cl_2$ (4) in CH_3CN , without TEA/ or with TEA, were analysed using a mobile phase of CH_3CN/H_2O 70/30 containing 0.02 M KNO_3 and detection wavelengths of 280 or 430 nm and a flow rate 2.0 $cm^3\ min^{-1}$. The temperature control was set at 24^o C.

6.2.3 Preparation of Samples for Photo-Catalysis.

Preparation of sample solutions was carried out in the absence of ambient light, and solutions were wrapped in aluminium foil and carefully sealed to avoid exposure to light, and evaporation. Samples were always prepared fresh,

immediately prior to the measurements. Photolysis experiments carried out in acetonitrile only were carried out in aerated solutions. Samples investigated under photocatalytic conditions containing triethylamine (TEA) were deoxygenated using argon for 30 minutes to copy the conditions used. A ~ $1x10^{-4}$ M solution of the complexes in acetonitrile was used for irradiations both without TEA and with TEA. For the experiments carried out under photocatalytic conditions a TEA concentration of $1x\ 10^{-4}$ M was used. The photochemical experiments were carried out an LED with 470nm blue light as described in Chapter 2.

6.3 Results and Discussion

6.3.1 HPLC Behaviour of the Compounds Studied.

The chromatographic behaviour of the compounds discussed in this chapter is similar to that observed for the compounds discussed in Chapters 3-5. It was however observed that the retention times of the compounds is strongly temperature dependent. An example of this is shown in Figure 6.6 below for compound **3**.

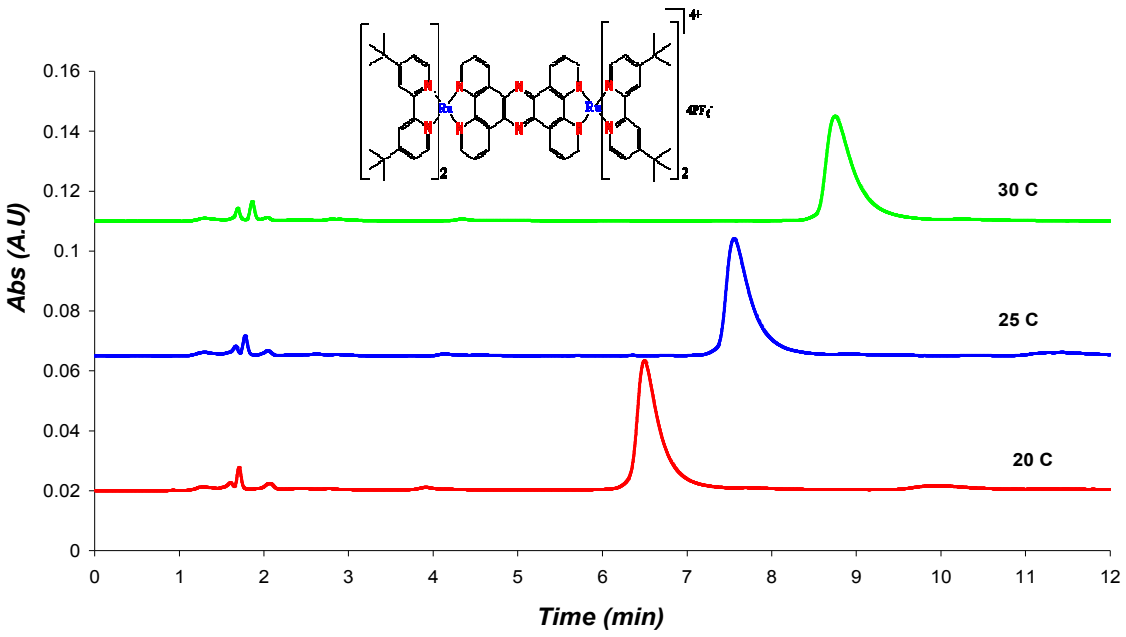

Figure 6.6 *HPLC trace for sample 3 at depending temperatures, in CH_3CN $1*10^{-4}$ M Mobile phase CH_3CN/H_2O 70/30 containing 0.02 M KNO_3 at 430 nm and flow rate 2.0 cm^3 min^{-1}.*

This figure shows that the retention time of peak obtained for compound **3** is strongly dependent on the temperature. The same behaviour is observed for both fractions in compounds **1** and **2**. No temperature dependence was observed for compound **4**. The reason for this temperature dependence was not further investigated but is most likely related to the presence of the bridging ligand. As a result of this observation all further experiments were carried out at 24°C using a column heater. Due to the large variations in temperature that may occur in the laboratory, temperature effect could not always be avoided completely.

A typical set of chromatograms for compounds **1-3** is shown in Figure 6.7 below.

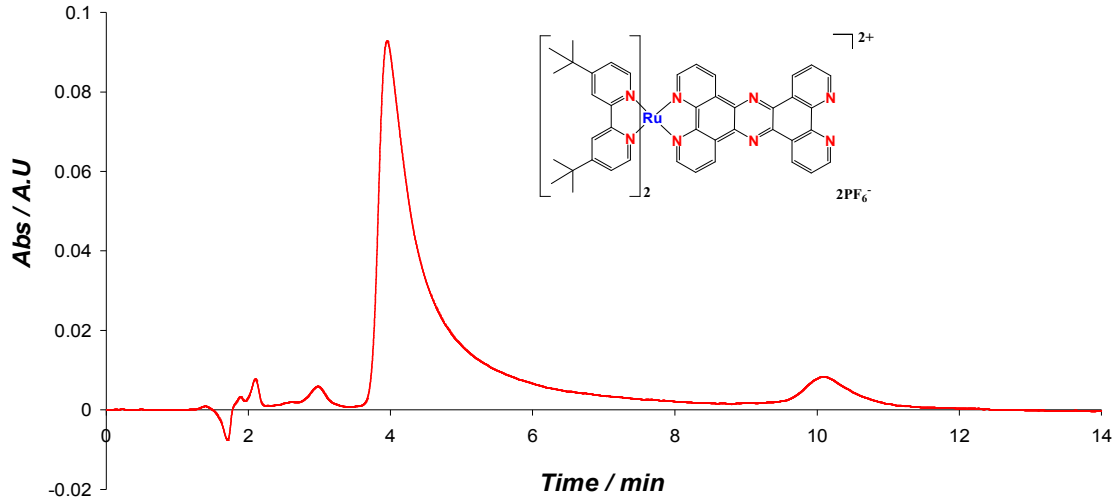

a

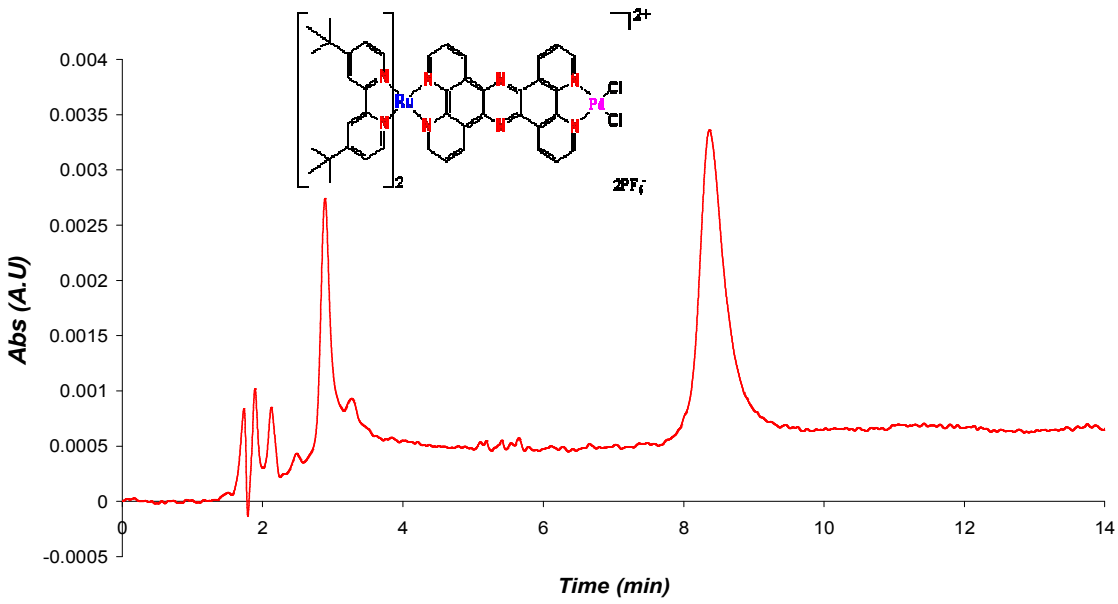

b

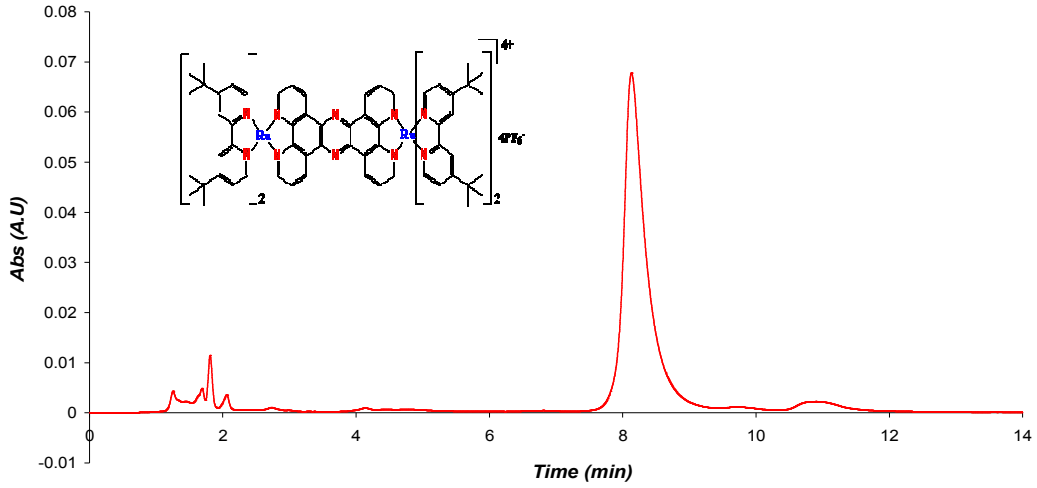

c

Figure 6.7 *HPLC traces of compounds* ***1-3*** *in* CH_3CN $1*10^{-4}$ *M Mobile phase* CH_3CN/H_2O *70/30 containing 0.02 M* KNO_3 *at 430 nm and 24° C flow rate 2.0* cm^3 min^{-1}.

The retention times obtained for these compounds, together with these obtained in the presence of TEA are shown in Table 6.1. The table shows that the retention times, especially for compound 3 vary in the presence of TEA.

Table 6.1*. Retention times of compounds* ***1-4*** *in acetonitrile and in acetonitrile containing triethylamine.*

Compounds	Retention Time (min)	
	with TEA	without TEA
1	2.68	3.95
2	2.64	2.83
3	4.64	8.14
4	1.60	1.80

The separation of the compounds is dependent on the charge of the complexes. So compound **3** has a charge of +4 this compound shows the longest retention time. However the nature of the ligands is also important. The tert-butyl groups located at the bpy ligands will shield the positive charge located on the ruthenium centre from the mobile phase. As a result the retention times observed are rather short, especially when compared with these observed for the dinuclear compounds in Chapters 3 and 4. The small variation of retention times, especially in the 1-3 minutes range leads to a considerably amount of overlap and this complicates the identification of the compounds formed as photoproducts. Note that the strong peak observed for compound **2** at about 8 min is assigned as compound **3** present as an impurity, based on the absorption spectrum of this peak. The peak for compound **2** is observed at about 3 minutes.

The chromatograms obtained for compounds **1** and **2** show a considerable amount of tailing. For compound 1 this is not unexpected since the free nitrogen atoms are most likely interacting with the stationary phase. Tailing for compound **2** is less and maybe this is related to the loss of chloride at the palladium centre. For compounds **3** and **4** no significant tailing is observed. A complication for the identification of the species observed in the chromatograms for compounds **1-3** containing the tpphz ligand, is that these have the same optical absorption properties in the visible part of the spectrum. The formation of photoproducts can therefore be observed by HPLC but their identification by their spectral features is not possible in cases where the tpphz ligands is still bound. The one exception is

that for compound 3 the intensity ratio of some of the peaks is slightly different. Part of the spectrum associated with the MLCT band, the broad feature, is more intense that the doublet of sharper peaks at higher energy. For the other tpphz containing compounds this is the other way around.

The chromatographic features observed for the compounds when TEA was added to the irradiated solutions to allow the study of the photochemical behaviour under "catalytic conditions" are shown in Figure 6.8 below.

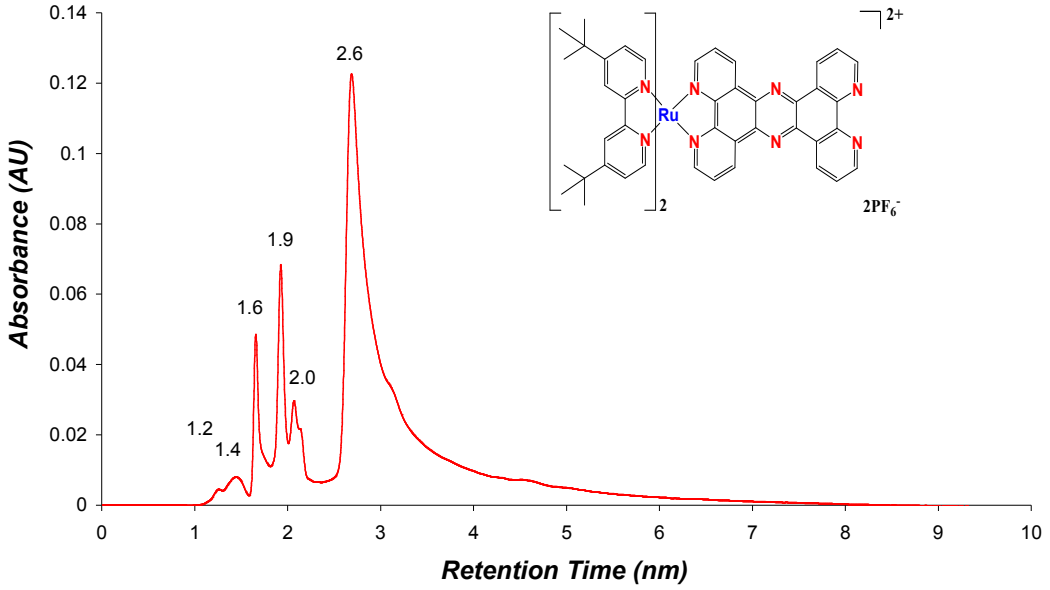

a

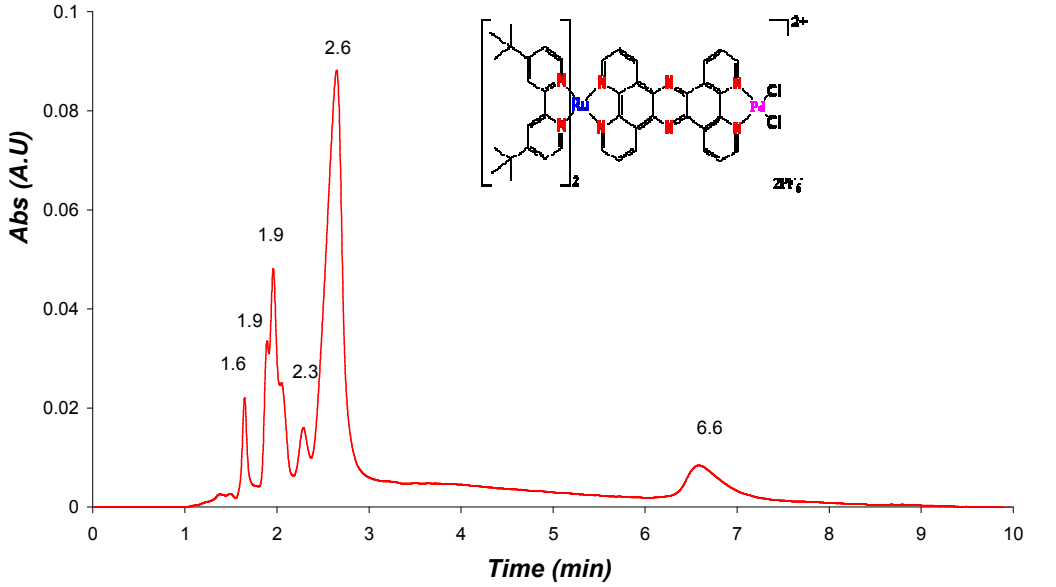

b

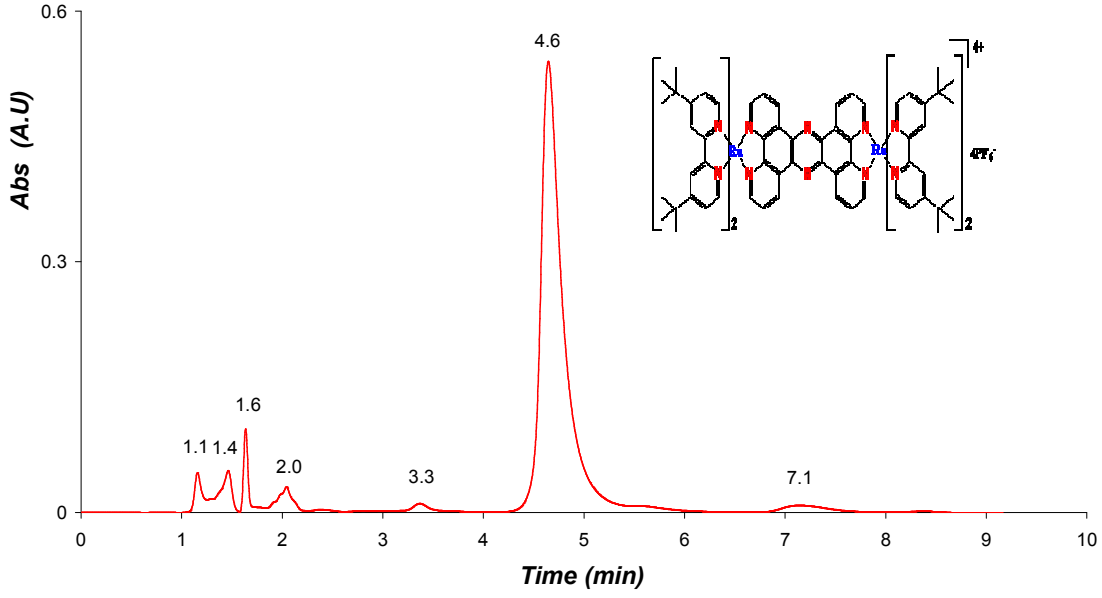

c

Figure 6.8 *Chromatograms obtained for compound 1-3 in CH_3CN $1*10^{-4}$ M Mobile phase CH_3CN/H_2O 70/30 containing 0.02 M KNO_3 at 280 nm and 24° C flow rate 2.0 cm^3 min^{-1}.*

By comparing Figures 6.7 and 6.8 and the data presented in Table 6.1 it is clear that the retention times of compounds **1-3** are changed upon the addition of TEA. For compound 4 no major changes are observed in it chromatographic behaviour in the presence if TEA.

6.3.2 Photolysis of Compounds 1-4 in Acetonitrile.

As outlined in the last section in order to limit the effect of temperature of the chromatography all experiments were carried out at 24^{o}C. The purpose of this chapter is to investigate the stability of compound **2** with respect to light. Since this compound is under investigation as a photocatalyst for the generation of hydrogen its photochemical behaviour needs to be determined. Compounds **1, 3** and **4** were investigated as well as model compounds. The first step in this study was the investigation of the photochemical stability of the compounds upon irradiation in acetonitrile. It has been shown before that this solvent can lead to light induced ligand exchange processes [15]. The samples were irradiated for up to 2 hours and it was found that all 4 are largely photostable under these conditions. Typical HPLC examples of this are shown in Figures 6.9 and 6.10 for compounds **1** and **3**. Similar results are obtained for the other two compounds.

These results clearly show that under the conditions used in these experiments the compounds are photostable for up to 2 hours. The photocatalytic experiments used to achieve hydrogen generation with compound **2** include the presence of a

high concentration of TEA as a sacrificial agent as outlined in the introduction of this chapter. In the next section the photochemical behaviour of the compounds will be discussed in the presence of this sacrificial agent.

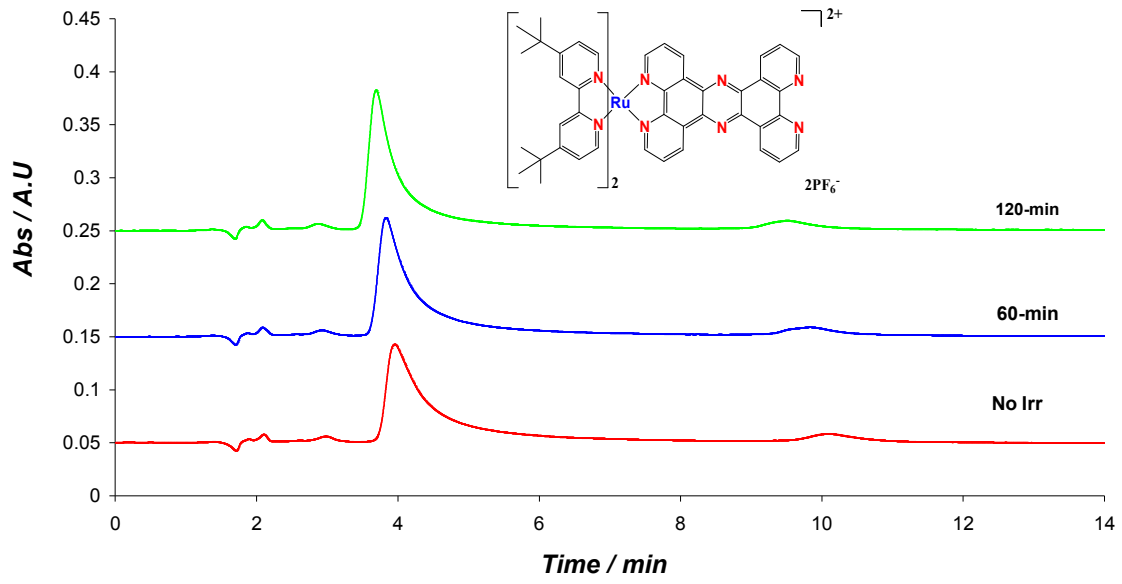

Figure 6.9 *Irradiation of compound* ***1*** *- [(tbbpy)$_2$ Ru (tpphz)](PF$_6$)$_2$ (1x10^{-4} M) in ACN at 24^o C Detection wavelength 430 nm, Mobile Phase CH$_3$CN: H$_2$O 70:30 0.02 M KNO$_3$. Flow rate 2.0 cm^3/min*

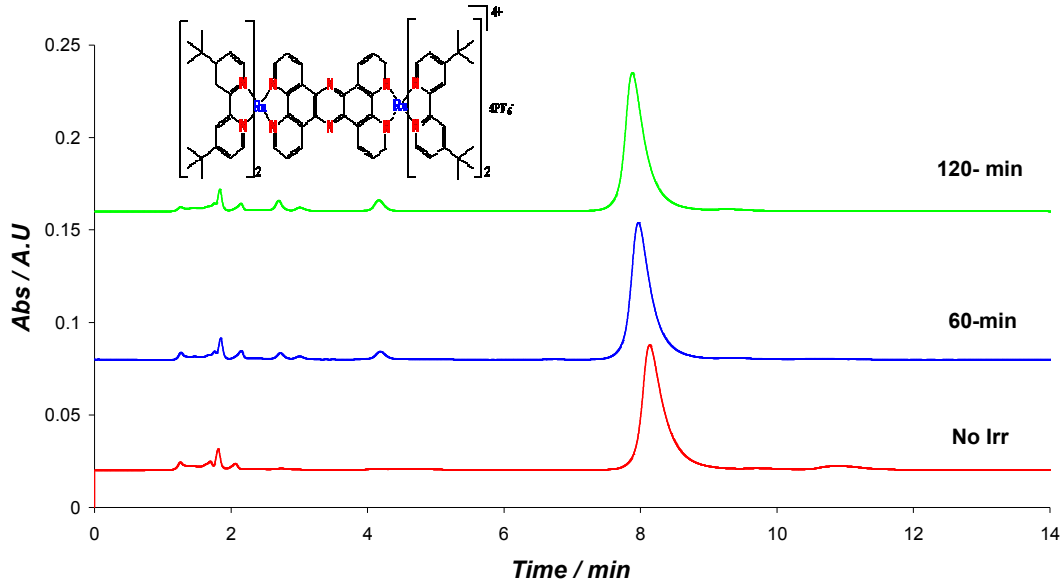

Figure 6.10 *Irradiation of compound* ***3*** *[(tbbpy)$_2$ Ru (tpphz)Ru(tbbpy)$_2$](PF$_6$)$_4$ in ACN 1*10^{-4} M at 24^o C detection wavelength 430 nm, Mobile Phase CH$_3$CN: H2O 70:30; 0.02 M KNO$_3$ Flow rate 2.0 cm^3/min.*

6.3.3 Photolysis of Compounds 1-4 in the Presence of TEA.

In the last section has been shown that in acetonitrile all the compounds are photostable for up to 2 hours under irradiation with visible light. In this section the stability of the compounds towards irradiation under catalytic conditions will be investigated. The major difference between the two irradiation conditions is the presence of triethylamine (TEA) which acts as a sacrificial agent in the photocatalytic process as outlined in the introduction. In addition the samples were also deaerated with argon before irradiation to mirror the conditions used for the photocatalytic process.

6.3.3.1 Compound 4.

The photochemical behaviour of compound **4** is outlined in Figure 6.11.

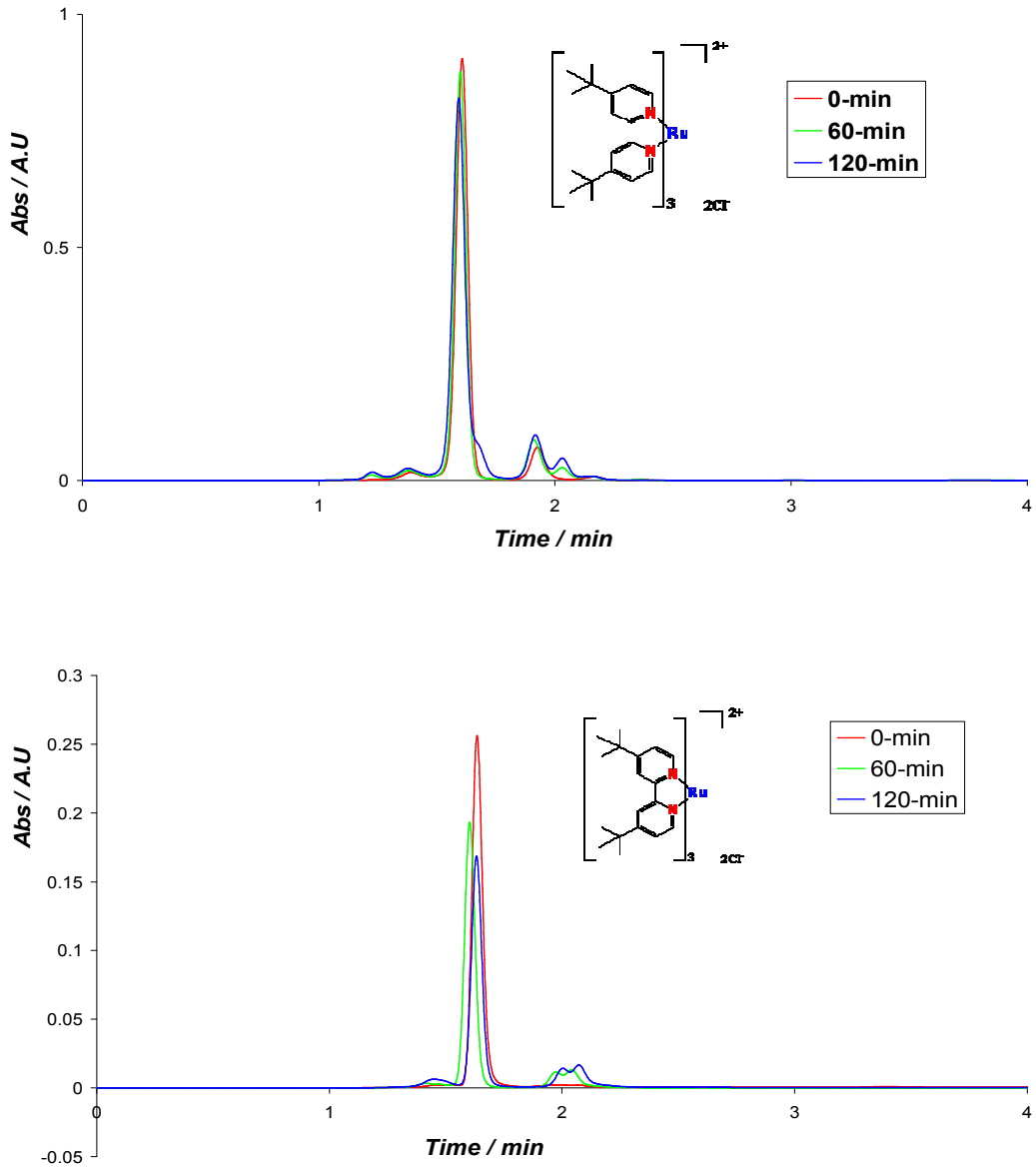

Figure 6.11 *Compound **4** $[(tbbpy)_3 Ru]Cl_2$ $1*10^{-4}$ M Temperature 24° C Irradiated in in ACN in presence of TEA (2 M) using 470 nm LED irradiation from (0-120min) degassing with Ar before irradiation detection wavelength; (top) 280 and (botom)*

430 nm, Mobile Phase CH_3CN: H_2O 70:30 containing 0.02 M KNO_3 Flow rate 2.0 cm^3/min.

This figure shows that a change in detection wavelength of the HPLC detector does not greatly affect the traces observed. It is also clear that although the compound is not totally stable the amount of decomposition observed is small. A small shift on the components is also observed due to small temperature variations. The retention time observed for compound **4** is 1.6 minutes. A small amount of three different products is observed at 1.4, 1.9 and 2.0 minutes retention times. The absorption spectra of two of the compounds are shown in Figure 6.12 below.

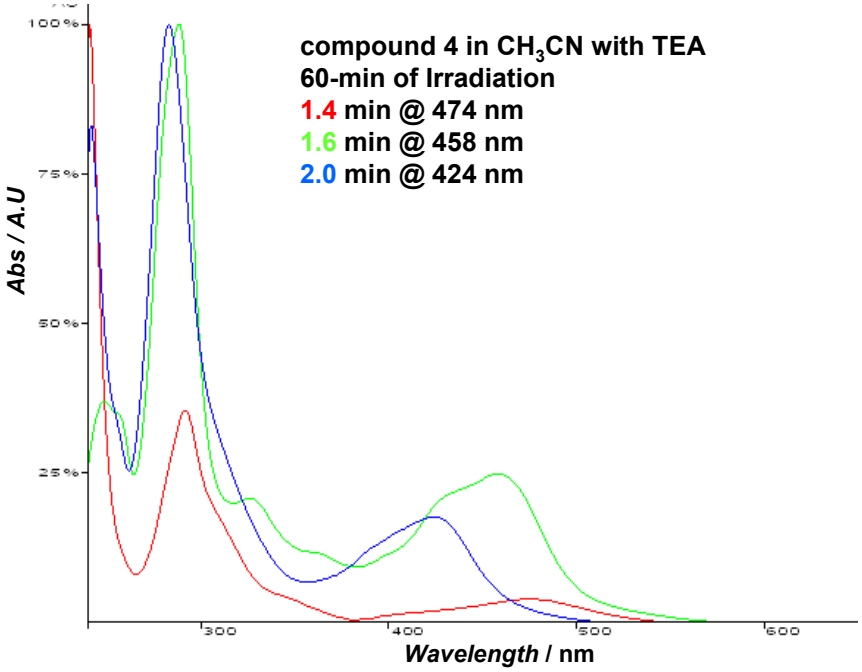

Figure 6.12 *Absorption spectra of species detected in Figure 6.8 above after 60 minutes of irradiation. Detection wavelength 430 nm.*

The spectrum observed for the species with a retention time of 1.4 can be identified from related studies as $[Ru(tbbpy)_2(CH_3CN)Cl]^+$ [16]. The formation of this compound can be explained by the presence of chloride counter ions in compound **4**. The species found at 2.0 min is the related $[Ru(tbbpy)_2(CH_3CN)_2]^{2+}$ compound [16]. The formation of these compounds indicates that upon irradiation a tbbpy ligand is replaced. The shoulder observed at 1.9 minutes has an absorption maximum of 280 nm (not shown) and is assigned to this replaced ligand.

6.3.3.2 Compound 3.

The HPLC traces obtained upon irradiation of this compound are shown in Figure 6.13 below.

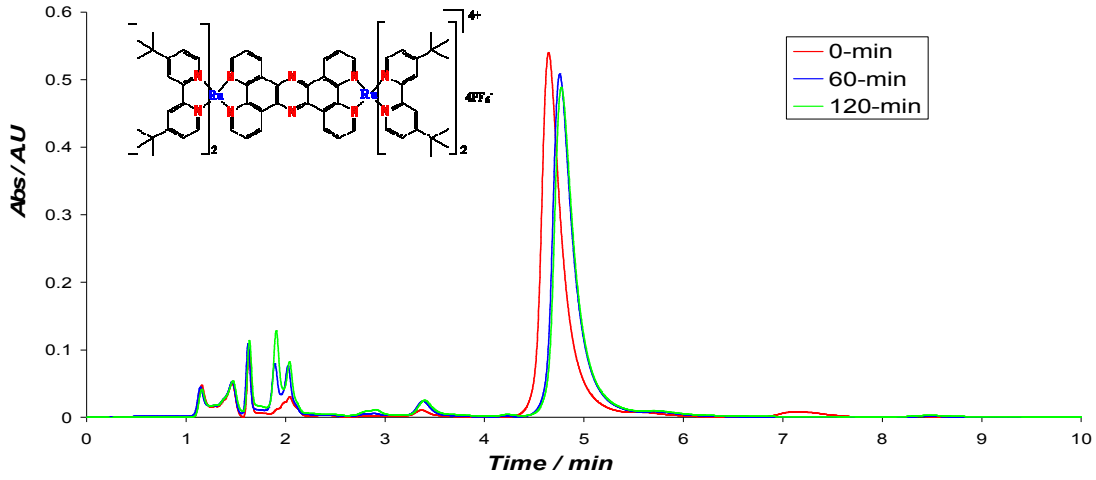

***Figure 6.13** . HPLC traces obtained upon photolysis of compound **3**. Temperature 24° C. Irradiated in ACN in presence of TEA (2 M) using 470 nm LED irradiation from (0-120min) degassing with Ar before irradiation detection wavelength; 280 nm, Mobile Phase CH_3CN: H_2O 70:30 containing 0.02 M KNO_3 Flow rate 2.0 cm^3 min^{-1}*

The figure shows that there is only a small decrease of the main signal, attributed to compound **3**. There are however a number of small peaks already present in the solution before irradiation. These are found at 1.1, 1.4 and 1.6 minutes. The absorption spectra of these species are shown in Figure 6.14 below.

The spectra observed can by comparison with independently prepared samples and other related studies [10,16] be identified as $[Ru(tbbpy)_2Cl_2]$, (red) as

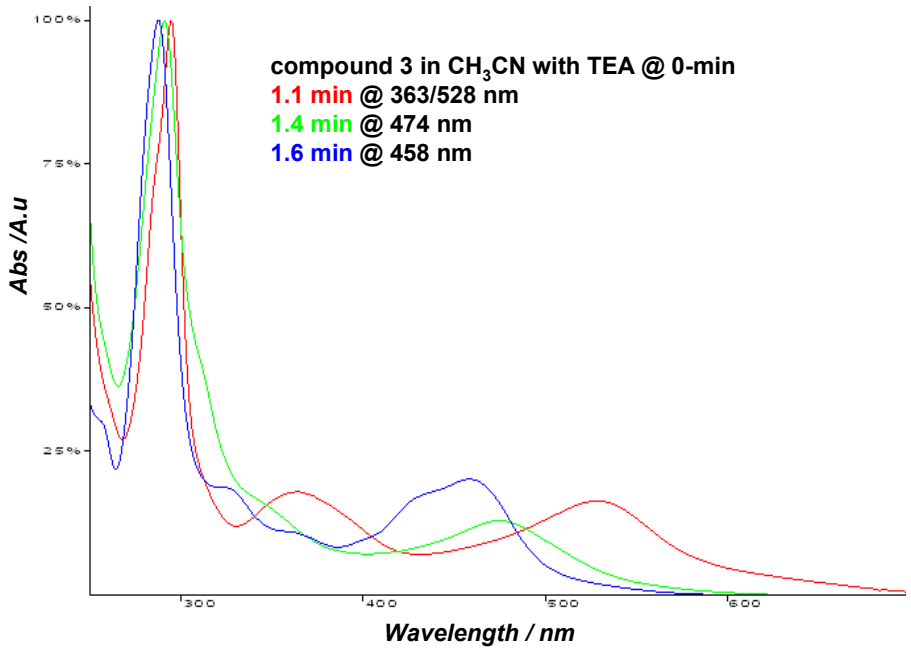

***Figure 6.14**. Absorption spectra obtained for the species observed at 1.1, 1.4 and 1.6 minutes retention times in Figure 6.13.*

$[Ru(tbbpy)_3]^{2+}$ (blue) and as $[Ru(tbbpy)_2(CH_3CN)Cl]^{+}$ (green). All three are related to the synthetic procedure, which involves the use of $[Ru(tbbpy)_2Cl_2]$ as the main starting material. The compound $[Ru(tbbpy)_3]^{2+}$ may be present as a small impurity

in this starting material while $[Ru(tbbpy)_2(CH_3CN)Cl]^+$ is formed by chloride loss from $[Ru(tbbpy)_2Cl_2]$ upon dissolution in the mobile phase.

Upon irradiation two small peaks are growing at 1.9 and 2.1 minutes, respectively. These can be assigned as a small amount of free ligand, most likely the bridging ligand, (1.9 min) and $[Ru(tbbpy)_2(CH_3CN)_2]^{2+}$ according to the equation below;

$$[(tbbpy)_2\ Ru\ (tpphz)Ru(tbbpy)_2]^{2+} \xrightarrow{h\nu} [(tbbpy)_2\ Ru\ (tpphz)]^{2+} + [(tbbpy)_2\ Ru(CH_3CN)_2]^{2+} + tpphz. \quad \textit{Eq 6.1}$$

A very weak signal at 2.8 min is indicative of the formation of $[(tbbpy)_2\ Ru\ (tpphz)]^{2+}$ (compound 1), while the nature of the species formed at 3.3 min could not be identified from its absorption spectrum.

These results show that compounds **3** and **4** are largely photostable under irradiation with 470 nm light for 2 hours. As the next section shows compounds **1** and **2** behave very differently. The HPLC traces observed for compound **1** under the same conditions are shown in Figure 6.15.

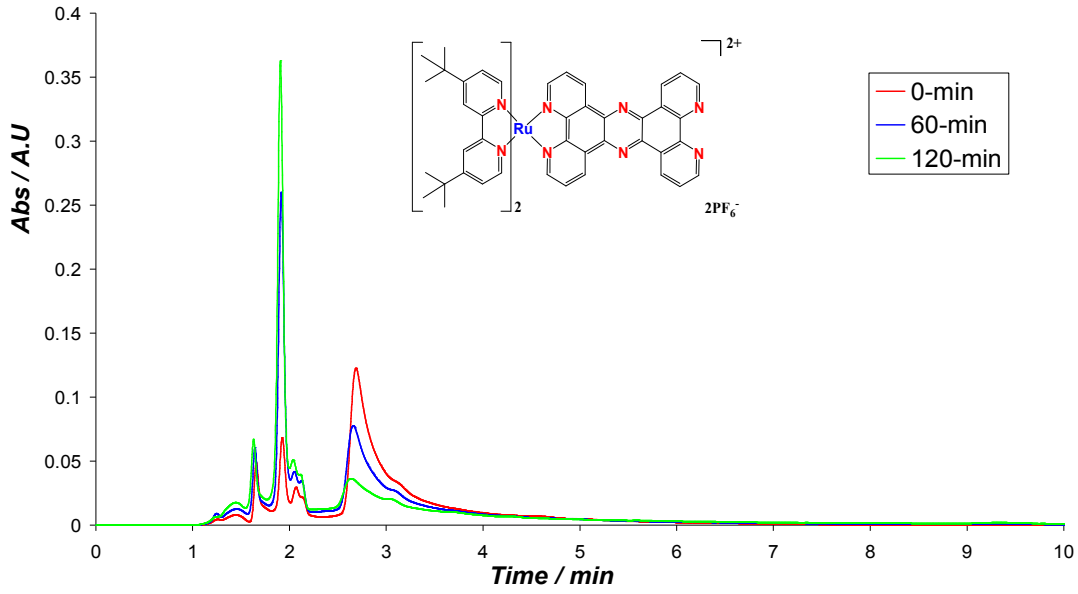

Figure 6.15 *. HPLC traces obtained upon photolysis of compound 1. Temperature 24^{o} C. Irradiated in ACN in presence of TEA (2 M) using 470 nm LED irradiation from (0-120min) degassing with Ar before irradiation detection wavelength; 280 nm, Mobile Phase CH_3CN: H_2O 70:30 containing 0.02 M KNO_3 Flow rate 2.0 cm^3 min.*

As observed for compound **3** a number of synthesis related impurities are observed before irradiation has taken place. It can however not be ruled out that some of these species were formed during the sample preparation. Compound **1** is more reactive to light than **3** and **4**. The absorption spectra obtained at t = 0 are shown in the following figure.

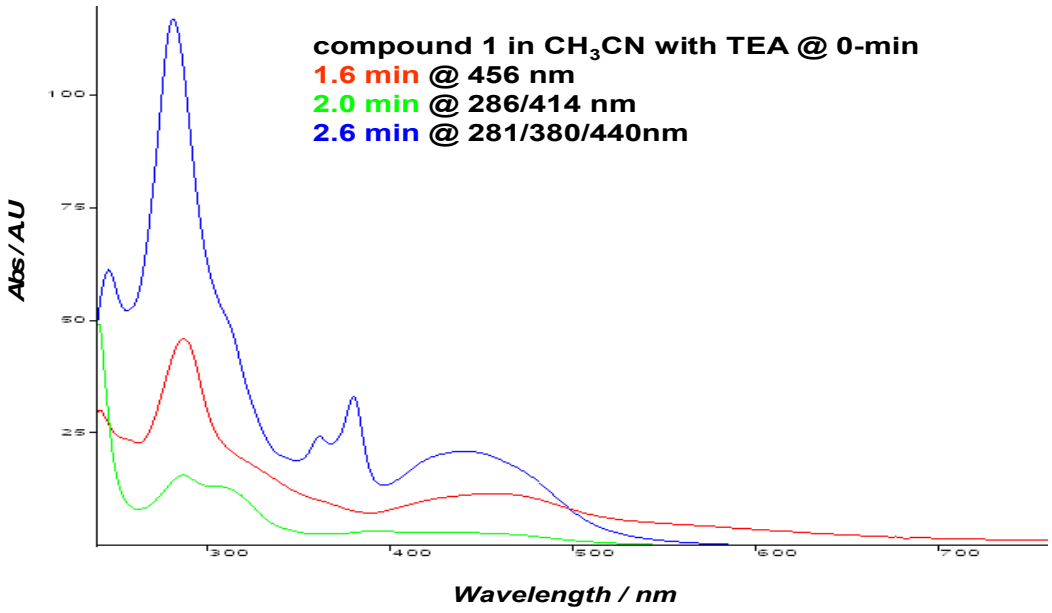

***Figure 6.16**. Absorption features of peaks identified in Figure 6.15.*

These spectra indicate the presence of $[Ru(tbbpy)_3]^{2+}$ at 1.6 min and at 2.6 minutes the presence of compound **1**. The composite peak at about 2.0 min indicates the presence of both free ligand and the $[(tbbpy)_2\ Ru(CH_3CN)_2]^{2+}$ complex. The presence of the latter two species suggests that some light induced ligand exchange may have taken place already during the sample preparation. The HPLC traces in the figure above show a continuing decrease of the peak at 2.6 minutes, compound **1**, and an increase of the composite peak at about 2.0 minutes, which can, on the basis of the absorption spectra obtained, be assigned to a combination of the bridging ligand tpphz and the bis(CH_3CN) complex. The absorption spectra obtained from the hlpc experiments indicate that a species is formed with a retention time of about 2 minutes that has an absorption maximum at 280 nm. This indicates the formation of an organic species and this is therefore expected to be a ligand. Based on the spectral data observed it is not possible to

determine whether this ligand is tpphz or tbbpy. However, based on the results obtained in Chapters 3-5 and other investigations reported in the literature [17], it is most likely that the tpphz ligand is lost. This photoinduced ligand exchange is clearly more efficient that observed for compounds 3 and 4 and can, on the basis of the absorption spectra obtained for the various species formed, be explained by the following reaction;

$$[(tbbpy)_2\ Ru\ (tpphz)]^{2+} \xrightarrow{h\nu} [(tbbpy)_2\ Ru(CH_3CN)_2]^{2+} + tpphz \qquad \textbf{Eq 6.2}$$

The HPLC results obtained during the photolysis of compound 2 are shown in Figure 6. 17 below:

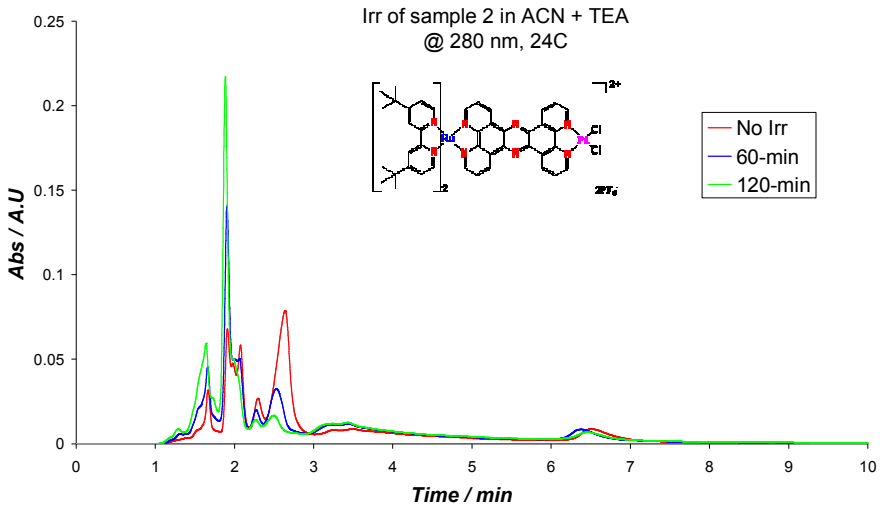

Figure 6.17 *. HPLC traces obtained upon photolysis of compound 2. Temperature 24^o C. Irradiated in ACN in presence of TEA (2 M) using 470 nm LED irradiation from (0-120min) degassing with Ar before irradiation detection wavelength at 280 nm, Mobile Phase CH_3CN: H_2O 70:30 containing 0.02 M KNO_3 Flow rate 2.0 cm^3 min.*

The HPLC results obtain for compound **2** look considerable more complicated than those obtained for the other three compounds. They do resemble those of compound **1** the most. The chromatogram obtained before any irradiation has taken place together with the absorption spectra obtained for the main species is shown below in Figure 6.18 the peak observed at 1.6 min can be assigned to compound **4** as shown above. A strong signal and 1.9 has been observed in all chromatograms and is organic in nature. What is most obvious is that the absorption spectra associated with tpphz complexes can be found over a wide range, the double absorptions at around 370 nm are found from 1.9 to 3.5 minutes. Apart from that one feature the traces obtained for compound **2** look similar to those shown for compound **1** earlier. It is clear that there is a strong overlap between different species. For example it proved not to be possible to improve the chromatographic conditions so that the retention time of compounds **1** and **2** would be different. This is not totally unexpected since the size and the charge of both compounds are the same. This will make the possible formation of compound **1** upon irradiation of **2** difficult to detect.

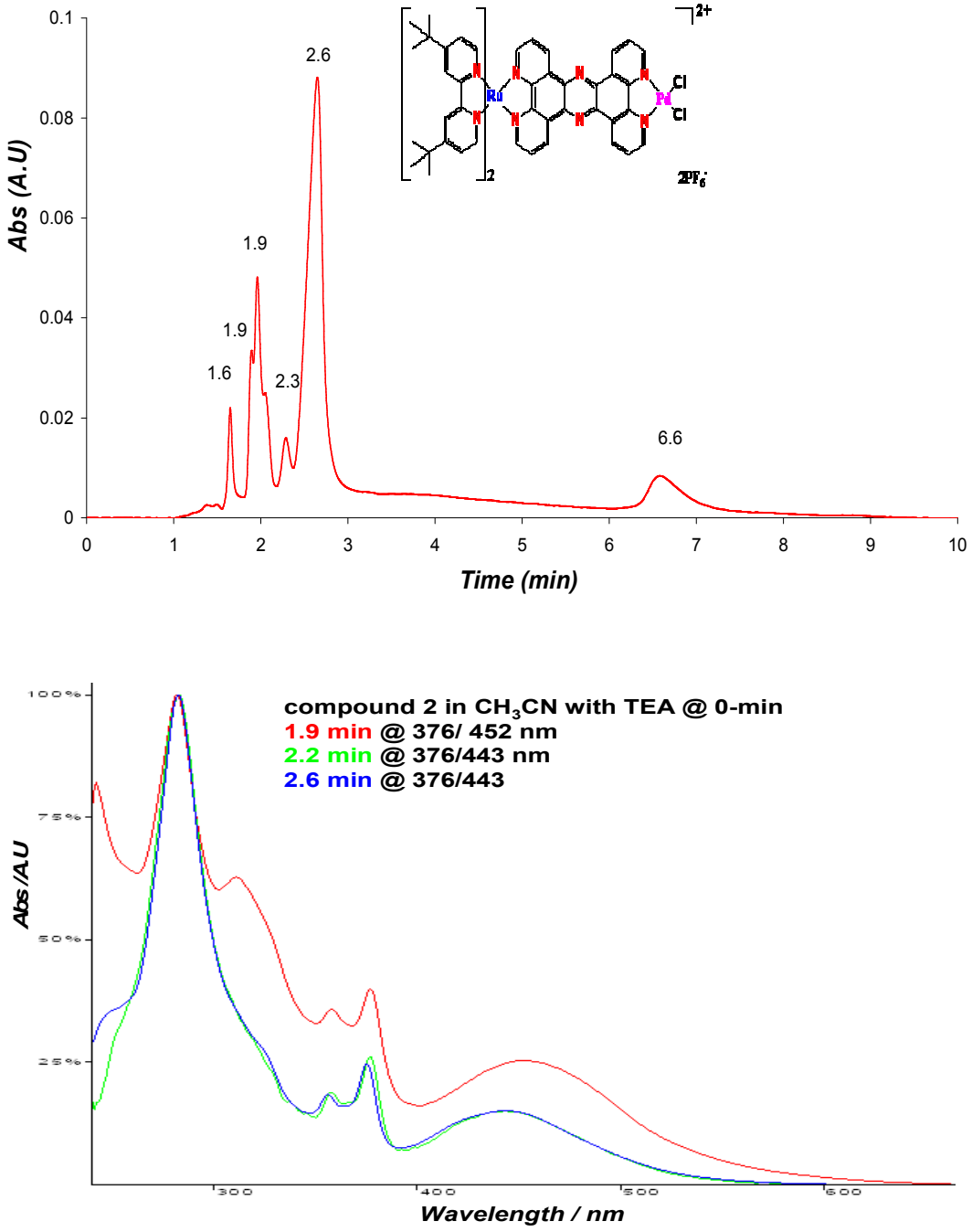

Figure 6.18. *Chromatogram (top) and absorption spectra (botom) of most important peaks of compound* ***2*** *before photolysis.*

Both compound **1** and **2** show quite a bit of tailing and this may suggest that their chromatographic behaviour is not as straight forward as that observed for compounds **3** and **4**. The reasons for this behaviour might be the presence of a free binding site on compound **1** and the possible liability of the chlorides of the palladium centre Another important point is that since the compound contains a $PdCl_2$ group, chloride ions are available and literature studies have shown that these will speed up photochemically induced ligand exchange processes [16].

A set of absorption spectra and the appropriate chromatogram obtained after photolysis for 120 min is shown below in Figure 6.19.

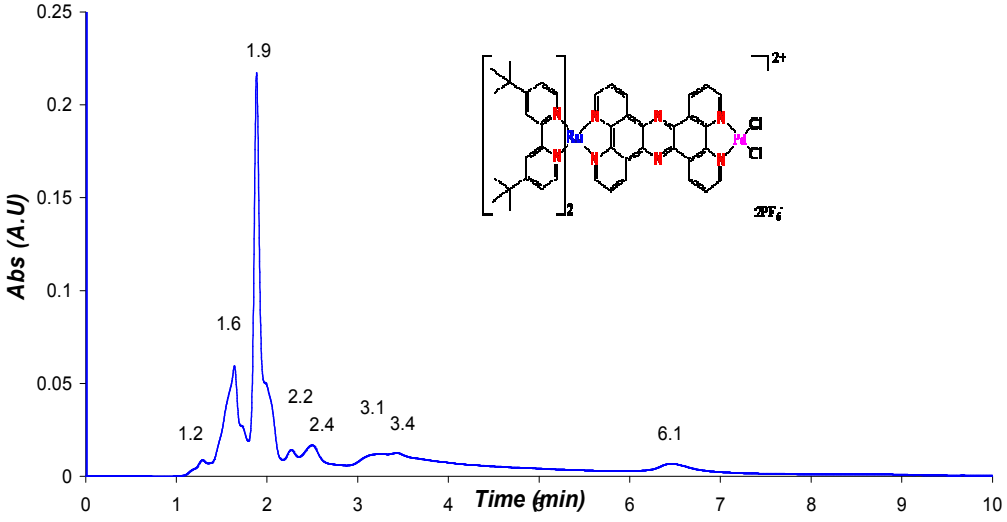

a

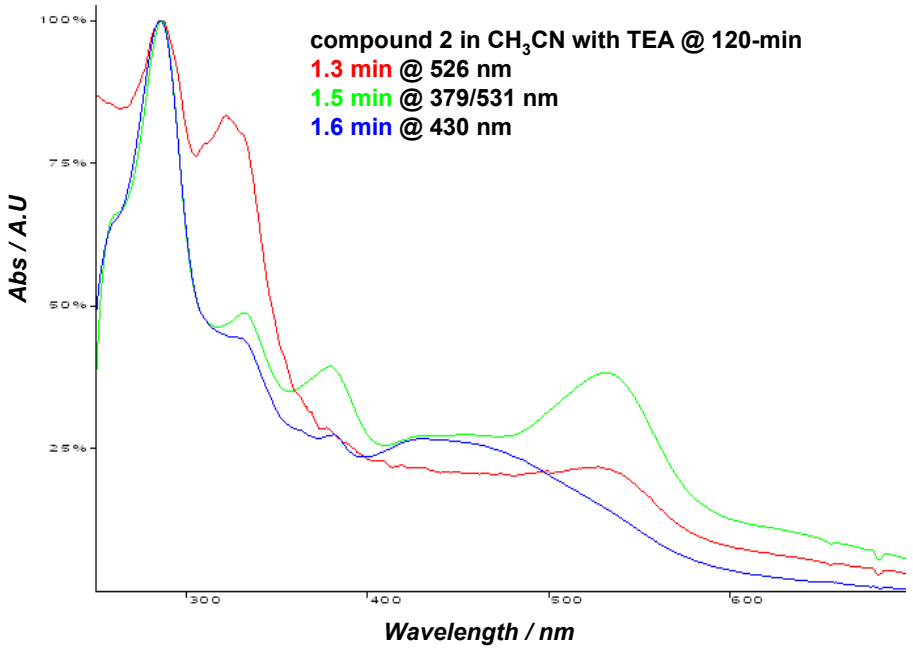
compound 2 in CH3CN with TEA @ 120-min
1.3 min @ 526 nm
1.5 min @ 379/531 nm
1.6 min @ 430 nm
Abs / A.U
100%
75%
50%
25%
300
400
500
600
Wavelength / nm

b

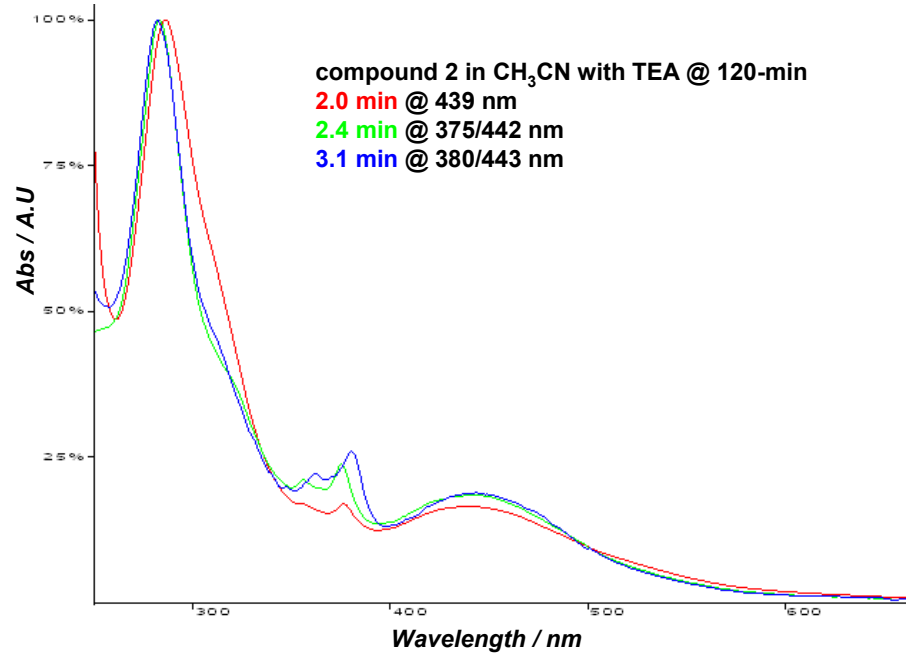
compound 2 in CH3CN with TEA @ 120-min
2.0 min @ 439 nm
2.4 min @ 375/442 nm
3.1 min @ 380/443 nm
Abs / A.U
100%
75%
50%
25%
300
400
500
600
Wavelength / nm

c

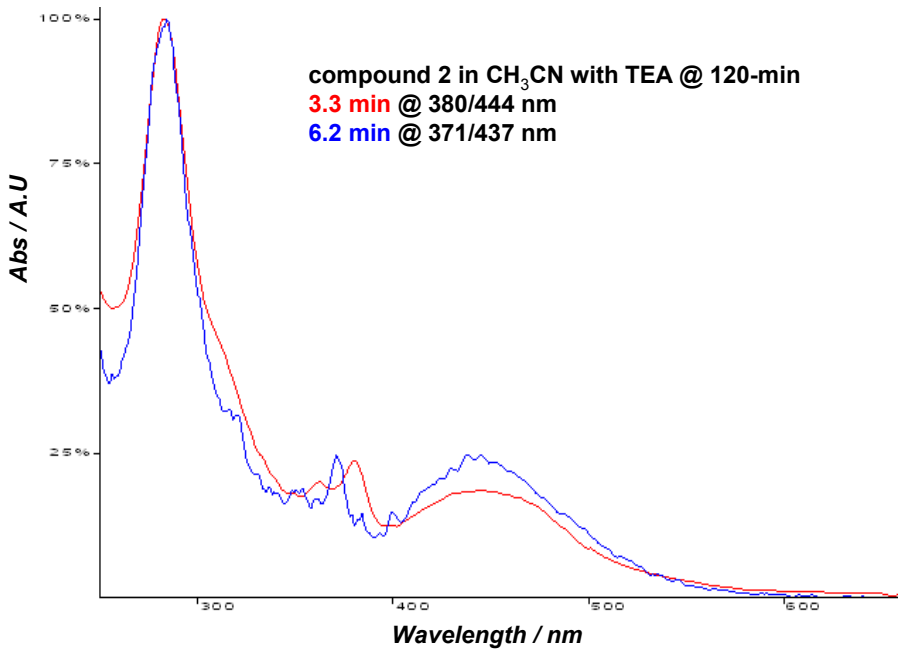

d

Figure 6.19 *Chromatogram (a) and absorption spectra (b,c,d) obtained for compound* ***2*** *after 120 min of irradiation.*

The chromatogram shows that after 2 hours of irradiation very little of compound 2 can be found in the reaction mixture. The main peaks observed are at 1.8 min, the so called organic peak, at 1.6 min, this is compound 4 present as an impurity from the synthetic process an unchanged peak at 6.4 min and a very broad signal covering the retention time range from 1.9 to 5 min.

The absorption spectra obtained for peaks below 2 min retention time indicate a strong overlap between the different species and are therefore not that informative. The presence of absorption peaks at about 520 nm (retention time 1.3 min) indicates the presence of $[Ru(tbbpy)_2Cl_2]$ as outlined before. Other species can not be determined with certainly, but the presence of free tpphz bridging ligand and

$[Ru(tbbpy)_2(CH_3CN)_2]^{2+}$ (retention times of 1.8 and 2.2 respectively) are likely to be present. The next section of the chromatogram, from 2 min to 6 min shows a number of species that all show the typical tpphz spectra features. A feature of these spectra is that they are not sensitive to the coordination pattern of the molecule. They can therefore not be used to identify the species present. As pointed out above also for compound **1** tailing of the peak is observed, but the signals at 3 min are not observed for any of the other compounds. In addition the peaks between 2 and 2.5 min also show tpphz features any may be related to the formation of compound **1**.

From the strong tailing of the peaks in the 2-5 min region it is difficult to determine the amount of material present and the absorption data present do not allow for a detailed analysis of the species formed. It is important however that in the photocatalytic process concerned with the generation of hydrogen, no hydrogen is formed in the first hour or so and that hydrogen formation continues for up to 24 hours.[10] The chromatographic data suggest that up on photolysis a new species is formed and that therefore the original compound **2** is unlikely to be the photocatalyst, but may be acting as a precatalyst. It has been suggested [10] that compound **2** needs to lose a chloride ligand before it can act as a catalyst for hydrogen reduction. This lability of the chloride, already confirmed by the formation of $[Ru(tbbpy)_2Cl_2]$, as outlined above would lead to the formation of species like $[(tbbpy)_2Ru(tpphz)PdClS]^{3+}$ and $[(tbbpy)_2Ru(tpphz)PdS_2]^{4+}$, where S is a solvent that could be water or acetonitrile. Quite a number of compounds

could therefore be formed upon release of the chloride ions. All would have a higher charge and would therefore be retained on the column for longer times as observed. The important observations of these studies is therefore that the data suggest that compound 2 is a pre catalyst and that during the photocatalytic process new, so far not identified tpph species are formed which could carry out the photocatalytic process.

6.4 Conclusion

In this chapter the photostability of the photocatalyst compound 2 and the model compounds 1,3 and 4 have been investigated both in acetonitrile and in acetonitrile containing triethylamine. In acetonitrile all 4 compounds are photostable for upto 2 hours. However, upon irradiation under “catalytic conditions”, that is in the presence of TEA, both compounds **1** and **2** show photo induced rearrangements. The photolysis of the photocatalyst, compound **2**, shows that after the two hour irradiation the compound is transformed in a range of compounds. The nature of these can not be established, apart from the fact that like for compound **1** the bis(acetonitrile) compound is observed as a product. The most interesting observation is however that other tpphz complexes are formed. These can not include compound **1** since this compounds decomposes to the acetonitrile complex and free bridging ligand. The identification of the new products, which have retention times of between 2-5 minutes can at this stage, not be established mainly because of the fact that all tpphz complexes show absorption spectra which are indistinguishable. The fact that the photo produced species are observed at longer

retention times suggests that they have a more positive charge. It is therefore postulated that the species which is assumed to be the active catalyst is formed. DFT calculations indicate that chloride loss from the Pd centre has to occur before hydrogen generation can take place. In addition the hydrogen formation has incubation time of about 2 hours. This would therefore agree quite well with the results obtained in this study. At this stage we can not identify the species formed, mainly because of the fact that the absorption features of the different tpphz complexes are identical. Nevertheless is seems likely from the hlpc experiments that such species are formed further research needs however to be carried out to establish this more fully.

References:

[1] (a) B. O`Regan and M. Grätzel, Nature, 1991, 353, 737; (b) M. K. Nazeeruddin, *Coord. Chem. Rev*., **2004**, 248, 1161.

[2] E. Amouyal in Water Splitting: *from Molecular to Supramolecular Photochemical Systems Homogenous Photocatalysis*, Vol. 2 (Ed.: M. Chanon), Wiley, Chichester, **1997**, pp. 263.

[3] K. Kalyanasundaram, J. Kiwi, M. Grätzel, Helv. *Chim. Acta*, **1978**, 61, 2720.

[4] S. Rau, D. Walther, J. G. Vos., *Dalton Trans*, **2007**, 915.

[5] A. Moradpour, E. Amouyal, P. Keller, H. Kagan, Nouv. *J. Chim*., **1978**, 2, 547

[6] M. Grätzel, Acc. *Chem. Res*., **1981**, 14, 376.

[7] J. Hawecker, J.-M. Lehn, R. Ziessel, *J. Chem. Soc. Chem.Commun*. **1983**, 536.

[8] J. M. Lehn, J.-P. Sauvage, Nouv. *J. Chim* **1977**, 1, 449.

[9] A. Currao, V. R. Reddy, M. K. van Veen, R. E. I. Schropp, G. Calzaferri, *Photochem. Photobiol. Sci*. **2004**, 3, 1017, and references therein.

[10] S. Rau, B. Schäfer, D. Gleich, E. Anders, M. Rudolph, M. Friedrich, H. Gorls, W. Henry, and J. G. Vos, *Angew. Chem. Int. Ed*. **2006**, 45, 6215.

[11] S. Rau, PhD thesis University of Jena.

[12] Ozawa, M. Haga, K. Sakai, *J. Am. Chem. Soc.* **2006**, 128, 4926 .

[13] B. Dietzek, W. Kiefer, J. Blumhoff, L. BMttcher, S. Rau, D. Walther, U. Uhlemann, M. Schmitt, J. Popp, *Chem. Eur. J*. **2006**, 12, 5105.

[14] S. Tschierlei, M. Presselt, C. Kuhnt, A. Yartsev, T. Pascher, V. Sundstrom, M. Karnahl, M. Schwalbe, B. Schäfer, S. Rau, M. Schmitt, B. Dietzek, Jurgen Popp., *Chem. Eur. J*. **2009**, 15, 7678.

[15] (a) B.P. Sullivan, T. J. Meyer, Inorg. Chem. **1982**, 21, 1037, (b) B. Durham, S. R. Wilson, D. J. Hodgson, T. J. Meyer, J. Am. Chem. Soc **1980**, 103, 600; (c) B. Durham, J.V. Caspar, J.K Nagle, T.J. Meyer, J. Am. Chem. Soc. **1982**, 104,

4803; (d) B. Durham, J.L.Walsh, C.L. Carter, T.J. Meyer, Inorg. Chem. **1980**, 19, 860.
[16] B.E. Buchanan, H. Hughes, P. Degn, J.M. Pavon Velasco, B.S. Creaven, C. Long, J.G. Vos, R. A. Howie, R. Hage, J.H. van Diemen, J.G. Haasnoot, and J. Reedijk. *J. Chem. Soc., Dalton Trans*., **1992**, 1177.

[17] CCR review this year.

CHAPTER 7

Conclusion & Future Work

7.1 Conclusion

The results reported here in chapters 3, 4, 5, and 6 shows that the HPLC method described, based on a cation exchange column can be very useful for the study of the photochemical properties of ruthenium compounds. Following these reactions with HPLC clearly has an advantage over the use of the more traditional spectroscopic methods. With only minor modifications we have used this method successfully to optimise reaction conditions for a range of ruthenium compounds. When HPLC is used in combination with a photodiode array detector, the species formed can be identified. Also the detection of coordination isomers is greatly facilitated by this method. One has however to take into account the possibility of changes of the ligand compositions of the species injected on the column because of their interaction with the mobile phase. Our results show that ligand exchange processes do occur in some cases and also that deprotonation of ligands can take place. This in itself however yields useful information about the stability of the compounds concerned.

In case of $\{[Ru(bpy)_2]_2(bpt)\}^{3+}$ (**1**) in Chapter 3 after three hours of irradiation at 430 nm the isomers constituting fraction A are converted into the isomers forming fraction B as detected through ^1H NMR spectroscopy. For both fractions **A** and **B** of complex **1**, further irradiation produces the fragmentation of the dimetallic complex into monometallic species. Such a photolytic reaction is catalysed by the

presence of chloride anions. In particular, photofragmentation of complex consists of the loss of the ruthenium centre bound to the N4-site of triazole ring. In case of complex, after three hours of irradiation at 430 nm the isomers constituting fraction A are converted into the isomers of fraction B. Analogously the irradiation of fraction B of complex leads initially to a process of photoisomerization into the components of fraction A. For both fractions A and B of the complex, further irradiation produces the fragmentation of the dimetallic complex into monometallic species. Such a photolytic reaction is catalysed by the presence of chloride anions. In particular, photofragmentation of the complex consists of the loss of the ruthenium centre bound to the N4-site of triazole ring.

In case of $\{[Ru(bpy)_2]_2(bpzt)\}(PF_6)_3$ in chapter 4 the loss of one metal centre takes place in less than nine hours.

The photochemical properties in chapter 5 are studied of $[Ru(bpy)_2(pztr)]^+$ **1**, and $[Ru(bpy)_2(pytr)]^+$ **2** and their protonated analogues **1H** and **2H**. Earlier studies have shown that for **1**, **2** and **2H** the LUMO and lowest emissive ^{3}MLCT state is based on the bpy ligands, while for **1H** the LUMO and lowest emissive ^{3}MLCT state is pyrazine based. The purpose of this study is therefore to investigate whether the difference in the location of the LUMO/MLCT state affects the photolability of the complexes. The deprotonated complexes **1** and **2** are both photostable in acetonitrile and acetone. This is not unexpected since the activation parameters (see Table 5.1) chapter five, for these compounds indicate the population of the ^{3}MC excited state is not significant. The photochemical behaviour of **1H** and **2H** in

CH_3CN is again the same, with ligand loss occurring with the formation of $[Ru(bpy)_2(CH_3CN)_2]^{2+}$ as the final product. Differences are however observed upon photolysis in acetone. As reported earlier photoinduced interconversion of the N2 and N4 isomers of **2H** is observed in CH_2Cl_2, with steady-state equilibrium of N4:N2 of 4:1. Upon irradiation of **1H** however, it was found that the N4 isomer is photostable while the N2 species isomerises to the N4 species via an intermediate. The results obtained therefore indicate that for these compounds the location of the LUMO in **1H** and **2H** does not affect the photolytic behaviour fundamentally. The photostability of the N4 isomer of **1H** is however an important point but is likely to be associated with the thermal stability of the primary photoproduct, i.e the species that contains a monodentate coordinated ligand.

In chapter 6, the photostability of the photocatalyst compound 2 and the model compounds 1,2,4 have been investigated both in acetonitrile and in acetonitrile containing triethylamine. In acetonitrile all 4 compounds are photostable for up to 2 hours. However, upon irradiation under “catalytic conditions”, that is in the presence of TEA, both compounds 1 and 2 show photo induced rearrangements. The photolysis of the photocatalyst compound 2 shows that after the two hour irradiation the compound is transformed into a range of compounds. The nature of these can not be established, apart from the fact that for compound **1** the bis(acetonitrile) complexed species is observed as a product. The most interesting observation is however that other tpphz complexes are obtained. These cannot include compound **1** since this compound decomposes to the acetonitrile complex

and the free bridging ligand. The identification of the new products, which have retention times of between 2-5 minutes can at this stage, not be established mainly because of the fact that all tpphz complexes show absorption spectra which are indistinguishable. The fact that the photo produced species are observed at longer retention times suggests that they have a more positive charge. It is therefore postulated that a species which is assumed to be the active catalyst is formed. DFT calculations indicate that chloride loss from the Pd centre has to occur before hydrogen generation can take place. In addition the hydrogen formation has incubation time of about 2 hours. This would therefore agree quite well with the results obtained in this study. At this stage we can not identify the species formed, mainly because of the fact that the absorption features of the different tpphz complexes are identical. Nevertheless is seems likely from the hlpc experiments that such species are formed further research needs however to
be carried out to establish this more fully.

7.2 Future Work

For the complexes described in Chapter 6, the photochemistry of the complexes needs to be investigated further in order to be explained better. The photochemical properties have only been investigated with condition described so special attention should be paid to the photochemical properties of the tpphz complexes **1-4** in other solvent conditions, another issue is the fact that the separation obtained between the products cannot be evaluated through changes of optical spectra. The compounds need to be investigated using other HPLC conditions (mobile phase, columns types, and many other).

Appendix A Posters and Publications

(Posters)

APPLICATION OF HPLC IN THE INVESTIGATION OF THE PHOTOCHEMICAL REACTIONS OF BIMETALLIC COMPLEXES $\{[Ru(bpy)_2]_2bpt\}^{3+}$ AND $\{[Ru(bpy)_2]_2bpzt\}^{3+}$

Hamid M.Y. Ahmed, **Nadia Coburn, Danilo Dini, Johannes G. Vos**

Solar Energy Conversion SRC, School of Chemical Sciences, Dublin City University, Dublin 9, Ireland. E-mail: hamid.ahmed2@mail.dcu.ie

An abstract has been accepted on 18th ISPPCC International Symposium on the Photochemistry and Photophysics of Coordination Compounds, Sapporo Japan

Development of a New Synthetic Strategy for obtaining $[Ir^{III}(bpy\text{-}N,N')_2Cl_2]^+$ and its analogues in High Purity and Yield, Study of its Mechanism and Deuteriation Effect on the Formation of $[Ir^{III}(bpy\text{-}N,N')_2(bpy\text{-}C,N')^-]^{2+}$ Complexes.

Suraj Soman,[a] Hamid Younis,[a] , Laura Cleary,[a] Johannes G. Vos,[a] Mary T. Pryce,[a] Wesley R. Browne[b]

*(**a**) SRC for Solar Energy Conversion: School of Chemical Sciences, Dublin City University, Dublin 9, Ireland;(**b**) Faculty of Mathematics and Natural Sciences, Stratingh Institute, University of Groningen, The Netherlands.*

A poster has been presented at Trinity College Dublin on 8th Annual Symposium on Supramolecular Chemistry in Ireland 30th March 2009.

Application of HPLC in the investigation of the photochemical reactions of bimetallic complexes $\{[Ru(bpy)_2]_2bpt\}^{3+}$ and $\{[Ru(bpy)_2]_2bpzt\}^{3+}$

Hamid M.Y. Ahmed, Nadia Coburn, Danilo Dini, Johannes G. Vos

SRC for Solar Energy Conversion - School of Chemical Sciences, Dublin City University, Dublin 9, Ireland

Abstract

Bimetallic ruthenium complexes $\{[Ru(bpy)_2]_2(bpt)\}(PF_6)_3$ (**1**) [bpy = 2,2'-bipyridine, bpt = 3,5-bis-(pyridin-2'-yl)-1,2,4-triazole], and $\{[Ru(bpy)_2]_2(bpzt)\}(PF_6)_3$ (**2**) [bpzt = 3,5-bis(pyrazin-2- yl)-1,2,4-triazole], have been synthesized and their photolysis processes have been analysed with ^1H-NMR, UV/vis spectroscopy, and HPLC. HPLC separation of **1** and **2** affords two fractions: A (with the smaller retention time) and B (with the larger retention time). Each fraction is constituted by a enantiomeric pair. In case of **1**, after three hours of irradiation at 430 nm the isomers constituting fraction A are converted into the isomers of fraction B. Analogously the irradiation of fraction B of **1** leads initially to a process of photoisomerization into the components of fraction A. For both fractions A and B of **1**, further irradiation produces the fragmentation of the dimetallic complex into monometallic species. Such a photolytic reaction is catalysed by the presence of chloride anions. In particular, photofragmentation of complex **1** consists of the loss of the ruthenium centre bound to the N4-site of triazole ring. In case of $\{[Ru(bpy)_2]_2(bpzt)\}(PF_6)_3$ (**2**) photoisomerization is completed within one hour of irradiation whereas the loss of one metal centre takes place in less than nine hours.

The syntheses of $\{[Ru(bpy)_2]_2(bpt)\}(PF_6)_3$ (**1**) and $\{[Ru(bpy)_2]_2(bpzt)\}(PF_6)_3$ (**2**) (Figure 1) have been accomplished following previously reported procedures.[1]

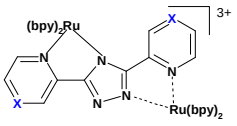

X = CH, N bpy = 2,2'-bipyridine

Figure 1: *Structures of bimetallic Ru complexes **1 (X = CH) and** 2 (X = N).*

The HPLC traces of complexes **1** (Figure 2) and **2** (Figure 3) in acetonitrile (ACN) present two main peaks here indicated as fraction A and fraction B at shorter and longer retention times, respectively. These two fractions refer to the pairs of enantiomers Λ,Λ/Δ,Δ (fraction A) and Λ,Δ/Δ,Λ (fraction B).[2]

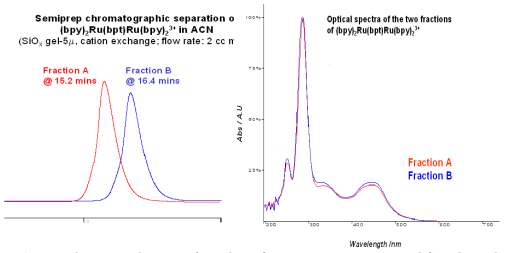

Figure 2: *Chromatographic traces of complex **1** after semipreparative separation (left), and optical spectra of fractions A and B of **1** (right).*

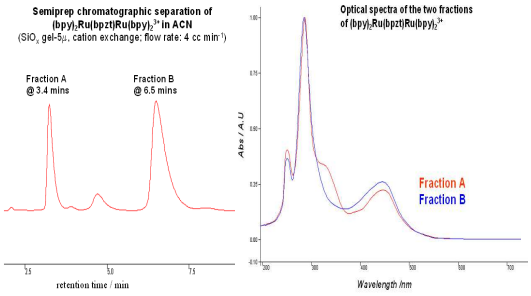

Figure 3: *Chromatographic trace of complex **2** after preparation (left), and optical spectra of fractions A and B of **2** after semipreparative separation (right).*

Visible irradiation of the separated fractions A and B in acetonitrile first primes a reaction of photoisomerization A →B / B →A as verified through the combined analysis of the HPLC traces of photolysis products and their optical and ^{1}H NMR spectra (complex **1**, Figures 4 and 5). Photoisomerization is then followed by the fragmentation of the bimetallic species into monomeric species (peaks 3-5 in Figure 4, left) and uptaking of ACN solvent molecules in order to complete the coordination spheres of the non bridged metal cations.[3]

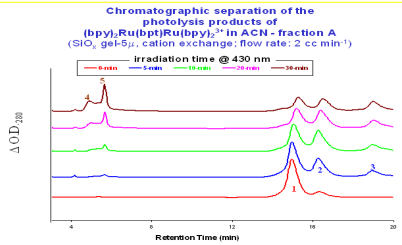

Figure 4: *Compound **1**- HPLC separation of the products of photolysis of fraction A.. Peaks 1 and 2 refer to fractions A and B, respectively. Peaks 3-5 are related to the species obtained from the fragmentation of the bimetallic complexes.*

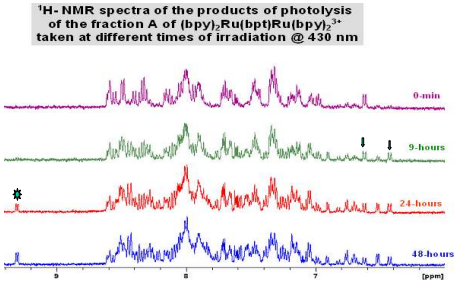

Figure 5: *Compound **1**- Variations of the ^{1}H NMR spectrum of the fraction A in d3-acetonitrile upon photolysis at 430 nm. Down arrows indicate signals derived from isomerization,green star indicate the signal derived from complex decomposition.*

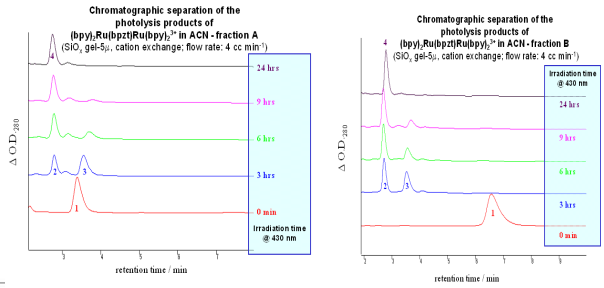

Figure 6: *Compound 2- (left) HPLC separation of the products of photolysis of fraction A and (right) fraction B. The optical spectrum of peak 4 is coincident with that of peak 5 in Figure 4 and is ascribed to the monomeric species $Ru(bpy)_2ACN_2^{2+}$.*

References

1. (a) Hage, R.; Dijkhuis, A.H.J.; Haasnoot, J.G.; Prins, R.; Reedijk, J.; Buchanan, B.E.; Vos, J.G. *Inorg. Chem.* **1988**, *27*, 2185; (b) Gerald, J.F.; Lions, F. *J. Org. Chem.* **1965**, *30*, 318; (c) Hage, R.; Haasnoot, J.G.; Reedijk, J.; Wang, R.; Vos, J.G. *Inorg. Chem.* **1991**, *30*, 3263. 2. Browne, W.R.; O'Connor, C.M.; Villani, C.; Vos, J.G. *Inorg. Chem.* **2001**, *40*, 5461. 3. (a)Hughes, H.P.; Vos, J.G. *Inorg. Chem.* **1995**, *34*, 4001; (b) Hughes, H.P.; Martin, D.; Bell, S.; McGarvey, J.; Vos, J.G. *Inorg. Chem.* **1993**, *32*, 4402.

Acknowledgements

The authors would like to thank SFI (Advanced Biomimetic Materials for Solar Energy Conversion), the General People's Committee Secretary for Higher Education of Libya, and the Louth County Council for their financial support.

(Publications)

1 Photoinduced Ligand Isomerisation in a Pyrazine Containing Ruthenium Polypyridyl Complex. S. Horn, **H. M. Younis Ahmed**, H. P Hughes, S. Soman, W. R. Browne and J. G. Vos *Photochem. Photobiol. Sci.*, **2010**, 9, 985

2 Excited State Localization and Internuclear Interactions in Asymmetric Ruthenium(II) and Osmium(II) bpy/tpy Based Dinuclear Compounds. Yvonne Halpin, Danilo Dini, **Hamid M. Younis Ahmed**, Lynda Cassidy, Wesley R. Browne, and Johannes G. Vos, *Inorg. Chem*. **2010**, 49, 2799–2807 2799.

3 Development of a New Synthetic Strategy for obtaining $[Ir^{III}(bpy\text{-}N,N')_2Cl_2]^+$ and its analogues in High Purity and Yield, Study of its Mechanism and Deuteriation Effect on the Formation of $[Ir^{III}(bpy\text{-}N,N')_2(bpy\text{-}C,N')^-]^{2+}$ Complexes. Suraj Soman, **H. M. Younis Ahmed**, , Laura Cleary, Johannes G. Vos, Mary T. Pryce, Wesley R. Browne. (to be published).

4 SOMO delocalisation in mixed valent Ruthenium Polypyridyle complexes through CD spectroelectrochemistry. **Hamid. M.Younis Ahmed**, Nadia Coburn, Danilo Dini, Wesly R. Brown, Jaap J. D. de Jong, Claudio Villani, L. Feringa, Johannes G. Vos. (to be published).

Photoinduced ligand isomerisation in a pyrazine-containing ruthenium polypyridyl complex†

Sabine Horn,[a] Hamid M. Y. Ahmed,[a] Helen P Hughes,[a] Suraj Soman,[a] Wesley R. Browne[b] and Johannes G. Vos*[a]

Received 10th March 2010, Accepted 13th April 2010
First published as an Advance Article on the web 14th May 2010
DOI: 10.1039/c0pp00054j

Photochemically-induced ligand rearrangements for the N2 and N4 coordination isomers of the complex $[Ru(bpy)_2(Hpztr)]^{2+}$ and its deprotonated analogue $[Ru(bpy)_2(pztr)]^{+}$, where bpy is 2,2′-bipyridyl and Hpztr is pyrazine-1,2,4-triazole ligand, are reported. ^{1}H NMR spectroscopic and HPLC studies indicate that in acetone and acetonitrile the complexes are photostable when the triazole ring is deprotonated. Irradiation of the protonated N2 isomer in acetone results in formation of the N4 isomer, with the N4 isomer being photostable. In acetonitrile both isomers show photolability of the triazole-based ligand and full dissociation to form $[Ru(bpy)_2(CH_3CN)_2]^{2+}$ is observed. The activation parameters for the population of the ^{3}MC state from the lowest ^{3}MLCT manifold, as obtained from temperature-dependent emission lifetime studies, are reported and their relevance to the observed photochemical behaviour is considered. The results obtained are discussed in relation the analogous pyridine-triazole complexes.

Introduction

Following the early work of Adamson[1] and others,[2] the investigation of photoinduced processes has developed substantially over the last 50 years. This development was further intensified with the application of ruthenium polypyridyl complexes as dyes for solar cells,[3] oxygen sensors,[4] and as bioprobes[5] and molecular machines and devices, such as molecular wires, motors and switches.[6] Recently these studies have received further interest due to the potential application of polypyridyl compounds in the development of sustainable and environmentally friendly energy such as photocatalytic hydrogen generation[7] and CO_2 reduction.[8]

Over the last number of years we have reported a series of studies of photoinduced ligand rearrangements of ruthenium polypyridyl complexes containing pyridine-1,2,4-triazole (Hpytr) ligands. Recently such ligands have seen widespread application in iridium(III) based OLED systems also.[9] The complex $[Ru(bpy)_2(pytr)]^{+}$ (Fig. 1), which contains a deprotonated pyridine-1,2,4-triazolato ligand is photostable upon irradiation in basic acetone and acetonitrile. This photostability is related to the strong σ-donor capacity of the deprotonated triazole ring that provides for a considerable destabilization of the ^{3}MC state that has been identified as being involved in the photochemical activity of ruthenium polypyridyl complexes.[10] Because of the destabilisation this excited state is not populated significantly at room temperature. However, for complexes containing protonated or methylated triazole ligands the ^{3}MC level is stabilised and photolability observed.[11,12,13] As a result photoinduced ligand dissociation processes are observed where the triazole ligand is not anionic. For $[Ru(bpy)_2(Hpytr)]^{2+}$ there are two coordination isomers possible where the Hpytr ligand is bound *via* either the N2 or the N4 nitrogen atom of the triazole ring (Fig. 2). Irradiation in CH_2Cl_2 of either the N2 or N4 isomer leads to a photostationary state with a N4 : N2 ratio of 4 : 1.

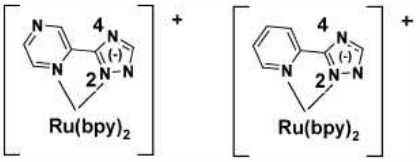

Fig. 1 N2 isomers of $[Ru(bpy)_2(pztr)]^{2+}$ **1**, (left) and $[Ru(bpy)_2(pytr)]^{2+}$ **2**, (right); bpy = 2,2′-bipyridine.

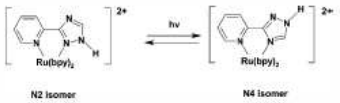

Fig. 2 Reversible N2–N4 isomerisation observed for compound **2H**.

For the analogous pyrazine triazole (Hpztr) based complexes (*e.g.*, Fig. 1) photochemically induced ligand isomerisations have not been reported. There have however been extensive photophysical studies[14,15] that have shown that contrary to that which is observed for the Hpytr based complexes, where the emitting state is bpy based, the lowest energy triplet state in complexes containing the protonated ligand is based on the pyrazine ring.

[a]*Solar Energy Conversion SRC, School of Chemical Sciences, Dublin City University, Dublin 9, Ireland. E-mail: han.vos@dcu.ie; Fax: +353-1-7005503; Tel: +353-1-7005307*
[b]*Center for Systems Chemistry, Stratingh Institute for Chemistry and Zernike Institute for Advanced Materials, Faculty of Mathematics and Natural Sciences, University of Groningen, Nijenborgh 4, 9747AG, Groningen, The Netherlands*

† This article is published as part of a themed issue in appreciation of the many important contributions made to the field of molecular photophysics by Jan Verhoeven.

In this contribution we report the photochemically induced rearrangements observed for the complex $[Ru(bpy)_2(Hpztr)]^{2+}$ (**1H**). The photochemical processes observed are discussed in terms of the structure and the electronic properties of the complex and are compared with those observed for the analogous complex **2H** based on the Hpytr ligand.

Experimental

Synthesis and materials

All solvents employed in spectroscopic measurements were of spectroscopic grade (Sigma-Aldrich). All other solvents were of HPLC grade or better. *cis*-$Ru(bpy)_2Cl_2{\cdot}2H_2O$,[16] and the N2 and N4 isomers of $[Ru(bpy)_2(pztr)](PF_6)_2$ **1**[14a] were prepared as reported before. $[Ru(bpy)_2(CH_3CN)_2](PF_6)_2$ was available from earlier studies.[13b]

N2-/N4-isomer $[Ru(bpy)_2(pztr)]PF_6$

cis-$[Ru(bpy)_2Cl_2]{\cdot}2H_2O$ (185 mg, 0.36 mmol) and Hpztr-H (80 mg, 0.54 mmol) were added to a mixture of EtOH (30 mL) and H_2O (30 mL). After heating at reflux for 8 h, EtOH was removed *in vacuo* and the reaction mixture was left to stand overnight. The crude product was flash chromatographed on a silica column with 7 : 3 (v/v) CH_3CN–H_2O saturated with KNO_3. A drop of NH_3 solution and NH_4PF_6 (30 mg, 0.18 mmol) was added in turn to each of the two fractions collected. Each solution was washed with dichloromethane (3 × 20 mL) and the solvent was evaporated. The N2-isomer (second fraction of silica column) was purified further by column chromatography on an alumina column (neutral) with CH_3CN as eluant. The solvent was evaporated *in vacuo* and the solid was recrystallised by slow evaporation from 2 : 1 MeOH–H_2O. The N4-isomer (first fraction from the silica column) was chromatographed on an alumina column (neutral) with first CH_3CN, then 1 : 20 MeOH–CH_3CN, 1 : 10 MeOH–CH_3CN and 1 : 5 MeOH–CH_3CN. The solvent was evaporated *in vacuo* and the solid recrystallised by slow evaporation of 2 : 1 MeOH–H_2O. Yield: 51 mg of the N2-isomer (0.09 mmol, 25%), 90 mg of N4-isomer (0.16 mmol, 45%). The ^{1}H NMR spectra were in accordance with literature values.[15a,c]

^{1}H-NMR spectra were recorded on a Bruker Advance 400 MHz NMR spectrometer. Data are relative to residual solvent absorptions. UV/vis absorption spectra were recorded on a JASCO 570 UV/vis/NIR spectrophotometer using a 1 cm pathlength quartz cells. Temperature dependent luminescence lifetime studies were carried out using a Spectra Physics Q-switched Nd-YAG laser system as described elsewhere.[14e] Analytical High Performance Liquid Chromatography (HPLC) experiments were carried out using an analytical HPLC system consisting of a Varian Prostar HPLC pump fitted with a 20 µL injection loop, a Varian Prostar PDA detector connected to a dedicated PC, and a HiChrom Partisil P10SCX-3095 cation exchange column. Mobile phase CH_3CN : H_2O : CH_3OH with volume ratio 75 : 20 : 5 containing 0.12 M KNO_3. Flow rate: 2.0 cm^3 min^{-1}; detection wavelength: 430 nm. The photochemistry of complexes **1**, **2**, **1H** and **2H** was monitored by HPLC and ^{1}H NMR spectroscopy. HPLC samples were irradiated in acetonitrile or acetone with an array of 60 Kingbright L-7113PBC-Gblue 470± 20 nm LEDs. Photolysis studies monitored by ^{1}H NMR spectroscopy were carried out by irradiating the compounds in NMR tubes and placing them before a 20 W tungsten filament light source slide projector (Kodak Carousel S-AV 2020). Sample heating was prevented using a water filter. The protonation state of the triazole ring of the complexes was controlled by addition of 100 µl triethylamine or trifluoroacetic acid to the 2 mL NMR sample.

Results and discussion

Both isomers show strong ^{1}MLCT bands in the visible part of the spectrum as expected.[15c] The absorption maxima of both protonated compounds are very similar with a λ_{max} of 440 nm for the N2 isomer and a value of 439 nm for the N4 species. Upon deprotonation the absorption maxima of the N2 and N4 isomers shift to 456 and 457 nm respectively. Because of the similarity of these values and also in the shape of the absorption spectra these features can not be used to discriminate between the two isomers.

Irradiation in acetonitrile

The photochemical properties of **1** and **1H** were investigated using ^{1}H NMR spectroscopy and HPLC. Irradiation of the compounds was carried out in both acetonitrile and acetone.

The HPLC chromatogram obtained for a mixture of the N2 and N4 isomers is shown in Fig. 3. The N4 isomer is observed to have a retention time of 5.4 min, while the N2 is observed at 6.7 min. The same elution order is observed for the pyridinetriazole analogues (*e.g.*, **2**).[11] In contrast to **2**, the UV/Vis spectra of the two isomers of **1**/**1H** are almost identical and cannot be used for identification as a result. The two species are identified by their ^{1}H NMR spectra however. Of most importance for the identification of the nature of the isomer obtained are the ^{1}H NMR absorptions than can be attributed to the pyrazine and the triazole rings. The pyrazine absorptions appear as a singlet (H3) in the range 9.1–9.5 ppm, while H5 appears at *ca.* 7.8 ppm and H6 at *ca.* 8.2 ppm; the exact location depending on whether the compound is protonated or not. The most indicative feature identifying the isomeric form is the position of the H5 proton of the triazole ring. For the protonated N2 isomer (*N2***1H**) this proton is observed at 8.91 ppm and for the deprotonated N2 isomer at 8.0 ppm. For the N4 isomer the corresponding values are at *ca.* 8.4 and 7.4 ppm respectively. These values were obtained in acetone and vary substantially depending on the amount of acid added and the water content of the solvent. The rather large difference between the values observed for the

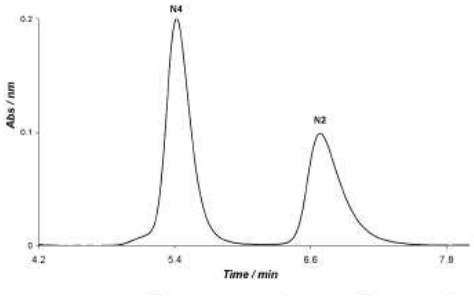

Fig. 3 HPLC trace of N2 and N4 isomers of **1**. Mobile phase CH_3CN : H_2O : CH_3OH with volume ratio 75 : 20 : 5, 0.12 M KNO_3, flow rate: 2.0 cm^3 min^{-1}; detection wavelength: 430 nm, 20 °C.

H5 protons for the two isomers is related to the through space interaction between these protons and neighbouring bpy ligands especially in the case of the N4 isomer.[15c,16] This through space interaction results in the considerable shift to lower ppm values for the proton in the N4 isomer compared with the N2 species.

HPLC and ^{1}H NMR spectroscopic studies indicate that both isomers of the deprotonated compound **1** are photostable in the presence of the base TEA in acetonitrile and in acetone. This is in agreement with the reported behaviour of compound **2**.[11] However, acidification of the solution prior to irradiation allows for photoinduced changes to be observed. The photoinduced changes observed for *N4***1H** in acetonitrile monitored by HPLC are shown in Fig. 4.

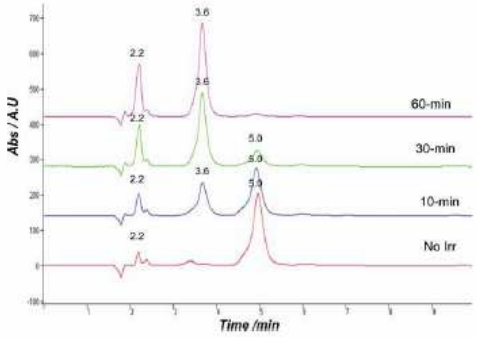

Fig. 4 HPLC trace following the irradiation of the N4 isomer in CH_3CN with CF_3CO_2H (mobile phase CH_3CN : H_2O : CH_3OH with volume ratio 75 : 20 : 5, 0.12 M KNO_3). Flow rate: 2.0 cm^3 min^{-1}; detection wavelength: 430 nm, 20 °C.

The decrease in the signal for the N4 isomer (retention time of 5.0 min) with irradiation is accompanied by the appearance of a new peak at 3.6 min. This signal which shows an absorption maximum at 425 nm is identified as the $[Ru(bpy)_2(CH_3CN)_2]^{2+}$ by comparison with an authentic sample. The appearance of a second product with a retention time of 2.2 min ($\lambda_{max} = 472$ nm) is observed also. The nature of these species could not be determined unambiguously but may be related to the intermediate observed in the ^{1}H NMR spectrum in Fig. 5. The irradiation of *N2***1H** in acetonitrile was monitored by ^{1}H NMR spectroscopy also (Fig. 5). ^{1}H NMR spectra show that upon irradiation of both the N2 and the N4 isomers of **1H** in acidic acetonitrile results in formation of the same final product, $[Ru(bpy)_2(CH_3CN)_2]^{2+}$, which was confirmed by comparison with the spectrum of an authentic sample.

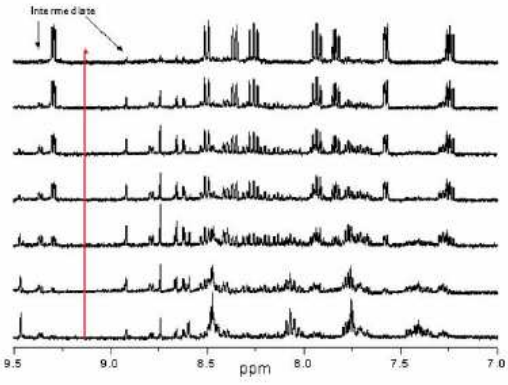

Fig. 5 Irradiation of N2 isomer of $[Ru(bpy)_2(Hpztr)]^{2+}$ in acetonitrile with CF_3CO_2H.

As observed in the HPLC traces an intermediate is observed with signals at 8.0, 8.9 pm and 9.3 pm which disappear upon further photolysis. The observed isomerisation process could suggest that in this intermediate the pyrazine ring remains attached to the metal centre, since this allows for reorientation of the triazole ring in the sterically most favoured position. However, our earlier studies have shown that an alternative intermediate species is formed upon photolysis of the related complex $[Ru(bpy)_2(L\text{-}L')]^{2+}$ where L-L′ is 4-methyl-3-(pyridine-2-yl)-1,2,4-triazole. In this intermediate the triazole ring is bound to the N1 atom as shown in Fig. 6.[13b] Such a species can be formed starting from both **1H** isomers and hence the formation of the isomer where the triazole ring is coordinated to the metal centre *via* the N1 atom of the triazole ligand can not be excluded.

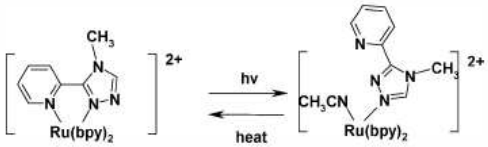

Fig. 6 Photo- and thermally-induced coordination changes for $[Ru(bpy)_2(L\text{-}L')]^{2+}$ where L-L′ is 4-methyl-3-(pyridine-2-yl)-1,2,4-triazole.

Irradiation in acetone

The photostability of the protonated complex **1H** in acetone was investigated. Surprisingly, irradiation of the N4 isomer of **1H** does not result in any observed changes over at least a 2 h period. The N2 isomer, by contrast, shows photoreactivity as illustrated in Fig. 7. Initially the N2 isomer is observed at a retention time of 7.4 min. After irradiation the N4 isomer is present as the main product with a retention time of 5.6 min. As observed in the ^{1}H NMR spectra the formation of other minor products is observed also (Fig. 8).

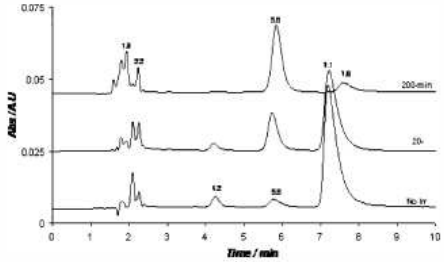

Fig. 7 HPLC assessment of the photoisomerisation of N2 isomer of **1H** in acetone in the presence of CF_3COOH.

Most indicative for the isomerisation from the N2 to the N4 isomer are the changes observed for the pzH3 peak which changes from 9.63 ppm for the N2 isomer to 9.54 pm. Additionally the peak

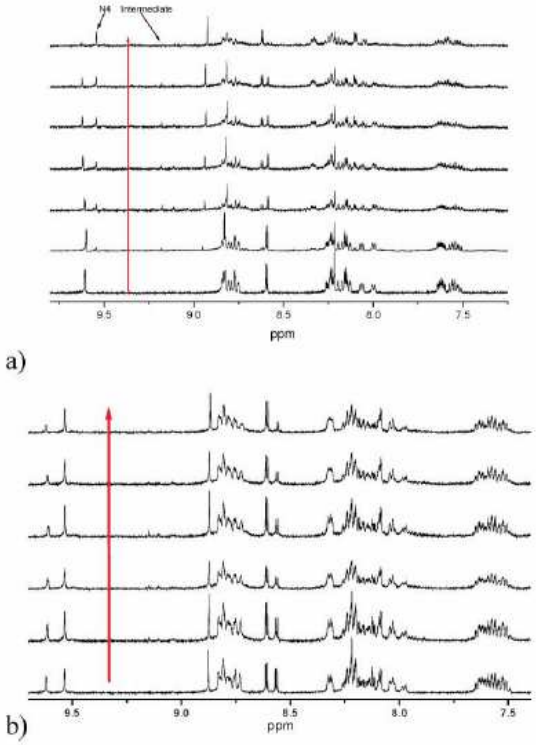

Fig. 8 (a) Irradiation of the N2 isomer of $[Ru(bpy)_2(Hpztr)]^{2+}$ (**1H**) in acetone with CF_3CO_2H. (b) Irradiation of a 1 : 1 mixture of the N2 and N4 isomer of $[Ru(bpy)_2(Hpztr)]^{2+}$ (**1H**) in acetone with CF_3CO_2H. Spectra run from bottom to top in each case.

of the pzH5 shifts from 8.58 pm to 8.61 pm. During irradiation two peaks appear at 9.1 pm and 9.17 pm and disappear in the final spectrum, indicating (as in the HPLC traces, *i.e.* at 4.2 and 2.0 min) the formation of a small amount of an intermediate. The concentrations of these species are however to low to allow for definitive assignment.

Activated crossing from the ^{3}MLCT to ^{3}MC states

Ligand exchange *via* cleavage of metal–ligand bonds is a paradigm photochemical reaction and is central to results discussed here. Meyer and co-workers,[17] in their studies of ruthenium(II) polypyridyl complexes, identified the triplet metal centred (^{3}MC) state as being responsible for the photochemical ligand dissociation observed for these compounds. The state corresponds to population of the antibonding (e_g) orbitals which is accessed at room temperature from the lowest ^{3}MLCT state manifold. This process is thermally activated and the difference in energy between the ^{3}MLCT and ^{3}MC states can be estimated indirectly from the temperature dependence of the emission lifetime. The activation parameters obtained in an ethanol–methanol (4 : 1) solvent system over the temperature range 150–300 K are shown in Table 1 and are compared with related data for Hpytr based compounds *N2***2** and *N4***2**. For example values of the ^{3}MLCT–^{3}MC energy gap for **1H** complexes are similar to those obtained for their **2H** analogues.

Table 1 Activation parameters and kinetic data for ruthenium(II) pyrazine triazole complexes and related pyridine triazole analogues

	E_a/cm^{-1} [a]	A/s^{-1}	k_{77K}/s^{-1}
*N4***1**	1300	5.1×10^{9}	2.2×10^{5}
*N2***1**	1200	3.6×10^{9}	2.4×10^{5}
*N4***1H**	2950	1.5×10^{13}	1.5×10^{5}
*N2***1H**	2200	9.0×10^{11}	1.4×10^{5}
*N4***2**[b]	600	3.1×10^{7}	6.4×10^{5}
*N2***2**[b]	550	4.7×10^{7}	4.1×10^{5}
*N4***2H**[b]	2850	9.2×10^{13}	2.8×10^{5}
*N2***2H**[b]	1700	6.0×10^{10}	2.8×10^{5}

[a] Data obtained in ethanol–methanol (4 : 1) at temperatures 150–300 K. Rate constant errors ± 5%, activation parameters ± 10%. [b] Values obtained from reference 11.

The temperature dependent lifetime data in the temperature range 150–300 K were analysed by assuming that the excited state decay consists of a temperature independent intrinsic decay from the ^{3}MLCT state and a single thermally activated non-radiative decay process according to eqn (1):

$$\frac{1}{\tau_{obs}} = k_{77K} + A\exp\left(\frac{-E_a}{RT}\right) \quad (1)$$

where $k_{77K} = k_{nr} + k_r$ (the sum of the temperature-independent radiative and non-radiative decays from the ^{3}MLCT direct to the ground state), A is the preexponential factor and E_a is the activation energy for crossing from the ^{3}MLCT to the ^{3}MC excited state. k_{77K} is obtained at 77 K, assuming that k_{nr} and k_r are temperature independent above 77 K and that population of the ^{3}MC states is effectively prevented at 77 K

Activation parameters obtained for ruthenium polypyridyl complexes usually fall into one of two categories:

(a) small activation energies (<800 cm^{-1}) and low prefactors (<10^9 s^{-1});

(b) large activation energies (>2000 cm^{-1}) and large prefactors (>10^{11} s^{-1}).

Complexes exhibiting the former behaviour are typically unreactive towards photosubstitution. This is indeed observed for the deprotonated species. The low prefactor suggests the process involves the population of an MLCT state of largely singlet character that is weakly coupled to the ^{3}MLCT state.[18] Complexes exhibiting the second type of behaviour are typically photochemically active and the activation process has been ascribed as being due to population of a ^{3}MC state. If relaxation of the ^{3}MC state is rapid relative to crossover from the ^{3}MC state back to the ^{3}MLCT state, the measured E_a represents the activation energy for ^{3}MLCT–^{3}MC internal conversion. For such a process the prefactor is expected to be large (10^{13}–10^{14}). The N4 isomers for both **1H** and **2H** fall in this catagory.

The N2 isomer of $[Ru(bpy)_2(Hpztr)]^{2+}$ (*i.e. N2***1H**) intermediate behaviour was observed, with an activation barrier of 2200 cm^{-1} and a prefactor of 9.0×10^{11}. This may indicate that the ^{3}MLCT and ^{3}MC states are in equilibrium. In this case the measured activation energy corresponds approximately to the energy gap between the two states.[19] For compound *N2***2H** this intermediate behaviour was also observed.[11]

Population of the ^{3}MC state is a key step in the photochemistry of the protonated pyrazyltriazole complexes. pK_a data indicate

that triazole is a stronger σ-donor when coordinating *via* the N2 nitrogen than *via* the N4 nitrogen.[11,14a] Hence for the N2 isomers of **1H** and **2H** the ^{3}MC state would be expected to lie higher in energy than the for the corresponding N4 isomers. Consequently the larger activation energy for population of the ^{3}MC state from the ^{3}MLCT state is expected to be higher for the N2 isomers compared with the N4 isomers. However, this is not found to be the case, suggesting that population of the ^{3}MC excited state is not the rate determining step in the photochemistry of the protonated pyrazoletriazole complexes. Instead, the rate-determining step may be governed by the formation of the monodentate species during the photoisomerisation and the subsequent ground state thermal self-annealing process. This may be related to the difference observed between the N4 and N2 isomers in the deactivation mechanism for the ^{3}MC state. While the prefactors for the N2 isomers suggest the existence of an equilibrium with the ^{3}MCLT state, fast deactivation of the ^{3}MC state is taking place *via* other pathways.

Conclusions

The aim of this study is to compare the photochemical properties of the $[Ru(bpy)_2(pztr)]^+$ **1**, and $[Ru(bpy)_2(pytr)]^+$ **2** and their protonated analogues **1H** and **2H**. Earlier studies have shown that for **1**, **2** and **2H** the LUMO and lowest emissive ^{3}MLCT state is based on the bpy ligands,[11] while for **1H** the LUMO and lowest emissive ^{3}MLCT state is pyrazine based.[14d,e] The purpose of this study is therefore to investigate whether the difference in the location of the LUMO/^{3}MLCT state affects the photolability of the complexes. The deprotonated complexes **1** and **2** are both photostable in acetonitrile and acetone. This is not unexpected since the activation parameters (Table 1) for these compounds indicate the population of the ^{3}MC excited state is not significant. The photochemical behaviour of **1H** and **2H** in CH_3CN is again the same, with ligand loss occurring with the formation of $[Ru(bpy)_2(CH_3CN)_2]^{2+}$ as the final product. Differences are however observed upon photolysis in acetone. As reported earlier photoinduced interconversion of the N2 and N4 isomers of **2H** is observed in CH_2Cl_2, with a steady-state equilibrium of N4 : N2 of 4 : 1. Upon irradiation of **1H** however, it was found that the N4 isomer is photostable while the N2 species isomerises to the N4 species *via* an intermediate. The results obtained therefore indicate that for these compounds the location of the LUMO in **1H** and **2H** does not affect the photolytic behaviour fundamentally. The photostability of the N4 isomer of **1H** is however an important point but is likely to be associated with the thermal stability of the primary photoproduct, *i.e.* the species that contains a monodentate coordinated ligand.

Acknowledgements

SS and JGV thank the Environmental Protection Agency for financial support under grant Nr 2008-ET-MS-3-S2. HMYA thanks the Libyan Government for Financial support. Science Foundation Ireland has contributed to this research under Grant No. 07/SRC/B1160 Advanced Biomimetic Materials for Solar Energy Conversion.

Notes and references

1 (*a*) A. W. Adamson, *J. Phys. Chem.*, 1967, **71**, 798; (*b*) A. W. Adamson, *Adv. Chem. Series, No. 49*, American Chemical Society, Washington, D. C., 1965.
2 L. G. Vanquickenborne and A. Ceulemans, *J. Am. Chem. Soc.*, 1977, **99**, 2208.
3 (*a*) B. O'Regan and M. Grätzel, *Nature*, 1991, **353**, 737; (*b*) A. Hagfeldt and M. Grätzel, *Acc. Chem. Res.*, 2000, **33**, 269.
4 (*a*) A. P. Doherty, M. A. Stanley, D. Leech and J. G. Vos, *Anal. Chim. Acta*, 1996, **319**, 111; (*b*) A. Lobnik, I. Oehme, I. Murkovic and O. S. Wolfbeis, *Anal. Chim. Acta*, 1998, **367**, 159; (*c*) J. N. Demas and B. A. DeGraff, *J. Chem. Educ.*, 1997, **74**, 690.
5 (*a*) J. K. Barton, A. T. Danishefsky and J. M. Goldberg, *J. Am. Chem. Soc.*, 1984, **106**, 2172; (*b*) J. K. Barton, J. M. Goldberg, C. V. Kumar and N. J. Turro, *J. Am. Chem. Soc.*, 1986, **108**, 2081; (*c*) J. M. Kelly, A. B. Tossi, D. J. McConnell and C. OhUigin, *Nucleic Acids Res.*, 1985, **13**, 6017; (*d*) L. Jacquet, J. M. Kelly and A. Kirsch-De Mesmaeker, *J. Chem. Soc., Chem. Commun.*, 1995, 913; (*e*) L. Jacquet, R. J. H. Davies, A. Kirsch-De Mesmaeker and J. M. Kelly, *J. Am. Chem. Soc.*, 1997, **119**, 11763; (*f*) L. M. Wilhelmsson, F. Westerlund, P. Lincoln and B. Norden, *J. Am. Chem. Soc.*, 2002, **124**, 12092.
6 (*a*) V. Balzani, M. Venturi and A. Credi, *Molecular Devices and Machines*, Wiley-VCH, Weinheim, 2003; (*b*) J-P. Sauvage, *Acc. Chem. Res.*, 1998, **31**, 611; (*c*) V. Balzani, *Small*, 2005, **1**, 278; (*d*) P. Mobian, J-M. Kern and J-P Sauvage, *Angew. Chem., Int. Ed.*, 2004, **43**, 2392.
7 S. Rau, D. Walther and J. G. Vos, *Dalton Trans.*, 2007, 915, and references therein.
8 (*a*) H. Takeda, K. Koike, H. Inoue and O. Ishitani, *J. Am. Chem. Soc.*, 2008, **130**, 2023; (*b*) Y. Hayashi, S. Kita, B. S. Brunschwig and E. Fujita, *J. Am. Chem. Soc.*, 2003, **125**, 11976.
9 (*a*) S-C Lo, C. P. Shipley, R. N. Bera, R. E. Harding, A. R. Cowley, P. L. Burn and I. D. W. Samuel, *Chem. Mater.*, 2006, **18**, 5119; (*b*) E. Orselli, G. S. Kottas, A. E. Konradsson, P. Coppo, R. Fröhlich, L. De Cola, A. van Dijken, M. Büchel and H. Börner, *Inorg. Chem.*, 2007, **46**, 11082; (*c*) M. Felici, P. Contreras-Carballada, Y. Vida, J. M. M. Smits, R. J. M. Nolte, L. De Cola, R. N. Williams and M. C. Feiters, *Chem.–Eur. J.*, 2009, **15**, 13124; (*d*) C-H. Yang, S-W. Li. Y Chi, Y-M. Cheng, Y-S. Yeh, P-T. Chou, G-H. Lee, C-H. Wang and C-F. Shu, *Inorg. Chem.*, 2005, **44**, 7770.
10 (*a*) W. M. Walcholtz, R. A. Auerback, R. H. Schmehl, M. Ollino and W. R. Cherry, *Inorg. Chem.*, 1985, **24**, 1758; (*b*) G. H. Allen, R. P. White, D. P. Rillema and T. J. Meyer, *J. Am. Chem. Soc.*, 1984, **106**, 2613; (*c*) F. Barigelletti, A. Juris, V. Balzani, P. Belser and A. von Zelewsky, *Inorg. Chem.*, 1983, **22**, 3335.
11 (*a*) R. Wang, J. G. Vos, R. H. Schmehl and R. Hage, *J. Am. Chem. Soc.*, 1992, **114**, 1964; (*b*) B. E. Buchanan, J. G. Vos, M. Kaneko, W. J. M. Van Der Putten, J. M. Kelly, R. Hage, R. Prins, J. G. Haasnoot, J. Reedijk and R. A. G. de Graaff, *J. Chem. Soc., Dalton Trans.*, 1990, 2425.
12 S. Fanni, F. M. Weldon, L. Hammarström, E. Mukhtar, W. R. Browne, T. E. Keyes and J. G. Vos, *Eur. J. Inorg. Chem.*, 2001, 529.
13 (*a*) B. E. Buchanan, H. Hughes, J. van Diemen, R. Hage, J. G. Haasnoot, J. Reedijk and J. G. Vos, *J. Chem. Soc., Chem. Commun.*, 1991, 300; (*b*) B. E. Buchanan, H. Hughes, P. Degn, J. M. Pavon Velasco, B. S. Creaven, C. Long, J. G. Vos, R. A. Howie, R. Hage, J. H. van Diemen, J. G. Haasnoot and J. Reedijk, *J. Chem. Soc., Dalton Trans.*, 1992, 1177.
14 (*a*) H. P. Hughes and J. G. Vos, *Inorg. Chem.*, 1995, **34**, 4001; (*b*) H. E. B. Lempers, J. G. Haasnoot, J. Reedijk, R. Hage, F. M. Weldon and J. G. Vos, *Inorg. Chim. Acta*, 1994, **225**, 67; (*c*) R. Hage, H. E. B. Lempers, J. G. Haasnoot, J. Reedijk, F. M. Weldon and J. G. Vos, *Inorg. Chem.*, 1997, **36**, 3139; (*d*) T. E. Keyes, C. M. O'Connor and J. G. Vos, *Chem. Commun.*, 1998, 889; (*e*) T. E. Keyes, C. M. O'Connor, U. O'Dwyer, C. C. Coates, P. Callaghan, J. J. McGarvey and J. G. Vos, *J. Phys. Chem. A*, 1999, **103**, 8915.
15 (*a*) H. A. Nieuwenhuis, J. G. Haasnoot, R. Hage, J. Reedijk, T. L. Snoeck, D. J. Stufkens and J. G Vos, *Inorg. Chem.*, 1991, **30**, 48; (*b*) R. Hage, J. G. Haasnoot, J. Reedijk, R. Wang and J. G. Vos, *Inorg. Chem.*, 1991, **30**, 3263; (*c*) R. Hage, J. G. Haasnoot, H. A. Nieuwenhuis, J. Reedijk, R. Wang and J. G. Vos, *J. Chem. Soc., Dalton Trans.*, 1991, 3271; (*d*) C. G. Coates, T. E. Keyes, H. P. Hughes, P. M. Jayaweera, J. J. McGarvey and J. G Vos, *J. Phys. Chem. A*, 1998, **102**, 5013; (*e*) W. R. Browne, N. M. O'Boyle, W. Henry, A. L. Guckian, S. Horn, T. Fett, C. M. O'Connor, M. Duati, L. De Cola, C. G. Coates, K. L.

Ronayne, J. J. McGarvey and J. G. Vos, *J. Am. Chem. Soc.*, 2005, **127**, 1229.
16 B. E. Buchanan, R. Wang, J. G. Vos, R. Hage, J. G. Haasnoot and J. Reedijk, *Inorg. Chem.*, 1990, **29**, 3263.
17 (*a*) B. P. Sullivan and T. J. Meyer, *Inorg. Chem.*, 1982, **21**, 1037; (*b*) B. Durham, S. R. Wilson, D. J. Hodgson and T. J. Meyer, *J. Am. Chem. Soc.*, 1980, **102**, 600; (*c*) B. Durham, J. V. Caspar, J. K Nagle and T. J. Meyer, *J. Am. Chem. Soc.*, 1982, **104**, 4803; (*d*) B. Durham, J. L. Walsh, C. L. Carter and T. J. Meyer, *Inorg. Chem.*, 1980, **19**, 860.
18 (*a*) T. J. Meyer, *Pure Appl. Chem.*, 1986, **58**, 1193; (*b*) Y. Kawanishi, N. Kitamura and S. Tazuke, *Inorg. Chem.*, 1989, **28**, 2968; (*c*) E. M. Kober and T. J. Meyer, *Inorg. Chem.*, 1982, **21**, 3967.
19 W. F. Wacholtz, R. A. Auerbach and R. H. Schmehl, *Inorg. Chem.*, 1986, **25**, 227.

Inorganic Chemistry
Article

Inorg. Chem. **2010**, *49*, 2799–2807 **2799**
DOI: 10.1021/ic902140t

Excited State Localization and Internuclear Interactions in Asymmetric Ruthenium(II) and Osmium(II) bpy/tpy Based Dinuclear Compounds

Yvonne Halpin,[†] Danilo Dini,[†] Hamid M. Younis Ahmed,[†] Lynda Cassidy,[†] Wesley R. Browne,[‡] and Johannes G. Vos*[,†]

[†]*Solar Energy Conversion SRC, School of Chemical Sciences, Dublin City University, Dublin 9, Ireland, and* [‡]*Center for Systems Chemistry, Stratingh Institute for Chemistry and Zernike Institute for Advanced Materials, Faculty of Mathematics and Natural Sciences, University of Groningen, Nijenborgh 4, 9747AG Groningen, The Netherlands*

Received October 28, 2009

The synthesis of two asymmetric dinuclear complexes with the formula $[M(bpy)_2(bpt)Ru(tpy)Cl]^{2+}$, where M = Ru (**1a**), Os(**2a**); bpy = 2,2′-bipyridyl; Hbpt = 3,5-bis(pyridin-2-yl)1,2,4-triazole and tpy = 2,2′,6′,2″-terpyridine, is reported. The compounds obtained are characterized by mass spectrometry, ^{1}H NMR, UV/vis/NIR absorption, luminescence, and resonance Raman spectroscopy. Deuterium isotope labeling facilitates assignment of the ^{1}H NMR and resonance Raman spectra. The interaction between the two metal centers, mediated by the bridging 1,2,4-triazolato moiety in the mixed valent state, is assigned as type II based on the observation of metal to metal charge transfer absorption bands at 7090 and 5990 cm^{-1} for **1a** and **2a**, respectively. The extent of localization of the emissive excited state was determined by transient resonance Raman and emission spectroscopy. Both **1a** and **2a** show phosphorescence at the same wavelengths; however, whereas for compound **1a** the emission is based on the Ru(tpy)Cl- center, for **2a** the emissive state is localized on the $Os(bpy)_2$- unit. This indicates that also in the excited state there is efficient interaction between the two metal centers.

Introduction

The remarkable combination of spectroscopic and electrochemical properties of ruthenium and osmium based polypyridyl complexes,[1,2] which can be tuned in a predictable manner synthetically and by electrochemical oxidation or reduction, has led to their widespread application to molecular machines,[3] dye-sensitized solar cells,[4] electro- and optical sensors,[5] chemiluminescent devices[6] and electrochromic displays,[7] and have proven invaluable in the development of nonlinear optics,[8] artificial photosynthesis,[9] and molecular electronics.[10] Multinuclear metal polypyridyl complexes are of particular interest in regard to transfer either electronic charge or excitation from one site of coordination to the other via π-delocalized bridging ligands manifested in near-infrared (NIR) absorptions.[11] In principle, such intramolecular charge transfer in binuclear complexes can be exploited

*To whom correspondence should be addressed. E-mail: han.vos@dcu.ie. Fax: 00353 1 700 5503. Phone: 00353 1 700 5307.

(1) (a) Juris, A.; Balzani, V.; Barigelletti, F.; Campagna, S.; Belser, P.; von Zelewsky, A. *Coord. Chem. Rev.* **1988**, *84*, 85–277. (b) Lytle, F. E.; Hercules, D. M. *J. Am. Chem. Soc.* **1969**, *91*, 253–257.

(2) Vos, J. G.; Kelly, J. M. *Dalton Trans.* **2006**, 4869–4883.

(3) (a) Balzani, V.; Bergamini, G.; Ceroni, P. *Coord. Chem. Rev.* **2008**, *252*, 2456–2469. (b) Balzani, V.; Bergamini, G.; Marchioni, F.; Ceroni, P. *Coord. Chem. Rev.* **2006**, *250*, 1254–1266.

(4) (a) O'Regan, B.; Grätzel, M. *Nature* **1991**, *353*, 737–740. (b) Hagfeldt, A.; Grätzel, M. *Acc. Chem. Res.* **2000**, *33*, 269–277.

(5) (a) Rajagopolan, C. R.; Aoki, A.; Heller, A. *J. Phys. Chem.* **1996**, *100*, 3719–27. (b) Doherty, A. P.; Stanley, M. A.; Leech, D.; Vos, J. G. *Anal. Chim. Acta* **1996**, *319*, 111–120. (c) Doherty, A. P.; Vos, J. G. *J. Chem. Soc., Faraday Trans.* **1992**, *88*, 2903–2907. (d) Demas, J. N.; DeGraff, B. A. *Anal. Chem.* **1991**, *63*, 829A–837A. (e) Lippitsch, M. E.; Pusterhofer, J.; Leiner, M. J. P.; Wolfbeis, O. S. *Anal. Chim. Acta* **1988**, *205*, 1–6. (f) Demas, J. N; DeGraff, B. A. *Chem. Educ.* **1997**, *74*, 690–695. (g) Malins, C.; Fanni, S.; Glever, H. G.; Vos, J. G.; MacCraith, B. D. *Anal. Commun.* **1999**, *36*, 3–4.

(6) (a) Chen, C. H.; Shi, J. M. *Coord. Chem. Rev.* **1998**, *171*, 161–174. (b) Armstrong, N. R.; Wightman, R. M.; Gross, E. M. *Annu. Rev. Phys. Chem.* **2001**, *52*, 391–422.

(7) (a) Marcaccio, M.; Paolucci, F.; Paradisi, C.; Roffia, S.; Fontanesi, C.; Yellowlees, L. J.; Serroni, S.; Campagna, S.; Denti, G.; Balzani, V. *J. Am. Chem. Soc.* **1999**, *121*, 10081–91. (b) Stagni, S.; Palazzi, A.; Zacchini, S.; Ballarin, B.; Bruno, C.; Marcaccio, M.; Paolucci, F.; Monari, M.; Carano, M.; Bard, A. J. *Inorg. Chem.* **2006**, *45*, 695–709. (c) Marcaccio, M.; Paolucci, F.; Paradisi, C.; Carano, M.; Roffia, S.; Fontanesi, C.; Yellowlees, L. J.; Serroni, S.; Campagna, S.; Balzani, V. *J. Electroanal. Chem.* **2002**, *532*, 99–112. (d) Roffia, S.; Casadei, R.; Paolucci, F.; Paradisi, C.; Bignozzi, C. A.; Scandola, F. *J. Electroanal. Chem.* **1991**, *302*, 157–171.

(8) (a) Feuvrie, C.; Maury, O.; Le Bozec, H.; Ledoux, I.; Morrall, J. P.; Dalton, G. T.; Samoc, M.; Humphrey, M. G. *J. Phys. Chem. A* **2007**, *111*, 8980–8985. (b) Girardot, C.; Cao, B.; Mulatier, J. C.; Baldeck, P. L.; Chauvin, J.; Riehl, D.; Delaire, J. A.; Andraud, C.; Lemercier, G. *ChemPhysChem* **2008**, *9*, 1531–1535. (c) Maury, O.; Le Bozec, H. *Acc. Chem. Res.* **2005**, *38*, 691–704.

(9) Sun, L.; Hammarström, L.; Åkermark, B.; Styring, S. *Chem. Soc. Rev.* **2001**, *30*, 36–49.

(10) Albrecht, T.; Moth-Poulsen, K.; Christensen, J. B.; Guckian, A.; Bjornholm, T.; Vos, J. G.; Ulstrup, J. *Faraday Discuss.* **2006**, *13*, 265-279 and references therein.

(11) Balzani, V.; Juris, A.; Venturi, A.; Campagna, S.; Serroni, S. *Chem. Rev.* **1996**, *96*, 759–833.

Published on Web 02/08/2010

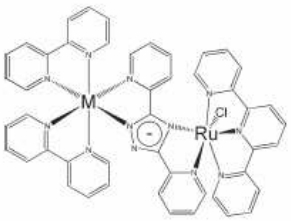

Figure 1. Structure of dinuclear complexes **1a** (M = Ru) and **2a** (M = Os).

for the realization of miniaturized sub-nanoscale devices where electrons or photons dispatch "information" between specific sites within distances of the order of a few angstroms.[12] A key challenge therefore is to be able to control not only the strength of the interaction between the two metal centers in both the ground and the excited state but also the direction. This can be achieved through the structural modification of the bridging ligand and the variation of the nature of the coordinating metal centers. In this regard dinuclear complexes bridged by negatively charged 1,2,4-triazolato moieties including homonuclear and heteronuclear 2,2′-bipyridyl based Ru(II) and Os(II) complexes[13−20] as well as cyclometalated complexes based on Rh and Ir[21] have been investigated by our group over recent years, in particular with respect to the ground state and excited state intercomponent interaction.

Here we report the synthesis and characterization of two binuclear complexes of ruthenium and osmium, containing both bpy (2,2′-bipyridine) and tpy (2,6-bis(pyridin-2′-yl)-pyridine) as peripheral ligands of the general formula $[(bpy)_2M(bpt)Ru(tpy)Cl]^{2+}$ where M = Ru (**1a**) and Os (**2a**) (Figure 1). In compounds **1a** and **2a** the bridging ligand 3,5-bis(pyridin-2′-yl)-1,2,4-triazolato (bpt) is negatively charged. In contrast to related pseudo-symmetric systems,[13,14] in **1a** and **2a** the non-bridging polypyridyl ligands at each center are geometrically and photophysically distinct, that is, $(bpy)_2$ versus (tpy)Cl. The extent and directionality of the interaction between the triazolato bridged metal centers is found to be highly dependent on the nature of the metal center. The corresponding deuterated isotopologues $[(d_8\text{-bpy})_2M(bpt)Ru(tpy)Cl]^{2+}$ [M = Ru (**1b**), Os (**2b**)] were prepared to facilitate assignment of the chemical shifts of the protons in the bridging bpt- ligand and tpy peripheral ligand as well as the vibrational and electronic spectroscopic features. The results obtained show that in these systems the location of the lowest emissive excited state and the first oxidation can be switched by judicious choice of the metal centers. Importantly this can be done with only minimal perturbation of the photophysical properties including electronic absorption and emission spectra.

Experimental Section

Materials. All solvents employed in spectroscopic measurements were of spectroscopic grade (Sigma-Aldrich). All other solvents were of HPLC grade or better, *cis*-$Ru(bpy)_2Cl_2\cdot 2H_2O$,[22] $Ru(d_8\text{-bpy})_2Cl_2\cdot 2H_2O$, $Os(bpy)_2Cl_2$[23] and $Ru(tpy)Cl_3$,[24] d_8-bpy[25] and 3,5-bis(pyridin-2-yl)-1,2,4-triazole (Hbpt)[26] were prepared by reported procedures. Gold colloid for SERS measurements was prepared by standard methods.[27]

The syntheses of the mononuclear complexes were as reported in the literature.[13]

$[Ru(bpy)_2(bpt)](PF_6)\cdot 1/2H_2O$: Yield: 92 mg (0.12 mmol), 51%, ^{1}H NMR (CD_3CN, 298 K) δ/ppm: 8.53 (1H, d), 8.43 (4H, m), 8.15 (1H, d), 7.92 (8H, m), 7.90 (1H, d), 7.83 (1H, dd), 7.75 (1H, dd), 7.52 (1H, d), 7.37 (4H,m), 7.23 (1H, dd), 7.14 (1H, dd). Elemental analysis for $C_{32}H_{24}N_9RuPF_6\cdot 1/2H_2O$: Calcd: C 48.7%, H 3.17%, N 15.96%. Found: C 48.4%, H 3.22%, N 15.91%.

$[Ru(d_8\text{-bpy})_2(bpt)](PF_6)\cdot 1/2H_2O$: Yield: 55 mg (0.06 mmol), 31%, ^{1}H NMR (CD_3CN, 298 K) δ/ppm: 8.50 (1H, d), 8.15 (1H, d), 8.01 (1H, d), 7.90 (1H, t), 7.70 (1H, t), 7.55 (1H, d), 7.20 (1H, t), 7.15 (1H, t). Elemental analysis for $C_{32}H_8D_{16}N_9RuPF_6\cdot 1/2H_2O$: Calcd: C 47.7%, H 3.10%, N 15.65%. Found: C 48.4%, H 2.97%, N 15.49%.

$[Os(bpy)_2(bpt)](PF_6)\cdot 2H_2O$. 82 mg (0.09 mmol), 43%, ^{1}H NMR (CD_3CN, 298 K) δ/ppm: 8.55 (1H, d), 8.43 (4H, m), 8.18 (1H,d), 7.92 (8H, m), 7.95 (1H, d), 7.88 (1H, dd), 7.65 (1H, dd), 7.40 (1H, d), 7.15 (1H, dd), 7.37 (4H, m), 7.05 (1H, dd). Elemental Analysis for $C_{32}H_{24}N_9OsPF_6\cdot 2H_2O$: Calcd: C 42.4%, H 3.09%, N 13.92%. Found: C 42.9%, H 3.08%, N 13.80%.

$[Os(d_8\text{-bpy})_2(bpt)](PF_6)\cdot 2H_2O$. Yield: 16 mg (0.02 mmol), 9%, ^{1}H NMR (CD_3CN, 298 K) δ/ppm: 8.55 (1H, d), 8.15 (1H, d), 8.01 (1H, d), 7.75 (1H, dd), 7.72 (1H, d), 7.42 (1H), 7.25 (1H, dd), 7.15 (1H, dd). Elemental analysis for $C_{32}H_8D_{16}N_9OsPF_6\cdot 2H_2O$: Calcd: C 41.7%, H 3.04%, N 13.68%. Found: C 41.6%, H 2.95%, N 13.62%.

$Ru(tpy)Cl_3$. A 981 mg portion (4.1 mmol) of $RuCl_3\cdot 2H_2O$ was dissolved in 150 cm^3 of ethanol, the solution was refluxed and 1 equiv of 2,2′;6′,2″ terpyridine (tpy), dissolved in 20 cm^3 of ethanol, were dropped in the reaction bulk. The reaction mixture was heated for 2 h and filtered hot. A dark solid was collected and washed with ethanol, water, and diethyl ether. Yield: 681 mg (1.6 mmol), 80%.

Synthesis of Dinuclear Complexes. $[Ru(bpy)_2(bpt)Ru(tpy)Cl](PF_6)_2\cdot 2H_2O$ (1a). $Ru(tpy)Cl_3$ (100 mg, 0.13 mmol) was dissolved in 10 cm^3 ethanol/water (1:1 v/v). $[Ru(bpy)_2(bpt)]PF_6\cdot 1/2H_2O$ (119 mg, 0.13 mmol) was added, and the mixture was left to heat at reflux for 8 h. The reaction was cooled to room

(12) (a) D'Alessandro, D. M.; Keene, F. R. *Pure Appl. Chem.* **2008**, *80*, 1–16. (b) D'Alessandro, D. M.; Keene, F. R. *Chem. Rev.* **2006**, *106*, 2270–2298. (c) Launay, J. P. *Chem. Soc. Rev.* **2001**, *30*, 386–397.
(13) Hage, R.; Dijkhuis, A. H. J.; Haasnoot, J. G.; Prins, R.; Reedijk, J.; Buchanan, B. E.; Vos, J. G. *Inorg. Chem.* **1988**, *27*, 2185–2189.
(14) Hage, R.; Haasnoot, J. G.; Nieuwenhuis, H. A.; Reedijk, J.; De Ridder, D. J. A.; Vos, J. G. *J. Am. Chem. Soc.* **1990**, *112*, 9245–9251.
(15) De Cola, L.; Barigelletti, F.; Balzani, V.; Hage, R.; Haasnoot, J. G.; Reedijk, J.; Vos, J. G. *Chem. Phys. Lett.* **1991**, *178*, 491–496.
(16) Di Pietro, C.; Serroni, S.; Campagna, S.; Gandolfi, T.; Ballardini, R.; Fanni, S.; Browne, W. R.; Vos, J. G. *Inorg. Chem.* **2002**, *41*, 2871–2878.
(17) Browne, W. R.; Weldon, F.; Guckian, A.; Vos, J. G. *Collect. Czech. Chem. Commun.* **2003**, *68*, 1467–1486.
(18) Weldon, F.; Hammarström, L.; Mukhtar, E.; Hage, R.; Gunneweg, E.; Haasnoot, J. G.; Reedijk, J.; Browne, W. R.; Guckian, A. L.; Vos, J. G. *Inorg. Chem.* **2004**, *43*, 4471–4481.
(19) Hage, R.; Haasnoot, J. G.; Reedijk, J.; Wang, R.; Vos, J. G. *Inorg. Chem.* **1991**, *30*, 3263–3269.
(20) Hage, R.; Lempers, H. E. B.; Haasnoot, J. G.; Reedijk, J.; Weldon, F. M.; Vos, J. G. *Inorg. Chem.* **1997**, *36*, 3139–3145.
(21) (a) Van Diemen, J. H.; Haasnoot, J. G.; Hage, R.; Reedijk, J.; Vos, J. G.; Wang, R. *Inorg. Chem.* **1991**, *30*, 4038–4043. (b) Van Diemen, J. H.; Hage, R.; Haasnoot, J. G.; Lempers, H. E. B.; Reedijk, J.; Vos, J. G.; De Cola, L.; Barigelletti, F.; Balzani, V. *Inorg. Chem.* **1992**, *31*, 3518–3522.
(22) Sullivan, B. P.; Salmon, D. J.; Meyer, T. J. *Inorg. Chem.* **1978**, *17*, 3334–3341.
(23) Lay, P. A.; Sargeson, A. M.; Taube, H.; Chou, M. H.; Creutz, C. *Inorg. Synth.* **1986**, *24*, 291–299.
(24) Constable, E. C.; Thompson, A. M. W. C.; Tocher, D. A.; Daniels, M. A. M. *New J. Chem.* **1992**, *16*, 855–867.
(25) Browne, W. R.; O'Connor, C. M.; Killeen, J. S.; Guckian, A. L.; Burke, M.; James, P.; Burke, M.; Vos, J. G. *Inorg. Chem.* **2002**, *41*, 4245–4251.
(26) Geldard., J. F.; Lions, F. *J. Org. Chem.* **1965**, *30*, 318–319.
(27) Lee, P. C.; Meisel, D. *J. Phys. Chem.* **1982**, *86*, 3391–3395.

temperature and evaporated to dryness after which 10 cm^3 water was added, followed by precipitation of the product by the addition of aqueous NH_4PF_6. The product was isolated by filtration, washed with water and diethyl ether, and dried under vacuum. **1a** was isolated by column chromatography (stationary phase silica, mobile phase 80:20, acetonitrile:water, 0.05 M KNO_3). The compound was obtained after precipitation with aqueous NH_4PF_6 and subsequent recrystallization from acetone/water 1:1. Yield: 40 mg (0.04 mmol), 33%. ^{1}H NMR (CD_3CN, 298 K) δ/ppm: 10.08 [1H, d, H6(B)], 8.75 [1H, d, H3(B)], 8.70 [1H, d, H3′], 8.65 [5H, md, H3(1), H3′(1), H3(2), H3′(2), H3″], 8.47 [1H, d, H3], 8.20 [3H, m, H4′, H5′, H4(B)], 7.99 [3H, m, H4″, H6″, H4], 7.92 [2H, t, H4(1), H4′(2)], 7.72−7.81 [4H, md, H4(2), H4′(1), H5(B), H6], 7.60 [1H, t, H5″], 7.56 [1H, d, H6(A)], 7.51 [1H, d, H6(1)], 7.23−7.37 [5H, dm, H6′(2), H6′(1), H6(2), H5, H4(A)], 7.08−7.19 [4H, m, H5(1), H5′(1), H5(2), H5′(2)], 7.02 [1H, t, H5(A)], 6.47 [1H, d, H3(A)]. MS. Found: 502.5 (M^{2+}); Calcd: 502. Elemental Analysis for $Ru_2C_{47}H_{35}N_{12}ClP_2F_{12}\cdot 2H_2O$: Calcd: C 42.4%, H 2.93%, N 12.62%. Found: C 42.4%, H 2.95%, N 12.53%.

[Ru(d$_8$-bpy)$_2$(bpt)Ru(tpy)Cl](PF$_6$)$_2\cdot$ 2H$_2$O (1b). Yield: 15 mg (0.01 mmol), 11.5%. ^{1}H NMR (CD_3CN, 298 K) δ/ppm: 10.05 [1H, d, H6(B)], 8.78 [1H, d, H3(B)], 8.67 [1H, d, H3′], 8.58 [1H, d, H3″], 8.45 [1H, d, H3], 8.15 [3H, m, H4′, H5′, H4(B)], 7.95 [3H, m, H4″, H6″, H4], 7.79 [1H, m, H5(B)], 7.72 (1H, d, H6), 7.58 [1H, t, H5″], 7.53 [1H, d, H6(A)], 7.24 [2H, m, H5, H4(A)], 6.96 [1H, t, H5(A)], 6.43 [1H, d, H3(A)]. MS. Found 510 (M^{2+}); Calcd: 510. Elemental analysis for $Ru_2C_{47}H_{19}D_{16}N_{12}ClP_2F_{12}\cdot 2H_2O$: Calcd: C 41.9%, H 2.89%, N 12.47%, Found: C 41.8%, H 2.97%, N 12.33%.

[Os(bpy)$_2$(bpt)Ru(tpy)Cl](PF$_6$)$_2\cdot$H$_2$O (2a). Yield: 10 mg (0.01 mmol), 8%. ^{1}H NMR in CD_3CN at 298 K, δ/ppm: 10.01 [1H, d, H6(B)], 8.69 [1H, d, H3(B)], 8.52 [1H, d, H3′], 8.37−8.45 [5H, md, H3(1), H3′(1), H3(2), H3′(2), H3″], 8.27−8.35 [1H, d, H3], 8.15−8.25 [2H, m, H4′, H5′], 8.08−8.15 [1H, t, H4(B)], 8.00−8.07 [2H, m, H4(1), H4′(2)], 7.80−7.99 [5H, m, H4′(1), H4(2), H4″, H6″, H4], 7.65−7.80 [2H, m, H5(B), H6(1)], 7.58−7.65 [1H, d, H6], 7.45−7.52 [1H, t, H5″], 7.40−7.45 [1H, d, H6(A)], 7.26−7.37 [4H, m, H6(2), H6′(1), H5(1), H4(A)], 7.15−7.24 [2H, m, H6′(2), H5′(2)], 7.01−7.22 [3H, t, H5, H5′(1), H5(2)], 7.00−7.05 [1H, t, H5(A)], 6.35−6.46 [1H, d, H3(A)]. MS. Found: 548.2 (M^{2+}); Calcd: 548. Elemental analysis for $OsRuC_{47}H_{35}N_{12}ClP_2F_{12}\cdot H_2O$: Calcd: C 40.2%, H 2.64%, N 11.98%. Found: C 40.5%, H 2.75%, N 12.01%.

[Os(d$_8$-bpy)$_2$(bpt)Ru(tpy)Cl](PF$_6$)$_2\cdot$H$_2$O (2b). As above for **1a**. Yield: 46 mg (0.04 mmol), 34%. ^{1}H NMR in CD_3CN at 298 K, δ/ppm: 10.09 [1H, d, H6(B)], 8.56−8.63 [1H, d, H3(B)], 8.50−8.55 [1H, d, H3′], 8.38−8.44 [1H, d, H3″], 8.27−8.37 [1H, d, H3], 8.15−8.23 [2H, m, H4′, H5′], 8.06−8.13 [1H, t, H4(B)], 7.86−7.95 [3H, m, H4″, H6″, H4], 7.78−7.85 [1H, t, H5(B)], 7.60−7.68 [1H, d, H6], 7.47−7.52 [1H, t, H5″], 7.37−7.46 [1H, d, H6(A)], 7.25−7.36 [1H, t, H4(A)], 7.15−7.23 [1H, t, H5], 6.95−7.05 [1H, t, H5(A)], 6.4 [1H, d, H3(A)]. MS. Found 556.2 (M^{2+}); Calcd: 556. Elemental analysis for $OsRuC_{47}H_{19}D_{16}N_{12}ClP_2F_{12}\cdot H_2O$: Calcd: C 39.8%, H 2.61%, N 11.85%. Found: C 39.7%, H 2.66%, N 11.77%.

Instrumental Methods. ^{1}H NMR spectra were recorded on a Bruker Advance 400 MHz NMR spectrometer. All measurements were carried out in $CDCl_3$ for ligands and in d_3-acetonitrile for complexes. Data are relative to residual solvent. UV/vis absorption spectra were recorded on a JASCO 570 UV/vis/NIR or a JASCO 600 UV/vis spectrophotometer using a 1 cm path length quartz cells. Absorption maxima are ± 2 nm: molar absorptivities are ± 10%. Emission spectra were recorded at 298 K in 10 mm path length cells on a JASCO-7200 spectrofluorimeter equipped with a red sensitive Hamamatsu R928 detector. The excitation source is corrected between 200 and 600 nm. Emission spectra are not corrected for detector response. The emission lifetimes were determined by means of a Time Correlated Single Photon Counter using an Edinburgh Instruments nf900 ns flashlamp and CD900 TAC. Solvent was Uvasol grade acetonitrile. Emission lifetimes (±5%) were calculated using a single exponential fitting function. Mass spectra were recorded on a Bruker-EsquireLC_00050 mass spectrometer using electrospray ionization with positive polarity and a cap-exit voltage of 167 V. Spectra were recorded in the scan range of 50−2200 m/z with an acquisition time of between 300 and 900 μs and a potential of between 30 and 70 V. Each spectrum was recorded by the summation of 20 scans. Electrochemical measurements were carried out with analyte concentrations of typically 0.5−1.0 mM in anhydrous CH_3CN with 0.1 M tetrabutylammonium hexafluorophosphate ($TBAPF_6$) using a CH Instruments Version 6.24 software controlled potentiostat (CHI 750C). A glassy carbon electrode, Pt wire and saturated calomel electrode (SCE) were used as working, counter and reference electrodes, respectively. Prior to each experiment the solutions were deoxygenated with argon and a blanket of argon was maintained during analysis. Spectroelectrochemistry was carried out in both UV/vis and NIR regions using a model 760c potentiostat (CH Instruments). Platinum gauze working electrode (Aldrich), Pt wire auxiliary electrode, and an SCE were used as the working, counter and reference electrodes, respectively. A custom-made 2 mm path length 1.2 mL volume quartz cuvette was employed for all spectroelectrochemical measurements. UV/vis/NIR spectra were recorded on a JASCO 570 UV/vis/NIR spectrophotometer.

Raman spectra were obtained with excitation at 400.8 (50 mW at source, PowerTechnology), 449 nm (35 mW at source, PowerTechnology), 473 (100 mW at source, Cobolt Lasers), 532 nm (300 mW at source, Cobolt Lasers), 561 nm (100 mW at source, Cobolt Lasers), and 355 nm (10 Hz 3 mJ per pulse, Spitlight 200, Innolas) to the sample through a 5 cm diameter plano convex lens (f = 6 cm) and Raman scattering collected in a 180° backscattering arrangement. The collimated Raman scattering was focused by a second 5 cm diameter plano-convex lens (f = 6 cm) through an appropriate long pass edge filter (Semrock) into a Shamrock300 spectrograph (Andor Technology) with a 1200 L/mm grating blazed at 500 nm and collected by a Newton EMCCD (Andor Technology) operating in conventional ccd mode. Data were recorded and processed using Solis (Andor Technology) with spectral calibration performed using the Raman spectrum of acetonitrile/toluene 50:50 (v:v). Samples were held in quartz 10 mm path length cuvettes.

Analytical High Performance Liquid Chromatography (HPLC) experiments were carried out using an analytical HPLC system consisting of a Varian Prostar HPLC pump fitted with a 20 μL injection loop, a Varian Prostar PDA detector connected to a dedicated PC, and a HiChrom Partisil P10SCX-3095 cation exchange column. The mobile phase used was acetonitrile:water 80:20 (v:v) containing 0.01−0.08 M $LiClO_4$; the flow rate was 2.0 cm^3/min. The monitoring wavelength used was 280 nm. Photostability of complexes **1a**/**2a** was monitored by HPLC. Samples were irradiated at 470 nm with a 9 W LED-array.

Results and Discussion

Synthesis. The dinuclear complexes **1a**/**1b** and **2a**/**2b** were prepared by addition of the soluble mononuclear complexes $[Ru(bpy)_2(bpt)]^+$/$[Ru(d_8\text{-}bpy)_2(bpt)]^+$ and $[Os(bpy)_2(bpt)]^+$/$[Os(d_8\text{-}bpy)_2(bpt)]^+$, respectively, to a solution containing the mononuclear complex Ru(tpy)Cl_3 in EtOH/H_2O followed by heating at reflux and isolation by chromatography.

^{1}H NMR Spectroscopy. The ^{1}H NMR spectroscopic and mass spectral data for the mononuclear complexes are in agreement with previous reports.[13] For the dinuclear complexes the availability of **1b** and **2b** allow for analysis of the proton chemical shifts in bpt$^-$ and tpy

Table 1. Spectroscopic and Electrochemical Data for Complexes **1a** and **2a** and Related Analogues[a]

	absorption λ_{max} /nm (ε/10^4 M^{-1} cm^{-1})	emission[a] λ_{max} /nm	τ/ns[a]	V vs SCE [ΔEp /mV]
1a	428 (0.95), 467 (1.55), 520 (sh)	757	58	0.72 [65], 1.19 [60]
2a	488 (0.69), 608 (0.40)	768	13	0.65 [65], 0.86 [60]
$[Ru(bpy)_2(bpt)]^{+}$ [b,c]	475 (1.13)	678	160	0.85
$[Os(bpy)_2(bpt)]^{+}$ [c,d]	486 (1.08), 610 (0.28)	762	55	0.49
$[Ru(tpy)(phen)Cl]^{+}$ [e]	380, 439(0.60), 502(0.93)	710		0.78
$[Ru(bpy)_2(bpt)Ru(bpy)_2]^{3+}$ [b,c]	453 (2.26)	648	100	1.04, 1.34
$[Os(bpy)_2(bpt)Os(bpy)_2]^{3+}$ [d]	460 (1.82), 475 (1.82), 600 (0.44)	756	30	0.64, 0.85
$[Os(bpy)_2(bpt)Ru(bpy)_2]^{3+}$ [d]	453 (2.37), 580 (sh), 670 (sh)	762	25	0.65, 1.30

[a] Solutions purged with Ar at 298 K. [b] From ref 13. [c] From ref 15. [d] From ref 14. [e] From ref 30.

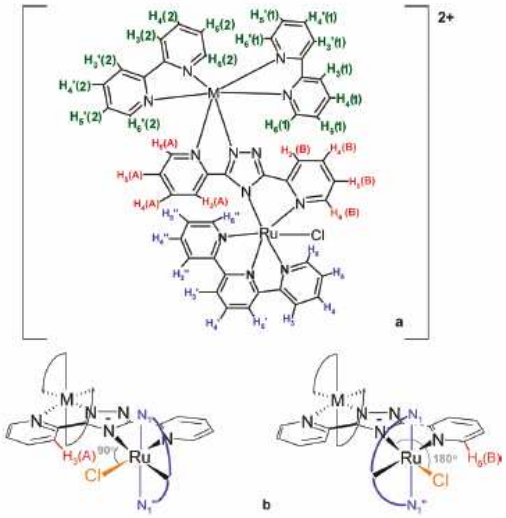

Figure 2. Numbering scheme used for the protons (a) and the structures of the two possible isomers (b) for the dinuclear complexes **1a** and **2a**. The proximity of the chlorido ligand to H3(A) and H6(B), respectively, used to identify the structure of the isolated complexes. Blue lines indicate the tpy ligand.

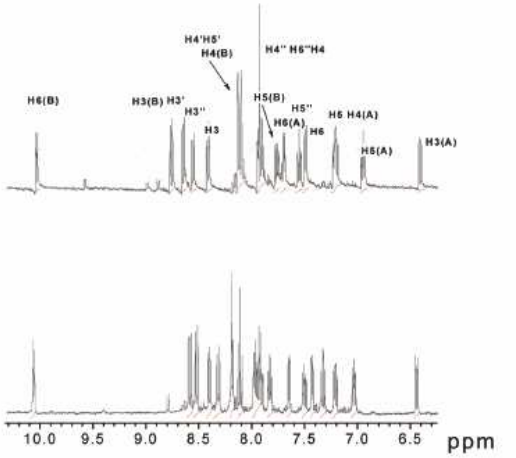

Figure 3. ^{1}H NMR spectra of (upper) $[Ru(d_8\text{-}bpy)_2(bpt)Ru(tpy)Cl]^{2+}$ **1b** and $[Os(d_8\text{-}bpy)_2(bpt)Ru(tpy)Cl]^{2+}$ (lower) **2b**, in CD_3CN.

ligands. The coordination mode of the Ru(tpy)Cl- unit in **1** and **2** can, potentially, be such that the chlorido ligand is trans to either the triazolato or the pyridyl ring of the bpt^- bridging ligand (Figure 2b).

The ^{1}H NMR spectra of **1b** and **2b** are shown in Figure 3. Further ^{1}NMR and COSY spectra are shown in Supporting Information, Figures S1−S3. ^{1}H COSY NMR spectroscopy together with comparison of the chemical shifts with those of related complexes allows for assignment of the absorptions of the bpt and tpy ligands.

From the analysis of the ^{1}H NMR spectra of the isotopologues **1b** and **2b** (Figure 3) it is apparent that only one geometric isomer, where the chlorido ligand is trans to the triazolato ring of the bpt^- ligand, is isolated. This assignment is based on the downfield shifted doublet at about 10.1 ppm with a coupling constant J of 5.6 Hz for both **1b** and **2b** (Figure 3). The chemical shift and the corresponding coupling constant indicate through-space interaction between an H6 type proton of a pyridine ring of the bpt^- and the chlorido ligand. In the case of the chlorido ligand being cis to the triazolato ligand then the H3(A) ligand would be influenced by the chlorido ligand with a chemical shift similar to that observed but with a larger coupling constant (7−9 Hz). Further support for this assignment is the upfield shift of the H3(A) resonance at about 6.40 ppm (J = 8.0 Hz) because of shielding by the ring current of the tpy ligand.

Examination of the resonances of the tpy ligand in complexes **1** and **2** gives additional support for this structural assignment. The protons Hn and Hn″ on the py rings of the tpy ligand are not chemically equivalent in complexes **1** and **2**. This is shown by the fact that the chemical shifts of H3 and H3″, H5 and H5″, and H6 and H6″, are different. This asymmetry indicates that the chlorido ligand is not equidistant to the two pyridyl rings of the tpy ligand, that is, it does not lie in the plane formed from the Ru−N bonds with the pyridyl and triazolato rings of the bpt^- ligand and hence the Ru(tpy)Cl center is in a distorted octahedral geometry.

UV/vis Absorption and Emission Spectroscopy. Electronic absorption and emission data for the mononuclear and dinuclear complexes are listed in Table 1. All complexes exhibit absorption and emission properties that are characteristic of ruthenium(II) and osmium(II) based polypyridyl complexes with triazolato containing bridging ligands.

The absorption spectra for **1a** and **2a** are shown in Figure 4. In the UV region (< 350 nm) the absorptions are assigned to $\pi-\pi^*$ intraligand electronic transitions associated with the bpy, tpy, and bridging triazolato ligands,[1,13] whereas those in the visible region (400−570 nm) are assigned to ^{1}MLCT (metal ligand charge transfer) transitions.[1] The shoulder at about 525 nm is typical for

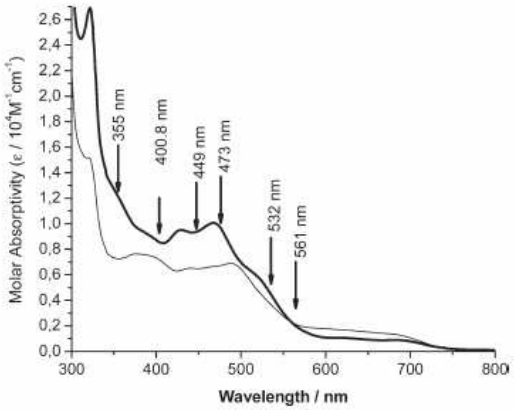

Figure 4. Absorption spectra of **1a** $[Ru(bpy)_2(bpt)Ru(tpy)Cl]^{2+}$ (thin line) and $[Os(bpy)_2(bpt)Ru(tpy)Cl]^{2+}$ **2a** (black line) in CH_3CN. Laser excitation lines used for acquiring Raman spectra are indicated with arrows.

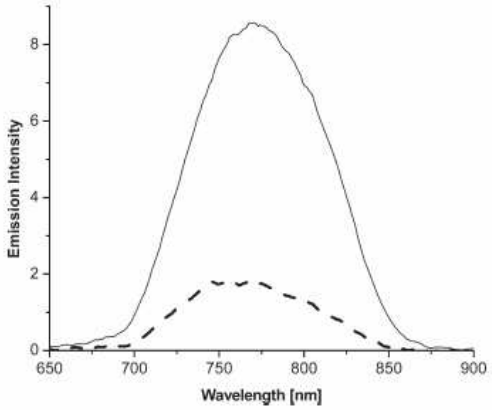

Figure 5. Emission spectra of **1a**$[Ru(bpy)_2(bpt)Ru(tpy)Cl]^{2+}$ (dashed line, λ_{exc} 482 nm) and $[Os(bpy)_2(bpt)Ru(tpy)Cl]^{2+}$ **2a** (solid line λ_{exc} 468 nm) in CH_3CN. The absorbance of the two solutions at the excitation wavelengths were the same. The concentrations were approximately $1-2 \times 10^{-5}$ M.

ruthenium(II)(N5)chlorido complexes.[28] The absorptions >570 nm are assigned to ^{3}MLCT transitions in the case of **2a**; however, for **1a** a significant absorption is observed in this region also, which are reminiscent of the absorption spectrum of $[Ru(tpy)_2]^{2+}$.[29] These assignments are supported by resonance Raman spectroscopy (vide infra).

The emission spectra of both **1a** and **2a** show maxima at 757 and 768 nm, respectively (Figure 5). In both cases the emission energy and lifetime (Table 1) is typical of emission from a ^{3}MLCT excited state, localized either on a bpy or on a tpy ligand. The near coincidence in energy of the emission of the two complexes could suggest that the emission is localized at the same metal center for both complexes, that is, the $[Ru(tpy)Cl]^+$ center. However, the differences in emission lifetimes and intensities indicate otherwise. For **1a**, the emissive ^{3}MLCT state is assigned to be localized on the $[Ru(tpy)Cl]^+$ moiety on the basis that the related complex[13,15] $[Ru(bpy)_2(bpt)Ru(bpy)_2]^{3+}$ has an emission maximum at 648 nm (Table 1). The lifetime of the emission of **1a** is considerably longer (58 ns) than that expected for compounds such as $[Ru(tpy)(phen)Cl]^+$ for which the lifetimes are <1 ns[30] and is closer to that of $[Ru(bpy)_2(bpt)Ru(bpy)_2]^{3+}$ (100 ns);[15] however, the substitution of the bpy ligand of $[Ru(tpy)(bpy)Cl]^+$ with the strongly σ-donating triazolato ligand will raise the energy of the ^{3}MC excited state which is typically the major excited state deactivation channel for ruthenium(II) polypyridyl complexes.[1] In the case of **2a** the shorter lifetime of the emission (13 ns) and the similarity in emission energy to the related complexes[15] $[Os(bpy)_2(bpt)Os(bpy)_2]^{3+}$ and $[Os(bpy)_2(bpt)Ru(bpy)_2]^{3+}$ suggests that the emissive excited state is localized on the $Os(bpy)_2$ moiety. Furthermore, the relatively higher intensity of emission for **2a** over **1a** despite the shorter excited state lifetime (Figure 5) indicates that **2a** has a shorter radiative lifetime in accordance with a switch from a ruthenium(tpy) to an osmium(bpy) centered emission between **1a** and **2a**.

Photostability. Previously it was shown for complexes of the type $[Ru(bpy)_2(L)Cl]^+$ where L = pyridine,[31] 4-vinyl-imidazole[32] and poly-4-vinyl-pyridine,[33] that rapid loss of a chlorido ligand can be observed by photochemical or thermal activation and photoinduced ligand loss has been observed for $[Ru(tpy)(bpy)Cl]^+$ also.[28a] The photostability under visible excitation of **1a** and **2a** in acetonitrile was determined by HPLC. Formation of a main photolysis product is detected only on extended photolysis after 48 and 72 h irradiation for **1a** and **2a**, respectively. This product manifests itself in the appearance of a peak in the HPLC chromatogram at a retention time longer than observed for **1a** and **2a** (see Figures S4 and S5 in Supporting Information), which indicates that the photoproduct is more positively charged. Comparison of the absorption spectra of **1a** and **2a** and the primary photolysis product indicates the loss of the chlorido ligand (see Supporting Information, Figure S6). This indicates that cleavage of the Ru−Cl bond is unlikely to be significant on the time scale of the absorption and Raman spectroscopic studies (vide infra).

Resonance Raman Spectroscopy. Resonance Raman spectra for compounds **1a**/**1b** and **2a**/**2b** were recorded in acetonitrile solution at room temperature upon excitation at 355, 400.8, 449, 473, 532, and 561 nm (see Figure 4 for absorption spectra). Isotopic labeling indicates that between 400 and 473 nm the Raman spectra are dominated by resonance enhanced bands from vibrational modes of the bpy (Figure 6). At 532 nm, the Raman spectrum shows contributions from vibrational modes

(28) (a) Suen, H. F.; Wilson, S. W.; Poimerantz, M.; Walsh, J. L. *Inorg. Chem.* **1989**, *28*, 786–791. (b) Patra, S.; Sarkar, B.; Ghumaan, S.; Patil, M. P.; Mobin, S. M.; Sunoj, R. B.; Kaim, W.; Lahiri, G. K. *Dalton Trans.* **2005**, 1188–1194.

(29) Coe, B. J.; Thompson, D. W.; Culbertson, C. T.; Schoonover, J. R.; Meyer, T. J. *Inorg. Chem.* **1995**, *34*, 3385–3395.

(30) Bonnet, S.; Collin, J.-P.; Gruber, N.; Sauvage, J.-P.; Schofield., E. R. *Dalton Trans.* **2003**, 4654–4662.

(31) Clear, J. M.; Kelly, J. M.; Pepper, D. C.; Vos, J. G. *Inorg. Chim. Acta* **1979**, *33*, L139–L140.

(32) Geraty, S.; Vos, J. G. *J. Electroanal. Chem.* **1984**, *176*, 389–393.

(33) Haas, O.; Kriens, M.; Vos, J. G. *J. Am. Chem. Soc.* **1981**, *103*, 1318–1319.

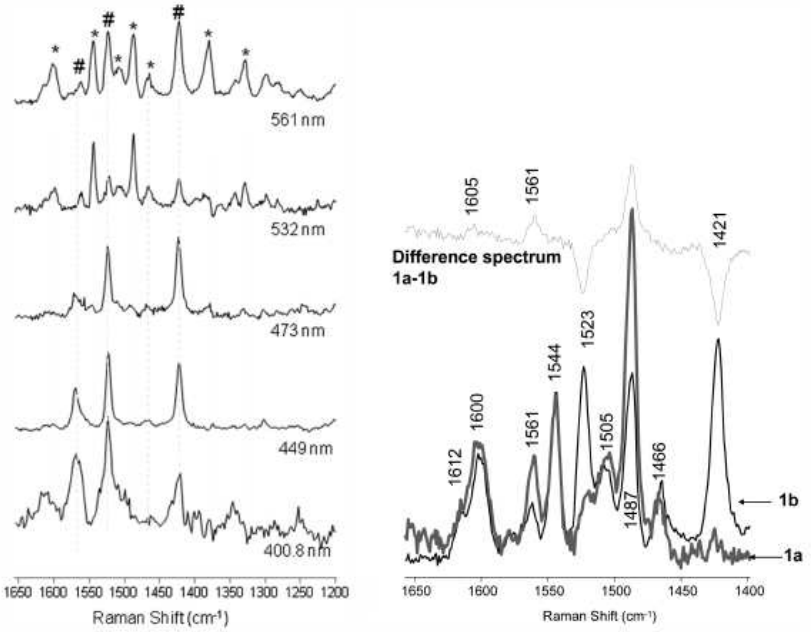

Figure 6. (Left) Resonance Raman spectra in CH_3CN of $[Ru(d_8\text{-bpy})_2(bpt)Ru(tpy)Cl]^{2+}$ **1b** at selected excitation wavelengths. (Right) Resonance Raman spectra in CH_3CN of $[Ru(bpy)_2(bpt)Ru(tpy)Cl]^{2+}$ **1a** and $[Ru(d_8\text{-bpy})_2(bpt)Ru(tpy)Cl]^{2+}$ **1b** at 561 nm. The difference spectrum (**1a**-**1b**) shows the characteristic Raman bands of h_8- and d_8-bpy. Solvent signals were subtracted. The * indicates tpy bands, and the # indicates d_8-bpy bands.

assignable to the other ligands, for example, tpy,[34] (1612, 1600, 1561, 1544, 1505, 1487, 1466 cm^{-1}) in addition to the characteristic bpy bands. Notably the relative contribution of bpy features[35] in the spectrum recorded at 561 nm is much greater than at 532 nm, indicating that bpy based MLCT states contribute to the red part of the absorption spectrum significantly. This suggests that the absorptions at the red edge of the visible absorption spectrum are dominated by $^1MLCT\ -(M^{II}\text{-tpy})$ with the more intense $^1MLCT\ -(M^{II}\text{-bpy})$ transitions dominating the spectrum between 400 and 500 nm (where M^{II} = Ru^{II} or Os^{II}).

The surface enhanced Raman spectra of **2a**/**2b** on gold colloid at 785 nm are shown in Figure S7 in the Supporting Information. Bands assignable to bpy ligands are readily identified on the basis of the effect of isotopic substitution and are in agreement with expected values.[35] Resonance Raman spectra obtained under ns-pulsed excitation at 355 nm show a distinct difference between the homo- (**1a**/**1b**) and hetero-(**2a**/**2b**) dinuclear complexes (Figure 7). In all cases bands at 1603 and 1558 cm^{-1} are observed; however, a band at 1518 cm^{-1} is observed only in the case of the d_8-bpy labeled complexes. For **2a** and **2b** bands assignable to the h_8-bpy and d_8-bpy anion radical of a bpy based ^3MLCT state are observed, respectively. For **1a** and **1b** similar excited state features are not observed. It should be noted that the $\pi-\pi^*$ transition of tpy is red-shifted with respect to that of bpy, and hence the tpy anion radical absorption will be expected to undergo a similar red-shift and will be out of resonance with the 355 nm excitation line. The data support the assignment of excited state localization made on the basis of emission spectroscopy (*vide supra*).

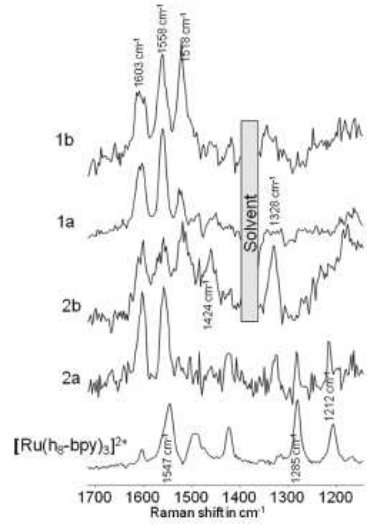

Figure 7. Transient resonance Raman spectra in CH_3CN of $[Ru(bpy)_3]^{2+}$, $[Ru(bpy)_2(bpt)Ru(tpy)Cl]^{2+}$ **1a**, $[Ru(d_8\text{-bpy})_2(bpt)Ru(tpy)Cl]^{2+}$ **1b**, $[Os(bpy)_2(bpt)Ru(tpy)Cl]^{2+}$ **2a**, and $[Os(bpy)_2(bpt)Ru(tpy)Cl]^{2+}$ **2b** at 355 nm (7 ns pulse width, 10−15 mJ per pulse). Solvent signals are subtracted.

(34) Bhuiyan, A. A.; Kincaid, J. R. *Inorg. Chem.* **1998**, *37*, 2525–2530.
(35) (a) Mallick, P. K.; Danzer, G. D.; Strommen, D. P.; Kincaid, J. R. *J. Phys. Chem.* **1988**, *92*, 5628–5634. (b) Strommen, D. P.; Mallick, P. K.; Danzer, G. D.; Lumpkin, R. S.; Kincaid, J. R. *J. Phys. Chem.* **1990**, *94*, 1357–66. (c) Mallick, P. K.; Strommen, D. P.; Kincaid, J. R. *J. Am. Chem. Soc.* **1990**, *112*, 1686–1690. (d) Manuel, D. J.; Strommen, D. P.; Bhuiyan, A.; Sykora, M.; Kincaid, J. R. *J. Raman Spectrosc.* **1997**, *28*, 933–938.

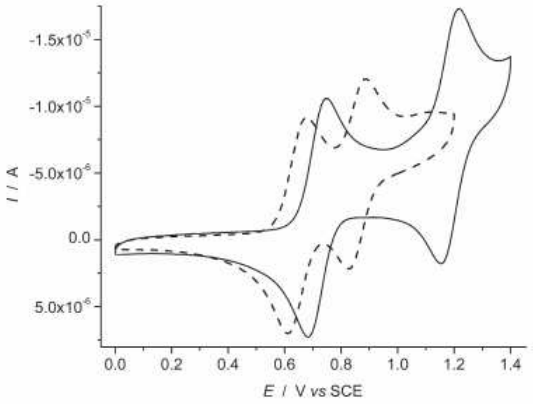

Figure 8. Cyclic voltammograms of $[Ru(bpy)_2(bpt)Ru(tpy)Cl]^{2+}$ **1a** (solid line) and $[Os(bpy)_2(bpt)Ru(tpy)Cl]^{2+}$ **2a** (dashed line) in 0.1 $TBAPF_6/CH_3CN$.

Electrochemical Properties. The redox properties of dinuclear complexes **1a** and **2a** are detailed in Table 1. Two reversible oxidative processes are observed for each complex, both of which are assigned to one-electron metal-centered oxidations (Figure 8).

The potential of the first oxidation step of the dinuclear complex **1a** is different than the value obtained for the related dinuclear compounds[13] $[Ru(bpy)_2(bpt)Ru(bpy)_2]^{3+}$ (Table 1). For **1a** (0.72 V vs SCE) the first oxidation is significantly less positive than for the related complex[13] $[Ru(bpy)_2(bpt)Ru(bpy)_2]^{3+}$ (1.04 V). The first oxidation of **1a** can be assigned to the $[Ru(tpy)Cl]^+$ moiety by comparison with the mononuclear complex $[Ru(tpy)(phen)Cl]^+$ (0.78 V vs SCE).[30] The less positive potential of the second oxidation of **1a** compared with[13] $[Ru(bpy)_2(bpt)Ru(bpy)_2]^{3+}$ reflects the increased electron density on the $Ru^{III}(tpy)Cl$ moiety compared with a $Ru^{III}(bpy)_2$ moiety (i.e., lower redox potential in the case of the former). The reductive electrochemistry of **1b** is shown in Figure S8 (see Supporting Information). Several reduction processes are observed at potentials typical of those of polypyridyl complexes; however, an irreversible reductive process at about −1.2 V versus SCE serves to distort the remaining reduction processes precluding a detailed analysis; similar reductive electrochemistry is observed for all complexes.

For complex **2a** the first oxidation is at the same potential (Figure 8) as the first oxidation of dinuclear complex[14] $[Os(bpy)_2(bpt)Ru(bpy)_2]^{3+}$ (Table 1) and is assigned (*vide infra*) to the $Os(bpy)_2$- moiety. The second oxidation of **2a** (0.86 V) is higher than the first oxidation of **1a** (0.72 V) indicating that the $Os^{III}(bpy)_2$ center reduces the σ-donor properties of the triazolato ligand compared with the $Ru^{II}(bpy)_2$ moiety in **1a**. The oxidation potential of Ru^{II} center of **2a** is comparable with that of the mononuclear complex[30] $[Ru(bpy)(tpy)Cl]^+$ (Table 1) as expected on the basis of the reduced σ-donor ability of the triazolato unit in $\mathbf{2a}^+$ than in **1a**.

Spectroelectrochemistry. Bulk electrolysis at 0.80 and 0.70 V for **1a** and **2a**, respectively, generates the mixed valence state. The fully oxidized state is obtained by electrolysis 1.35 V for **1a** and 0.95 V for **2a** (Figure 9). For complex **1a** the formation of a mixed valence state is manifested in the decrease in the intensity of the ^{1}MLCT absorption bands at 21000 cm^{-1} (475 nm) and the appearance of a broad absorption band centered at 11000−17000 cm^{-1} and at 7100 cm^{-1}. Notably for **1a** the first oxidation leads to a loss in intensity of the ^{1}MLCT absorption above 500 nm with minimal effect on the intensity at about 450 nm. This indicates that Ru-tpy ^{1}MLCT absorptions are absent in the mixed valence complex and hence that the first oxidation is localized predominantly on the Ru(tpy) moiety. Oxidation of the complex to the $Ru^{III}Ru^{III}$ state results in a disappearance of the absorption at 7100 cm^{-1} and a further decrease in the ^{1}MLCT bands at 21000 cm^{-1}. The disappearance of the 7100 cm^{-1} band upon full oxidation supports the assignment of the band as an metal to metal charge transfer (MMCT) transition.

Oxidation of **2a** at 0.70 V to form the $Os^{III}Ru^{II}$ redox state results in a decrease in intensity of the ^{1}MLCT absorptions at 20000 and 22500 cm^{-1}, and the ^{3}MLCT absorption (13000−17000 cm^{-1}). These changes are accompanied by the appearance of an absorption band at 6000 cm^{-1}. The latter feature is assigned to an MMCT transition on the basis of its subsequent disappearance upon oxidation of the second metal center at 0.95 V. In addition to a decrease in the MMCT band, the MLCT bands decrease further in the fully oxidized state (Figure 9).

Charge Transfer Band Analysis. The delocalization parameter (α^2) and the electronic coupling constant (H_{ab}) were calculated for **1a** and **2a** with eqs 1 and 2 from the spectroelectrochemical data (Table 2).[36]

$$\alpha^2 = \frac{(4.2 \times 10^{-4})\varepsilon_{max}\Delta\nu_{1/2}}{d^2 E_{op}} \quad (1)$$

$$H_{ab} = [\alpha^2 E_{op}^2]^{1/2} \quad (2)$$

where ε_{max} is the molar absorptivity of the MMCT band (M^{-1} cm^{-1}), $\Delta\nu_{1/2}$ is the peak width at half height of the MMCT band (in cm^{-1}), d is the nominal electron transfer distance between the metal centers (6.2 Å for bpt-bridged complexes **1a** and **2a**),[37] and E_{op} is the energy of the MMCT band in cm^{-1}.

Comparison of the delocalization parameters (α^2) (Table 2) shows that **1a** and $[(Ru(bpy)_2)_2bpt]^{3+}$ have the highest values of electronic delocalization among the bpt−bridged complexes in the mixed valence state. This is ascribed to the more effective overlap between the dπ orbitals of the Ru(III) center and a σ-orbital of the triazolato with respect to that of the dπ orbitals of the Os(III). Moreover, the larger electronic coupling in the mixed valence states of homobinuclear ruthenium

(36) Hush, N. S. *Electrochim. Acta* **1968**, *13*, 1005–1023.

(37) The use of the value 0.62 nm for the electron transfer distance is made on the basis of consistency with previous studies on related systems. Given the similarity in terms of the coordination environment and solvent condition employed in obtaining the absorption spectra of the mixed valence species, the inherent error in the value of d will be constant for all complexes considered in the present study. It should be noted that the electron transfer distance has been subject to extensive discussion in the literature in particular with respect to delocalization of the donor and acceptor orbitals. See for example: (a) Bublitz, G. U.; Laidlaw, W. M.; Denning, R. G.; Boxer, S. G. *J. Am. Chem. Soc.* **1998**, *120*, 6068–6075. (b) Browne, W. R.; Hage, R.; Vos, J. G. *Coord. Chem. Rev.* **2006**, *250*, 1653–1668 and references therein.

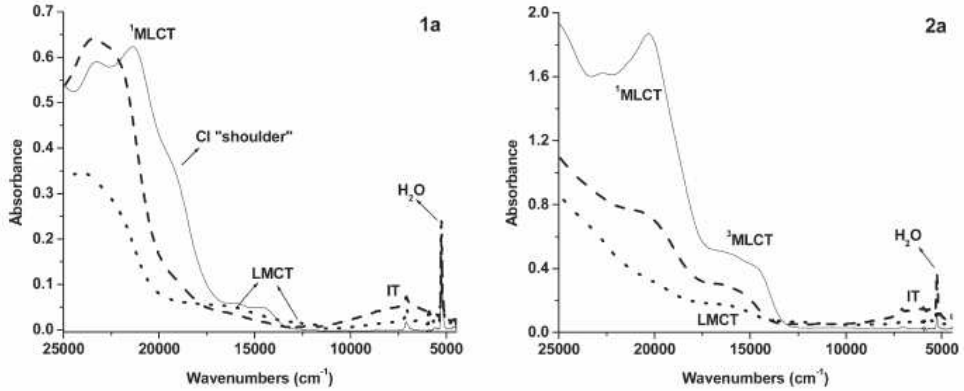

Figure 9. UV/vis/NIR absorption spectra of the dinuclear complexes **1a**$[Ru(bpy)_2(bpt)Ru(tpy)Cl]^{2+}$ (left) and $[Os(bpy)_2(bpt)Ru(tpy)Cl]^{2+}$ **2a** (right) in the $M_2^{II,II}$ (solid lines), $M_2^{II,III}$ (dashed lines), and $M_2^{III,III}$ (dotted lines) redox states.

Table 2. Spectroelectrochemical Data for **1a** and **2a** and Related Complexes[a]

	E_{op}[b]/cm^{-1}	ε_{max}/M^{-1} cm^{-1}	α^2	H_{ab}	ΔE[c]/mV	$\Delta\nu_{1/2calc}$/cm^{-1}	$\Delta\nu_{1/2}$/cm^{-1}	ref
1a	7100	1266	0.0102	716	470	3910	5200	
2a	6000	538	0.0046	406	210	3650	4660	
$[(Ru(bpy)_2)_2bpt]^{3+}$	5556	2452	0.0160	702	300	3341	3300	14
$[(bpy)_2Ru(bpt)Os(bpy)_2]^{3+}$	7143	1198	0.0070	598	470	3650	3800	14
$[(bpy)_2Os(bpt)Ru(bpy)_2]^{3+}$	8772	1133	0.0061	685	650	3700	4300	14
$[(Os(bpy)_2)_2bpt]^{3+}$	8333	455	0.0027	433	210	4170	4500	14

[a] In CH_3CN. [b] E_{op} and $\Delta\nu_{1/2}$ are $\pm$ 100 cm^{-1}. [c] $\Delta E = \pm 20$ mV.

complexes **1a** and $[(Ru(bpy)_2)_2bpt]^{3+}$ than either of the heteronuclear complexes **2a**, $[(bpy)_2Ru(bpt)Os(bpy)_2]^{3+}$ and $[(bpy)_2Os(bpt)Ru(bpy)_2]^{3+}$, indicates that such a larger intermetallic delocalization takes place through a $d\pi(Ru^{III})$-$\pi(L)$ orbital mixing (highest occupied molecular orbital (HOMO) mediated superexchange) rather than $d\pi(Ru^{II})$- $\pi^*(L)$ mixing (lowest unoccupied molecular orbital (LUMO) mediated superexchange). Analogously, the electronic coupling constants H_{ab} follow the same trend with the strongest coupling seen for the homobinuclear Ru complexes (Table 2). The determination of the type of metal-to-metal interaction in binuclear complexes is obtained from the comparison between the $\Delta\nu_{1/2}$ obtained from spectroelectrochemical data and the value $\Delta\nu_{1/2calc}$ determined from correlation of spectroelectrochemical and electrochemical data (eq 3).

$$\Delta\nu_{1/2calc} = [2310(E_{op} - \Delta E)]^{1/2} \quad (3)$$

where ΔE is the difference between the oxidation potentials of the metal centers in the binuclear complex (redox asymmetry[38]). In case of complexes **1a** and **2a** the value of $\Delta\nu_{1/2}$ determined directly from spectroelectrochemical data is larger than that calculated $\Delta\nu_{1/2calc}$ (Table 2), indicating that the system is best described as Type II (valence localized, $M^{II}M^{III}$) in the classification proposed by Robin and Day.[39] However, it should be noted that the use of ΔE, the difference in redox potentials, must take into account the electrostatic interaction between the metal centers, which can be approximated by the shift in the redox potential of the Ru(tpy) unit between complexes **1** and **2**, if other factors such as changes in backbonding and so on are ignored. From Table 1 this is calculated to be 140 mV, and hence the contributions from inherent difference in redox potentials between the metal centers are 330 mV and 70 mV and $\Delta\nu_{1/2calc}$ 3955 and 3700 cm^{-1} for **1** and **2**, respectively. Hence, even though these values are greater than in Table 2 with this correction the complex is still best described as valence localized.

Conclusions

Here, the synthesis, ^{1}H NMR, absorption, emission, and Raman spectral, spectroelectrochemical, and electrochemical characterization of the dinuclear complexes $[(bpy)_2Ru(bpt)Ru(tpy)Cl]^{2+}$ (**1a**) and $[(bpy)_2Os(bpt)Ru(tpy)Cl]^{2+}$ (**2a**) have been described together with their deuterated isotopologues **1b**/**2b**. ^{1}H NMR spectroscopy indicates that only one isomer is isolated for both **1b** and **2b** in which the chlorido ligand is trans to the triazolato ligand. Both complexes **1a** and **2a** are relatively photostable in contrast to related mononuclear chlorido containing systems. Emission and resonance Raman spectroscopy indicate that for compounds **1a**/**1b** the emissive excited state is localized on the [Ru(tpy)Cl] center, whereas for **2a**/**2b** the emissive state is localized on the $Os(bpy)_2$ unit. Electrochemistry and UV/vis/NIR spectroelectrochemistry

(38) It should be noted that the use of redox asymmetry, i.e., the difference in redox potential, to assess the degree of internuclear interaction in terms of delocalization is not advisable even in the case of fully symmetric systems, as the electrostatic contribution to asymmetry can be significant. In the present study the inherent asymmetry due to differences in the coordination environment of the metal centers contributes the most to redox asymmetry with delocalization and internuclear interaction making a second order contribution.

(39) (a) Robin, M. B.; Day, P. *Adv. Inorg. Chem. Radiochem.* **1967**, *10*, 247–422. (b) Demadis, K. D.; Hartshorn, C. M.; Meyer, T. J. *Chem. Rev.* **2001**, *101*, 2655–2685.

of **1a** and **2a** show that internuclear interaction in the mixed valence states is via bridging ligand HOMO mediated superexchange and that the site of the first oxidation switches from the M(tpy)Cl- unit to the $M(bpy)_2$- unit on going from **1a** to **2a**.

These systems show that the "direction" of energy and electron transfer in a multinuclear complex can be controlled by the switching of the metal center from Ru to Os and opens up considerable opportunities in application of these systems to molecular based electronic and photonic devices.

Acknowledgment. R. Megens is thanked for the preparation of gold colloid. Science Foundation Ireland has contributed to this research with under Grant 07/SRC/B1160 Advanced Biomimetic Materials for Solar Energy Conversion (D.D. and J.G.V.) and Grant 06/RFP/CHP029 Development of a Room Temperature Molecular Electronics (Y.H.), IRCSET (LC), the Libyan Government (HMYA), and The Netherlands Science Foundation (NWO, Vidi, WRB) are acknowledged for financial support.

Supporting Information Available: ^{1}H NMR spectra of $[Ru(bpy)_2(bpt)]^+$, $[Ru(d_8\text{-}bpy)_2(bpt)]^+$, $[Ru(bpy)_2(bpt)Ru(tpy)Cl]^{2+}$, and $[Os(bpy)_2(bpt)Ru(tpy)Cl]^{2+}$, COSY Spectrum for $[Os(d_8\text{-}bpy)_2(bpt)Ru(tpy)Cl]^{2+}$. HPLC chromatograms of $[Ru(bpy)_2(bpt)Ru(tpy)Cl]^{2+}$ and $[Os(bpy)_2(bpt)Ru(tpy)Cl]^{2+}$ before and after irradiation; normalized absorption spectra of **1a** and **2a** before and after irradiation; surface enhanced Raman spectra (Au colloid in water) of **2a**/**2b**. This material is available free of charge via the Internet at http://pubs.acs.org.

Development of a New Synthetic Strategy for obtaining $[Ir^{III}(bpy\text{-}N,N')_2Cl_2]^+$ and its analogues in High Purity and Yield, Study of its Mechanism and Deuteriation Effect on the Formation of $[Ir^{III}(bpy\text{-}N,N')_2(bpy\text{-}C,N')^-]^{2+}$ Complexes.

Suraj Soman,[a] Hamid Younis,[a] Gurmeet Singh Bindra,[a] Laura Cleary,[a] Johannes G. Vos,[a] Mary T. Pryce,[a] Wesley R. Browne[b]

*(**a**) SRC for Solar Energy Conversion: School of Chemical Sciences, Dublin City University, Dublin 9, Ireland;**(b)** Faculty of Mathematics and Natural Sciences, Stratingh Institute, University of Groningen, The Netherlands.*

Abstract

A novel rapid and efficient synthetic route for the preparation of $[Ir^{III}(bpy\text{-}N,N')_2Cl_2]^+$, $[Ir^{III}(phen)_2Cl_2]^+$, $[Ir^{III}(dmbpy)_2Cl_2]^+$, $[Ir^{III}(dtbpy)_2Cl_2]^+$ and the orthometallated complex, $[Ir^{III}(bpy\text{-}N,N')_2(bpy\text{-}C,N')^-]^{2+}$ is reported. All compounds obtained are characterized by HPLC, ^1H NMR and electronic spectroscopy. Deuteriated 2,2'-bipyridyl is used to obtain more detailed information on the reaction process. When predeuteriated 2,2'-bipyridyl was employed the amount of orthometallated complex formed is reduced.

Introduction

The ligand 2,2'-bipyridine (bpy) has been used extensively due to its rigidity which leads to a high preference for the bidentate binding mode and ease with which it chelates most transition metal ions[1]. Iridium (III) complexes of 2,2'-bipyridine (bpy) are difficult to prepare and purify[2] compared to the isoelectronic and isostructural analogues of Ru^{II} and Os^{II} due to its unexplored reaction mechanism and kinetically sluggish substitution rates[3-8]. Most of the d^6 ions of the group 8 transition metals are known to easily form complexes with bidentate-bound bpy, $Ru(bpy)_2Cl_2$, $Ru(bpy)_3$, $Os(bpy)_2Cl_2$, $Os(bpy)_3$ are some of the well known complexes studied. However, $[Ir^{III}(bpy\text{-}N,N')_2Cl_2]^+$ (**I**) is the principal product of the reaction of $IrC1_3.3H_2O$ with bpy,[9-12] along with a small fraction of $[Ir^{III}(bpy\text{-}N,N')_2(bpy\text{-}C,N')^-]^{2+}$ (**II**). Synthesis of complex **II** was reported[14] as obtained from **I** by its reaction with a good proton base in a poorly hydrogen-bonding solvent,[1,15] and also by the prolonged melting of $K_3IrCl_6.3H_2O$ with bpy.[18] But nobody has yet identified the formation of **II** along with **I** which has been considered as an "impurity" before.[5] $Ir(bpy)_3$ has been prepared by reaction of iridium sulphates with bpy in a halide-free medium.[13] It is apparently considerably more difficult to bind three bpy's to Ir(III) than it is to the other

metal ions mentioned above. Our work focus on the preparation of $[Ir^{III}(bpy\text{-}N,N')_2Cl_2]^+$ (**I**), $[Ir^{III}(phen)_2Cl_2]^+$ (**III**), $[Ir^{III}(dmbpy)_2Cl_2]^+$ (**IV**), $[Ir^{III}(dtbpy)_2Cl_2]^+$ (**V**) in high purity and yield, its mechanistic pathway going along with the reaction using NMR and HPLC, photophysical measurements and the effect of deuteriation on the formation of $[Ir^{III}(bpy\text{-}N,N')_2(bpy\text{-}C,N')^-]^{2+}$ (**II**).

Experimental Section.

Materials and Reagents

The reagents employed during the course of all experiments were purchased from Sigma-Aldrich and used without further purification. Deuteriated bipyridine was synthesized according to the procedure reported before.[39] All solvents used for HPLC analysis are of HPLC grade and spectroscopic grade solvents were used for photophysical measurements.

Methods and Instrumentation.

HPLC Measurements

High-Performance Liquid Chromatography (HPLC) was carried out using a Varian ProStar (model 335.71) photodiode array Detector, HPLC conjunction with Varian Star software, a Varian (model 210) pump, a 20 μl injector loop and a strong cation exchange Luna SCX 100A column (25cm X 4.6mm) provided by phenomenex . The column is packed with 5 μm particles and the operating pH range is between 2 and 8. The mobile phase for this work was 80:20 CH_3CN: H_2O: containing 0.1 M KNO_3. Filtered and degassed prior using the flow rate ranged 1.5 and 2 cm^3/min^{-1}.

NMR Spectroscopy

The ^1H NMR and COSY spectra were recorded on a Bruker AC400 (400 MHz) NMR spectrometer and Bruker Avance:3 (600MHz) instrument using deuteriated DMSO. The chemical shifts were recorded relative to TMS and spectra were converted from their free induction decay (FID) profiles using XWIN-NMR software.

Absorption and Emission Spectroscopy

The UV/Vis spectra were carried out on a gilent 8453 UV-Vis Spectrophotometer, the spectra were obtained in the ultraviolet region in the wavelength range 200 to 800nm. The emission spectra were obtained on a Perkin-Elmer LS50B luminescence spectrometer

Luminescence Lifetimes

Transient emission data were generated using a Q-switched Nd-YAG spectrum laser system. The data were plotted and analysed with the aid of Sigma Plot 8.0 software. All measurements were obtained in spectrometric grade acetonitrile at room temperature and all the solutions were degassed by bubbling nitrogen through the solution for 30 minutes. The lifetimes were calculated at the emission maxima.

Synthesis

Synthesis of h8-$[Ir(bpy)_2Cl_2]^+$ (I) and h8-$[Ir^{III}(bpy\text{-}N,N')_2(bpy\text{-}C,N')^-]^{2+}$(II)

Iridium trichloride hydrate (0.10g, 0.3349mmol) was reacted with 2,2'-bipyridyl (0.1046g, 0.6696mmol) dissolved in $2cm^3$ of glycerol. The reaction was heated at reflux (300^0C) for 25 minutes when the colour of the solution has changed from red to straw yellow. The solution was cooled to room temperature and $5cm^3$ of water was added. The mixture was filtered and washed with $5cm^3$ of diethyl ether. To the filtrate 10 ml saturated NaCl solution was added yielding $[Ir^{III}(bpy\text{-}N,N')_2Cl_2]^+$ (**I**) which is filtered and dried. ^1H NMR(400MHz, DMSO), δ(ppm): 7.51(t, 1H), 7.8275(d,1H), 8.116(t, 1H), 8.2045(t, 1H), 8.5165(t, 1H), 8.821(d, 1H), 8.932(d, 1H), 9.645(d, 1H). (Yield:0.120g).

The filtrate obtained after precipitating out fraction **I** is concentrated, dried and stirred with 20 ml of DCM, filtered and the process is repeated until all of excess bipyridine and any remaining fraction **I** are removed. The yellow residue is dried and 20 ml of dry methanol was added.. The solution is then stirred, filtered, concentrated and chromatographed on Sephadex (LH:20) using ethanol to yield $[Ir^{III}(bpy\text{-}N,N')_2(bpy\text{-}C,N')^-]^{2+}$ (**II**) in pure form. ^1H NMR(400MHz, DMSO), δ(ppm): 9.04(d, 1H), 9.01(d, 1H), 8.96(m, 2H), 8.45(m, 3H), 8.42(d, 1H), 8.38(m, 2H), 8.21(t, 1H), 8.01(d, 1H), 7.91(d, 1H), 7.90(d, 1H), 7.81(m, 2H), 7.72(d, 1H), 7.67(m, 3H), 7.48(t, 1H), 7.08(m, 1H), 6.58(d, 1H). (Yield:0.015g).

Synthesis of d8-$[Ir(bpy)_2Cl_2]^+$ (I) and d8-$[Ir^{III}(bpy\text{-}N,N')_2(bpy\text{-}C,N')^-]^{2+}$(II)

Iridium trichloride hydrate (0.10g, 0.3349mmol) was combined with deuteriated 2,2'-bipyridyl (0.1153g, 0.6696mmol) dissolved in $2cm^3$ of glycerol. The reaction was heated at reflux (300^0C) for 25 minutes until the colour of the solution changes from red to straw yellow. The solution was cooled to room temperature to which $5cm^3$ of water was added, filtered and washed with $5cm^3$ of diethyl ether. To the filtrate 10 ml saturated NaCl

solution was added in order to precipitate deuteriated $[Ir^{III}(bpy\text{-}N,N')_2Cl_2]^+$ (**I**) which is filtered and dried. (Yield:0.150g, 80%).

The filtrate obtained after precipitating out fraction **I** is concentrated, dried completely and stirred with 20 ml of DCM, filtered and the process is repeated until all of excess bipyridine and any remaining fraction **I** are removed completely along with the DCM. The yellow residue is dried to which 20 ml of dry methanol was added, stirred, filtered, concentrated and chromatographed on Sephadex (LH:20) using ethanol to get deuteriated $[Ir^{III}(bpy\text{-}N,N')_2(bpy\text{-}C,N')^-]^{2+}$ (**II**) pure. (Yield:0.020g).

Synthesis of $[Ir^{III}(phen)_2Cl_2]^+Cl$ (III)

Iridium trichloride hydrate (0.10g, 0.2836mmol) was combined with two equivalents of phenanthroline (0.102g, 0.567mmol) dissolved in 2 cm^3 of glycerol. The reaction mixture was heated at reflux (300^0C) for 25 minutes until the colour of the solution changes from red to straw yellow. The solution was cooled to room temperature and 5 cm^3 of deionised water was added. The mixture was filtered and extracted three times with diethyl ether and was heated using a heat gun for 10 minutes, cooled and 10 ml saturated NaCl solution was added yielding $[Ir^{III}(phen)_2Cl_2]^+Cl$ (**III**), which is vacuum filtered, dried and recrystallized from Acetone:water (1:1) mixture. ^{1}H NMR (400 MHz, DMSO), δ(ppm): 7.698(m, 1H), 8.077(d, 1H), 8.375(d, 1H), 8.486(m, 2H), 8.763(d, 1H), 9.157(d, 1H), 9.943(d, 1H). (Yield: 0.160g, 90.48%).

Synthesis of $[Ir^{III}(dmbpy)_2Cl_2]^+Cl$ (IV)

Iridium trichloride hydrate (0.10g, 0.2836mmol) was combined with two equivalents of 4,4'-dimethyl-2,2'dipyridyl (0.1045g, 0.5672mmol) dissolved in 2 cm^3 of glycerol. The reaction mixture was heated at reflux (300^0C) for 10 minutes, cooled and the turbid yellow solution was filtered, 10 cm^3 of deionised water was added to the filtrate and extracted three times with diethyl ether and then with DCM. The aqueous layer was heated for 10 minutes using a heat gun in order to remove residual solvents and 10 ml saturated NaCl solution was added resulting in the precipitation of $[Ir^{III}(dmbpy)_2Cl_2]^+Cl$ (**IV**)as yellow solid which is vacuum filtered, dried and recrystallized from Acetone:water(1:1) mixture. ^{1}H NMR (400 MHz, DMSO), δ(ppm): 2.557(s, 3H), 2.762(s, 3H), 7.316(dd, 1H), 7.597(d, 1H), 7.929(dd, 1H), 8.659(s, 1H), 8.756(s, 1H), 9.423(d, 1H). (Yield: 0.170g, 95%).

Synthesis of $[Ir^{III}(dtbpy)_2Cl_2]^+Cl$ (V)

Iridium trichloride hydrate (0.10g, 0.2836mmol) was combined with two equivalents of 4,4'-di tertiarybutyl-2,2'dipyridyl(0.1522g, 0.5672mmol) dissolved in 2 cm^3 of glycerol. The reaction mixture was heated at reflux (300^0C) for 10 minutes, cooled and the turbid yellow solution was filtered, 10 cm^3 of deionised water was added to the filtrate and extracted three times with diethyl ether and then with DCM. The aqueous layer was heated for 10 minutes using a heat gun in order to remove residual solvents and 10 ml saturated NaCl solution was added resulting in the precipitation of $[Ir^{III}(dtbpy)_2Cl_2]^+Cl$ (**V**) as yellow solid which is vacuum filtered, dried and recrystallized from Acetone:water(1:1) mixture. ^{1}H NMR (400 MHz, DMSO), δ(ppm): 1.360(s, 9H), 1.543(s, 9H), 7.479(dd, 1H), 7.622(d, 1H), 8.090(dd, 1H), 8.831(s, 1H), 8.929(s, 1H), 9.481(d, 1H). (Yield: 0.163, 71.8%).

Results and Discussion

Synthetic Considerations

Little work has been reported during the past 20 years on the chemistry of $[Ir(bpy)_2Cl_2]$. One of the factors that prevented its investigation is the multi step synthetic procedures reported before[14] resulting in low yields combined with the formation of a series of side products.[1,15,16,17] A trans isomer for **I** has also been reported.[12]

Because of the synthetic potential of this compound we carried out a series of experiments aimed at developing an efficient high yield synthetic method for $[Ir(bpy)_2Cl_2]$. In these studies a wide variety of solvents including ethylene glycol, ethanol, methoxyethanol, ethanol:H_20 (1:1) were investigated. In addition the reaction times were varied systematically from 25min to 3 days. The best results were obtained by the heating of $IrCl_3.3H_2O$ with bpy in glycerol under reflux for 25 minutes. By increasing the reaction temperature to 300^oC and by using a short reaction time we succeeded in suppressing the formation of other intermediate species also along with the trans isomer. With this method the reaction time is reduced considerably from one week to 25 min and $[Ir^{III}(bpy\text{-}N,N')_2Cl_2]^+$ (**I**) is obtained in high purity and in a good yield without the employment of further purification methods such as column chromatography. A second product, $[Ir^{III}(bpy\text{-}N,N')_2(bpy\text{-}C,N')^-]^{2+}$,(**II**), could be obtained from the reaction mixture by working up the remaining reaction mixture.

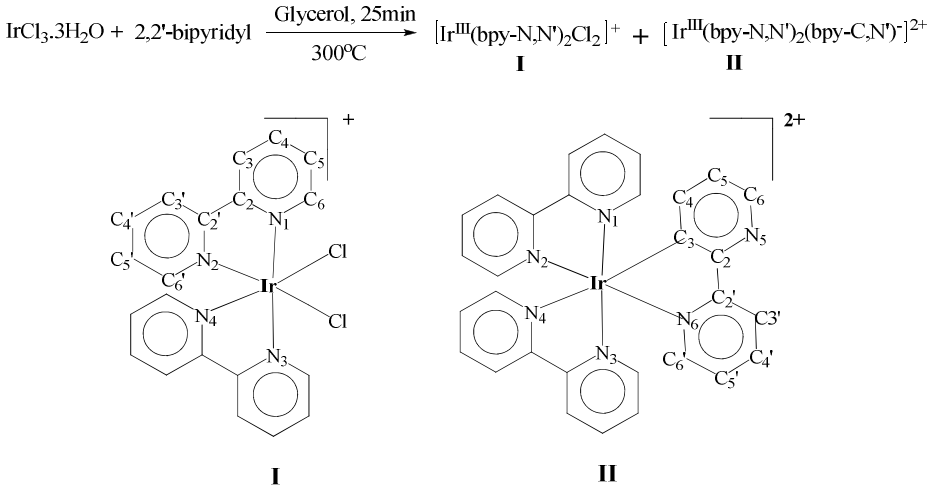

Figure 1. Schematic representation of the synthetic method followed.

cis-[Ir(phen)$_2$Cl$_2$]Cl was first described in 1964 by Chiswell *et al.*,[40] prepared in 27% yield by heating K_3IrCl_6 with 1,10-phenanthroline at 220 °C for 14 h. In 1971 Broomhead *et al.* reported a different synthesis.[41] In a first step [Ir(phen)-Cl$_4$]$_2$[phenH]$^+$ was prepared in 90% yield from (NH4)3IrCl6·2H2O and phen by reflux in acidic water for 2 h. The second step consisted of heating the phenanthrolinium salt in refluxing glycerol for 1 min, and gave *cis*-[Ir(phen)$_2$Cl$_2$]Cl as a yellow solid in 85% yield. These early examples reflect the synthetic difficulties usually encountered when preparing simple iridium (III) complexes. We successfully synthesised *cis*-[Ir(phen)$_2$Cl$_2$]Cl in high yield in a simple one step procedure. We also made two new novel complexes **III, IV** and **V** whose nmr data are given in Fig 2

The ^{1}H NMR spectra of the reaction mixture taken directly from the reaction mixture at the completion of the reaction (after 25 min) along with the purified complexes are given in Fig 2. By comparing the NMR spectrum of the mixture with those obtained for **I** and **II** we can conclude that apart from these two compounds no side products are obtained.

The ratio of the two products can be obtained both from the ^{1}HNMR as well as the hplc data (See Figure 3). NMR analysis of for example the spectrum shown in Figure 2A indicates that the ratio of **I:II** is 67:33, with hplc a ratio of 66:34 is obtained. For the deuteriated analogues an ratio of 75:25 is determined from hplc. This is in agreement with the increased bond strength of C-D bond over the C-H bond .

For complexes **III**, **IV** and **V** it was confirmed from nmr and hplc that the orthometallated tris complex as similar to bpy is not at all formed due to the steric hindrance caused by the bulky groups present on the bipyridine ring and for phenanthroline there is no free rotation possible.

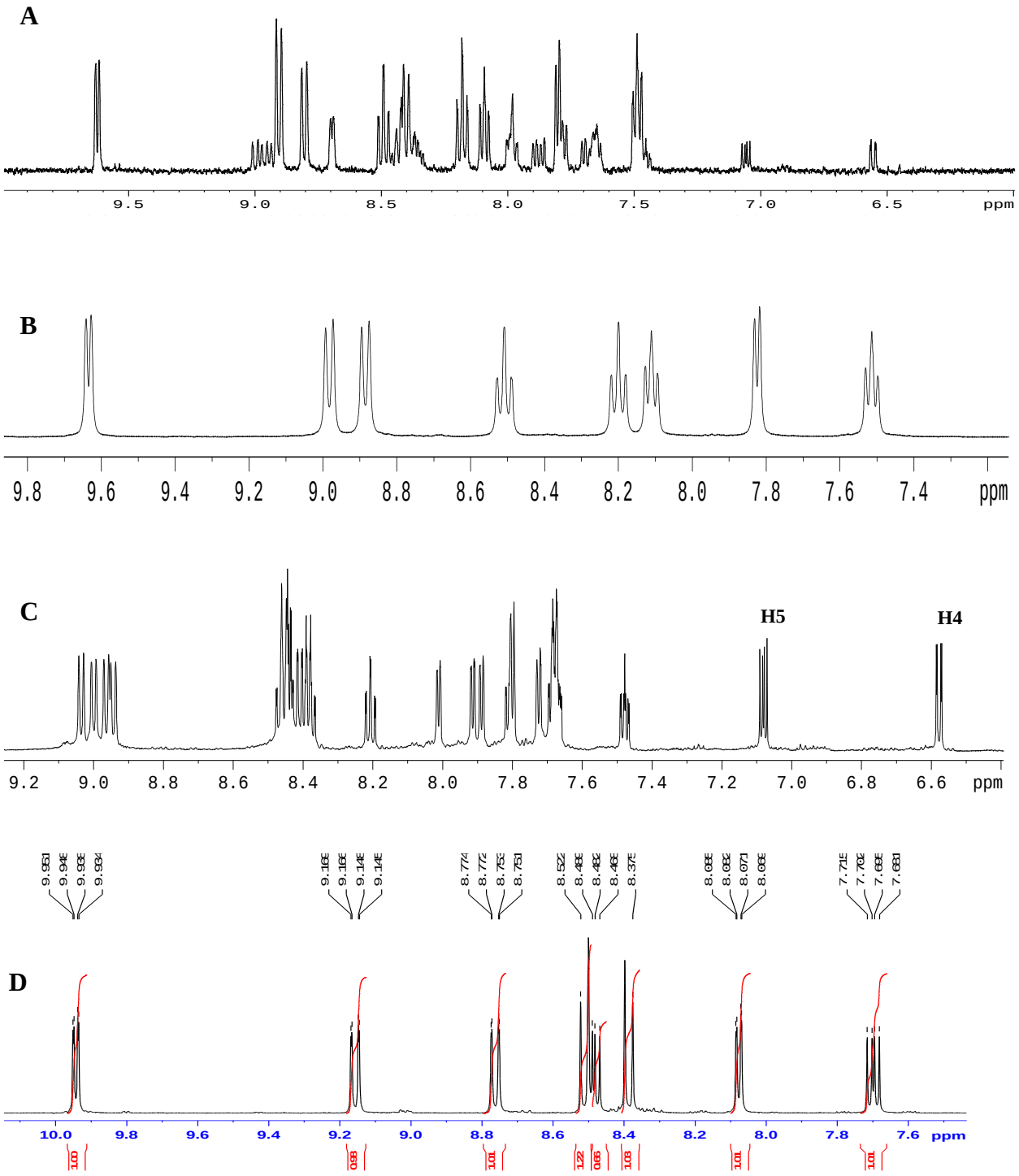

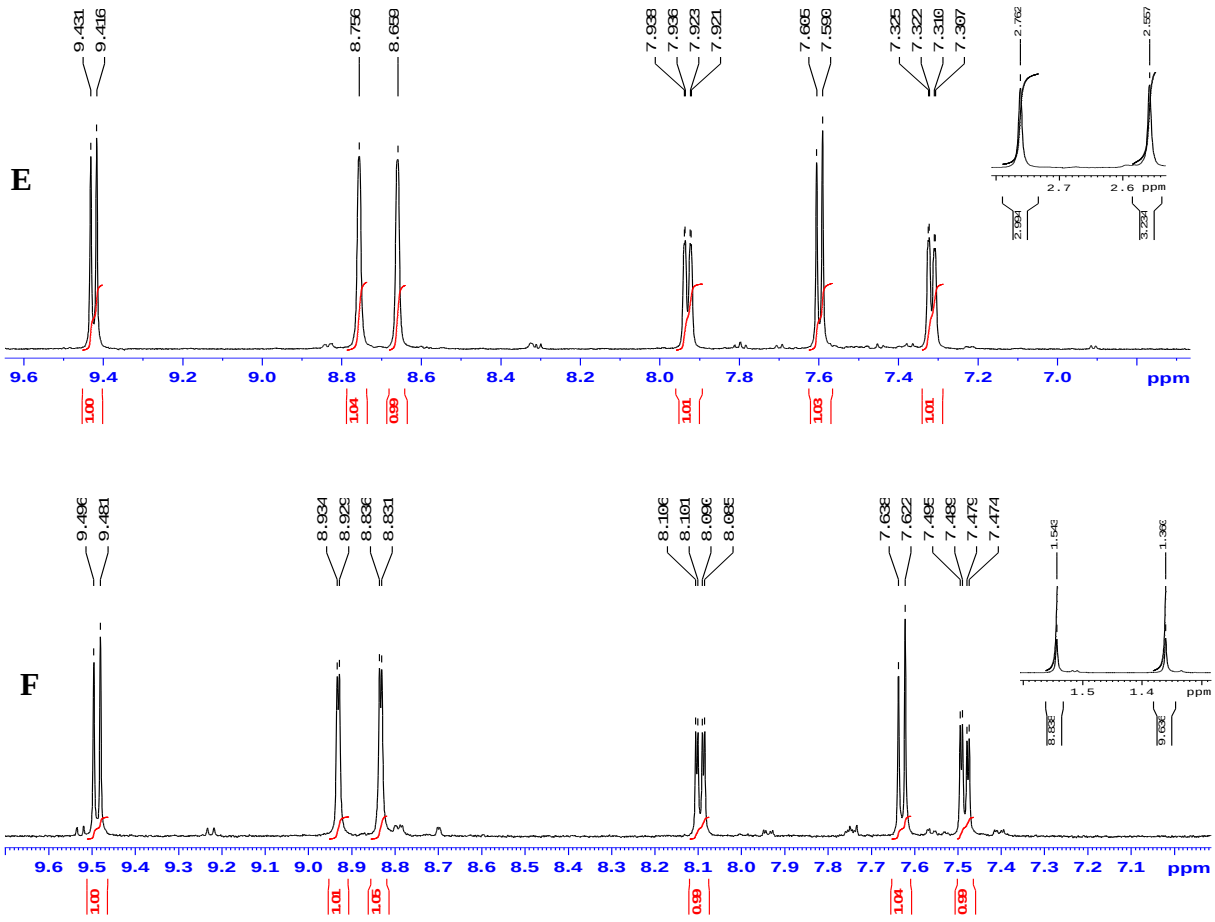

Figure 2. ^{1}H NMR spectra **(A)** directly taken from the reaction mixture for h8-bpy containing complex **I** and **II**, **(B)** $[Ir^{III}(bpy\text{-}N,N')_2Cl_2]^+$(**I**), **(C)** $[Ir^{III}(bpy\text{-}N,N')_2(bpy\text{-}C,N')^-]^{2+}$ (**II**), (D) $[Ir^{III}(phen)_2Cl_2]^+$ (**III**), $[Ir^{III}(dmbpy)_2Cl_2]^+$ (**IV**), $[Ir^{III}(dtbpy)_2Cl_2]^+$ (**V**) carried out in d^6 DMSO.

Characterisation. ^{1}H NMR spectroscopy

As shown in Figure 2B the spectrum of the iridium complex **I** shows the presence of two different types bpy rings, in agreement with a cis arrangement of the bpy ligands and the presence of chloride ligands, similar to that observed for the analogues compound $[Ru(bpy)_2Cl_2]$. complexes[12,21]

The ^{1}H NMR spectrum of **II** (Fig:2C) includes a doublet at δ 6.58 that integrates for 1 proton in a total of 23 protons and this can be assigned to the H4 proton of the C-bonded ring from the COSY measurements and also considering the fact that H4 proton is situated immediately above the pyridine ring of an adjacent ligand and therefore will experience a

high ring-current shielding which has been proved before for similar complexes using crystal structure.[14,16] The shift is 2 ppm upfield from the position of the H4 protons in the $[Ir(bpy\text{-}N,N')_3]^{2+}$ complex[19]. A similar upfield shift of ~2 ppm was also observed in the $[Pt(bpy\text{-}N,N')_2]^{2+}$ NMR spectrum where, on going from square-planar to a cis conformation, half of the H6 protons become shielded by an adjacent aromatic ring.[20]

To obtain further information concerning the reaction pathway as a function of time, HPLC (Fig:3) and NMR (Fig:4) data were obtained at intervals from the reaction mixture starting from 5 min upto a time limit of 25min which provides a good insight into the progress of the reaction. The HPLC data are clearly indicative of the formation of different species and by comparing with the NMR spectrum for the same time intervals the formation of both of fraction (**I**) and (**II**) started to form at 15min. This can be clearly distinguished from the peaks obtained for the nmr spectrum. By comparing (Fig: 3c) and (Fig:3d) with (Fig:4c) and Fig:4d) we obtain proof regarding the characteristic peaks for the orthometallated species, one double multiplet at δ 7.08 (m) and a doublet at δ 6.58 (d).

a **b**

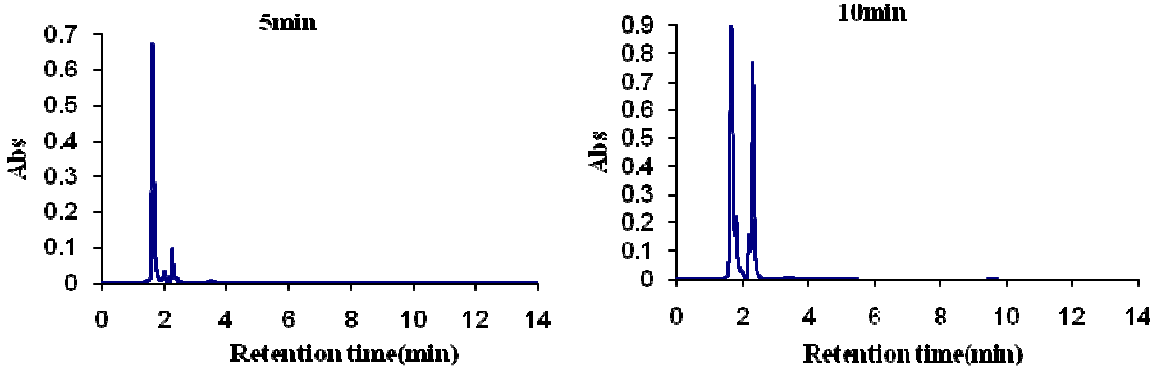

c **d**

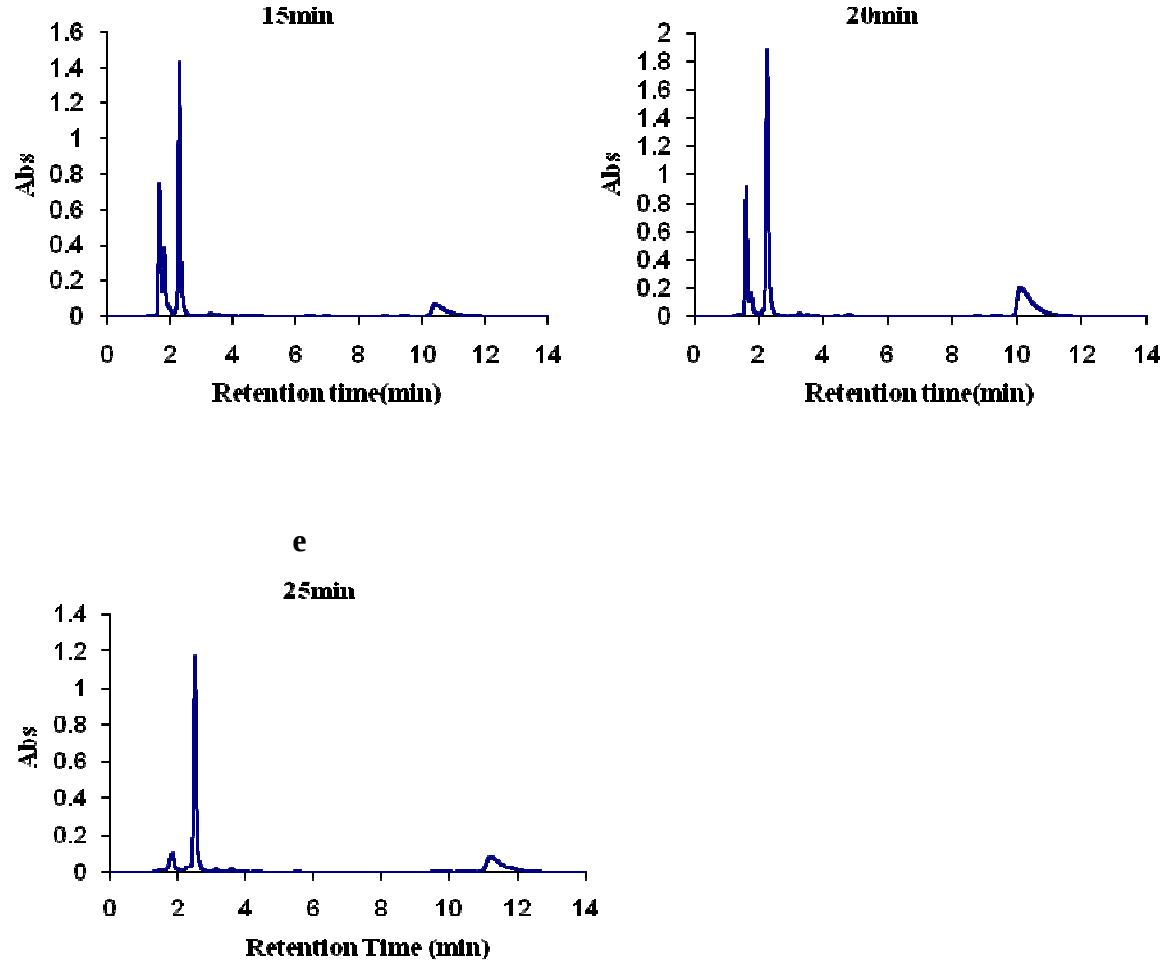

Figure 3. Time dependent HPLC data for reaction of $IrCl_3$ with h8 bpy at different time intervals ranging from 5min to 20min. a) 5min b) 10min c)15min d) 20min e) 25min

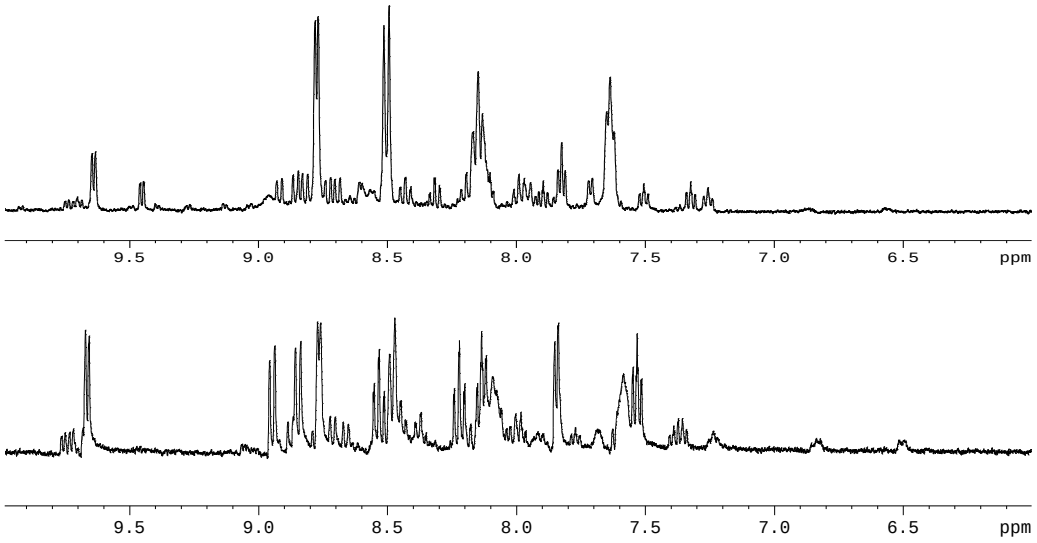

a) 5min

b) 10min

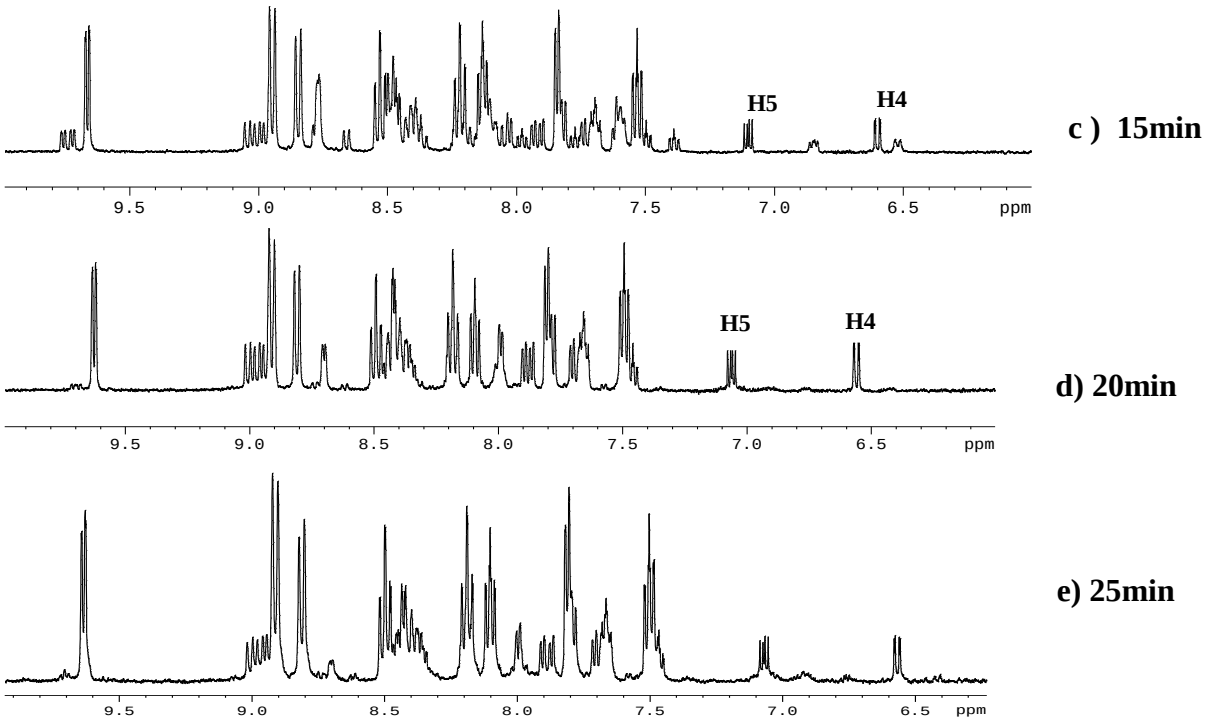

Figure 4. Time dependent nmr data for the reaction of $IrCl_3$ with h8 bpy at different time intervals ranging from 5min to 20min. a) 5min b) 10min c) 15min d) 20min. e)25min.

identify two peaks at retention time of 1.69min and at 2.33min after 5min of the starting of the reaction, former being the peak of bpy and latter of $[Ir^{III}(bpy\text{-}N,N')_2Cl_2]^+$ (**I**) . The ^1H NMR spectrum shown in Fig:4 supports the identity of both peaks. After 10min the intensity of 2nd peak has increased showing that more of complex **I** is formed by the reaction of starting materials, and the first peak has become more structured possibly because of the formation of an intermediate chloro bridged Iridium dimer in which one bpy complexed to each Ir metal undergo cyclometallation[22] which is clearly evident from the doublet at δ 6.5, multiplet at δ 6.85 and δ 9.75 given in Fig:4(b). At 15min the first peak in HPLC at 1.69min splits up into two, corresponding to the unreacted bpy and the intermediate species. In Fig 3(c) the upcoming 3rd peak at retention time 10.44min corresponds to $[Ir^{III}(bpy\text{-}N,N')_2(bpy\text{-}C,N')^-]^{2+}$ (**II**) evident from the δ 6.58 H4 proton doublet and δ7.08 multiplet. At 20min most of the intermediates get converted into complex **II** which is evident from HPLC Fig:3(d) and NMR Fig:4(d), as the peaks at δ values 6.5, 6.85 and 9.75 have disappeared on going from 15min to 20min. At 25min almost all of the bipyridine has reacted and we are left with the final two products. We

continued the study upto 1.5 hours which showed that most of the metal got charred at this higher temperature resulting in a decrease of yield to 30% at 1.5hour. We completely succeeded in eliminating quite a numerous side products in the conventional reaction of Ir metal with bpy by employing a higher temperature resulting in separation of only two products at the end of the reaction clearly proved using the HPLC and NMR data given in Fig:3 and Fig:4.

We had undertaken the deuteriation effect study which provided promising result on the formation of complex **II** through an intermediate species. When we employed deuteriated bpy (d8-bpy) due to the greater bond strength of C-D bond over the C-H bond the deuteron will not go off easily resulting in the reduced yield of complex **II**. The ratio of **I** and **II** for h8-bpy, d8-bpy tabulated using HPLC and NMR are given in Table 1.

For h8- and d8-bpy we obtained 3 distinguishable peaks at the end of the reaction, first peak corresponding to some amount of unreacted bpy at a retention time of 1.69min, second peak corresponding to complex **I** at retention time of 2.33min and the third peak corresponding to complex **II** at a retention time of 10.43min. The HPLC data obtained for all the 2 cases are given in supplementary information (Fig: S9 to S14).

Absorption and Emission Studies

The absorption spectrum of $[Ir^{III}(bpy\text{-}N,N')_2Cl_2]^+$ is dominated by Ir(III) to bpy charge-transfer bands (CTTL) in the visible and internal bpy bands (IL) in the ultraviolet. The visible absorption spectrum of $[Ir^{III}(bpy\text{-}N,N')_2Cl_2]^+$ consists of a weak band at 390 nm which has been assigned as CTTL transition. The CTTL band at 302 nm in $[Ir^{III}(bpy\text{-}N,N')_2Cl_2]^+$ moves to 310 nm in $Ir^{III}(bpy\text{-}N,N')_2(bpy\text{-}C,N')^-]^{2+}$ and the band at 390 moved into the tail end of the spectra, this can happen since the $(bpy)^-$ being a better π-donor than Cl^-, and should therefore lower the energy of the CTTL bands. The shoulder formed at 250-300nm range in both type of complexes are probably due to the CTTL transitions , the shoulder is much more clearly defined in case of complex **II** due to the presence of the more π-donating ligand $(bpy)^-$, suggesting that the CTTL band may be moved to slightly shorter wavelength in **II** where it is buried in the strong π-π* absorption peaks. The absorption spectrum of $[Ir^{III}(bpy\text{-}N,N')_2Cl_2]^+$ overlaps its emission spectrum.

The bands are therefore thought to arise from a transition between the ground state and the emissive state, Although the other iridium complexes fail to show a resolved absorption band in this region under the conditions employed, their absorption spectra do overlap their emission spectra significantly. Thus it is likely that the emissive state of each of the iridium complexes is actually seen in absorption but is clearly resolved only in the one case.[11] The absorption spectra of the tris complexes are noteworthy in that the ratios of the intensities of the highest and lowest energy bands decrease with change from N,N' to C,N' coordination.[31]

The photochemical and photophysical properties of bis-bidentate complexes of Ir(II1) such as $[Ir^{III}(bpy\text{-}N,N')_2Cl_2]^+$ and $[Ir^{III}(phen)_2Cl_2]^+$ are determined by the relatively unusual occurrence of light emission in competition with ligand substitutional activity,[2,24] coupled with the rare property of two close-lying emitting states of different orbital percentage. The primary ramification of the CT state in close proximity to the LF state appears to be enhanced emission intensity due to the combined increase of the radiative decay rate and substitutional unreactive nature of the CT state.[25,26] Both the bischelated iridium complexes, *cis*-$[Ir^{III}(bpy\text{-}N,N')_2Cl_2]^+$ and *cis*-$[Ir(phen)_2Cl_2]^+$ exhibit MLCT phosphorescence[2,11,27] but *cis*-$[Ir(5,6\text{-}Mephen)_2Cl_2]^+$ exhibits π-π^* emission.[25] The hetero-bischelated complexes, *cis*-$[Ir(bipy)(phen)Cl_2]^+$ and *cis*-$[Ir(phen)(5,6\text{-}Mephen)Cl_2]^+$, exhibit multiple emissions;[28] Watts established the multiple emissions for the latter from thermally nonequilibrated states of d-π^* and π-π^*, but there are however very slightly deviations from nonexponential luminescence decay which were observed for the former.[29,30]

Studies on the photophysics of cis-dichlorobis(2,2'-bipyridine)iridium(lII), $[Ir^{III}(bpy\text{-}N,N')_2Cl_2]^+$, and its deuteriated analogue $[Ir^{III}(d8\text{-}bpy\text{-}N,N')_2Cl_2]^+$ indicates that these ions have low-energy ligand field (LF) excited states. These states are believed to give rise to the chloride photoaquation which has been reported in several studies.[6a,6b,6c,23] Low energy charge-transfer (CT) excited states are also present in these complexes, at energies slightly above those of the LF states.[7a] These CT states also makes measurable contributions to the emission spectra in fluid solutions. Also the excited states of Iridium(III) complexes with such ligands as bipyridine, phenanthroline, and their derivatives are very sensitive to the environment and this can become an important factor in the reactivity of these complexes in various solvents.

It is quite interesting to note that for both complex **I** and complex **II** which is excited at an excitation wavelength at which OD is taken same for the 3 different cases showed that the emission intensity goes on increasing from h8 to d8 and the maximum for the (h8+d8) mixture for both the complexes. The emission of both complexes are found to be wavelength independent. The emission spectra of complex **II** also gives indication on dual emission, these emission can originate from impurities, such as a mixture of structural isomers or from a ground-state association process, and emission originating from a second, unequilibrated electronic excited state. The absence of evidence of impurities in TLC and NMR analysis and adherence of solutions to Beer-Lambert's law over the concentration range which was studied suggest that dual emission of complex **II** is not due to impurities but rather due to emission from an unequilibrated excited state.

The iridium system thus in fact clarifies the visible and near-ultraviolet spectra as there are no low energy charge-transfer bands to mask the $(bpy)^-$ transitions. These observations put beyond doubt the character of the redox-active orbitals of these and many other $d\pi^6$ bipyridyl complexes. Electrons entering such orbitals are effectively trapped on the individual ligands, with negligible communication between the neighboring chelate rings.[32] The d6 complexes of the second and third row transition metal ions all give a photoluminescence. The lowest empty orbital[7b] of the emitting species can be designated as a "localized orbital" (metal d type) or "delocalized orbital" (π type having ligand character and in some cases metal $d\pi$ character).[1,5]

The absorption and emission datas on h8,d8 and (1:1)h8+d8 for both complexes are tabulated in Table 2 and Table 3.

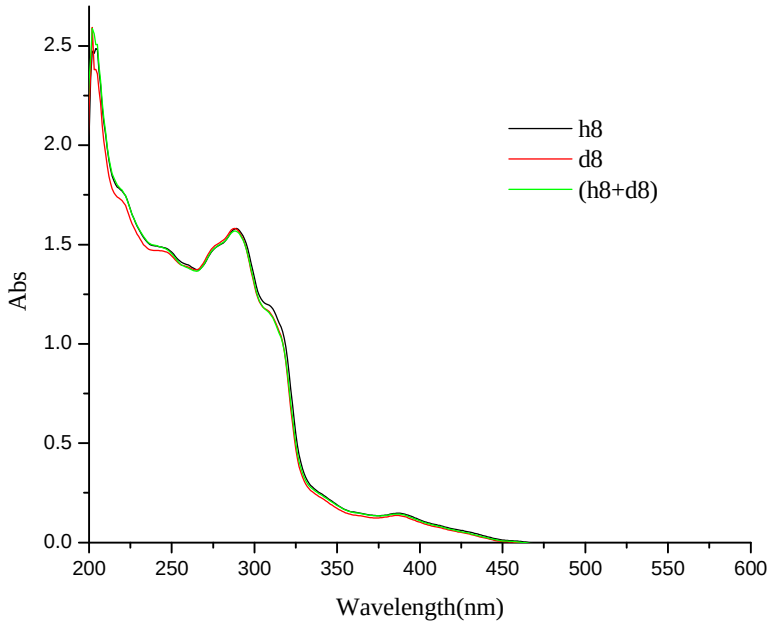

Figure 5. Absorption spectra of h8,d8 & (h8+d8) $[Ir^{III}(bpy\text{-}N,N')_2Cl_2]^+$ taken in spectrometric grade ACN (Conc. 1.37 $x10^{-4}$ moles/lit).

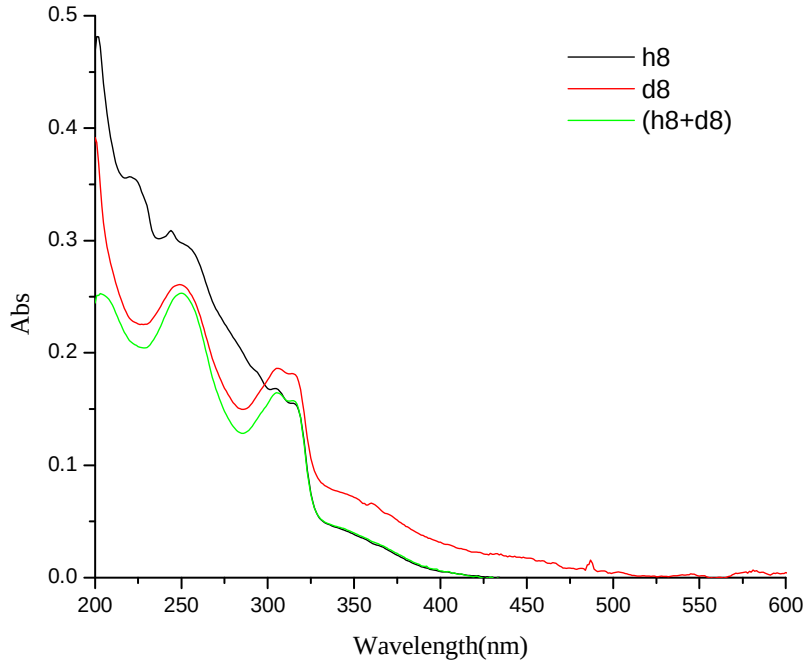

Figure 6. Absorption spectra of h8,d8 & (h8+d8) $[Ir^{III}(bpy\text{-}N,N')_2(bpy\text{-}C,N')^-]^{2+}$ in spectrometric grade ACN (Conc. 1.05 $x10^{-4}$ moles/lit).

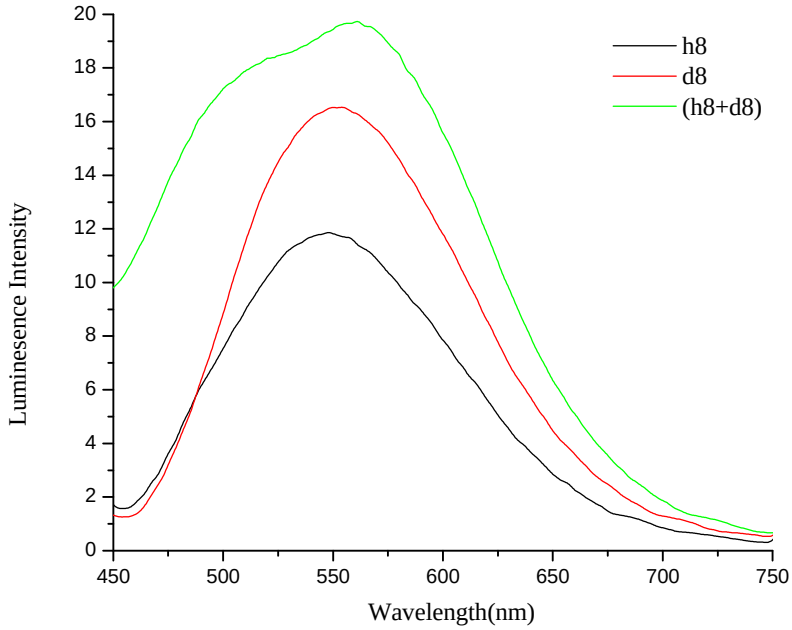

Figure 7. Emission spectra of h8,d8 & (h8+d8) $[Ir^{III}(bpy\text{-}N,N')_2Cl_2]^+$ taken in spectrometric grade ACN at an excitation wavelength of 390nm (Conc. 1.37 $x10^{-4}$ moles/lit).

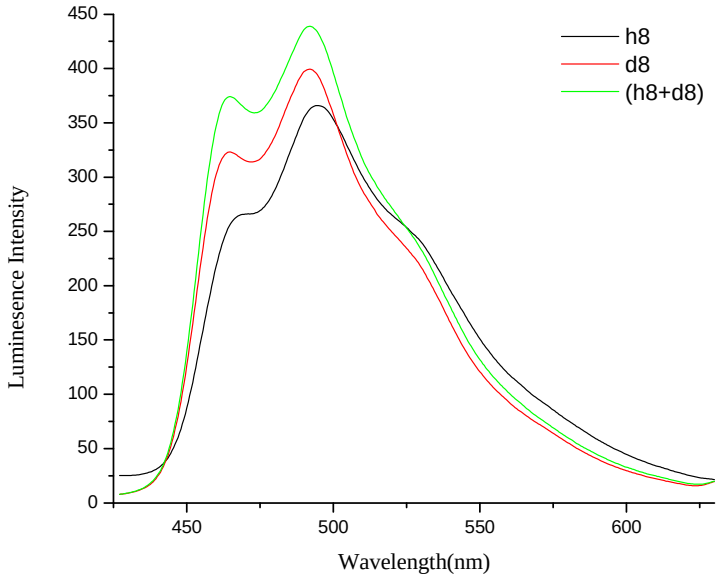

Figure 8. Emission spectra of h8,d8 & (h8+d8) $[Ir^{III}(bpy\text{-}N,N')_2(bpy\text{-}C,N')^-]^{2+}$ in spectrometric grade ACN excited at a wavelength of 310nm (Conc. 1.05 $x10^{-4}$ moles/lit).

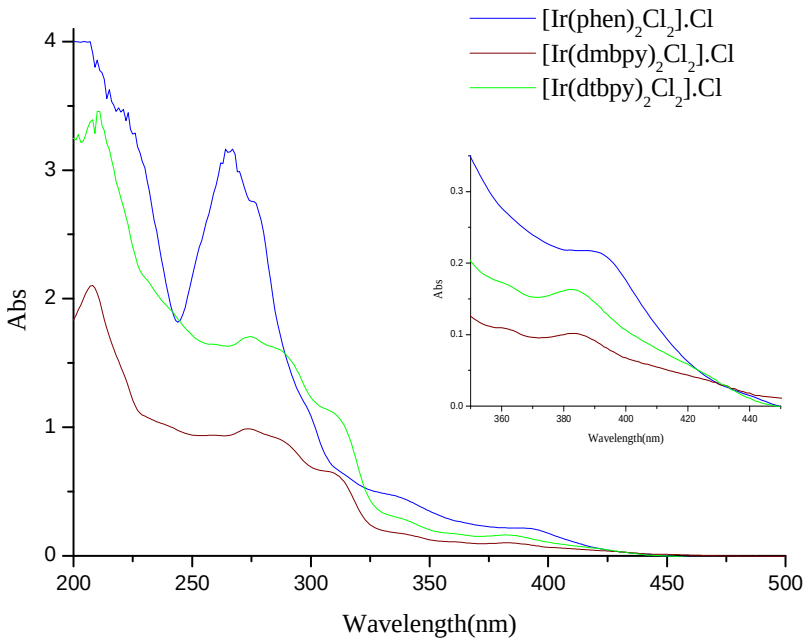

Figure 9. Absorption spectra of **III**, **IV** and **V** taken in spectrometric grade ACN.

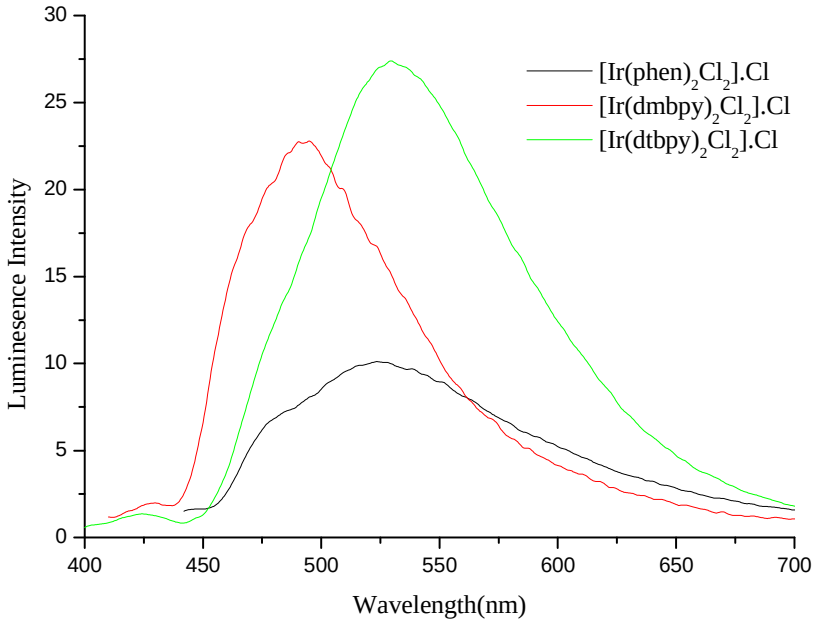

Figure 10. Emission spectra of **III**, **IV** and **V** in spectrometric grade ACN

Table 2.

$[Ir(bpy)_2Cl_2]^+$	Absorption λ_{abs} (nm) ε ($LM^{-1}cm^{-1}$)x 10^3	Emission λ_{max}(nm), λ_{ex}(nm)
h8	239(17.90), 280(17.99), 302(1.52), 380(1.73)	548, 380
d8	239(18.12), 280(18.67), 302(15.15), 380(1.62)	554, 380
(h8+d8)	239(18.19), 280(18.28), 302(15.07), 380(1.69)	561, 380

Table 3.

$[Ir(bpy)_2(bpy)^-]^{2+}$	Absorption λ_{abs} (nm) ε ($LM\text{-}^1cm^{-1}$)x 10^3	Emission λ_{max}(nm), λ_{ex}(nm)
h8	296(1.68), 310(1.50), 357(1.74)	495, 310
d8	304(1.77), 310(1.74), 350(1.50)	492, 310
(h8+d8)	300(1.46), 310(1.50), 355(1.61)	492, 310

Table 4.

Complex	Absorption λ_{abs} (nm) ε ($LM\text{-}^1cm^{-1}$)x 10^3	Emission λ_{max}(nm), λ_{ex}(nm)
$[Ir^{III}(phen)_2Cl_2]^+$	265(39.85), 275(34.86), 338(5.87), 390(2.74)	524, 390
$[Ir^{III}(dmbpy)_2Cl_2]^+$	275(13.67), 311(8.73), 341(2.38), 385(1.39)	492, 385
$[Ir^{III}(dtbpy)_2Cl_2]^+$	274(23.52), 308(15.44), 340(3.98), 383(2.22)	530, 383

Life Time Measurements

The life time of the complexes seemed to increase with deuteriation as mentioned in publications from our group before.[39] The experiments are carried out using Laser and the samples are completely deaerated by passing with nitrogen to avoid the quenching. The results are put together below.

Complex	**Excited State Life Time**
h8 – $[Ir(bpy)_2Cl_2]^+$	330ns
d8 – $[Ir(bpy)_2Cl_2]^+$	740ns

h8+d8 – $[Ir(bpy)_2Cl_2]^+$	497ns
h8-$[Ir^{III}(bpy\text{-}N,N')_2(bpy\text{-}C,N')^-]^{2+}$	976ns
d8-$[Ir^{III}(bpy\text{-}N,N')_2(bpy\text{-}C,N')^-]^{2+}$	1.33μs
(h8+d8)-$[Ir^{III}(bpy\text{-}N,N')_2(bpy\text{-}C,N')^-]^{2+}$	1.06μs
$[Ir(phen)_2Cl_2]^+$	411ns
$[Ir(dmbpy)_2Cl_2]^+$	917ns
$[Ir(tbbpy)_2Cl_2]^+$	270ns

Conclusion

The formation of $[Ir^{III}(bpy\text{-}N,N')_2Cl_2]^+$ and $[Ir^{III}(bpy\text{-}N,N')_2(bpy\text{-}C,N')^-]^{2+}$ have been confirmed by ^1H NMR, HPLC, UV-Vis and emission studies. The possible mechanistic significance of C coordination for reactions of Ir(III)-bipyridine complexes and the ratio of normal and orthometalated complex formed is discussed. The time dependent HPLC and NMR data gave us promising results on the mechanistic pathway for the synthesis of the title complexes. The luminescence lifetimes of $[Ir^{III}(bpy\text{-}N,N')_2Cl_2]^+$ and $[Ir^{III}(bpy\text{-}N,N')_2(bpy\text{-}C,N')^-]^{2+}$ complexes are long in liquid solutions. In view of their long lifetimes these complexes are excellent candidates for high-energy sensitizers.[33] A second possible application of these complexes could be in a flash pumped dye laser. Transition metal complexes containing ligands with extended π-systems (eg., pyridine, bipyridine) have generated tremendous interest because of their potential to participate as photocatalysts in solar-driven artificial photoconversion processes.[34,35,36,37,38] Iridium complexes reported here can easily coordinate water directly to the metal. Excitation of these species could lead to charge transfer to bpy, and, perhaps, reduction of coordinated water to a hydrogen atom. The novel substituted 2,2'-bipyridine Iridium complexes that we made **III**, **IV** and **V** , which we expect to be good candidates for Organic Light Emitting Devices (OLED's).

References

1. Watts, R. J.; Harrington, J. *S.;* Van Houten, J. *J. Am. Chem. Soc.* **1977**,99, 2179**.**
2. Ballardini, R.; Varani, G.; Moggi, L.; Balzani, V. *J. Am. Chem. Soc.* **1977**, 99, 6881.
3. B. Patrick Sullivan, B.; Thomas, J. M. *J. Chem. Soc., Chem. Commun.* **1984**, *403.*

4. Kahl, J. L.; Hanck, K. W.; DeArmond, K. *J. Phys. Chem.* **1979**, *83, 2606.*
5. Kahl, J. L.; Hanck, K. W.; DeArmond, K. *J. Phys. Chem.* **1978**, *82, 540.*
6. (a) Muir, M. M.; Luang, W. L. *Inorg. Chem.* **1973**, 12, 1930. (b) Broomhead, J. A.; Grumley, W. *Inorg. Chem.* **1971**,10, 2002. (c) Berka, L, H.; Philippon, G, E. *J.* *Inorg. Nucl. Chem.* **1970**, 32, 3355. (d) Divisia, B,; Ford, P. C.; Watts, R. J. *J. Am. Chem.Soc.* **1980**, 102, 7264.
7. (a) Watts, R. J.; Efrima, S.; Metrie, H. *J. Am. Chem. Soc.* **1979**, 101, 2742. (b) DeArmond, M. K.; Hills, J. E. *J. Chem. Phys.* **1971**, 54**,** 2247 (c) Ohashi, Y.; Kobayashi, T. *Bull. Chem. Soc. Jpn.***1979**, 52, 2214 (d) Cremers, T. L.; Crosby, G. A. *Chem. Phys.Lett.* **1980**, 73, 541.
8. (a) Marnot, P. A.; Ruppert, R. R.; Sauvage, J. *Nouv. J. Chim.***1981**, *5,* 543 (b) Hawecker, J.; Lehn, J. M.; Ziessel, R. J. *Chem. Soc., Chem. Commun.* **1983**, 531.
9. Gillard, R. D.; Heaton, B. T. *J. Chem. Soc.* A, **1969**, 451
10. Chisweli, B.; Livingstone, S. E.; *J. Inorg. Nucl. Chem.* **1964,** 26, 47**.**
11. Watts, R. J.; Crosby, G. A. *J. Am. Chem. Soc.* **1971,** 93, 3184.
12. De Simone, R. E.; Drago, R. S. *lnorg. Chem.* **1969,** 8, 2517.
13. Fiynn, C. M.; Demas, J. N. *J. Am. Chem. Soc.***1974**, 96, 1959; **1975**, 97, 1988.
14. Nord, G.; Hazell, A. C.; Hazell, R. G.; Farver, O. *Inorg. Chem*. **1983**, 22, 3429.
15. Gillard, R. D.; Lancashire, R**.** J.; Williams, P. A. *J. Chem.* Soc., *Dalton Trans.* **1979,** 193, 3429.
16. Wickramasinghe, W. A.; Bird, P. H.; Serpone, N. *J. Chem. Soc., Chem.Commun.* **1981,** 1284.
17. Watts, R. J.; Spellane, P. J. *Inorg. Chem*. **1981**, 20, 3561.
18. Martin, B.; Nord, G. *J. Chem.* Soc**. 1958**, 4284.
19. Kahl, J. L.; Hanck, K.; DeArmond, K. *J. Inorg. Nucl. Chem.* **1979**, 41, 495.
20. Farver, 0.; Monsted, O**.** Nord, G. *J. Am. Chem. Soc.* **1979**, 201, 6118.
21. Coombe, V. T.; Heath, G. A.; MacKenzie, A. J. *Inorg Chem*. **1984**, 23, 3423.
22. Garces, F. O.; Watts, R. J. *Inorg. Chem*. **1990**, 29, 582.
23. Broomhead, J. A.; Grumley, W. *J. Chem. Soc., Chem. Commun*, **1968**, 1211.
24. Ballardini, R.; Varani, G.; Moggi, L.; Balzani, V.; Olson, K. R.; Scandola, F.; Hoffman, M. Z. *J. Am. Chem. Soc*. **1975**, *97,* 728.
25. Watts, R. J.; White, T. P.; Griffith, B. G. *J. Am. Chem. Soc*. **1975**, 97, 6914.
26. Watts, R. J.; Missimer, D. *J. Am. Chem. Soc*. **1978**, *100,* 5350.
27. Crosby, G. A.; Watts, R. J.; Carstens, D. H. W. *Science*. **1970**, 170, 1195.
28. Lee, J. R.; Liou, Y. R.; Huang, W. L. *Inorganica Chimica Acta*. **2001**, 319, 83.
29. Watts, R. J. *J. Am. Chem. Soc*. **1974**, 96, 6186.
30. Watts, R. J.; Brown, M. J.; Griffith, B. G.; Harrington, J. S. *J. Am.Chem. Soc*. **1975**, 97, 6030.
31. Bosnich, B. *Acc.Chem. Res.* **1969**, *2,* 266.
32. Braterman, P. S.; Heath, G. A.; MacKenzie, A. J.; Noble, B. C.; Peacock, R. D.; Yellowlees, L. J. *Inorg. Chem.* **1984**, 23, 3425.
33. Watts, R. J.; Harrington, J. S.; Van Houten, J., *J. Am. Chem. Soc.* **1977**, 99, 2179**.**
34. Garces, F. O.; King, K. A.; Watts, R. J., *Inorg. Chem*. **1988**, 27, 3464.
35. Lowry, M. S.; Hudson, W. R.; Pascal, R. A.; Bernhard, S. *J. Am. Chem.Soc.* **2004**, 126, 14129.

36. Goldsmith, J. I.; Hudson, W. R.; Lowry, M. S.; Anderson, T. H.; Bernhard, S. *J. Am. Chem.Soc.* **2005**, 127, 7502.
37. Lowry, M.S.; Goldsmith, J. I.; Slinker, J. D.; Rohl, R.; Pascal, R. A.; Malliaras, G. G.; Bernhard, S., *Chem. Mater*. **2005,** 17, 5712.
38. Cline, E. D.; Adamson, S. E.; Bernhard, S. *Inorg. Chem*. **2008**, 47, 10378.
39. Browne, R. B.; Vos, G. J. *Coordination Chemistry Reviews*. **2001**, 219, 761.

Supplementary Datas

NMR Spectrum of d8 & (h8+d8) $[Ir^{III}(bpy\text{-}N,N')_2Cl_2]^+$

The nmr specrtrum of complexes are measured in 400MHz instrument using DMSO in which all of them are completly soluble.

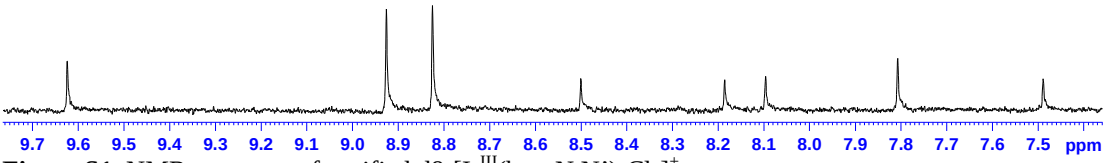

Figure S1. NMR spectrum of purified d8-$[Ir^{III}(bpy\text{-}N,N')_2Cl_2]^+$

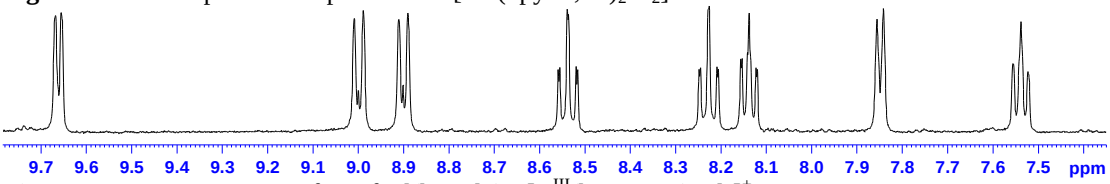

Figure S2. NMR spectrum of purified(h8+ d8) - $[Ir^{III}(bpy\text{-}N,N')_2Cl_2]^+$

NMR Spectrum of d8 & (h8+d8) $[Ir^{III}(bpy\text{-}N,N')_2(bpy\text{-}C,N')^-]^{2+}$

The nmr specrtrum of complexes are measured in 600MHz instrument using DMSO in which all of them are completly soluble.

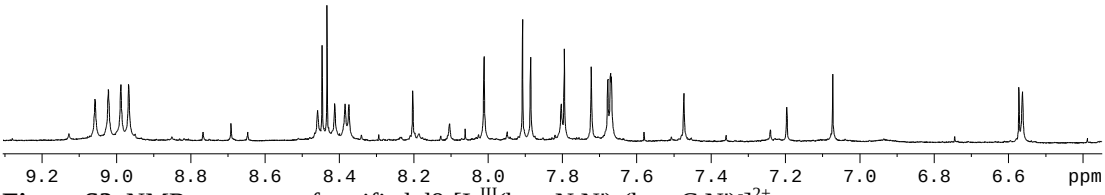

Figure S3. NMR spectrum of purified d8-$[Ir^{III}(bpy\text{-}N,N')_2(bpy\text{-}C,N')^-]^{2+}$

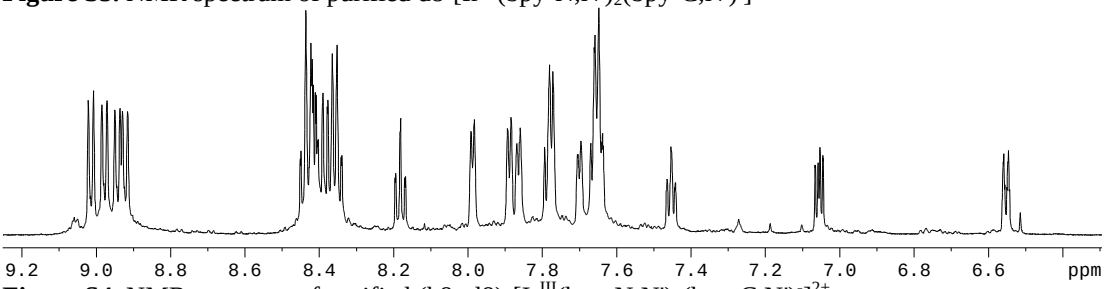

Figure S4. NMR spectrum of purified (h8+d8)-$[Ir^{III}(bpy\text{-}N,N')_2(bpy\text{-}C,N')^-]^{2+}$

COSY Spectrum of h8-$[Ir^{III}(bpy\text{-}N,N')_2Cl_2]^+$ & h8-$[Ir^{III}(bpy\text{-}N,N')_2(bpy\text{-}C,N')^-]^{2+}$

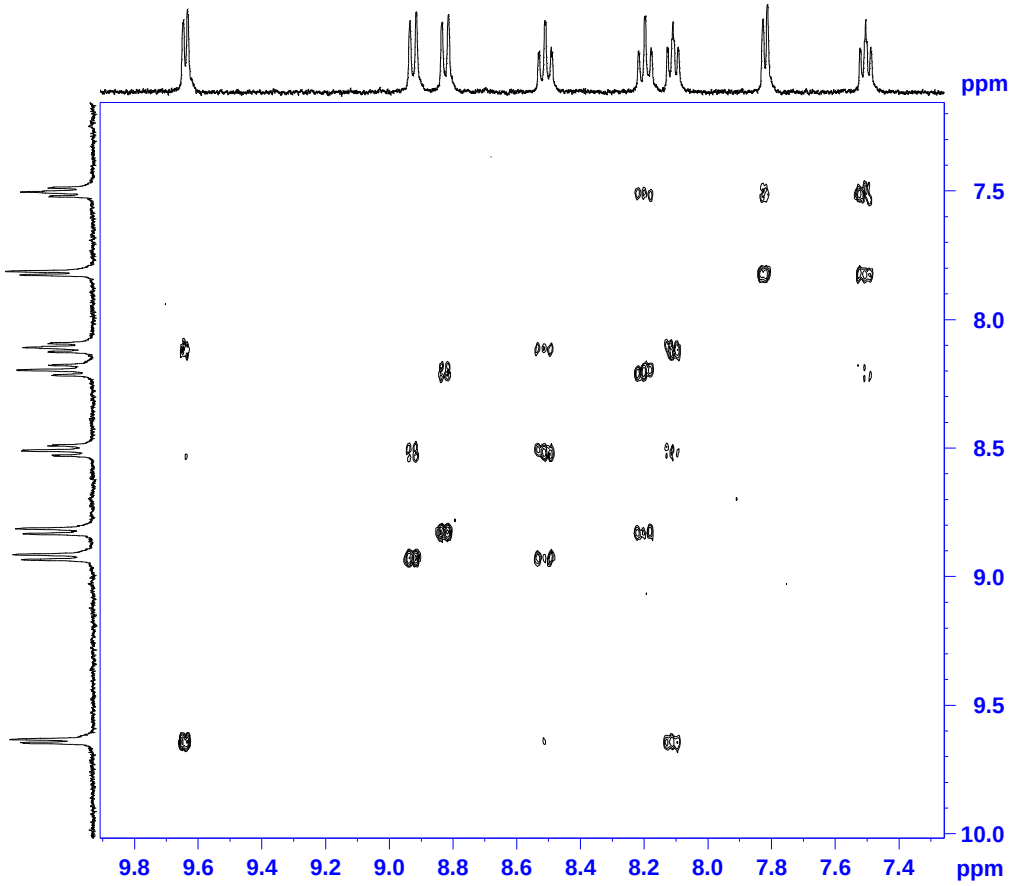

Figure S5. COSY spectrum of purified h8-$[Ir^{III}(bpy\text{-}N,N')_2Cl_2]^+$ taken in deuteriated DMSO.

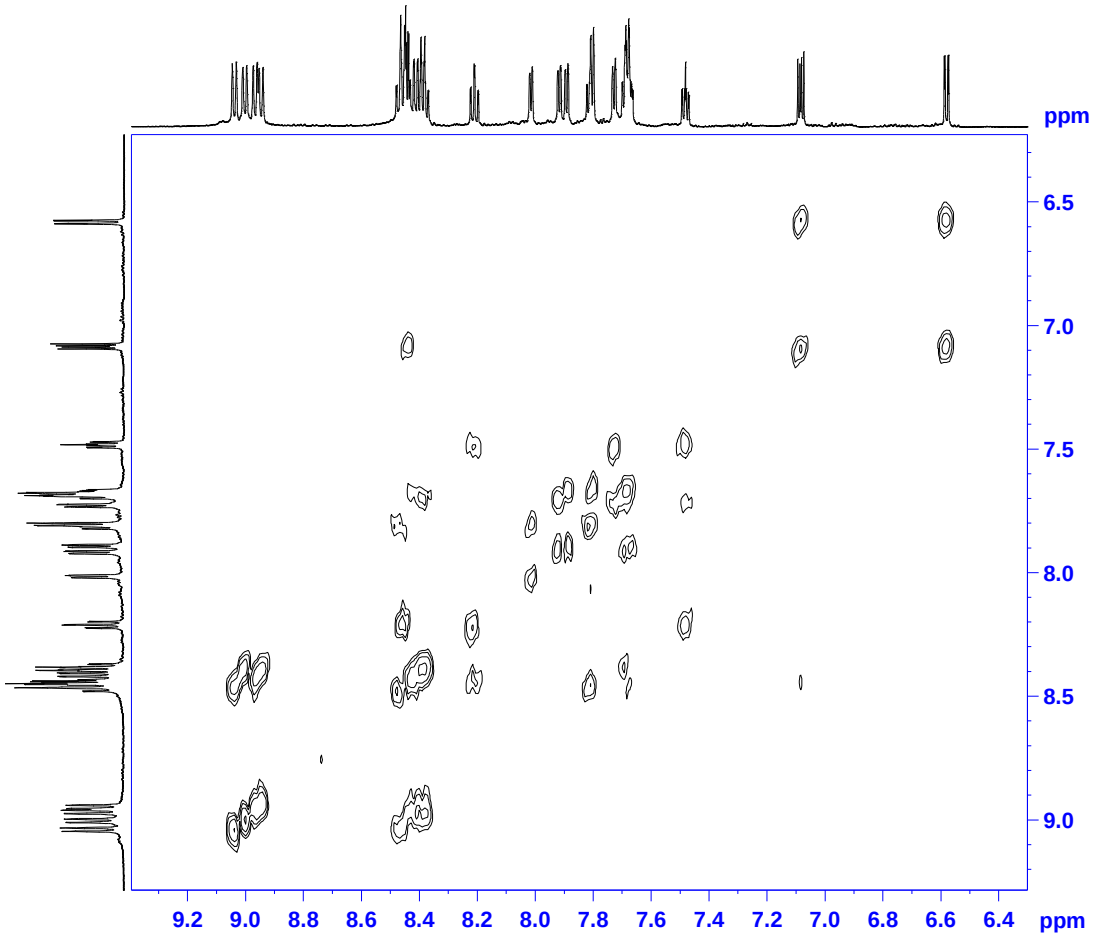

Figure S6. COSY spectrum of purified h8-[Ir^{III}(bpy-N,N')$_2$(bpy-C,N')$^-$]$^{2+}$ taken in deuteriated DMSO.

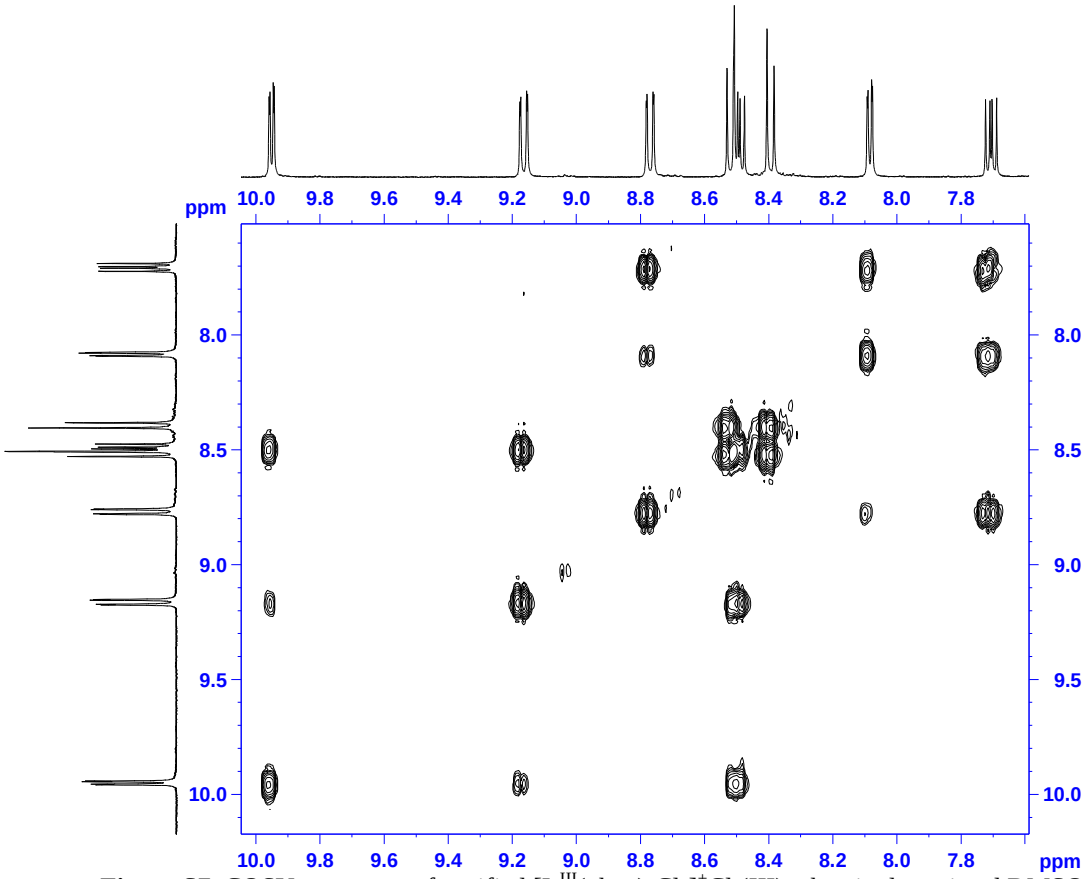

Figure S7. COSY spectrum of purified $[Ir^{III}(phen)_2Cl_2]^+Cl$ (III) taken in deuteriated DMSO.

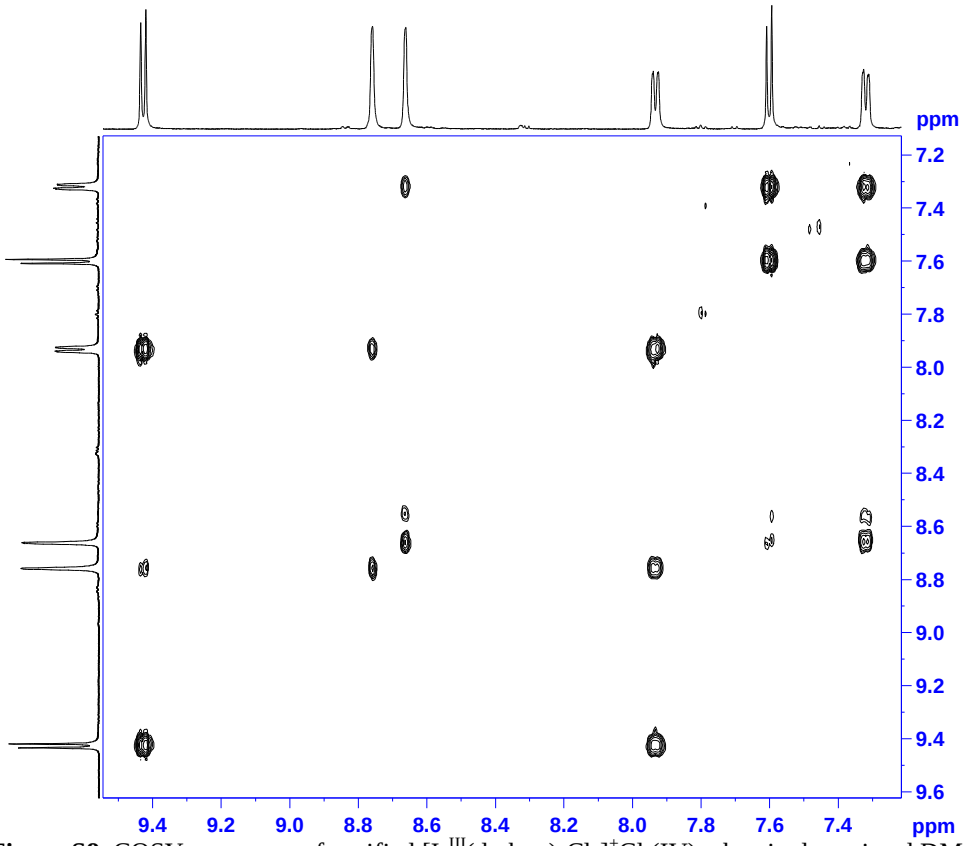

Figure S8. COSY spectrum of purified $[Ir^{III}(dmbpy)_2Cl_2]^+Cl$ (IV) taken in deuteriated DMSO.

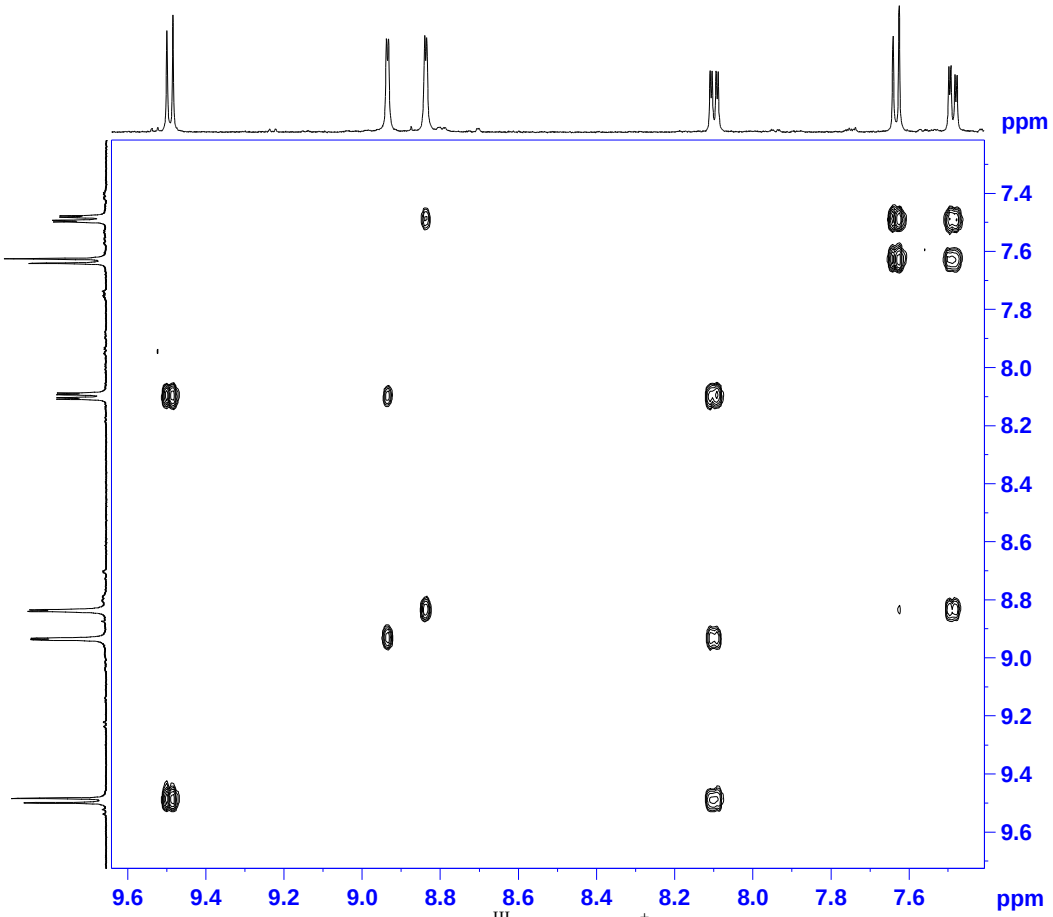

Figure S9. COSY spectrum of purified $[Ir^{III}(dtbpy)_2Cl_2]^+Cl$ (V) taken in deuteriated DMSO.

Time Dependent Study of the reaction mechanism of $IrCl_3$ with h8 bpy using HPLC and NMR

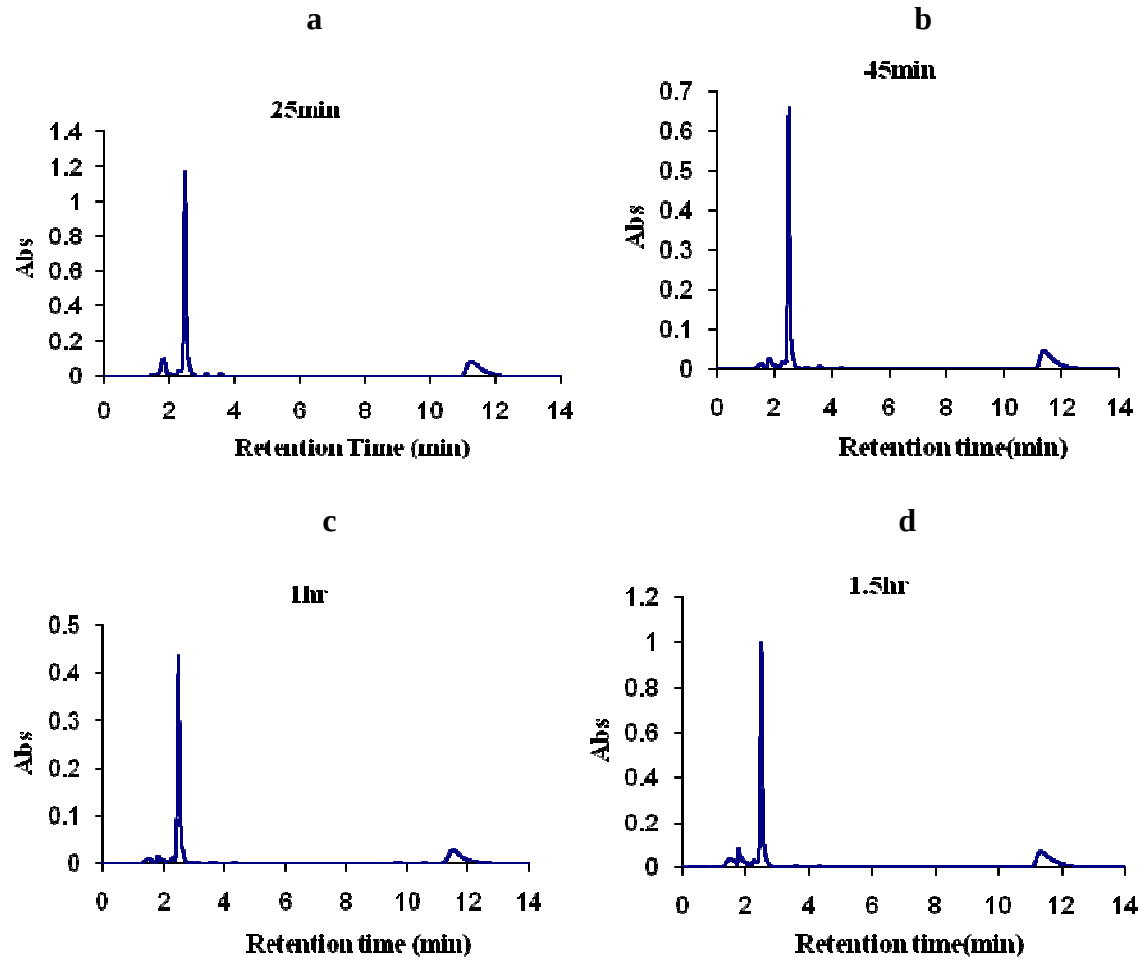

Figure S10. Time dependent HPLC data for reaction of $IrCl_3$ with h8 bpy at different time intervals ranging from 25min to 1.5hour. a) 25min b) 45min c)1hr d) 1.5hr.

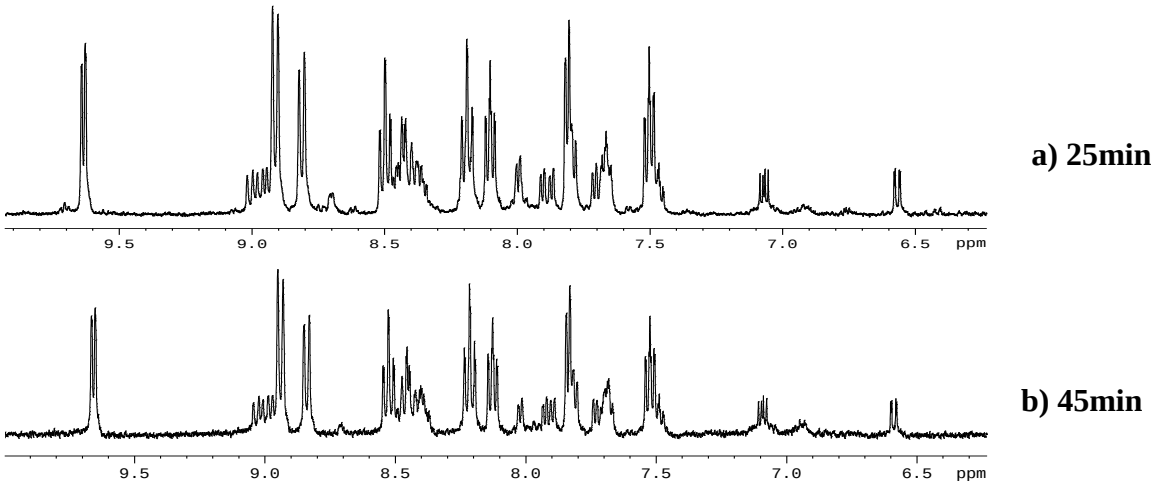

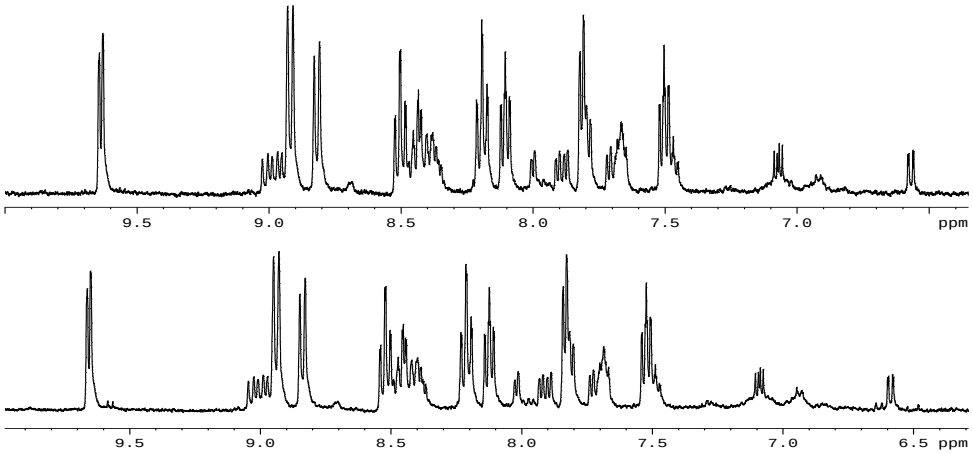

Figure S11. Time dependent nmr data for the reaction of $IrCl_3$ with h8 bpy at different time intervals ranging from 25min to 1.5hour. a) 25min b) 45min c) 1hr d) 1.5hr.

HPLC Measurements

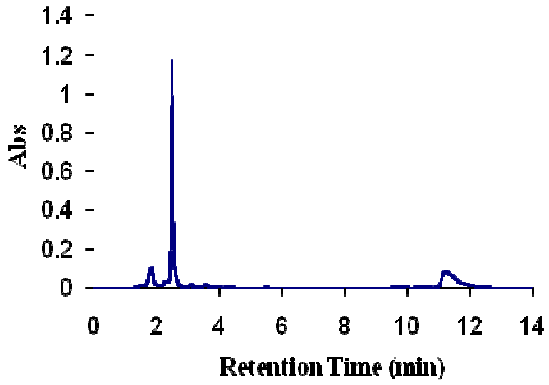

Fig S12.HPLC plot of h8-$[Ir^{III}(bpy\text{-}N,N')_2Cl_2]^+$directly from reaction mixture.

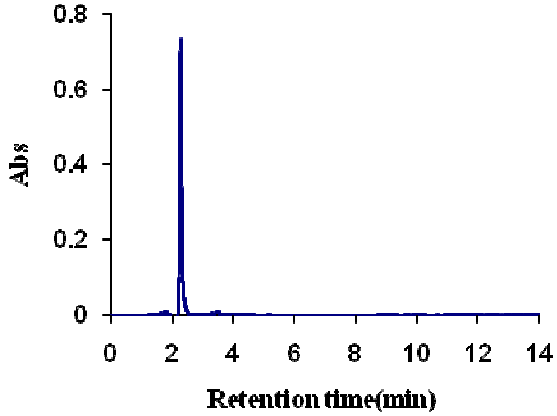

Fig S13. HPLC plot of purified h8-$[Ir^{III}(bpy\text{-}N,N')_2Cl_2]^+$

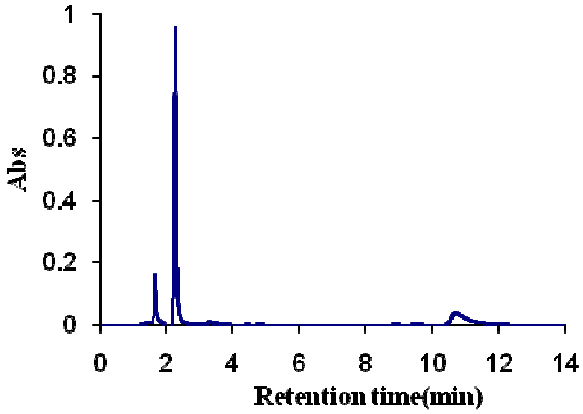

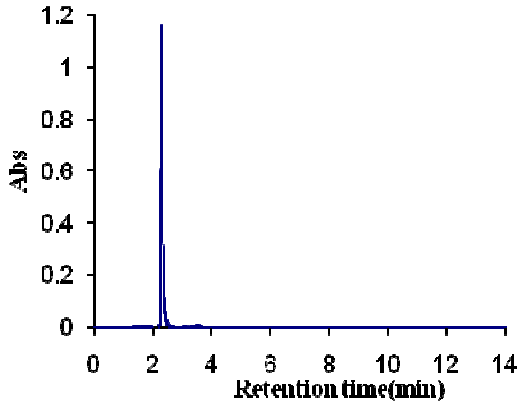

Fig S14.HPLC plot of d8-[Ir^{III}(bpy-N,N')$_2Cl_2$]$^+$directly from reaction mixture.

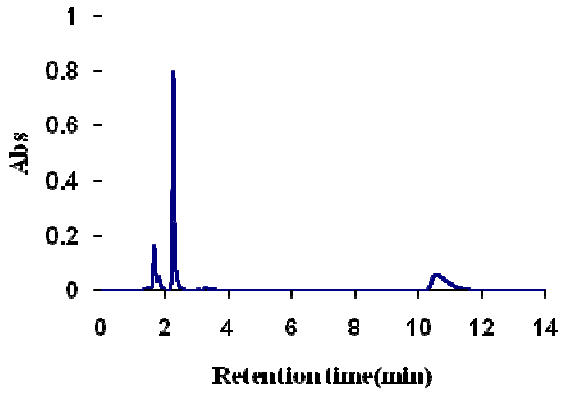

Fig S15. HPLC plot of purified d8-[Ir^{III}(bpy-N,N')$_2Cl_2$]$^+$

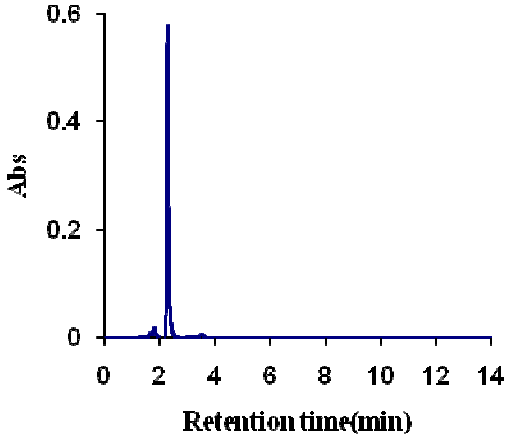

Fig S16.HPLC plot of (h8+d8)-[Ir^{III}(bpy-N,N')$_2Cl_2$]$^+$directly from reaction mixture.

Fig S17. HPLC plot of purified (h8+d8)-[Ir^{III}(bpy-N,N')$_2Cl_2$]$^+$

Life Time Measurements

h8 – [Ir(bpy)$_2$Cl$_2$]

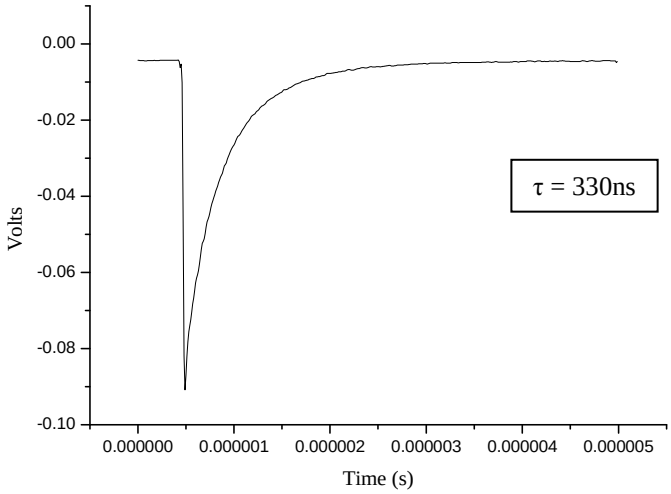

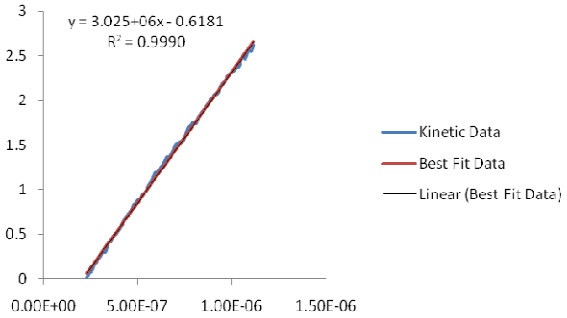

d8 – [Ir(bpy)$_2$Cl$_2$]$^+$

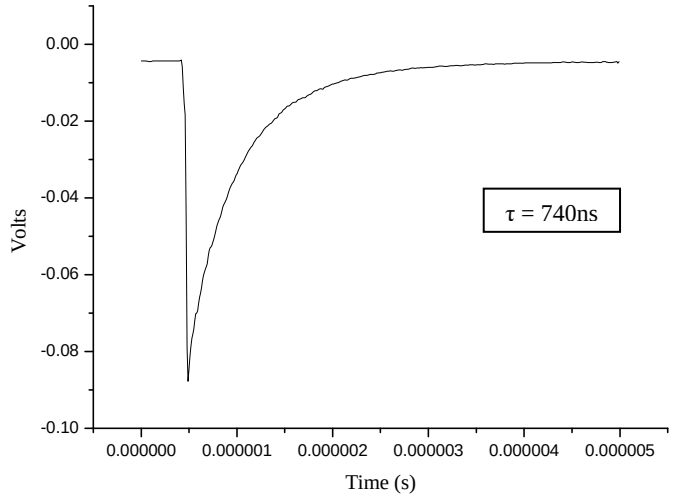

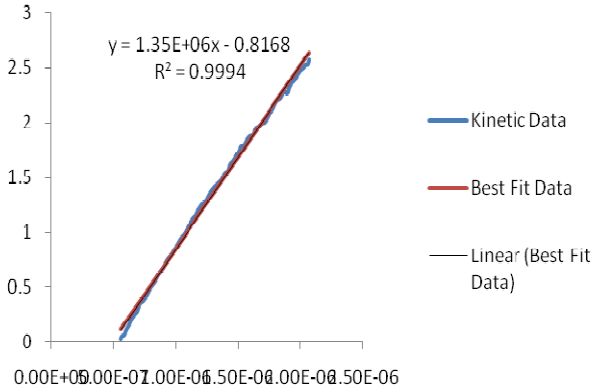

$(h8+d8) – [Ir(bpy)_2Cl_2]^+$

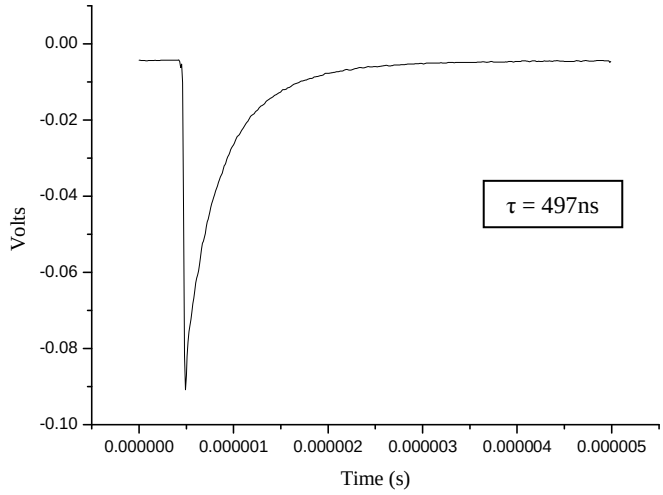

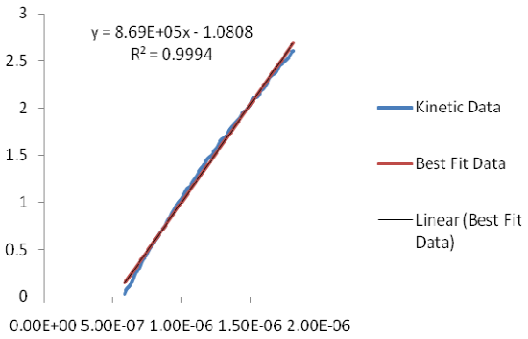

h8-[Ir^{III}(bpy-N,N')$_2$(bpy-C,N')$^-$]$^{2+}$

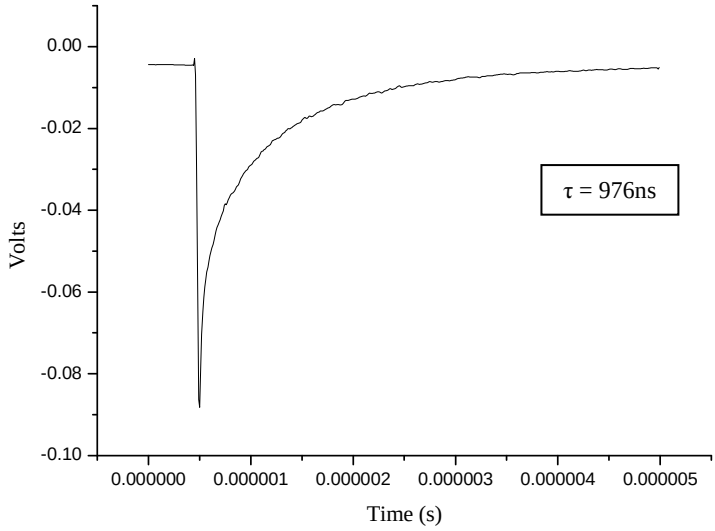

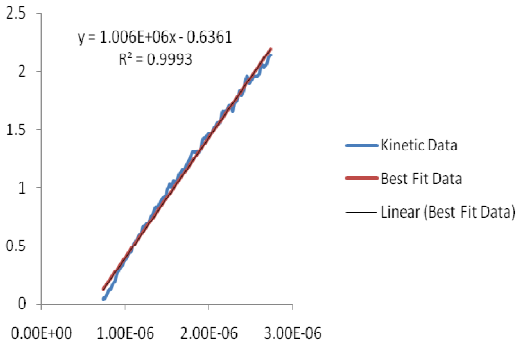

d8-[$Ir^{III}(bpy\text{-}N,N')_2(bpy\text{-}C,N')^-]^{2+}$

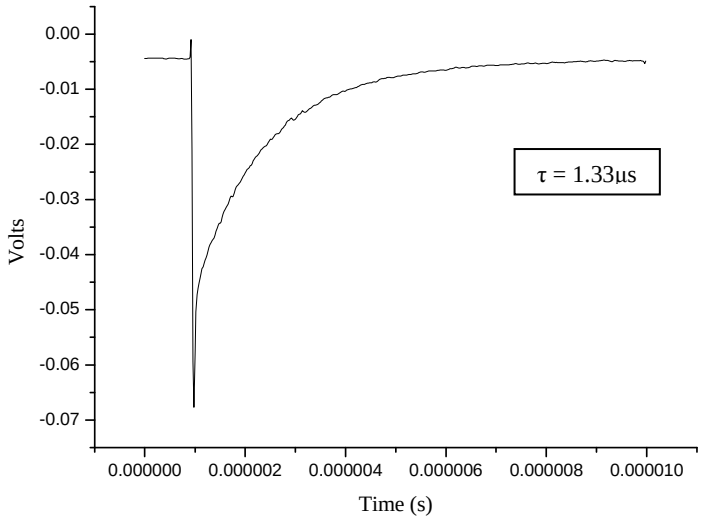

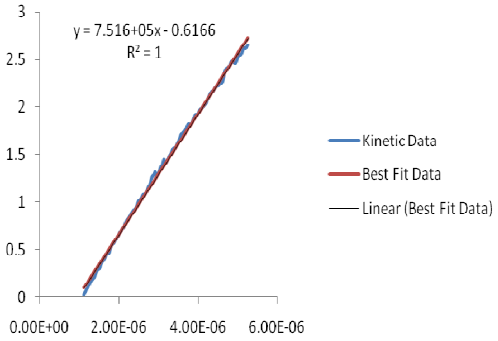

(h8+d8)-[$Ir^{III}(bpy\text{-}N,N')_2(bpy\text{-}C,N')^-]^{2+}$

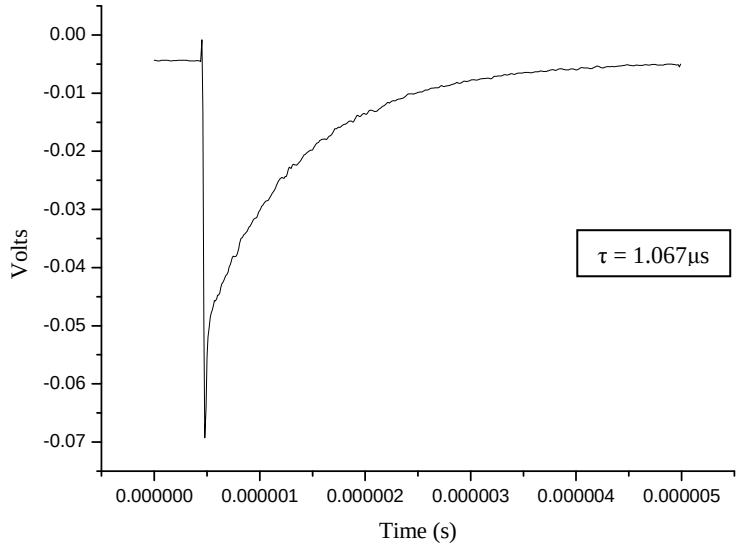

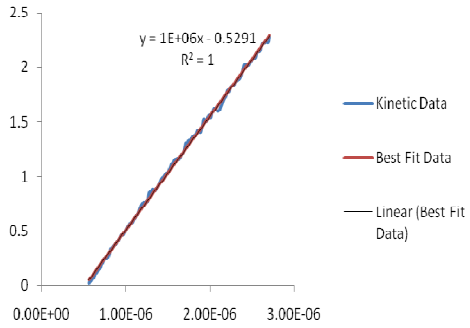

$[Ir(phen)_2Cl_2]^+$

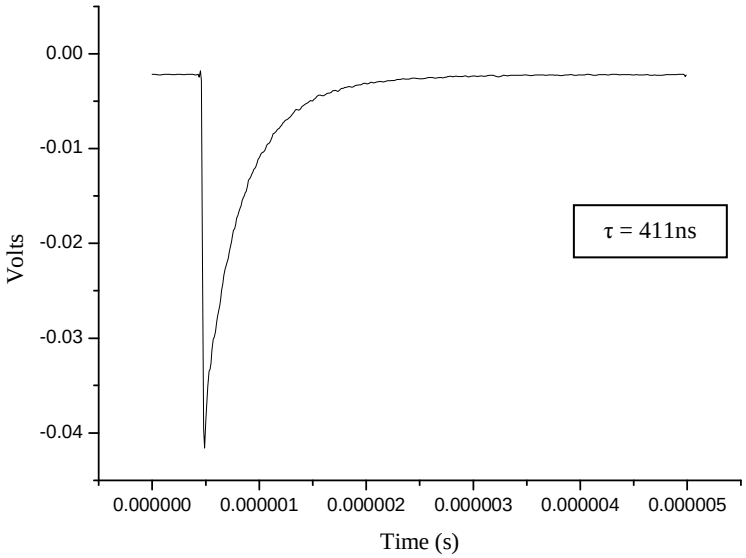

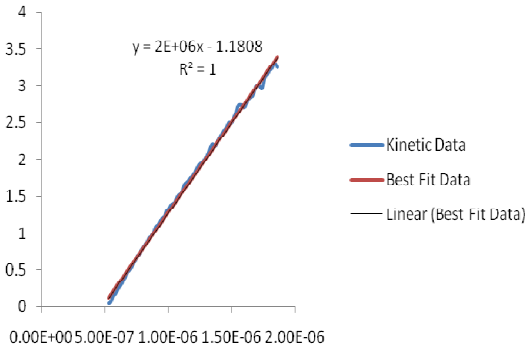

$[Ir(dmbpy)_2Cl_2]^+$

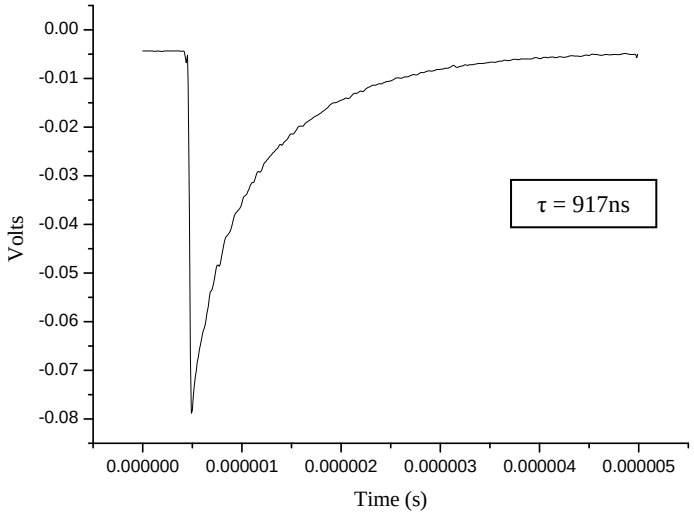
0.00
-0.01
-0.02
-0.03
-0.04
-0.05
-0.06
-0.07
-0.08
Volts
0.000000
0.000001
0.000002
0.000003
0.000004
0.000005
Time (s)
τ = 917ns

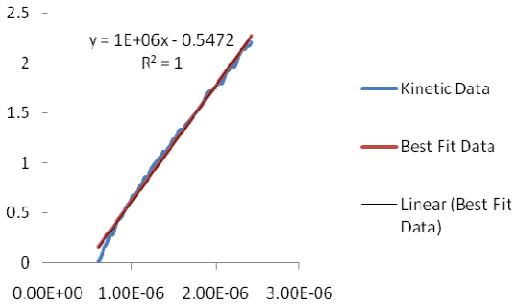
2.5
2
1.5
1
0.5
0
0.00E+00
1.00E-06
2.00E-06
3.00E-06
y = 1E+06x - 0.5472
R² = 1
Kinetic Data
Best Fit Data
Linear (Best Fit Data)

$[Ir(dtbpy)_2Cl_2]^+$

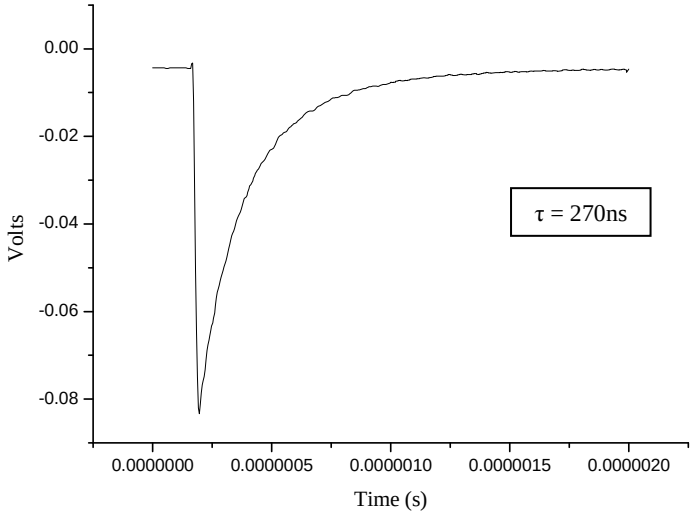

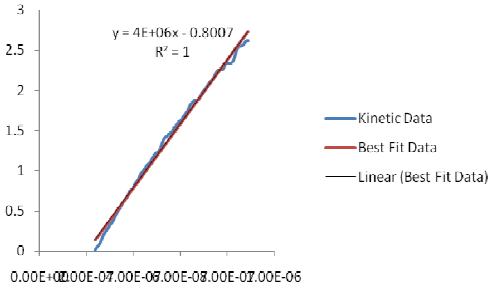

SOMO delocalisation in mixed valent Ruthenium Polypyridyl complexes through CD spectroelectrochemistry

Hamid Ahmed,[a] Nadia Coburn,[a] Danilo Dini,[a] Wesley R. Browne,[b] Jaap J. D. de Jong,[b] Claudio Villani,[c] Ben. L. Feringa[b], Johannes G. Vos[a]

[a]*National Centre for Sensor Research, School of Chemical Sciences, Dublin City University, Dublin 9, Ireland*

[b]*Organic and Molecular Inorganic Chemistry, Stratingh Institute, University of Groningen, Nijenborgh 4, 9747 AG, Groningen, The Netherlands. Fax: +31 50 3634296; Tel: +31 50 3634235*

[c]*Dipartimento di Studi di Chimica e Tecnologia delle Sostanze Biologicamente Attive, Universita' degli Studi di Roma "La Sapienza", P.le A. Moro 5 - 00185 Roma, Italy*

RECEIVED DATE (will be automatically inserted after manuscript is accepted)

Circular dichroism (CD) spectroelectrochemistry differentiates the spectral properties of the four diastereoisomers of $\{[Ru(bpy)_2]_2(bpt)\}^{3+}$ (1) [bpy = 2,2'-bipyridyl, bpt = 3,5-bis(pyridiyn-2'-yl)-1,2,4-triazolato anion] and allows the evaluation of the kinetic stability of 1 in the various possible oxidation states of the Ru centers.The extent of SOMO delocalization in $\{[Ru(bpy)_2]_2(bpt)\}^{3+}$ could be also evaluated through CD spectroscopic analysis of each redox state thus allowing new insight into the actual nature of mixed valence states.

Multinuclear transition metal complexes continue to receive widespread attention towards application in molecular based photonic devices such as electroluminescent devices[1] and conducting molecular wires.[2] Ru(II) and Os(II) polypyridyl based systems have formed the vanguard of many of these studies due to their exceptional electrochemical and photophysical properties.[3] The successful application of photonic devices based on transition metal polypyridyl complexes requires an understanding and, ultimately, controlling the nature and extent of interaction between electroactive units in multicomponent devices. With regard to binuclear complexes, of central concern is the strength of direct or ligand-mediated interaction between metal centers in their various oxidation states.

The extent of interaction in the mixed valence state of a bimetallic complex is conventionally described using the classification proposed by Robin and Day as Type I, II, II/III or III.[4] The occurrence of intervalence transfer (IT), i.e. the light induced electron transfer between metal centers, is verified through UV-vis-NIR spectroelectrochemistry. IT is analyzed with the approach of Hush that relates the strength of the metal-to-metal interaction (H_{ab}) and extent of electron delocalization (α^2) with the energy, width and molar extinction coefficient of the IT absorption band.[5] However, there are serious limitations to this approach since the spectral changes associated to an IT transition are not easily recognizable for their generally low intensity and for eventual overlap with absorption bands of other types in the NIR region.[6] In such situations it is difficult to determine unambiguously the features of the IT band and, consequently, assess if the mixed valence state has a localized character.[5] This contribution demonstrates that circular dichroism (CD) spectroscopy[7] can be employed for the analysis of mixed valence states in binuclear complexes. In order to establish the true potential of this spectroscopic technique we have analyzed the CD spectrum of binuclear complex $\{[Ru(bpy)_2]_2(bpt)\}^{x+}$ (**1**) [bpy = 2,2'-bipyridine, bpt = 3,5-bis(pyrid-2'-yl)-1,2,4-triazolato anion, and $3 \leq x \leq 5$, Figure 1], in the mixed valence state Ru(II)/Ru(III) ($x = 4$), which is known to be of the Type II/III.[8]

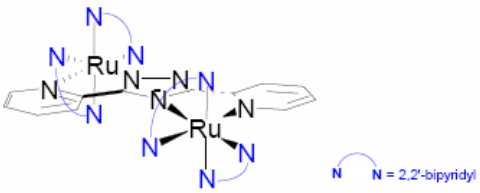

Figure 1. Molecular structure of the Λ,Λ diastereoisomer of $\{[Ru(bpy)_2]_2bpt\}^{3+}$ (**1**). For the complete listing of the different diasteroisomers of complex **1** see SI.

Oxidation of **1** to the mixed valence state and, subsequently, to the fully oxidised Ru(III)/Ru(III) state results in the decrease and broadening of the band at 285 nm that originates from a π-π* transition on bpy ligand, the gradual decrease of the metal-to-ligand charge transfer (MLCT) band at 440 nm, and the appearance of a broad ligand-to-metal charge transfer (LMCT) band at 700 nm (Figure 2). Oxidation of **1** to the Ru(II)Ru(III) state results also in a partial depletion in the ^{1}MLCT bands at 457 nm. The weak band centered at about 1050 nm appears only in the spectrum of Ru(II)/Ru(III) and derives from an IT type transition (Figure 2).[8]

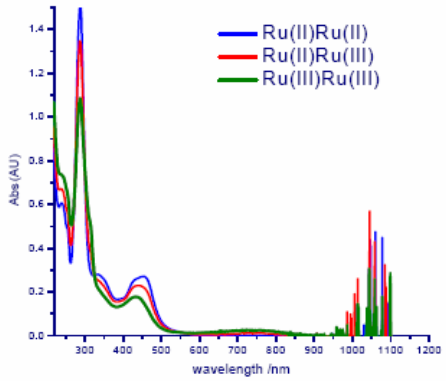

Figure 2. UV-vis-NIR spectroelectrochemistry of the Λ,Λ diastereoisomer of $\{[Ru(bpy)_2]_2(bpt)\}^{3+}$ (**1**).

CD spectra of **1** in the Ru(II)/Ru(II) state (Figure 3) are characterized by strong Cotton effects (CE's) in case of homochiral forms Δ,Δ/Λ,Λ (peaks/troughs at 295, 345, 480 nm, troughs/peaks at 220, 240, 270, 420 nm), and weak CE's for heterochiral isomers Λ,Δ/Δ,Λ (peaks/troughs at 205, 230, 270, 295, 470 nm, troughs/peaks at 240, 340, 400 nm).[7b]

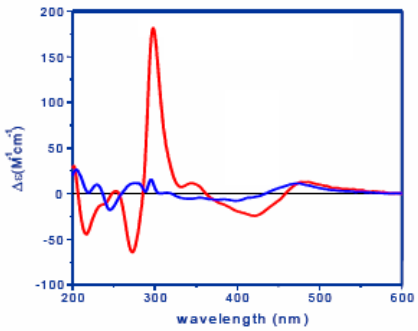

Figure 3. CD spectra of (red line) Δ,Δ and (blue line) Λ,Δ diastereoisomers of $\{[Ru(bpy)_2]_2(bpt)\}^{3+}$ (**1**) [Ru(II)/Ru(II) state]. CD spectra of Λ,Λ and Δ,Λ diastereoisomers of **1** have the opposite sign of the profiles of Δ,Δ and Λ,Δ, respectively.

In terms of chromophores chirality and CD activity, complex $\{[Ru(bpy)_2]_2(bpt)\}^{3+}$ (**1**) bears the inherently dissymmetric groups $(bpy)_2Ru(pyr{:}N_1\text{-}t)$ and $(bpy)_2Ru(pyr{:}N_4\text{-}t)$ ($pyr{:}N_x$-t = moiety of bpt bridging ligand coordinated by Ru through the N_x atom of triazole), and bpy/bpt ligands which are locally achiral but possess chiral character for their placement in an unsymmetrical environment.[9] The CD signals above 300 nm are associated with MLCT/LMCT type transitions from $(bpy)_2Ru(pyr)$ chromophores, whereas signals below 300 nm are related to bpy/bpt ligands centered (LC) transitions.[10] The CD spectra of Δ,Δ/Λ,Λ and Λ,Δ/Δ,Λ pairs of diastereoisomers (Figure 3) present the largest differences at wavelengths below 350 nm, i.e. in the spectral region where LC transitions are predominant.[10] These findings indicate that CD signal of $\{[Ru(bpy)_2]_2(bpt)\}^{3+}$ (**1**) [Ru(II)/Ru(II) state], is sensitive to the relative orientation of the four bpy's with respect to the plane of bpt bridging ligand. The largest variation of CD signal at about 300 nm is observed for the pair of diastereoisomers that do not change the relative orientation of the bpy's upon rotation of 180° around the central axis perpendicular to the triazole ring (Λ,Λ and Δ,Δ, see SI). This indicates that the CE generated by the bpy's surrounding one metal center adds to the CE from the other bpy's group when Λ,Λ/Δ,Δ isomers are considered. The pair of isomers Λ,Δ/Δ,Λ (see SI) displays a weaker CD signal at 300 nm (Figure 3) probably because the CE's generated by the coordination spheres of the two Ru centers are counteracting [bpy's of $Ru(pyr{:}N_1\text{-}t)$ mirror the bpy's of $Ru(pyr{:}N_4\text{-}t)$ in Λ,Δ/Δ,Λ isomers, see SI].[7b] When the Λ,Λ isomer is progressively oxidized a

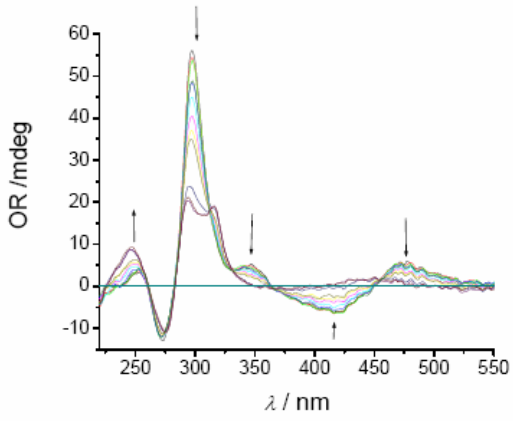

decrease of the main peak at 300 nm is observed together with the flattening of the profile for λ > 350 nm (Figure 4). The intensity of the band at 245 nm increases whereas no detectable CE could be discerned in correspondence of the LMCT band (~700 nm) generated upon Ru oxidation (Figure 4).

Figure 4. Spectral changes of optical rotation (OR) upon progressive conversion of Λ,Λ from the neutral to the mixed valence state. Arrows in correspondence of the peaks indicate the direction of variation of OR with the increase of the applied potential.

Such a signal depauperation at 300 nm indicates an increase of the degree of symmetry in the Λ,Λ isomer of **1** when passing from Ru(II)Ru(II) to Ru(II)Ru(III). This is mainly associated with the rearrangement of the bpy ligands around the oxidized Ru center as a consequence of the augmented positive charge on the metal. It is expected that the bpy's coordinated by the first oxidized center of Λ,Λ isomer tend to mirror the bpy's of the other Ru center when **1** passes from the neutral to the mixed valence state. Similar to neutral Ru(II)Ru(II) (Figure 3), when complex **1** is in the fully oxidized Ru(III)Ru(III) state the stronger CE's are displayed by the homochiral pair of isomers Λ,Λ/Δ,Δ with respect to the heterochiral pair Λ,Δ/Δ,Λ (not shown).

In the mixed valence state the four diasteroisomers of complex **1** show OR spectral profiles with comparable signal intensity in the UV-vis range. In particular, the OR spectra of Λ,Λ and Δ,Λ stereoisomers present a peak at 292 nm and a peak/trough at 317 nm, whereas their profiles almost overlap for λ > 340 nm (Figure 5). Analogous considerations hold when the OR spectra of Λ,Λ and Δ,Λ stereoisomers in the mixed valence state are compared.

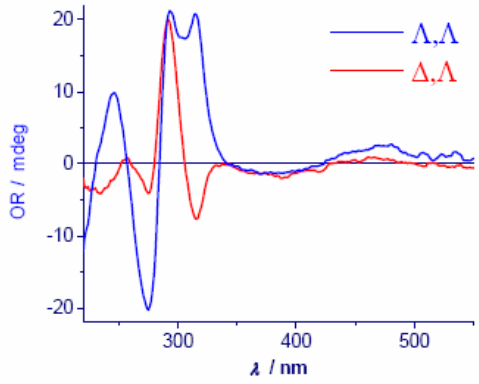

Figure 5. OR spectra of stereoisomers Λ,Λ (bl;ue curve), and Δ,Λ (red curve) in the mixed valence state Ru(II)Ru(III). The OR spectra of Δ,Δ and Λ,Δ diastereoisomers in the mixed valence state (not presented for clarity) have the opposite sign of Λ,Λ and Δ,Λ profiles, respectively.

Characteristic of the presence of Ru(III) in homochiral Λ,Λ (Δ,Δ) is the appearance of the peak (trough) at 317 nm (LC based transition) in the OR spectrum of the mixed valence state (Figure 5). Similar feature is shown by heterochiral Δ,Λ (Λ,Δ) with the observation of a less intense trough (peak) at the same wavelength upon oxidation of one Ru center. It is also found that the formation of the mixed valence state Ru(II)Ru(III) is not accompanied by considerable changes of the CD spectrum of **1** in correspondence of IVCT and LMCT bands. This combination of facts indicates that the SOMO of the mixed valence state[11] of **1** does not present a high degree of delocalization although the interaction between the two metal centers in the Ru(II)/Ru(III) state is strong (H_{ab} = 120 cm^{-1}), and the degree of delocalization calculated from the Hush method appears to be quite large.[8b,12] If the SOMO was delocalized over both metal centers or a hopping mechanism of the hole occurred between the inequivalent N2 and N4 coordination sites then the continuous fluctuation of charge between Ru(II) and Ru(III) would have resulted in a near complete cancellation of the CD spectrum with the averaging of the electronic properties of the two metal centres. The observation of a strong CD signal for both Λ,Λ and Δ,Λ (Figure 5) suggests that not only is the SOMO localized but that the inequivalence between the two sites is sufficient to prevent rapid 'hopping' between the two metal centers. In bimetallic Ru complexes the electrochemical formation of mixed valence states can also induce rapid reactions of linkage isomerism[13] which would result into a stereo-inversion in case of the mono-oxidation of $\{[Ru(bpy)_2]_2(bpt)\}^{3+}$ (**1**) (Figure 1). The differences of the OR spectra of the various isomers in the mixed valence state (Figure 5) reveal that **1** is generally stable with regard to stereo-inversion, isomerisation and ligand exchange as also confirmed by means UV-vis spectroscopy. This finding is particularly significant since it constitutes one of the first statements about the kinetic stability of the bimetallic complexes with Ru(III) towards stereo-inversion and ligand exchange processes. The photostability of the enantiomeric pairs Δ,Δ/Λ,Λ and Λ,Δ/Δ,Λ in the neutral state was followed by HPLC[14] and ^{1}H NMR[7b] upon irradiation at 430 nm. The study confirmed the occurrence of the irreversible transformation Δ,Δ/Λ,Λ→Λ,Δ/Δ,Λ whereas the chiral pair Λ,Δ/Δ,Λ did not undergo any photoisomerisation reaction (see SI).

The present study establishes the usefulness of CD spectroscopy in gaining a deeper insight into the conformational changes that are induced by redox processes in multinuclear complexes. Such a technique proved to be a valid tool for the analysis

of the stability of the complexes towards stereo-inversion in higher oxidation states. We have demonstrated that all four stereoisomers of binuclear complex **1** present distinctive patterns of the CD spectral profiles in the UV range (Figure 5), whereas UV-vis spectroscopy with non polarized light could not be as much sensitive to the nature of the diasteroisomers in their mixed valence state. It has been also recognized that CD spectroscopy has potential in providing information about the actual extent of SOMO delocalisation for those systems which exhibit weak IT bands in the mixed valence state.

Acknowledgments

The authors thank (JJDJ) the Materials Science Centre (MSC) and (WRB) the Dutch Economy, Ecology, Technology (EET) program for financial support.

References

1 (a) Kalyuzhny, G.; Buda, M.; McNeill, J.; Barbara, P.; Bard, A. J. *J. Am. Chem. Soc.* 2003, 125, 6272-6283 (b) Rudmann, H.; Shimada, S.; Rubner, M. F. *J. Am. Chem. Soc.* 2002, 124, 4918-4921; (c) Welter, S.; Brunner, K.; Hofstraat, J. W.; De Cola, L. *Nature* 2003, 421, 54-57 (d) Slinker, J.; Bernards, D.; Houston, P. L.; Abruna, H. D.; Bernhard, S.; Malliaras, G. G. *Chem. Commun.* 2003, 2392-2399.

2 (a) Nishihara, H.; Kanaizuka, K.; Nishimori, Y.; Yamanoi, Y. *Coord. Chem. Rev.* 2007, 251, 2674-2687; (b) Welter, S.; Lafolet, F.; Cecchetto, E.; Vergeer, F.; De Cola, L. *ChemPhysChem* 2005, *6*, 2417-2427; (c) Welter, S.; Salluce, N.; Belser, P.; Groeneveld, M.; De Cola, L. *Coord. Chem. Rev.* 2005, 249, 1360-1371; (d) De Cola, L.; Belser, P. *Coord. Chem. Rev.* 1998, 177, 301-346; (e) Barigelletti, F.; Flamigni, L. *Chem. Soc. Rev.* 2000, 29, 1-12; (f) Harriman, A.; Ziessel, R. *Chem. Commun.* 1996, 1707-1716; (g) Barbieri, A.; Ventura, B.; Barigelletti, F.; De Nicola, A.; Quesada, M.; Ziessel, R. *Inorg. Chem.* 2004; 43, 7359-7368.

3 (a) Juris, A.; Balzani, V.; Barigelletti, F.; Campagna, S.; Belser, P.; Von Zelewsky, A. *Coord. Chem. Rev.* 1988, 84, 85-277; (b) Bignozzi, C. A.; Schoonover, J. R.; Scandola, F. In *Progress in Inorganic Chemistry-Molecular Level Artificial Photosynthetic Materials*; Meyer, G.J., Ed.; Wiley: New York, 1996; Vol. 44, p.1-95; (c) Blanco, M.J.; Jime´nez, M. C.; Chambron, J.C.; Heitz, V.; Linke, M.; Sauvage, J.P. *Chem. Soc. Rev.* 1999, 28, 293-305; (d) Barigelletti, F.; Flamigni, L.; Collin, J.P.; Sauvage, J.P. *Chem. Commun.* 1997, 333-338; (e) Beer, P. D.; Szemes, F.; Balzani, V.; Sala', C. M.; Drew, M. G.; Dent, S. W.; Maestri, M. *J. Am. Chem. Soc.* 1997, 119, 11864-11875; (f) Vos, J.G.; Kelly, J. M. *Dalton Trans.,* 2006, 4869-4883.

4 Robin, M. B.; Day, P. *Adv. Inorg. Chem. Radiochem.* 1967, *10*, 247-422.

5 (a) Hush, N.S. *Prog. Inorg. Chem.* 1967, *8*, 391-444; (b) Hush, N.S. *Electrochim. Acta* 1968, *13*, 1005-1023.

6 Halpin, Y.; Cleary, L.; Cassidy, L.; Horne, S.; Dini, D.; Browne, W.R.; Vos, J.G. *Dalton Trans.,* 2009, 4146-4153.

7 (a) Nakanishi, K.; Berova, N.; Woody, R.W. *Circular Dichroism*; VCH Publishers: New York, 1994; (b) Browne, W.R.; O'Connor, C.M.; Villani, C.; Vos, J.G. *Inorg. Chem.*, 2001, *40*, 5461-5464; (c) Browne, W.R.; Hesek, D.; Gallagher, J.F.; O'Connor, C.M.; Killeen, J.S.; Aoki, F.; Ishida, H.; Inoue, Y.; Villani, C.; Vos, J.G. *Dalton Trans.* 2003, 2597-2602; (d) Eyring, H.; Liu, H.C.; Caldwell, D. *Chem. Rev.* 1968, 68, 525-540; (e) Richardson, F.S.; Riehl, J.P. *Chem. Rev.* 1977, 77, 773-792; (f) Ziegler, M.; Von Zelewsky, A. *Coord. Chem. Rev.* 1998, 177, 257-300.

8 (a) Hage, R.; Dijkhuis, A.H.J.; Haasnoot, J.G.; Prins, R.; Reedijk, J.; Buchanan, B.E.; Vos, J.G. *Inorg. Chem.* 1988, *27*, 2185-2189; (b) Hage, R.; Haasnoot, J.G.; Nieuwenhuis, H.A.; Reedijk, J.; De Ridder, D.J.A.; Vos, J.G. *J. Am. Chem. Soc.* 1990, 112, 9245-9251.

9 Snatzke, G. *Pure Appl. Chem.* **1979**, *51*, 769-785.

10 (a) Krausz, E.; Ferguson, J. In *Progress in Inorganic Chemistry*; Lippard, S.J., Ed.; Wiley: New York, 1989; Vol. 37, p.293-390; (b) Hug, S.J.; Boxer, S.G. *Inorg. Chim. Acta* 1996, 242, 323-327.

11 Browne, W.R.; Hage, R.; Vos, J.G. *Coord. Chem. Rev.* 2006, 250, 1653-1668.

12 Balzani, V.; Juris, A.; Venturi, M.; Campagna, S.; Serroni, S. *Chem. Rev.* 1996, 96, 759-833.

13 Johansson, O.; Lomoth, R. *Chem.Comm.* 2005, 1578-1580.

14 (a) Hughes, H.P.; Martin, D.; Bell, S.; McGarvey, J.; Vos, J.G. *Inorg. Chem.* 1993, 32, 4402-4408; (b) Hughes, H.P.; Vos, J.G. *Inorg. Chem.* 1995, 34, 4001-4003; (c) Gasparrini, F.; D'Acquarica, I.; Vos, J.G.; O'Connor, C.M.; Villani, C. *Tetrahedron: Asymm.* 2000, 11, 3535-3541.

Synopsis (Word Style "SN_Synopsis_TOC"). Authors are required to submit a 75-word synopsis accompanied by a structural diagram or other informative illustration. Synopsis artwork should be in color and designed such that, after reduction, it will fit either a 5 cm × 5 cm or a 12 cm × 5 cm (width × depth) window.

Insert Synopsis artwork here

SUPPLEMENTARY INFORMATION

The structures of the four diastereoisomers of $\{[Ru(bpy)_2]_2(bpt)\}^{3+}$ (**1**) are sketched in Figure SI1.

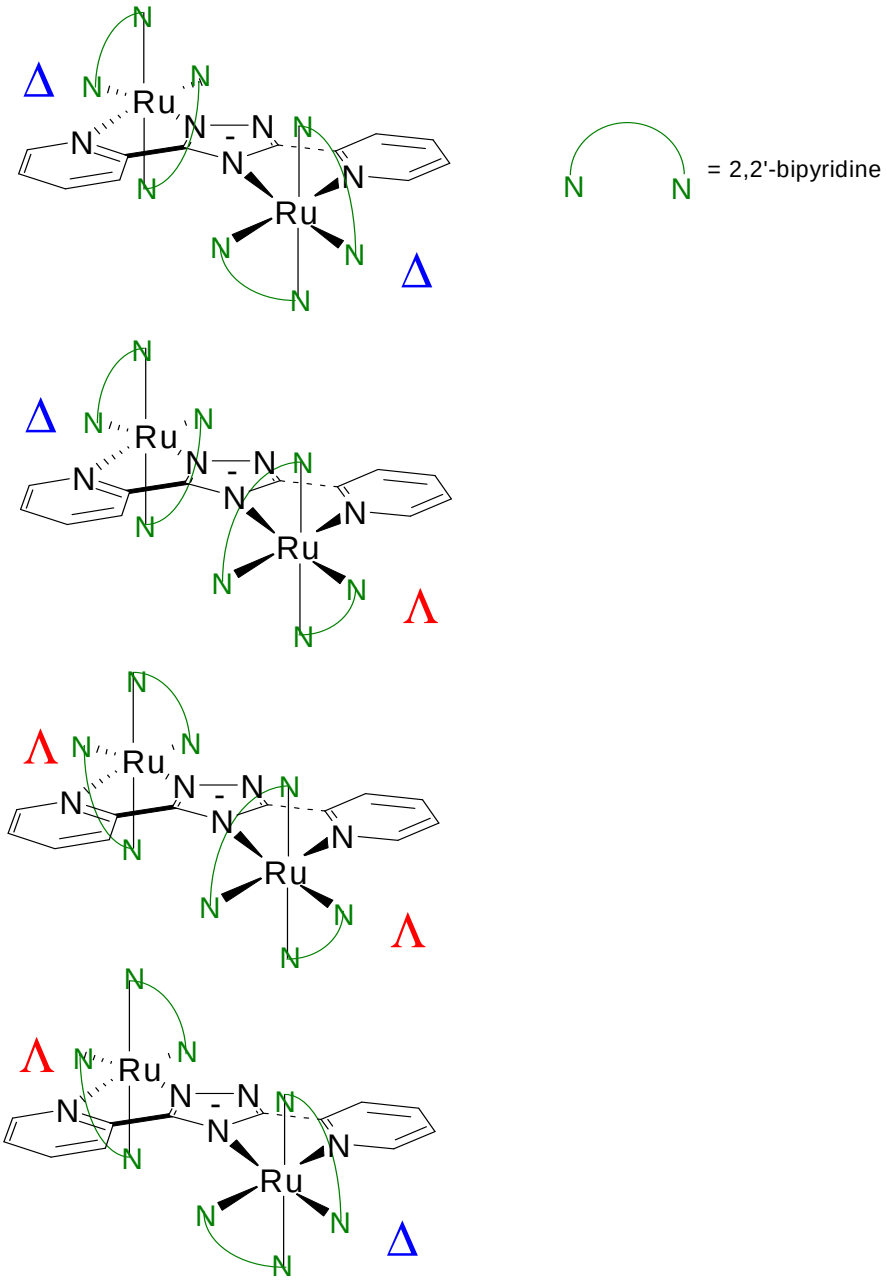

Figure SI1. *From top to bottom, structures of ΔΔ, ΔΛ, ΛΛ and ΛΔ diastereoisomers of complex* ***1****.*

EXPERIMENTAL DETAILS

Preparation and HPLC separation of all four diastereoisomers of **1** (Figure SI1), as well as their CD spectroscopic characterization were reported previously in ref. **SI1** and references therein. UV-vis spectra were taken with a Hewlett-Packard HP 8453 spectrophotometer whilst CD spectra were recorded on a JASCO J-715 spectropolarimeter using Uvasol-grade solvents (Merck). Spectroelectrochemical measurements were performed as described in ref. **SI2** with potential control provided by a CH Instruments CHI630B electrochemical workstation.

After preparation and column chromatography of **1** on alumina with acetonitrile as eluent, compound **1** was recrystallized from acetone:water (2:1) mixture. The recrystallised compound was used for being chromatographed with the Semiprep HPLC *Varian – Prostar* series (Mod.230 and 330).

The chromatogram of ruthenium complex **1** on Luna strong cation exchange (SCX) column from Phenomenex (particle size 5 μm, pore size 100 Å), presents two peaks (fractions A and B, Figure SI2), when mobile phase is constituted by acetonitrile:water mixture (volume ratio 80:20) with KNO_3 0.12 M, and flow rate is 2 cm^3 min^{-1}. The used column is based on a benzene sulfonic acid ligand that constitutes an ion-exchange reversed phase.

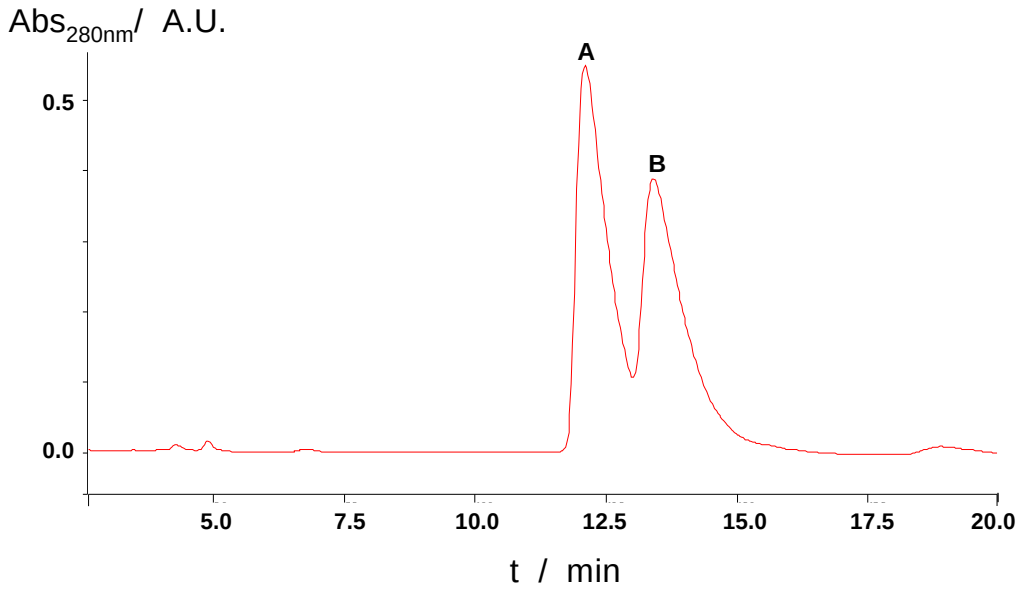

Figure SI2. *Chromatogram of dinuclear complex* $\{[Ru(bpy)_2]_2(bpt)\}^{3+}$ ***(1)*** *on Luna SCX column. On Y-axis the ordinate represents the absorbance of the sample at 280 nm.*

The ^{1}H NMR spectra (Figure SI3) of fractions A and B of $\{[Ru(bpy)_2]_2(bpt)\}^{3+}$ (**1**) in deuteriated acetonitrile are in full agreement with the ^{1}H NMR spectra of complex **1** previously reported [**SI1,SI3**].

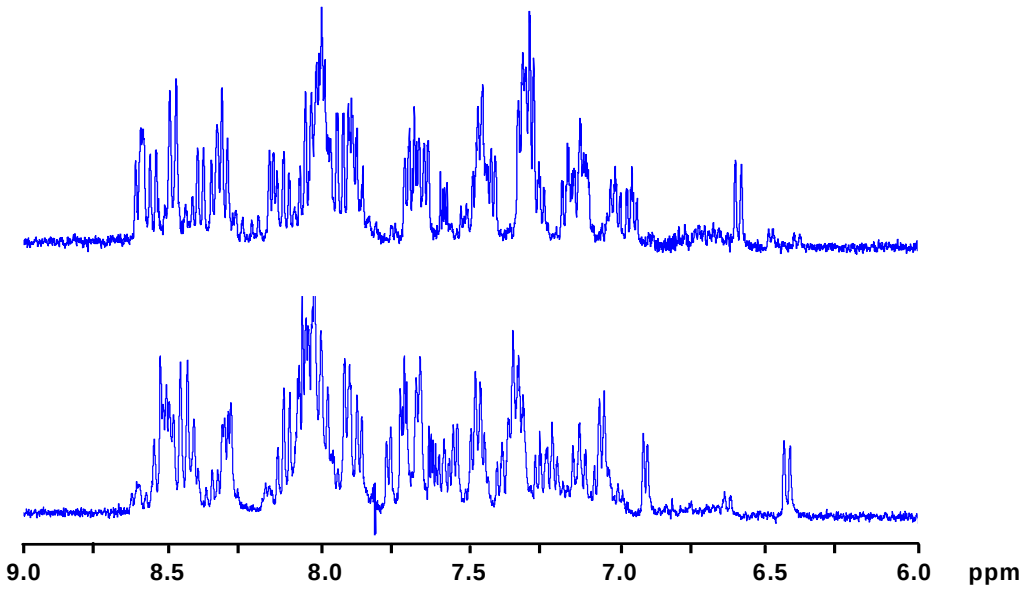

Figure SI3. *^{1}H-NMR spectra of fraction A (upper profile) and fraction B (lower profile) for complex {[Ru(bpy)$_2$]$_2$(bpt)}$^{3+}$ (**1**) in deuteriated acetonitrile.*

The chosen column affords the separation of the two racemic mixtures Λ,Λ/Δ,Δ and Λ,Δ/Δ,Λ, but not the separation of all four different diastereoisomers (Figure SI2) [**SI1,SI3,SI4**].

In case of {[Ru(bpy)$_2$]$_2$(bpt)}$^{3+}$ (**1**), after three hours of irradiation at 430 nm the isomers constituting fraction A are converted into the isomers forming fraction B as detected through ^{1}H NMR spectroscopy (Figure SI4).

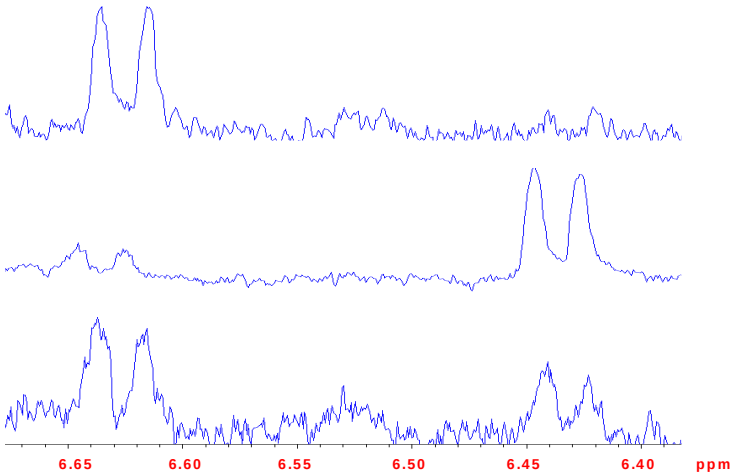

Figure SI4. *Comparison of the ^{1}H NMR spectra in deuteriated acetonitrile of fractions A (upper profile), B (middle) and fraction A of $\{[Ru(bpy)_2]_2(bpt)\}(PF_6)_3$ (**1**) after three hours of irradiation at 430 nm (lower profile) showing the photoisomerization process of fraction A.*

For both fractions A and B of **1**, further irradiation produces the fragmentation of the dimetallic complex into monometallic species [**SI5**]. Such a photolytic reaction is catalysed by the presence of chloride anions. In particular, photofragmentation of complex **1** consists of the loss of the ruthenium centre bound to the N4-site of triazole ring [**SI5**].

References

SI1. 1. (a) Hage, R.; Dijkhuis, A.H.J.; Haasnoot, J.G.; Prins, R.; Reedijk, J.; Buchanan, B.E.; Vos, J.G. *Inorg. Chem.* **1988**, *27*, 2185-2189; (b) Hage, R.; Haasnoot, J.G.; Reedijk, J.; Wang, R.; Vos, J.G. *Inorg. Chem.* **1991**, *30*, 3263-3269; (c) Browne, W.R.; O'Connor, C.M.; Villani, C.; Vos, J.G. *Inorg. Chem.*, **2001**, *40*, 5461-5464.

SI2. Browne, W.R.; O'Boyle, N.M.; Henry, W.; Guckian, A. L.; Horn, S.; Fett, T.; O'Connor, C. M.; Duati, M.; De Cola, L.; Coates, C. G.; Ronayne, K. L.; McGarvey, J. J.; Vos, J. G. *J. Am. Chem. Soc*. **2005** *127*, 1229-1241.

SI3. Hage, R.; Dijkhuis, A.H.J.; Haasnoot, J.G.; Prins, R.; Reedijk, J.; Buchanan, B.E.; Vos, J.G. *Inorg. Chem.* **1988**, *27*, 2185-2189.

SI4. Gasparrini, F.; D'Acquarica, I.; Vos, J.G.; O'Connor, C.M.; Villani, C. *Tetrahedron: Asymm.* **2000**, *11*, 3535-3541.

SI5. Hughes, H.P.; Vos, J.G. *Inorg. Chem.* **1995**, *34*, 4001-4003.

Appendix B HPLC traces for some standard compounds and work not shown in this thesis.

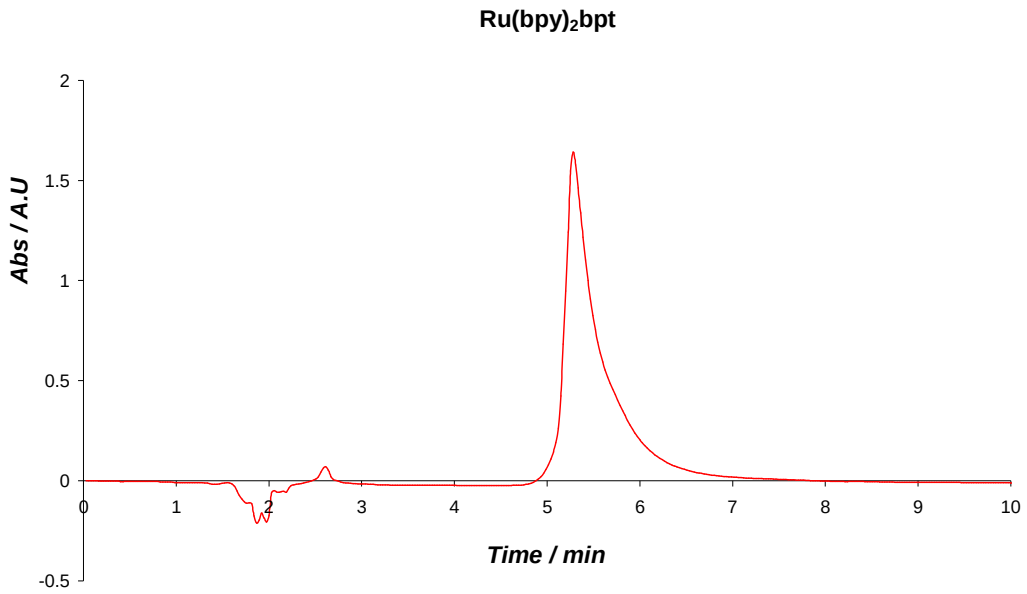

Figure B1 *HPLC trace for $[Ru(bpy)_2bpt]^+$ in CH_3CN (mobile phase CH_3CN: H_2O with volume ratio 80:20 containing 0.1 M KNO_3). Flow rate: 2.0 cm^3 min^{-1}; detection wavelength at 280 nm.*

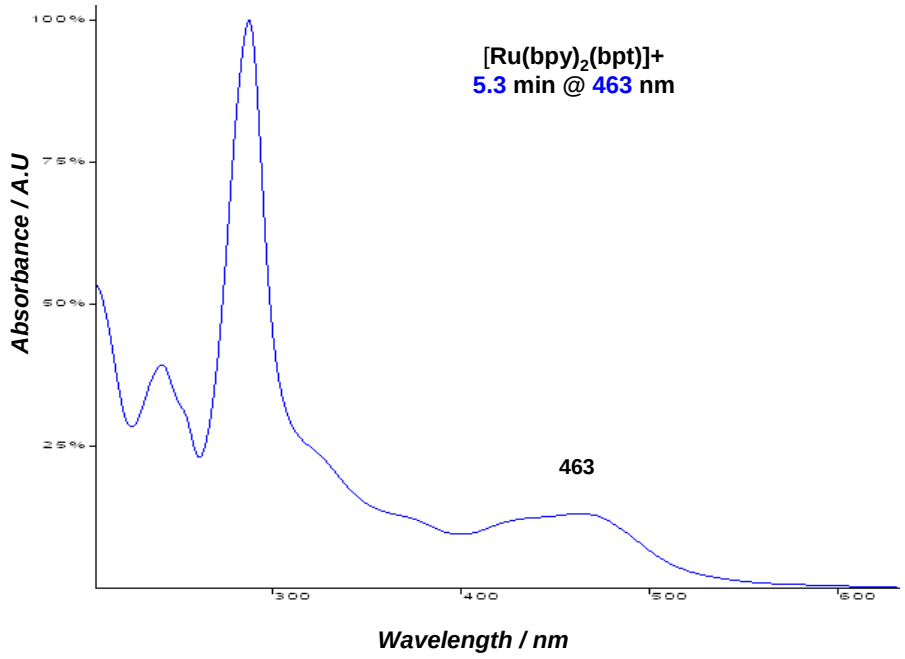

Figure B2 *UV/vis spectra for $[Ru(bpy)_2bpt]^+$ in CH_3CN (mobile phase CH_3CN: H_2O with volume ratio 80:20 containing 0.1 M KNO_3). Flow rate: 2.0 cm^3 min^{-1}; detection wavelength at 280 nm.*

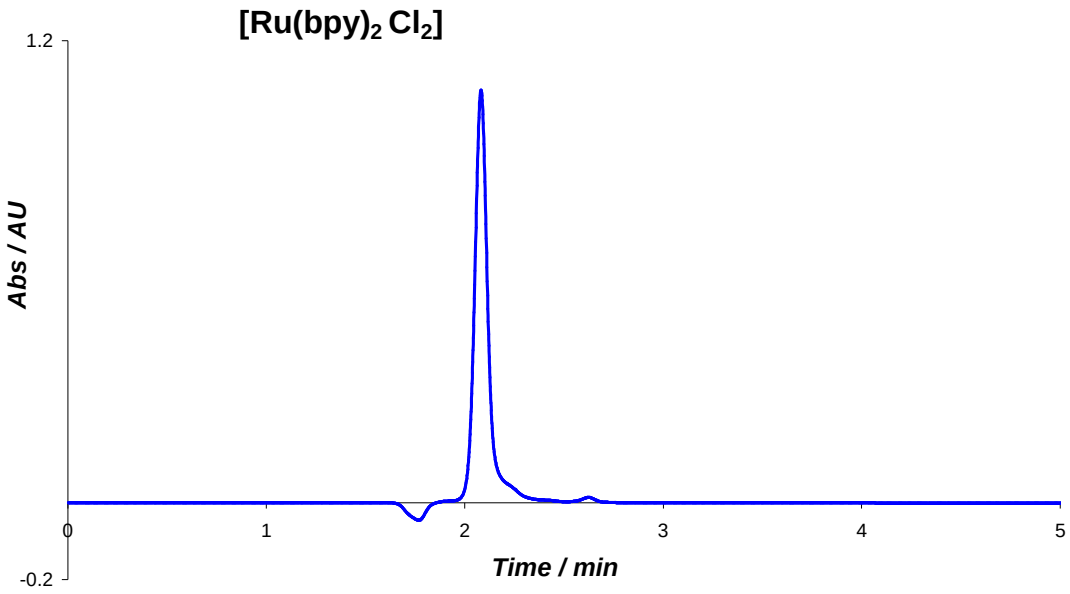

Figure B3 *HPLC trace for $[Ru(bpy)_2.Cl_2$ in CH_3CN (mobile phase CH_3CN: H_2O with volume ratio 80:20 containing 0.1 M KNO_3). Flow rate: 2.0 cm^3 min^{-1}; detection wavelength at 280 nm.*

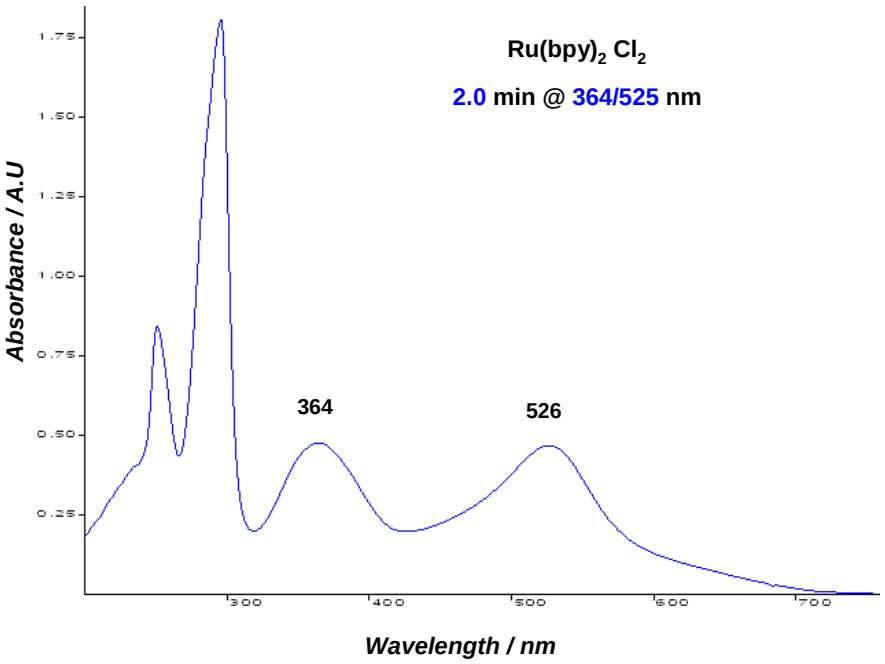

Figure B4 *UV/vis sapctra for $[Ru(bpy)_2.Cl_2$ in CH_3CN (mobile phase CH_3CN: H_2O with volume ratio 80:20 containing 0.1 M KNO_3). Flow rate: 2.0 cm^3 min^{-1}; detection wavelength at 280 nm.*

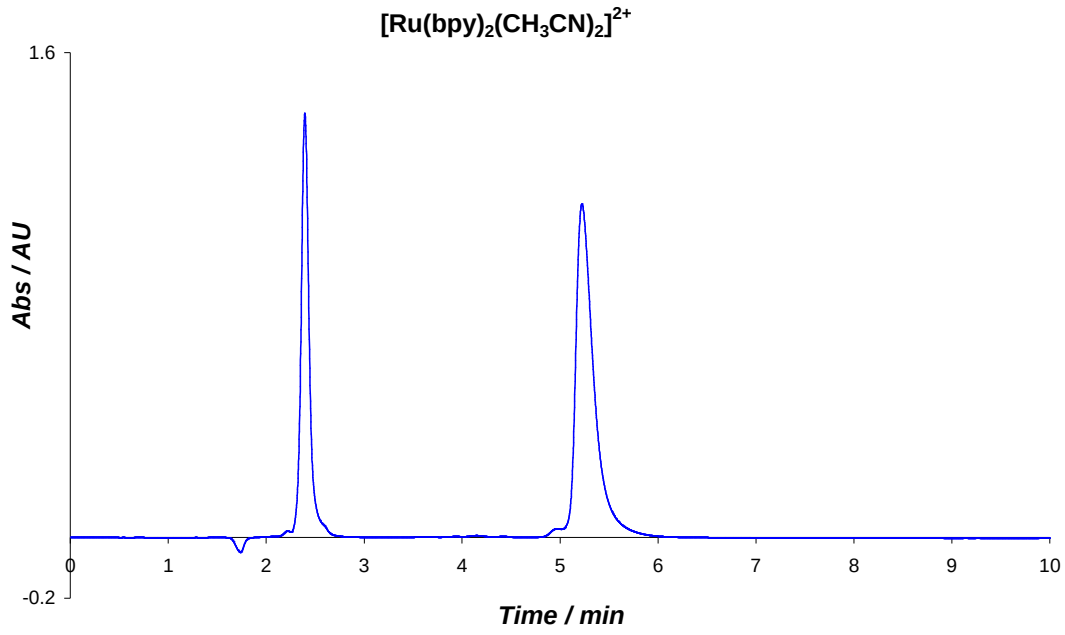

Figure B5 *HPLC trace for $[Ru(bpy)_2(CH_3CN)_2]^{2+}$ in CH_3CN (mobile phase CH_3CN: H_2O with volume ratio 80:20 containing 0.1 M KNO_3). Flow rate: 2.0 cm^3 min^{-1}; detection wavelength at 280 nm.*

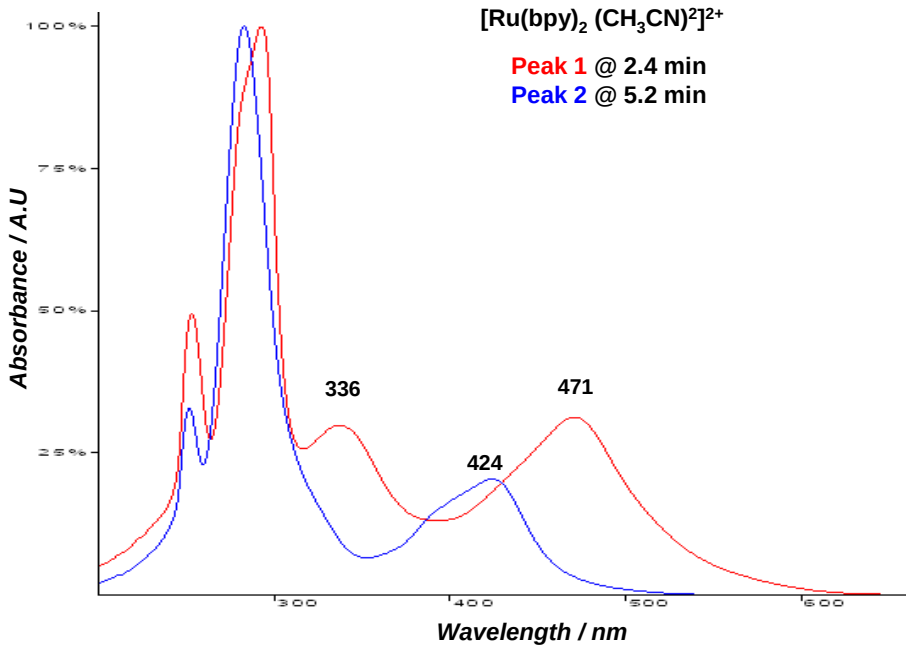

Figure B6 *UV/vis spectra of $[Ru(bpy)_2(CH_3CN)_2]^{2+}$ in CH_3CN (mobile phase CH_3CN: H_2O with volume ratio 80:20 containing 0.1 M KNO_3). Flow rate: 2.0 cm^3 min^{-1}; detection wavelength at 280 nm.*

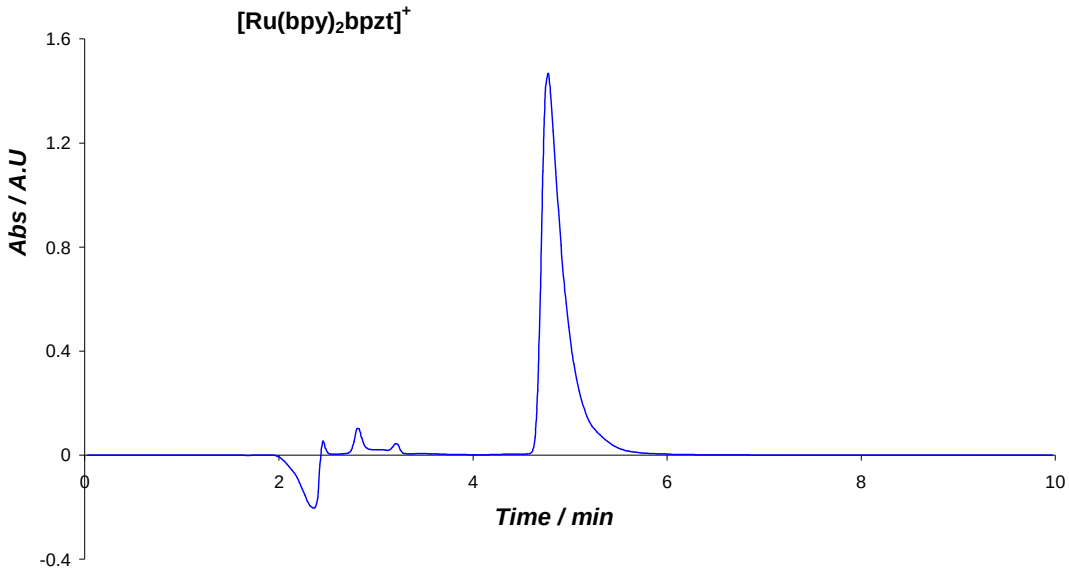

Figure B7 HPLC *trace for $[Ru(bpy)_2bpzt]^+$ in CH_3CN (mobile phase CH_3CN: H_2O with volume ratio 80:20 containing 0.1 M KNO_3). Flow rate: 2.0 cm^3 min^{-1}; detection wavelength at 280 nm.*

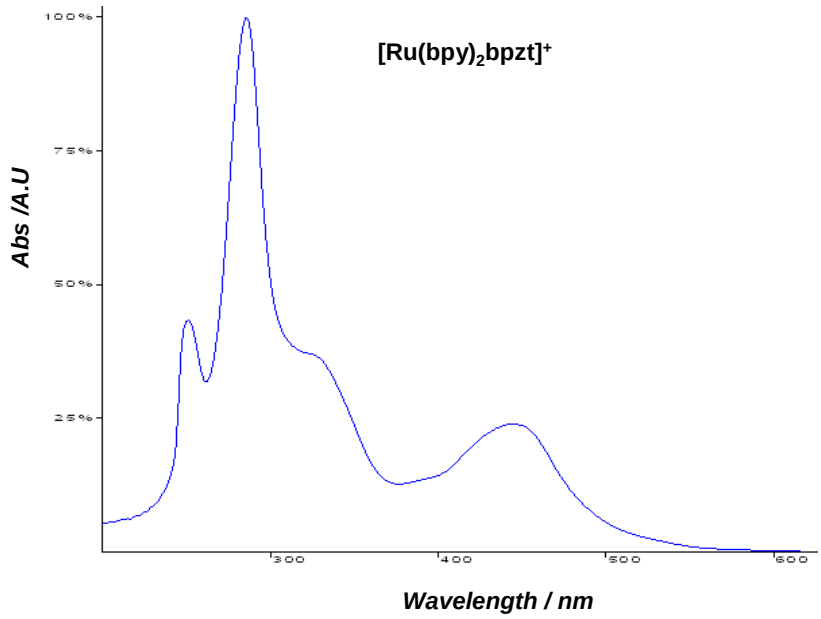

Figure B8 UV/*vis spectra for $[Ru(bpy)_2bpzt]^+$ in CH_3CN (mobile phase CH_3CN: H_2O with volume ratio 80:20 containing 0.1 M KNO_3). Flow rate: 2.0 cm^3 min^{-1}; detection wavelength at 280 nm.*

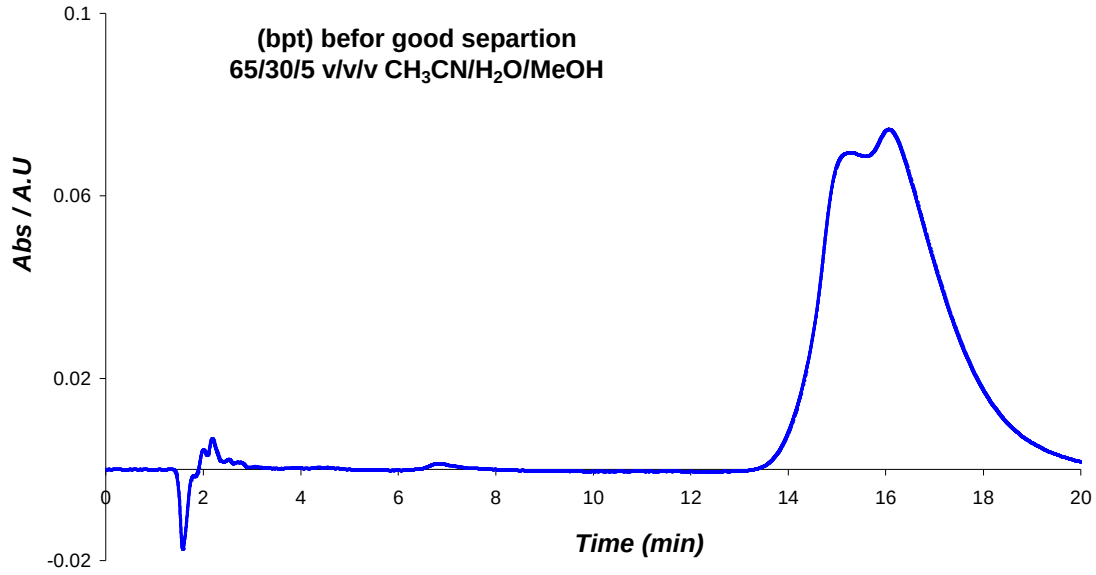

Figure B9 *HPLC trace for impure {[Ru(bpy)$_2$]$_2$ bpt}$^{3+}$ in CH_3CN (mobile phase CH_3CN: H_2O: CH_3OH with volume ratio 65:30:05 containing 0.12 M KNO_3). Flow rate: 2.0 cm^3 min^{-1}; detection wavelength at 280 nm.*

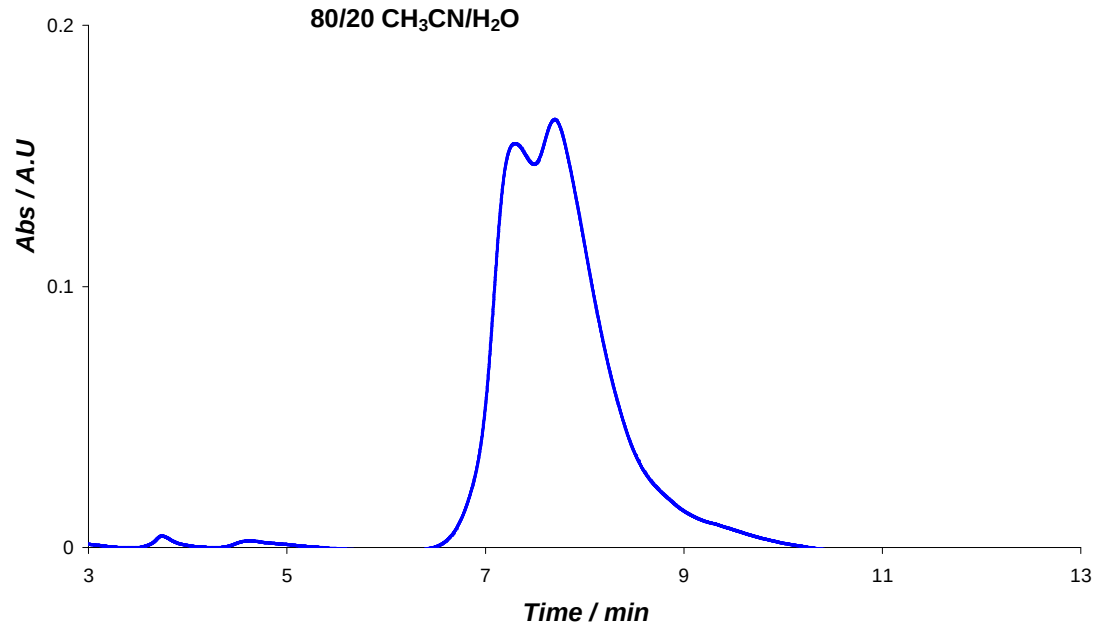

Figure B10 *HPLC trace for impure {[Ru(bpy)$_2$]$_2$ bpt}$^{3+}$ in CH_3CN (mobile phase CH_3CN: H_2O with volume ratio 80:20 containing 0.12 M KNO_3). Flow rate: 4.0 cm^3 min^{-1}; detection wavelength at 280 nm.*

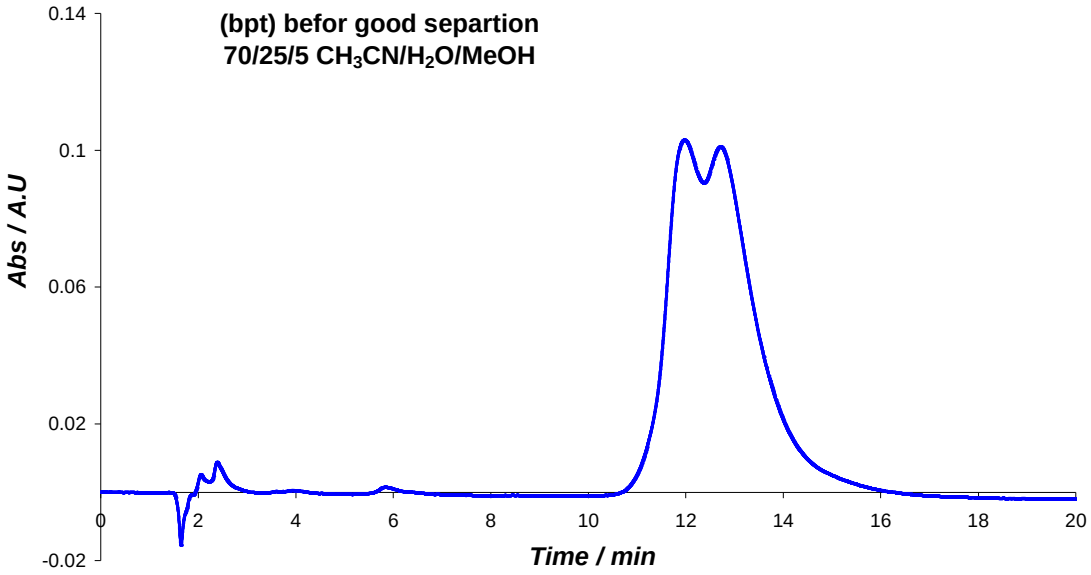

Figure B11 *HPLC trace for impure {[Ru(bpy)$_2$]$_2$ bpt}$^{3+}$ in CH_3CN (mobile phase CH_3CN: H_2O: CH_3OH with volume ratio 70:25:05 containing 0.12 M KNO_3). Flow rate: 4.0 cm^3 min^{-1}; detection wavelength at 280 nm.*

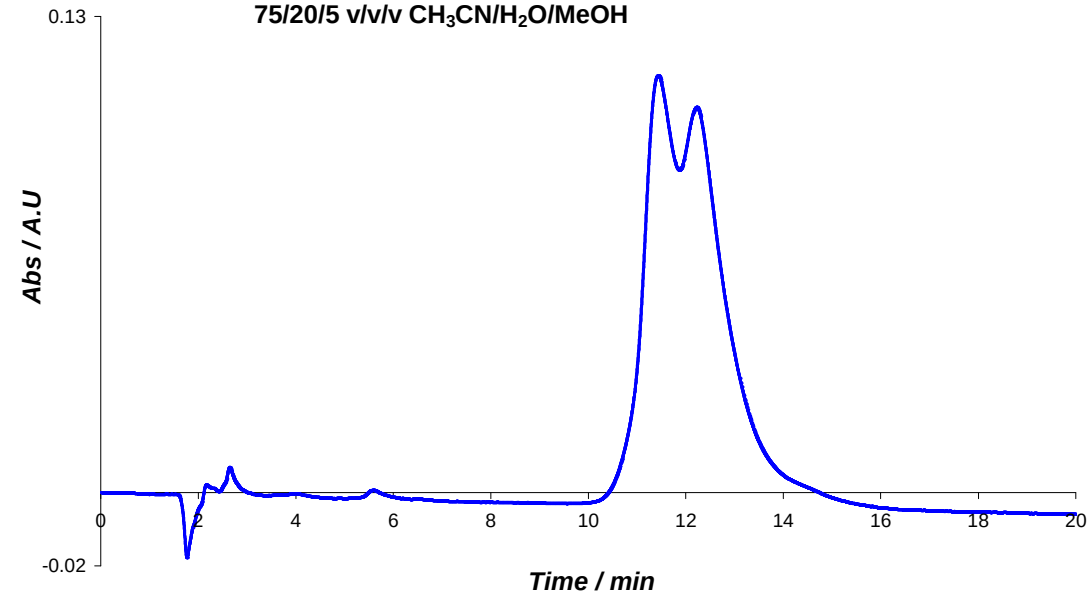

Figure B12 *HPLC trace for impure {[Ru(bpy)$_2$]$_2$ bpt}$^{3+}$ in CH_3CN (mobile phase CH_3CN: H_2O: CH_3OH with volume ratio 75:20:05 containing 0.12 M KNO_3). Flow rate: 4.0 cm^3 min^{-1}; detection wavelength at 280 nm.*

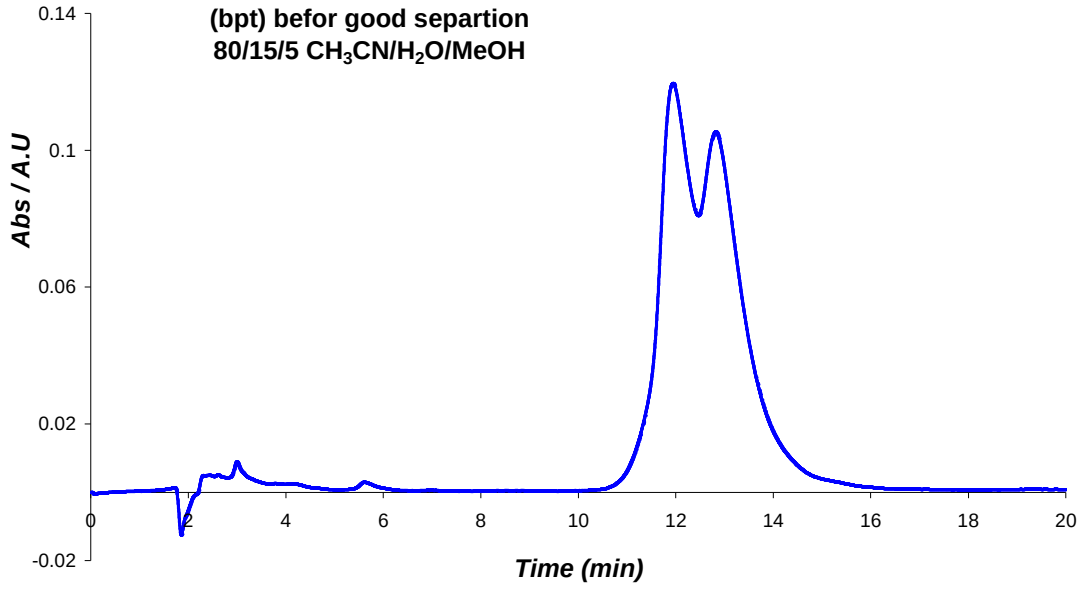

Figure B13 *HPLC trace for impure {[Ru(bpy)$_2$]$_2$ bpt}$^{3+}$ in CH_3CN (mobile phase CH_3CN: H_2O: CH_3OH with volume ratio 80:15:05 containing 0.12 M KNO_3). Flow rate: 4.0 cm^3 min^{-1}; detection wavelength at 280 nm.*

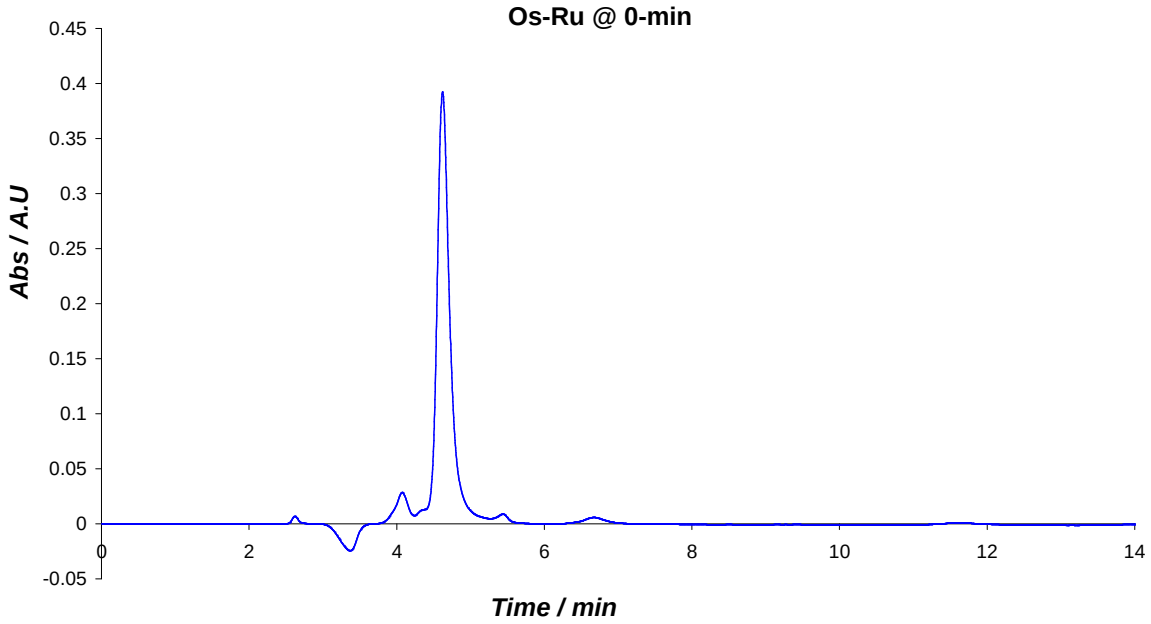

Figure B14 *HPLC trace for [Os(bpy)$_2$ (bpt) Ru(tpy)Cl]$^{2+}$ in CH_3CN (mobile phase CH_3CN: H_2O with volume ratio 80:20 containing 0.1 M KNO_3). Flow rate: 2.0 cm^3 min^{-1}; detection wavelength at 280 nm.*

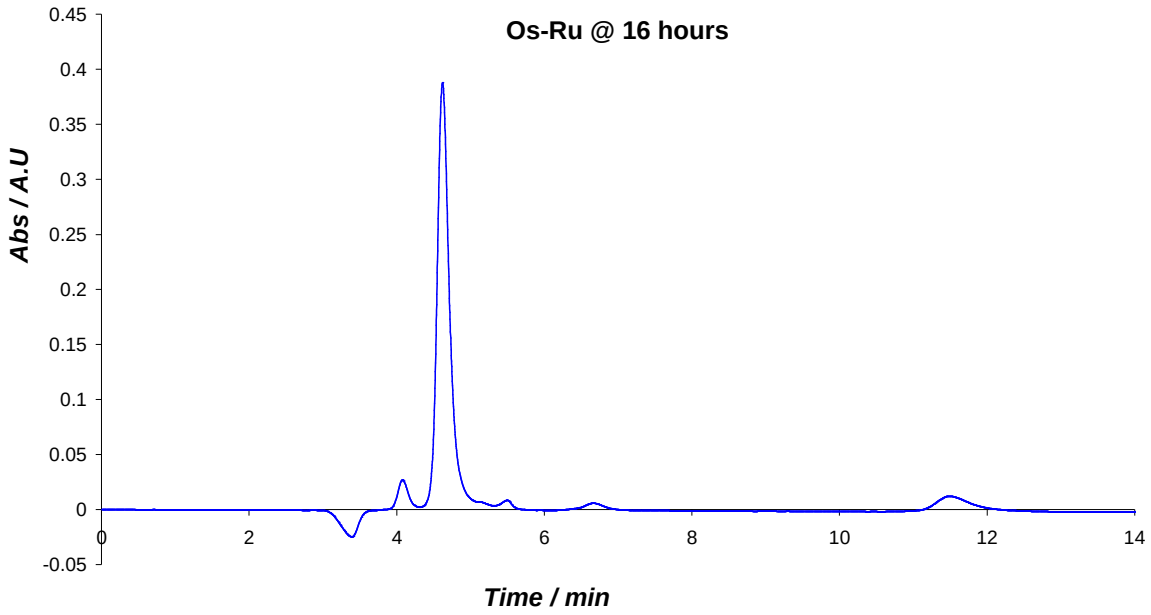

Figure B15 *HPLC trace during photolysis of $[Os(bpy)_2(bpt)Ru(tpy)Cl]^{2+}$ in CH_3CN (mobile phase CH_3CN: H_2O with volume ratio 80:20 containing 0.1 M KNO_3). Flow rate: 2.0 cm^3 min^{-1}; detection wavelength at 280 nm.*

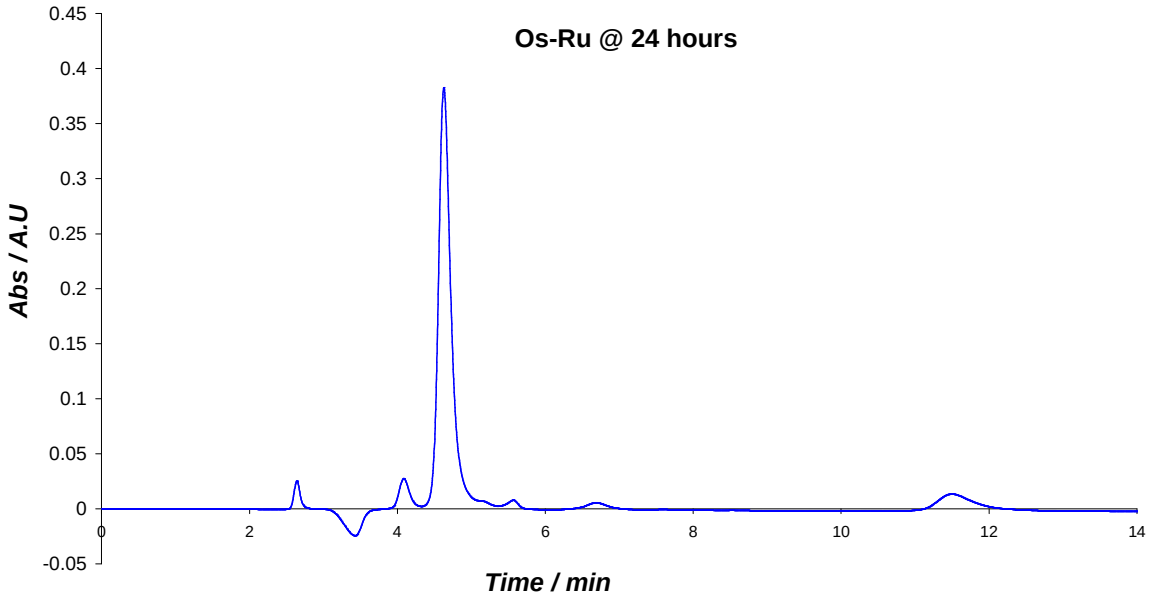

Figure B16 *HPLC trace during photolysis of $[Os(bpy)_2(bpt)Ru(tpy)Cl]^{2+}$ in CH_3CN (mobile phase CH_3CN: H_2O with volume ratio 80:20 containing 0.1 M KNO_3). Flow rate: 2.0 cm^3 min^{-1}; detection wavelength at 280 nm.*

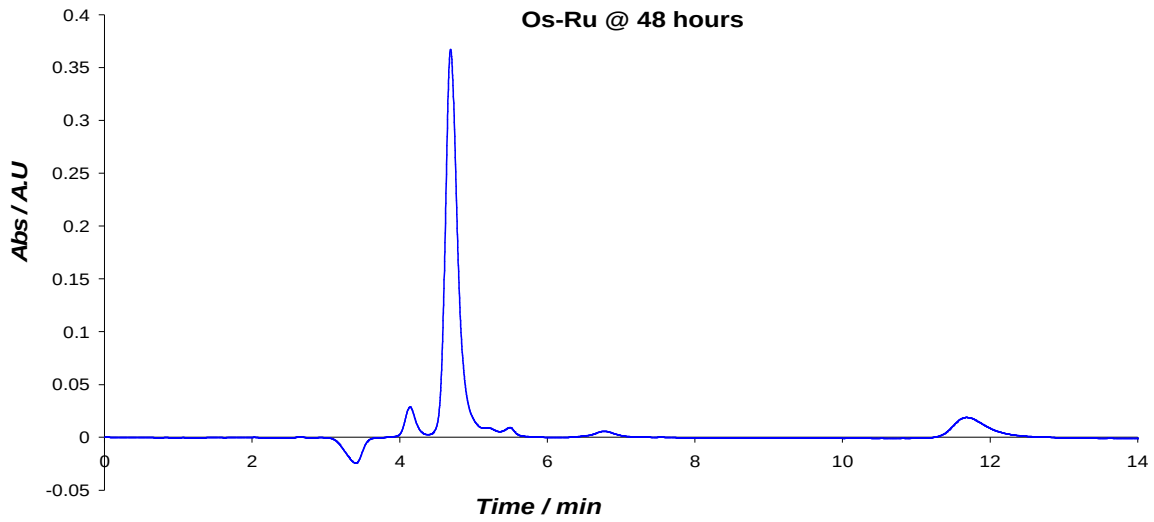

Figure B17 *HPLC trace during photolysis of $[Os(bpy)_2$ (bpt) $Ru(tpy)Cl]^{2+}$ in CH_3CN (mobile phase CH_3CN: H_2O with volume ratio 80:20 containing 0.1 M KNO_3). Flow rate: 2.0 cm^3 min^{-1}; detection wavelength at 280 nm.*

Results obtained during irradiation in the presence of Chloride ions

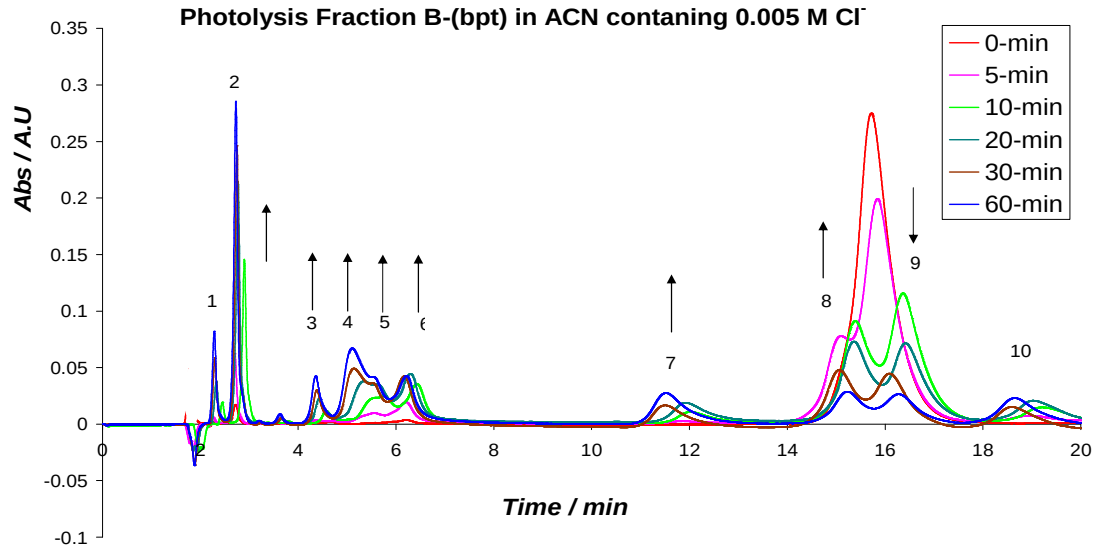

Figure B18 *HPLC trace during Photolysis of fraction B-(bpt) after semi prep. Retention time 15.0 min of $\{[Ru(bpy)_2]_2$ bpt$\}^{3+}$ in CH_3CN (mobile phase CH_3CN: H_2O: CH_3OH with volume ratio 75:15:10 containing 0.12 M KNO_3). Containing 0.005 M LiCl. Flow rate: 2.0 cm^3 min^{-1}; detection wavelength at 280 nm.*

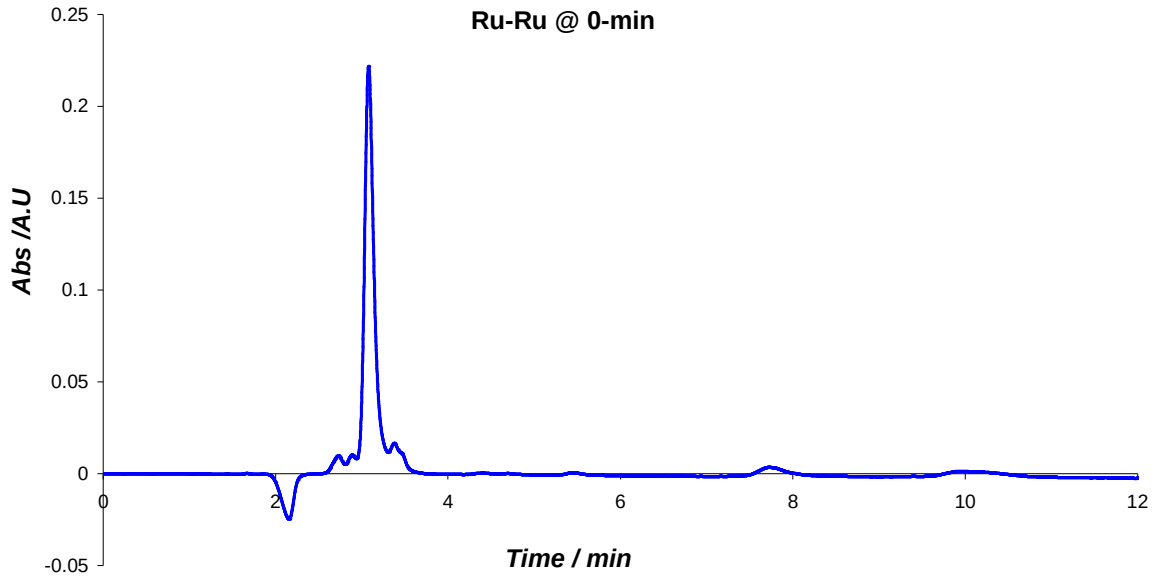

Figure B19 *HPLC trace for $[Ru(d_8\text{-}bpy)_2(bpt)Ru(bpy)Cl]^+$ in CH_3CN (mobile phase CH_3CN: H_2O with volume ratio 80:20 containing 0.1 M KNO_3). Flow rate: 2.0 cm^3 min^{-1}; detection wavelength at 280 nm.*

HPLC traces associated with paper 1.

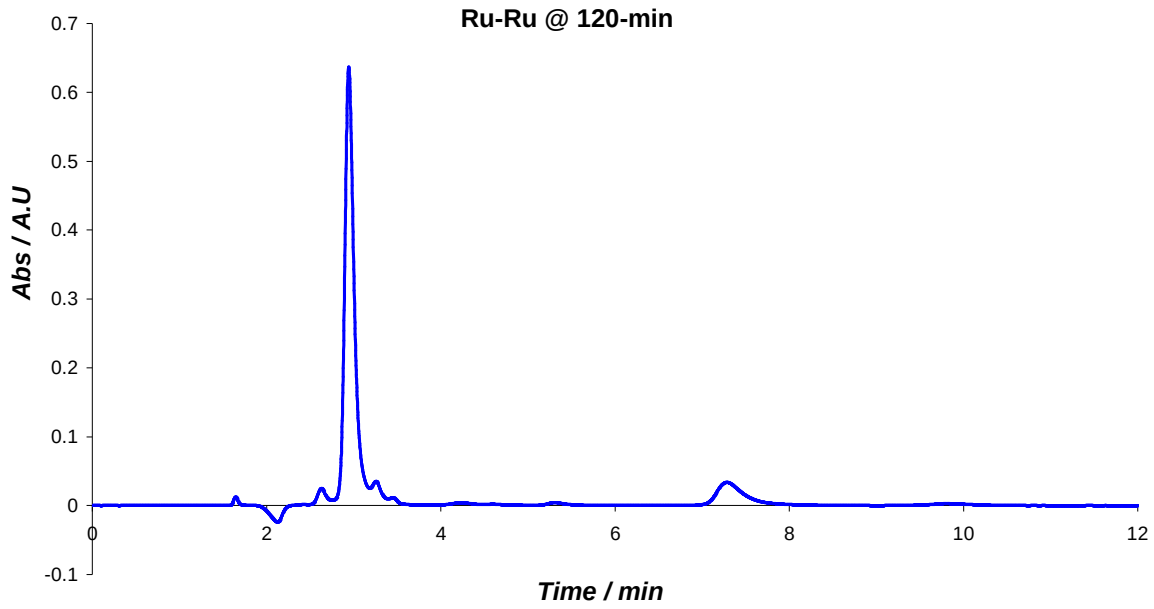

Figure B20 *HPLC trace during photolysis of $[Ru(d_8\text{-}bpy)_2(bpt)\ Ru(bpy)_2Cl]^{2+}$ in CH_3CN (mobile phase CH_3CN: H_2O with volume ratio 80:20 containing 0.1 M KNO_3). Flow rate: 2.0 $cm^3\ min^{-1}$; detection wavelength at 280 nm.*

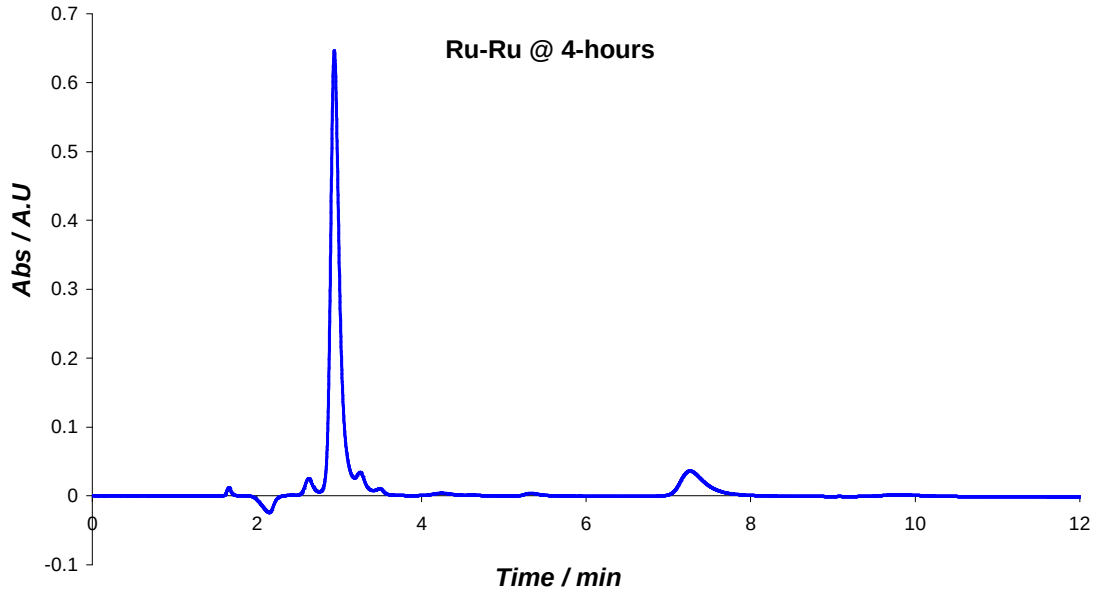

Figure B21 *HPLC trace during photolysis of $[Ru(d_8\text{-}bpy)_2\ (bpt)\ Ru(bpy)_2Cl]^{2+}$ in CH_3CN (mobile phase CH_3CN: H_2O with volume ratio 80:20 containing 0.1 M KNO_3). Flow rate: 2.0 $cm^3\ min^{-1}$; detection wavelength at 280 nm.*

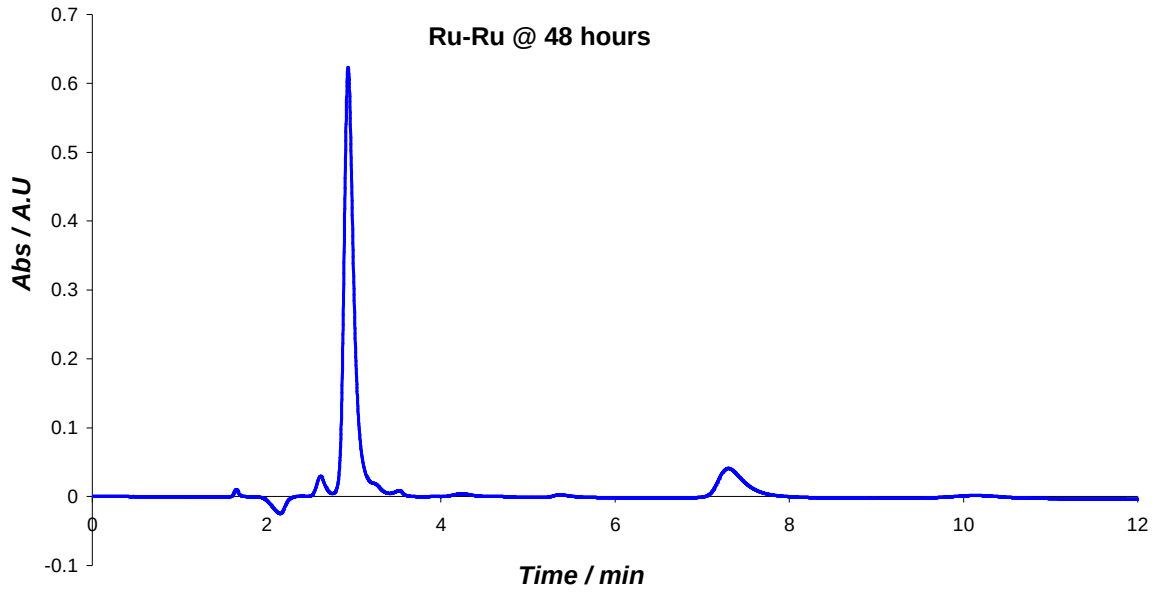

Figure B22 *HPLC trace during photolysis of [Ru(d_8-bpy)$_2$ (bpt) Ru(bpy)Cl]$^+$ in CH_3CN (mobile phase CH_3CN: H_2O with volume ratio 80:20 containing 0.1 M KNO_3). Flow rate: 2.0 cm^3 min^{-1}; detection wavelength at 280 nm.*

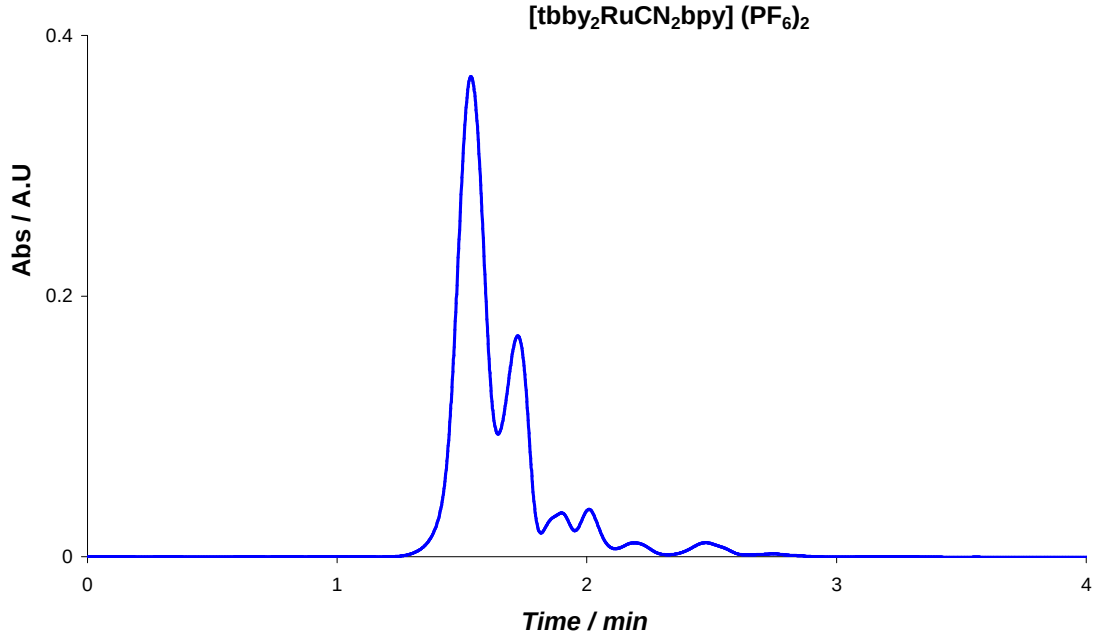

Figure B23 *HPLC trace during photolysis of [(tbby)$_2$RuCN$_2$] (PF$_6$)$_2$ in CH_3CN (mobile phase CH_3CN: H_2O: MeOH with volume ratio 75:20:05 containing 0.1 M KNO_3). Flow rate: 2.0 cm^3 min^{-1}; detection wavelength at 280 nm.*

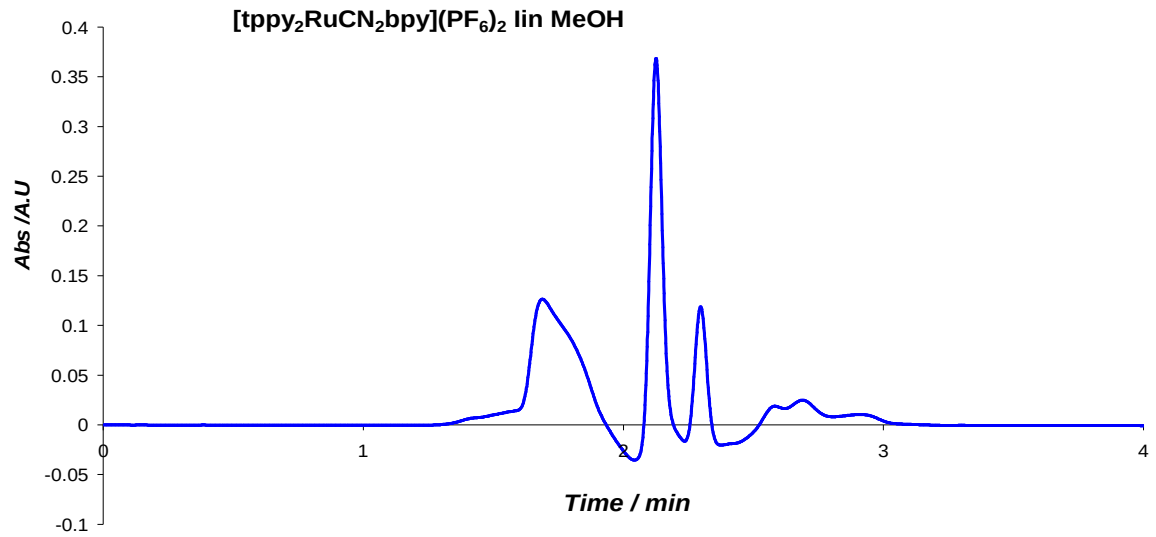

Figure B24 *HPLC trace during photolysis of [tbby$_2$RuCN$_2$] (PF$_6$)$_2$ in MeOH (mobile phase CH$_3$CN: H$_2$O: MeOH with volume ratio 75:20:05 containing 0.1 M KNO$_3$). Flow rate: 2.0 cm^3 min^{-1}; detection wavelength: at 280 nm.*

HPLC work related to paper 4.

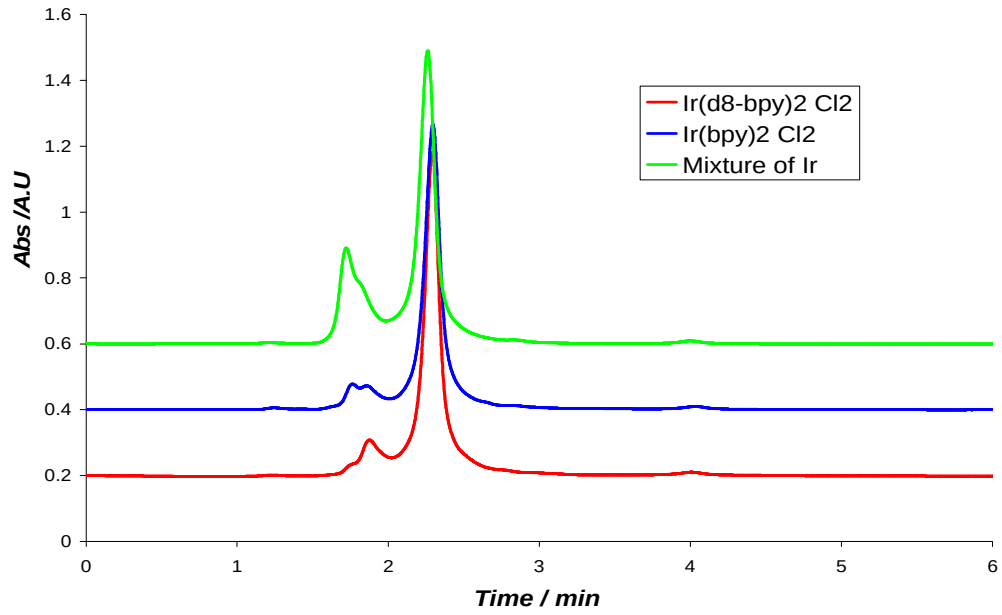

Figure B25 *HPLC trace for Ir(d$_8$-bpy)$_2$Cl$_2$, Ir(bpy)$_2$ Cl$_2$ and Mixture of Ir in CH$_3$CN (mobile phase CH$_3$CN: H$_2$O with volume ratio 80:20 containing 0.1 M KNO$_3$). Flow rate: 2.0 cm^3 min^{-1}; detection wavelength at 280 nm.*

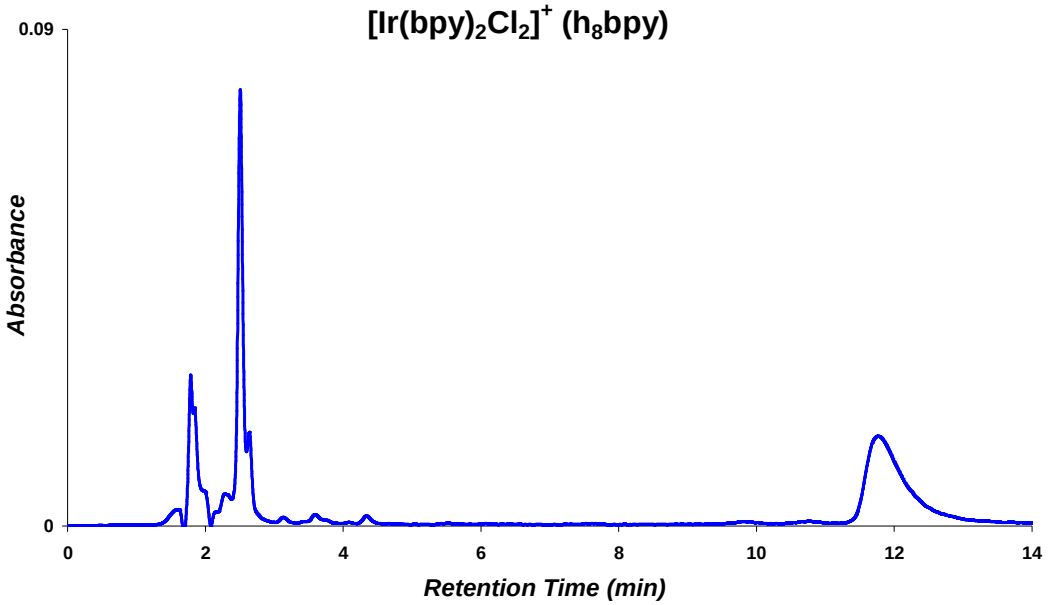

Figure B26 *HPLC trace for Ir(d_8-bpy)$_2$Cl$_2$, Ir(bpy)$_2$ Cl$_2$ and Mixture of Ir in CH_3CN (mobile phase CH_3CN: H_2O with volume ratio 80:20 containing 0.1 M KNO_3). Flow rate: 2.0 cm^3 min^{-1}; detection wavelength at 280 nm.*

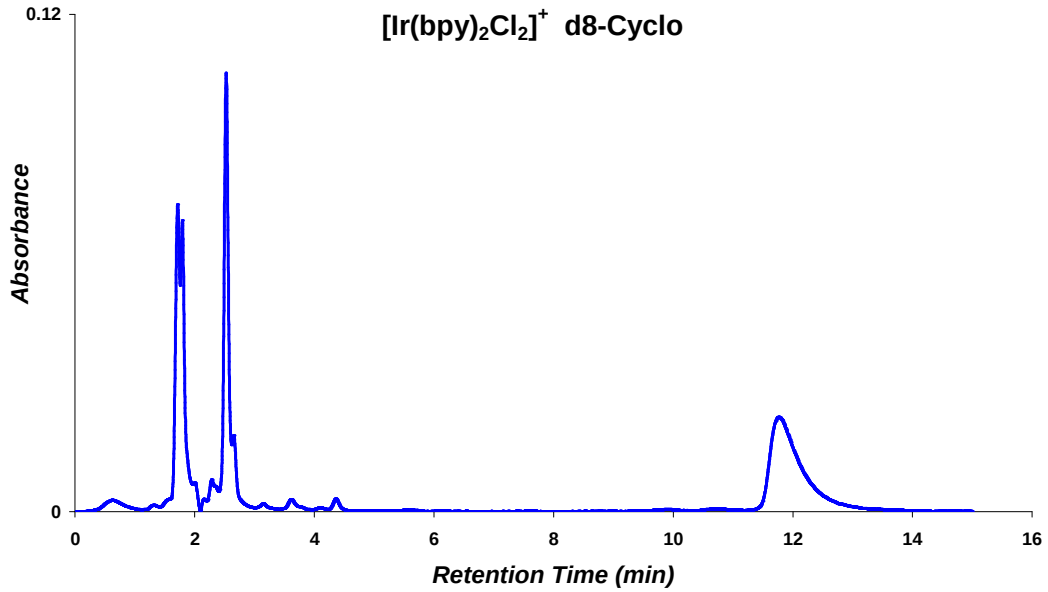

Figure B27 *HPLC trace for Ir(d_8-bpy)$_2$Cl$_2$, Ir(bpy)$_2$ Cl$_2$ and Mixture of Ir in CH_3CN (mobile phase CH_3CN: H_2O with volume ratio 80:20 containing 0.1 M KNO_3). Flow rate: 2.0 cm^3 min^{-1}; detection wavelength at 280 nm.*

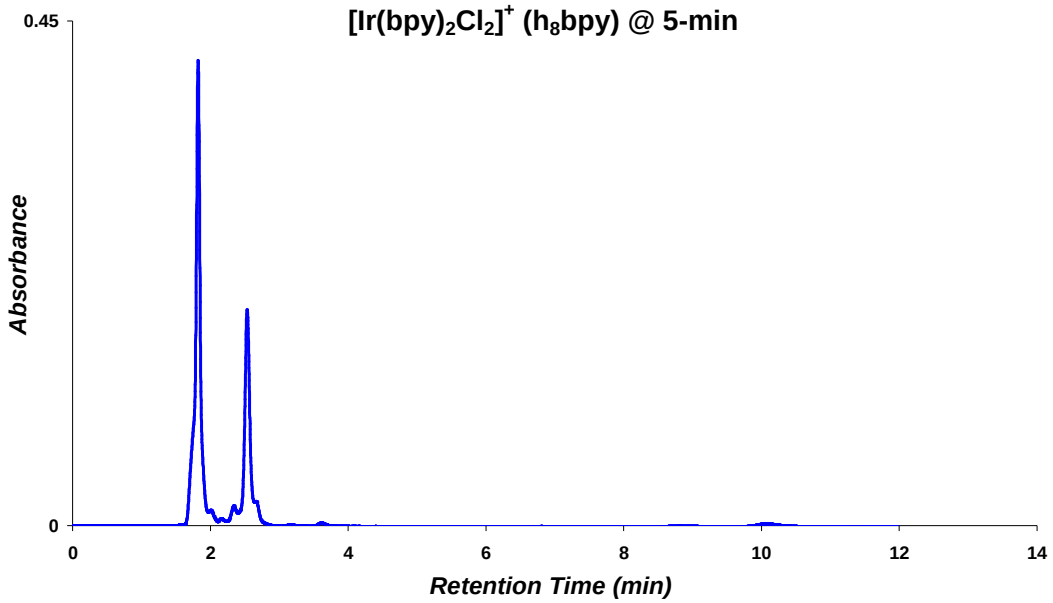

Figure B28 *HPLC trace for Ir(d_8-bpy)$_2$Cl$_2$, Ir(bpy)$_2$ Cl$_2$ and Mixture of Ir in CH_3CN (mobile phase CH_3CN: H_2O with volume ratio 80:20 containing 0.1 M KNO_3). Flow rate: 2.0 cm^3 min^{-1}; detection wavelength at 280 nm.*

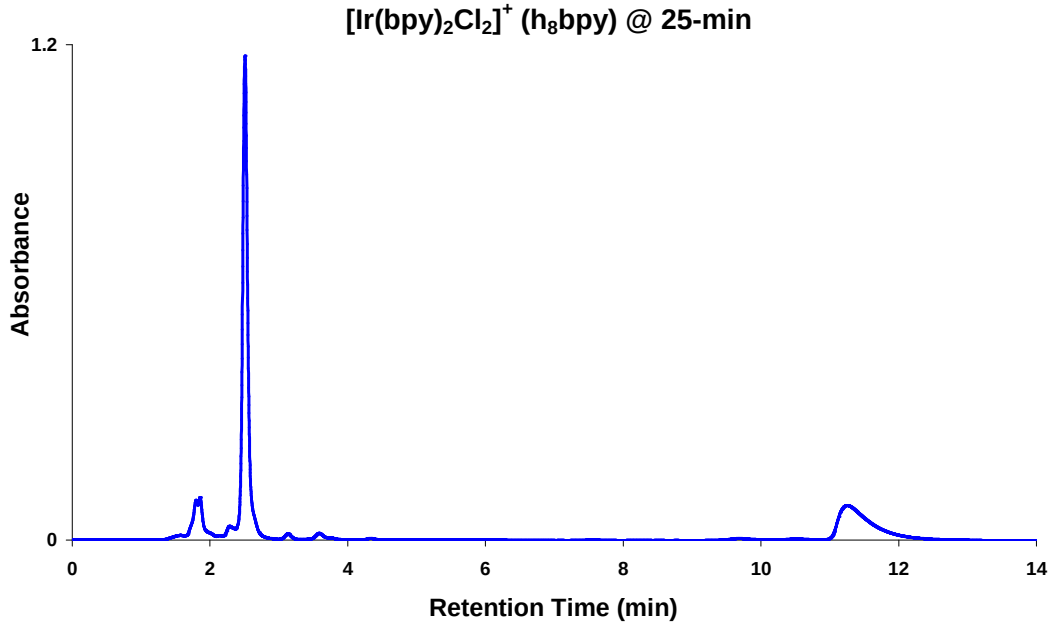

Figure B29 *HPLC trace for Ir(d_8-bpy)$_2$Cl$_2$, Ir(bpy)$_2$ Cl$_2$ and Mixture of Ir in CH_3CN (mobile phase CH_3CN: H_2O with volume ratio 80:20 containing 0.1 M KNO_3). Flow rate: 2.0 cm^3 min^{-1}; detection wavelength at 280 nm.*

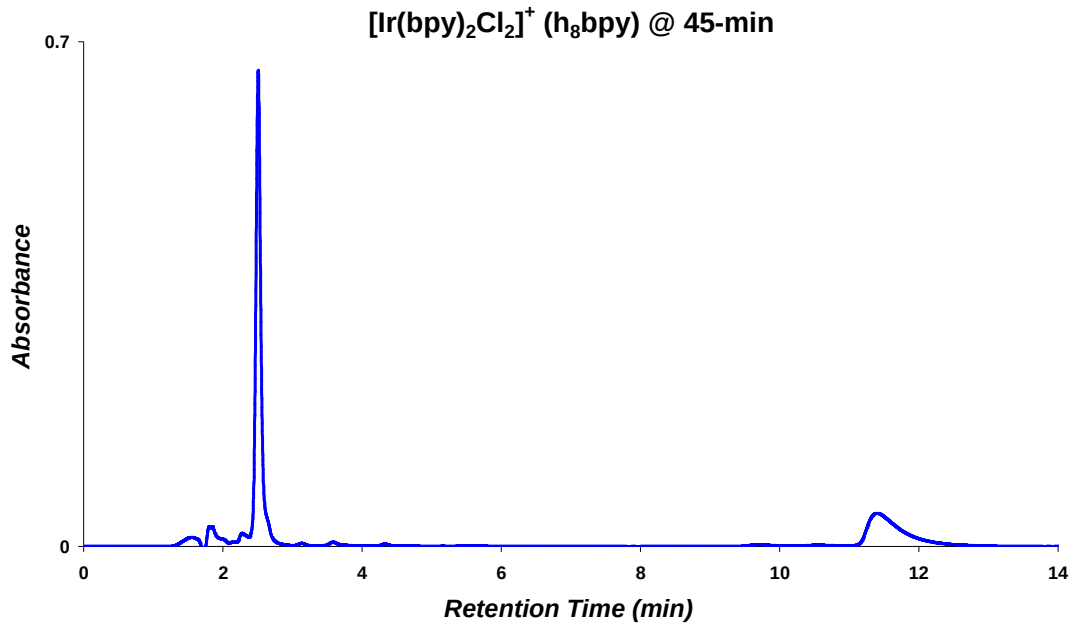

Figure B30 *HPLC trace for Ir(d_8-bpy)$_2$Cl$_2$, Ir(bpy)$_2$ Cl$_2$ and Mixture of Ir in CH_3CN (mobile phase CH_3CN: H_2O with volume ratio 80:20 containing 0.1 M KNO_3). Flow rate: 2.0 cm^3 min^{-1}; detection wavelength at 280 nm.*

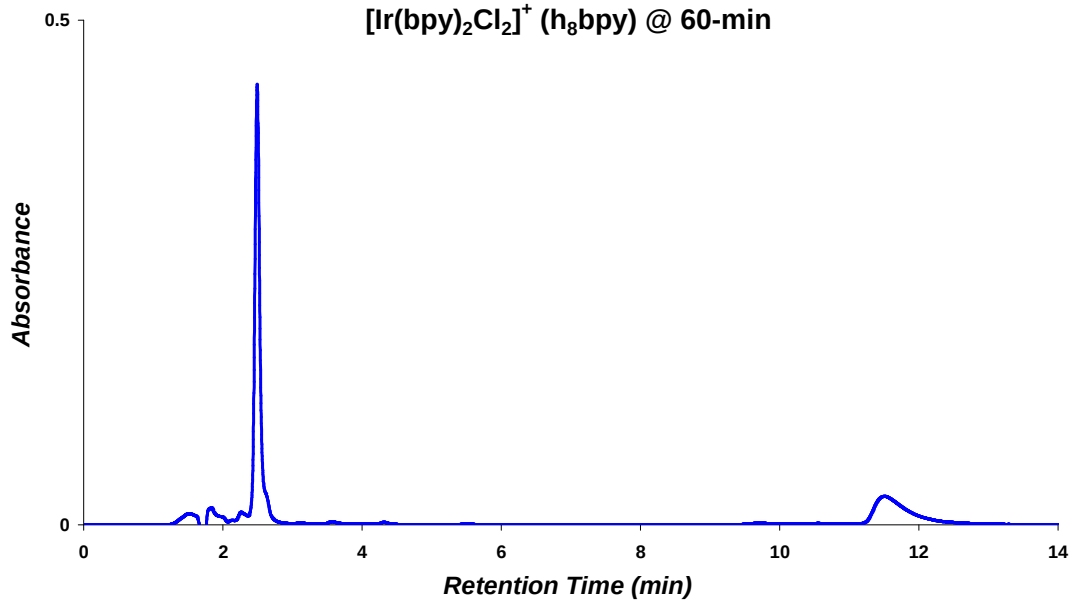

Figure B31 *HPLC trace for Ir(d_8-bpy)$_2$Cl$_2$, Ir(bpy)$_2$ Cl$_2$ and Mixture of Ir in CH_3CN (mobile phase CH_3CN: H_2O with volume ratio 80:20 containing 0.1 M KNO_3). Flow rate: 2.0 cm^3 min^{-1}; detection wavelength at 280 nm.*

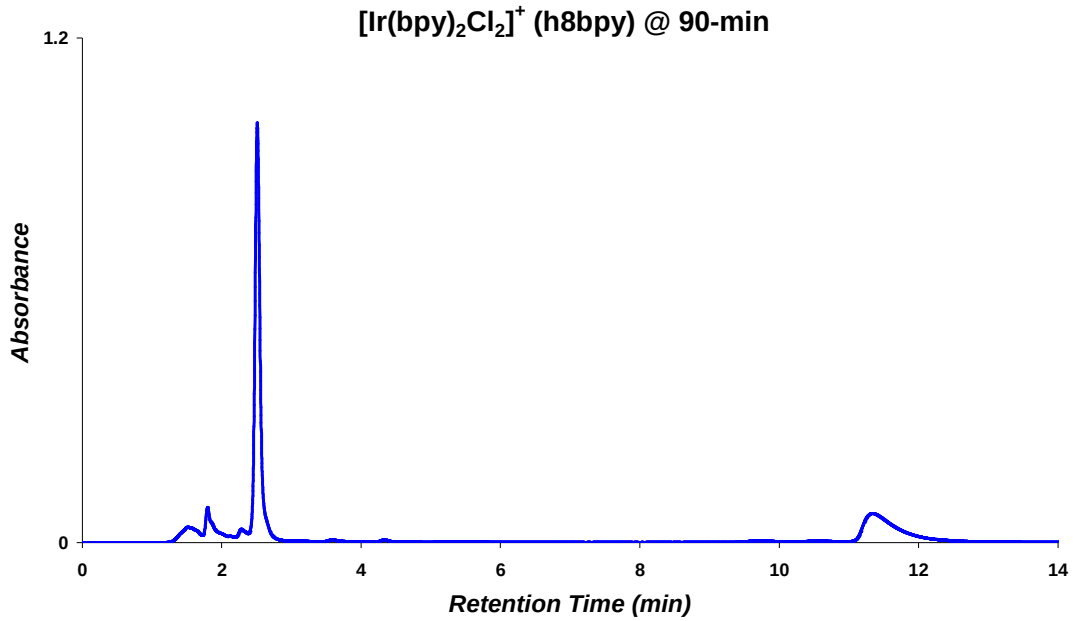

Figure B32 *HPLC trace for Ir(d_8-bpy)$_2$Cl$_2$, Ir(bpy)$_2$ Cl$_2$ and Mixture of Ir in CH_3CN (mobile phase CH_3CN: H_2O with volume ratio 80:20 containing 0.1 M KNO_3). Flow rate: 2.0 cm^3 min^{-1}; detection wavelength at 280 nm.*

Additional studies on effect of TEA on HPLC in Chapter 6.

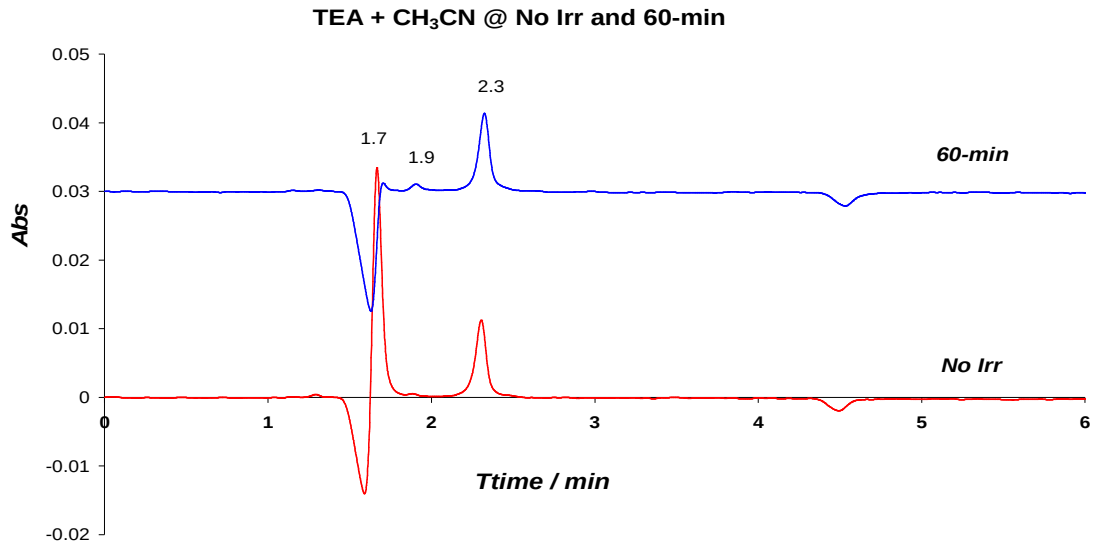

Figure B33 *HPLC trace during Irradiation of TEA with ACN at 24^{o} C detection wavelength at 430 nm, Mobile Phase CH_3CN: H_2O 70:30; 0.02 M KNO_3 Flow rate 2.0 cm^3 min^{-1}*

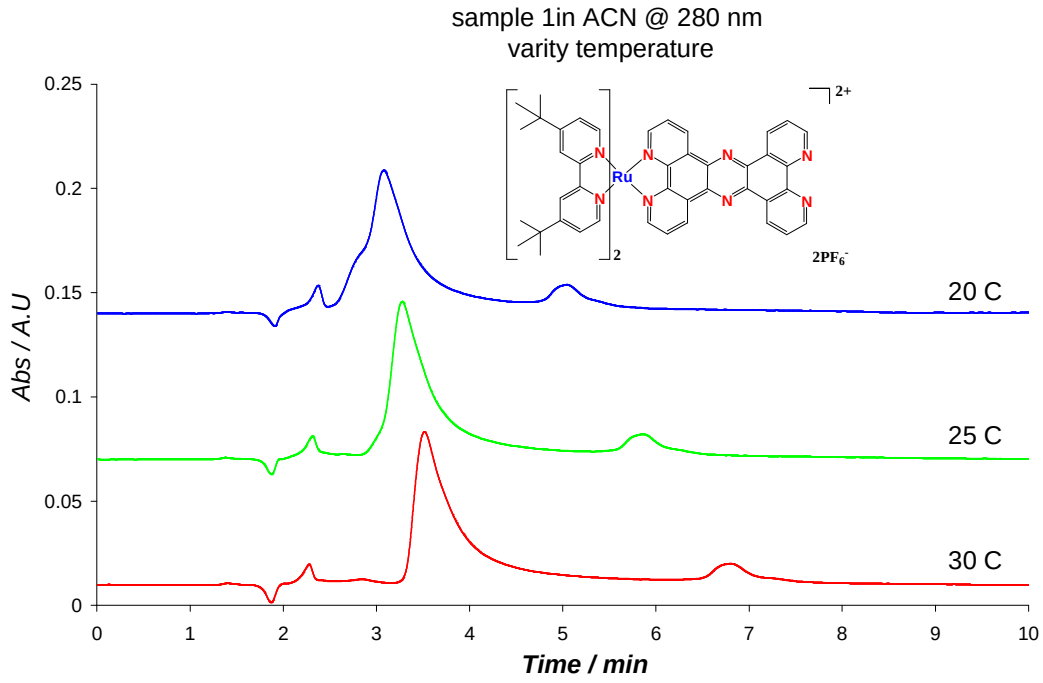

Figure B34 *HPLC trace for sample 1 at different temperatures.*

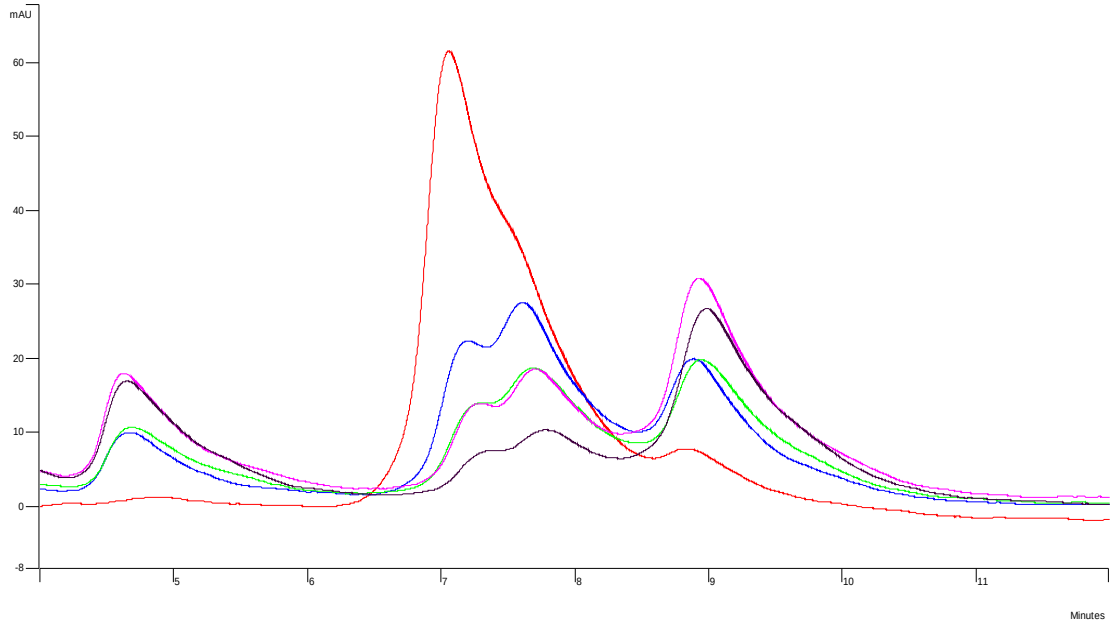

Figure B35 *HPLC trace for Fraction A-(bpt) in Acetone during photolysis from (0-120min) 80/20 acetonitrile/water 0.12 M KNO_3, Flow Rate 2.0 cm^3 min^{-1}.*

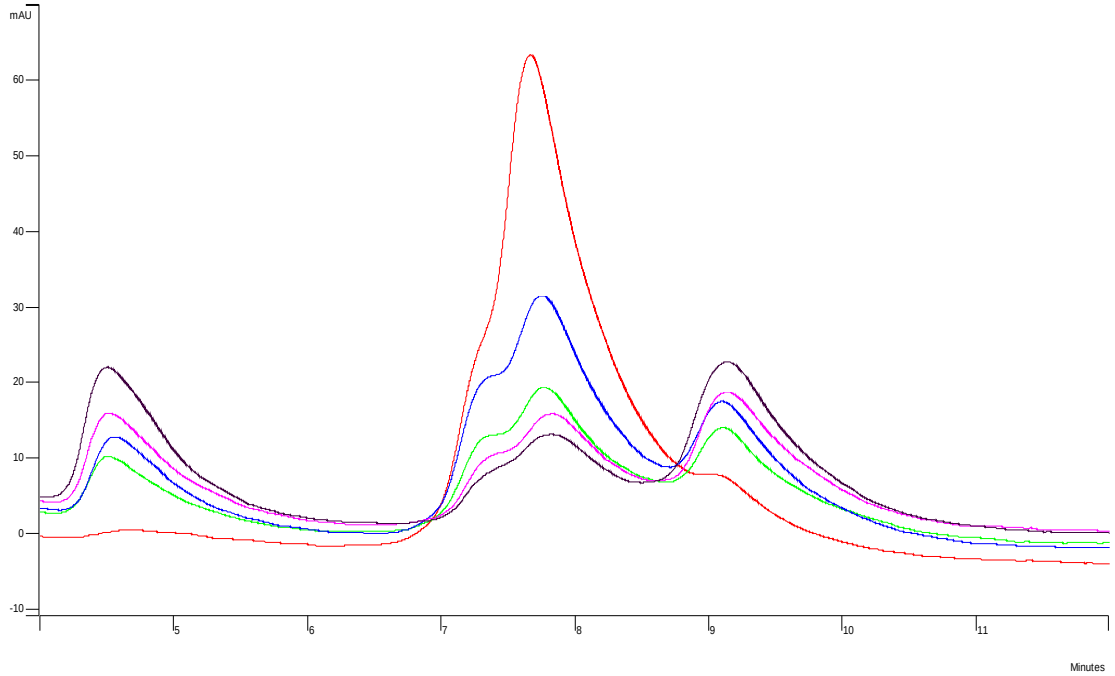

Figure B36 *HPLC trace for Fraction B-(bpt) in Acetone during photolysis from (0-120min) 80/20 acetonitrile/water 0.12 MKNO_3, Flow Rate 2.0 cm^3 min^{-1}.*